Caractérisation quantitative de la pulvérisation de pesticides par imagerie

Sofija Vulgarakis Minov

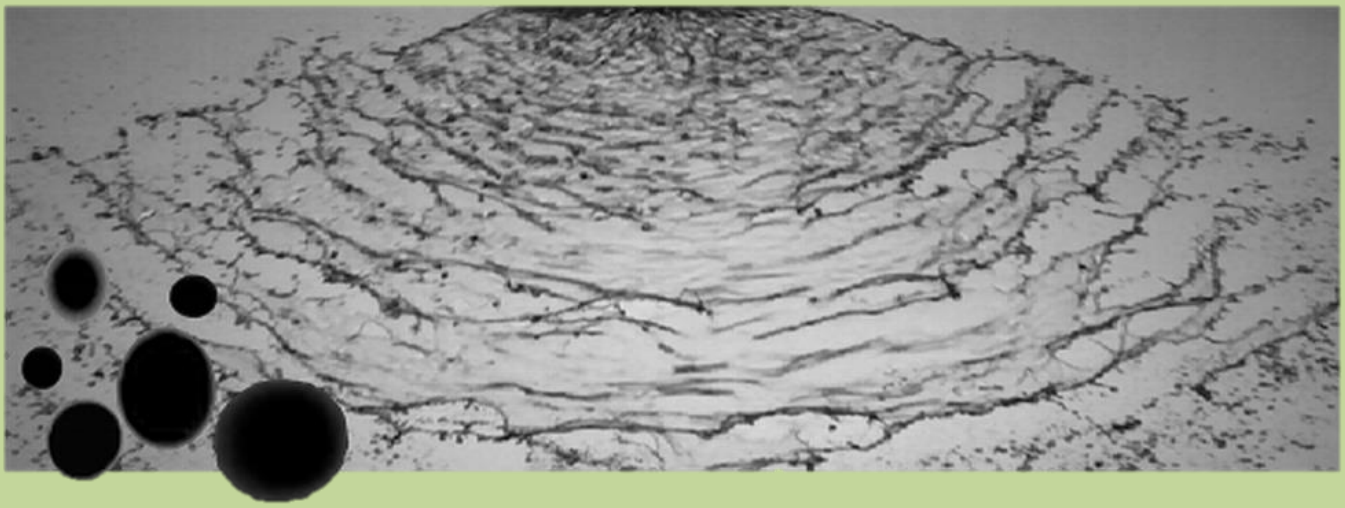

Integration of imaging techniques for the quantitative characterization of pesticide sprays

Sofija Vulgarakis Minov

ÉCOLE DOCTORALE ENVIRONNEMENT-SANTE THÈSE
Pour obtenir le grade de

Docteur de l'Université de Bourgogne
Discipline : Instrumentation et Informatique de l'Image

Thesis submitted in fulfillment of the requirements
for the degree of Doctor (PhD) in Applied Biological Sciences, Ghent University

Par

Sofija VULGARAKIS MINOV

06 Juillet 2015

Integration of imaging techniques for the quantitative characterization of pesticide sprays

Directeurs de thèse:
Michel PAINDAVOINE (Université de Bourgogne) & Jan G PIETERS (Ghent University)

Membre du Jury		
Marie-France Destain	Pr (Université de Liège)	Rapporteur
Christophe Ducottet	Pr (Université de Saint-Etienne)	Rapporteur
Paul Van Der Meeren	Pr (Université de Gand)	Examinateur
Jürgen Vangeyte	Dr. (ILVO)	Examinateur
Michel Paindavoine	Pr (Université de Bourgogne)	Directeur de Thése
Jan G Pieters	Pr (Université de Gand)	Directeur de Thése
Frédéric Cointault	MCF-HDR (AgroSup Dijon)	Co-encadrant de Thése
David Nuyttens	Dr. (ILVO)	Co-encadrant de Thése

Promotors: Prof. Dr. Jan G Pieters
Department of Biosystems Engineering, Ghent University

Prof. Dr. Michel Paindavoine
Learning and Development Laboratory (LEAD), University of Burgundy

Dean: Prof. Dr. ir. Guido Van Huylenbroeck

Rector: Prof. Dr. Anne de Paepe

Sofija Vulgarakis Minov

Integration of imaging techniques for the quantitative characterization of pesticide sprays

Thesis submitted in fulfillment of the requirements
for the degree of Doctor (PhD) in Applied Biological Sciences, Ghent University

Dutch translation of the title: Het gebruik van cameratechnieken voor de kwantitatieve karakterisatie van spuittoepassingen van gewasbeschermingsmiddelen

French translation of the title: Caractérisation quantitative de la pulvérisation de pesticides par imagerie

Cover picture:

Front - Spray angle image and differently sized droplets from TeeJet XR 110 04 nozzle

Vulgarakis Minov S. (2015). Integration of imaging techniques for the quantitative characterization of pesticide sprays. *PhD Thesis*. Ghent University, Belgium & University of Burgundy, France.

ISBN-number:

PREFACE

My journey towards this book has been an inspiring and challengeable personal experience. During the 4 years of research I have gained important knowledge and valuable skills. I prefer to believe that the sky is definitely not the limit. Without this foundation I probably would not have dared to start this work and cross boundaries in order to get where I am now.

However, passion alone with itself is not enough. The thesis has been supported by ILVO, the Region Burgundy and Nicéphore Cité. The PhD research was carried on in two institutes: ILVO, Merelbeke and AgroSup, Dijon. Therefore, while working, living and traveling between these two places, I have met many wonderful people. It is time to thank them.

Firstly, I would like to thank my supervisors: David and Frédéric**.**

David, thank you for accepting me to do this research into your group. It was you that believed that eventually something valuable would emerge from fuzzy words and images and guided me through the process of developing confidence as an academic. Your patience, flexibility and faith were more than valuable during the dissertation process. Working in two countries with different administration systems was more than difficult. I am thankful for your constant readiness to help.

Frédéric, thank you for the encouragement and unflagging support and advice.

Jürgen, although you were not really my supervisor, I appreciate your help, comments and guidance. Thank you for all the practical ideas.

Thank you to Prof. Pieters, for giving me a valuable guidance and a fast and constructive feedback. Besides, thanks to Prof. Paindavoine for supporting my research work.

I owe a debt of gratitude to Lieve Herman for accepting me to the Institute and supporting my research since the very beginning. Furthermore, I would like to thank you sincerely for the advices, help and tolerance for my personal life.

I would to like to acknowledge the jury members: Prof. Destain, Prof. Ducottet and Prof. Van Der Meeren for their fruitful comments and input to this work.

I also benefit a lot from the help of my colleagues, first the ILVO colleagues in Merelbeke then the AgroSup colleagues in Dijon. I want to thank to my Spray Tech colleagues from B27: Ingrid, Bert, Dieter and Donald for their participation in every occurred problem and for creating a nice Friday working environment. In particular, thanks to Donald for help with the spray measurements. Also, I appreciate all your effort you gave every time to repair my bike. Dieter, thanks for your emotional support and positive attitude since the beginning and I hope we go one more time to a Reggae festival. Ingrid, I deeply appreciate for your contribution to every text or presentation editing. Bert, thanks for being always open to talk or solve any problem. I hope you go to the Famelab final next year.

Furthermore, everyone in the T&V Unit, but especially: Veerle for the inspiration, conversations and emotional support. Stephanie, this work would have been much poorer without your help in statistics. Moreover, warm thanks to Sophie for the joyful train rides and comments on work-in-progress. I thank Gerlinde for the optimism and encouragement. In addition, thanks to Elsy for all the help with administrative tasks and optimistic talks. Nathalie, I wish you success with your thesis. Next, I would like to thank Luciano, Eva, Katrien, Johan, Philippe, Simon, Koen, Annelies, Raphael, and Jarissa with whom I spent a lot of lunch breaks and discussed everyday issues. Marie-José and Claudia, thanks for taking care of my desk to be proper and clean. I extend my special thanks to the T&V technicians.

Many thanks also to my AgroSup colleagues. More specifically, I want to thank Houda and Simeng who helped me with many necessary organization things while I was in Dijon (Merci!). Bastien: for your many inputs to my research and friendship.

While working in ILVO, I was partly living in Merelbeke. Here, I would like to thank Ruth and her mum Monique for all the PhD and non-PhD talks. Also, thanks for the nice atmosphere in the house.

I am enormously thankful to Azra and Osman. You were always there for me when I was far from home. I wish you many happy moments with baby Damir. Also, Milica and Backo, it is

hard to find words for all the support and help. I will remember all the beautiful trips spent together. Next trip will be with baby Daniel.

Thanks to my friends in Skopje for distant, but always present love and support: Bile, Kate, Dani, Sanja and Kristi.

Finally, I would like to thank my amazing family in law: teta Željka, cika Djordje and Biljana for their moral support, willingness to leave their obligations when necessary and completely dedicate to helping.

My sister Aneta, thanks for all the long Skype talks which helped me when I was far from home. In addition, to extent thank to my brother-in-law and my niece Emili.

Mamo and tato, thanks for all the unconditional support, love and believing in me through all the years. You were always proud of me.

And finally, my lovely husband Boris, without your support and encouragement, I could not have dared to begin and finish this work. I know that sometimes it was difficult taking care of two little boys. I can just say thanks cause you are sky full of stars. Beyond this, the happiest persons that this journey has come to an end are Filip and Stefan. Thanks for being good boys while I was away.

Sofija Vulgarakis Minov

July 2015, Utrecht, Netherlands

RESUME

CHAPITRE 1 INTRODUCTION ET CONTEXTE DE L'ETUDE

La protection des plantes est nécessaire pour prévenir des risques de pertes de rendement, dues à la présence de mauvaises herbes et de maladies (Rice *et al.*, 2007). Malheureusement, l'application de produits de protection des plantes (PPP) peut causer des pollutions de surface ou des eaux, aussi bien que des contaminations par des organismes nuisibles. Par conséquent, leur meilleure utilisation est un enjeu social, sanitaire et économique majeur, de plus en plus régulé par des lois environnementales internationales.

Ces PPP sont majoritairement appliqués par des solutions liquides utilisant différents types de pulvérisateurs équipés de buses hydrauliques. Ces buses atomisent le liquide pour produire un large spectre de tailles de gouttelettes (~ 10-1000 µm) et de vitesses (~ 0-25 m/s) (Nuyttens *et al.*, 2007a; 2009). Ces deux caractéristiques majeures influencent l'efficacité du jet projeté. En premier, les fines gouttelettes sont sujettes à des effets de dérive qui modifient la forme du jet et peuvent entrainer des pollutions environnementales (Nuyttens *et al.*, 2010). En second, les gouttes de taille importante ont une plus grande énergie cinétique qui augmente leur capacité à pénétrer la canopée mais aussi leur chance de rebondir ou d'éclater à l'impact sur le feuillage (Zwertvaegher *et al.*, 2014). Au-delà de ces deux caractéristiques, d'autres paramètres importants du jet influencent l'efficacité de l'application telles que : les directions de gouttes, la forme du volume de projection, la longueur de la nappe liquide et sa structure, la structure des gouttes individuelles et les dimensions 3D du jet (Miller & Ellis, 2000). Les caractéristiques du jet dépendent du type de buse, de leur taille, des propriétés du liquide projeté, de la pression utilisée pour pulvériser et des réglages du pulvérisateur (hauteur de la rampe par rapport à la végétation, vitesse d'avancement, …).

Ainsi, le challenge est de réduire les pertes de produits pendant le transport jusqu'au feuillage, de maximiser le dépôt de produit et de minimiser les pertes à l'impact en améliorant le processus de pulvérisation (Zabkiewicz, 2007); ceci en sélectionnant et utilisant les équipements adéquats et les meilleurs conditions de pulvérisation (matériel et produit) (Dorr *et al.*, 2007). Puisque les mécanismes de projection de gouttelettes quittant

une buse sont très complexes et délicats à quantifier ou modéliser, il est nécessaire de développer des techniques de quantification précises. Bien que certaines méthodes sont déjà disponibles pour la détermination de quelques caractéristiques des jets, aucune n'est cependant capable de caractériser en totalité le processus de pulvérisation. Par conséquent, l'ajustement des pulvérisateurs est toujours basé sur des expériences pratiques et des tests d'affinement, puisque prendre en considération toutes les combinaisons possibles est impossible. L'utilisation de modèles pourrait augmenter la connaissance des procédés de transport des gouttelettes et les effets des réglages du pulvérisateur et des conditions environnementales. La validation de ces modèles est cependant difficile et ne peut pas être réalisée avec des techniques de mesures traditionnelles, comme la mesure de la distribution du jet ou la mesure de la vitesse de l'air. Par conséquent, la disponibilité de systèmes non intrusifs est d'une grande importance.

Des techniques optiques quantitatives mais en fournissant pas d'images sont disponibles mais sont complexes, chères et dans la plupart des cas limitées à la mesure de petits volumes. Ces limitations concomittentes avec les récents développements des traitements d'images (augmentation de la sensibilité des systèmes et coût réduit) ont accru l'intérêt porté aux techniques d'imagerie rapide pour les applications agricoles et plus particulièrement pour la fertilisation (Vangeyte, 2013; Cool *et al.*, 2014) ou la pulvérisation. La petite taille des gouttes et leur vitesse élevée sont deux challenges intéressants à relever pour la caractérisation d'un jet. Ces caractéristiques microscopiques aussi bien que celles macroscopiques (jet réel) influencent l'efficacité du jet projeté. Ainsi, obtenir des informations plus précises sur ces paramètres peut permettre d'atteindre un usage de pesticides plus efficace. L'objectif général de ce projet de recherche est ainsi de développer des systèmes d'imagerie performants (acquisition et traitement) pour la visualisation et la détermination des caractéristiques des gouttelettes de produits phytosanitaires. Pour atteindre cet objectif, plusieurs sous-objectifs sont pointés correspondant chacun à un chapitre différent de la thèse.

CHAPITRE 2 ETUDE BIBLIOGRAPHIQUE SUR LES PROCESSUS DE PULVERISATION, LES TECHNIQUES D'APPLICATION EXISTANTES ET LES METHODES DE MESURE POUR LA CARACTERISATION DES JETS

Plutôt que d'utiliser des pesticides chimiques ou de synthèse, la gestion des infestations utilise une large gamme de méthodes de prévention et de contrôle. Cette thèse s'intéresse aux techniques d'application de jets de produits qui sont les plus utilisées pour appliquer des pesticides. Le processus de pulvérisation consiste en plusieurs sous-processus formant une chaîne de pulvérisation globale (Matthews, 2000). Chaque partie de la chaine peut influer sur l'efficacité du jet projeté: cuve, régimes de fonctionnement et d'atomisation (Figure 1), transport jusqu'à la cible et impact sur la cible (feuillage).

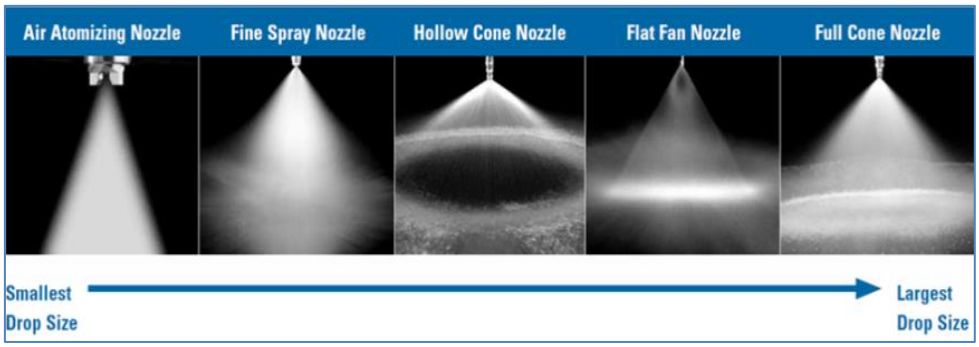

Figure 1. Les différentes formes de jets en fonction des buses utilisées (Schick, 1997)

Ce travail de thèse se focalisera donc sur deux phases essentielles de la pulvérisation : la formation des gouttes et l'atomisation et transport vers la cible. Les techniques d'acquisition d'images développées peuvent aussi être utilisées pour étudier l'impact des gouttes sur le feuillage et la rétention comme indiqué par Zwertvaegher *et al*. (2014). Pour notre étude, 3 sortes de buses ont été testées : buses à cône creux, buse à jet plat et buse à jet plat et inclusion d'air, qui sont les plus utilisées en arboriculture et viticulture.

La distribution du jet et le dépôt ont été utilisés pour évaluer les performances des buses pour des applications agricoles. Ces caractéristiques sont traditionnellement mesurées avec des techniques intrusives appelées méthodes d'échantillonnage qui peuvent affecter le comportement du jet (Rhodes, 2008). Ces nombreuses méthodes sont divisées en trois catégories: *méthodes mécaniques, électriques et optiques*.

Les *méthodes mécaniques* impliquent la collection d'échantillons de jet sur une surface solide ou sur une cellule contenant un liquide spécifique. Les *méthodes électriques* mesure la distribution des tailles de gouttes via la détection et l'analyse de pulses électroniques produits par les jets. Des informations sur cette technique peuvent être trouvées chez Gardiner (1964). Ceci étant, les méthodes les plus connues sont les techniques optiques qui sont divisées en plusieurs catégories : les systèmes de diffusion de lumière (Phase Doppler Particle Analyzers (PDPA) (Nuyttens *et al.*, 2007a; 2009), les analyseurs de diffraction laser (Malvern Analyzer (Stainier *et al.*, 2006)) et les sondes optiques (Teske *et al.*, 2002), et les méthodes d'imagerie rapide (caméra rapide avec une lumière à haut éclairage (Kim *et al.*, 2011) ou caméra standard et système stroboscopique associé (Cointault *et al.*, 2002; Kuang-Chao *et al.*, 2008; Hijazi *et al.*, 2010; Li *et al.*, 2010; Vangeyte, 2013).

Ces techniques peuvent fournir des informations additionnelles sur les trajectoires des gouttelettes, ce qui est nécessaire pour les travaux sur l'impact des gouttes. Cependant, les mécanismes d'atomisation, d'éjection et d'impact des gouttelettes sont très complexes et délicats à quantifier ou modéliser. Aucune méthode n'offre donc la possibilité de caractériser totalement le processus d'application de jets de pesticides. Néanmoins, les techniques d'imagerie sont non intrusives et ont prouvé leur efficacité pour de nombreuses applications. C'est pourquoi le développement d'outils spécifiques de caractérisation des gouttelettes et des jets est le premier axe de travail de cette thèse.

CHAPITRE 3 DEVELOPPEMENT DE SYSTEMES D'ACQUISITION D'IMAGES RAPIDES BASES SUR DES EXPERIMENTATIONS POUR DES GOUTTELETTES UNIQUES

Les caractéristiques des jets de pesticides générés par des buses agricoles jouent un rôle important dans la précision et l'efficacité des produits de protection des plantes, dans le domaine de l'agriculture de précision (Stafford, 2000).

La faible précision et les pertes des produits réduisent l'efficacité de leur application et augmentent la contimation à l'environnement et les risques pour l'opérateur. Le challenge à relever est de réduire les pertes pendant le transport vers la cible et de maximiser le dépôt de produits et donc le processus de pulvérisation (Zabkiewicz, 2007). Les caractéristiques les

plus importantes d'un jet de produit phytosanitaire influençant le processus de pulvérisation sont la taille et la vitesse des gouttelettes, la forme de la distribution du jet, la longueur de la nappe liquide et son épaisseur, la structure des gouttes seules et les dimensions 3D du jet (Miller & Ellis, 2000; Nuyttens *et al.*, 2009).

L'objectif de ce chapitre a été de développer deux systèmes d'acquisition d'images basés sur des images de gouttelettes uniques obtenues par un générateur de gouttelettes piézoélectriques dans son fonctionnement en mode « goutte à la demande » (Switzer, 1991; Yang *et al.*, 1997; Lee, 2003). Différents réglages de caméra rapide, différentes illuminations, différents diffuseurs et lentilles ont été testés en utilisant l'imagerie d'ombroscopie (pour le fond) (Lecuona *et al.*, 2000; Castanet *et al.*, 2013). Les évaluations de l'impact de ces paramètres ont été effectuées en mesurant trois paramètres de qualité d'une image (entropie, contraste et SNR), la stabilité de l'illumination et le rapport de sur-exposition, et la précision (de l'ordre de 1/2 pixel). Ces systèmes d'imagerie ont été utilisés pour caractériser les caractéristiques d'une goutte seule (chapitre 5) à partir d'algorithmes de traitement d'images (chapitre 4). De la même manière, ils ont permis de mesurer les caractéristiques d'un micro-jet (taille et vitesse des gouttes) (chapitre 6) et d'un jet réel (angle de jet, longueur de la nappe liquide, trajectoire) (chapitre 7).

Le développement et la conception des systèmes d'imagerie rapide ont été effectués en utilisant des gouttelettes contrôlées au niveau de leur taille dans le mode « goutte à la demande ». Pour cela, un générateur de gouttelettes (Université de Liége, Gembloux, Agro-Bio-Tech, Belgium) (Figure 2) a été utilisé dans cette étude. Il est composé d'une chambre d'alimentation en liquide avec un élément piézoélectrique qui peut être piloté avec des tensions jusqu'à 60V. Ce générateur est capable de produire des gouttelettes selon deux modes: «goutte à la demande » et mode continu (Rayleigh Breakup), qui sont détaillés plus finement dans le chapitre 5.

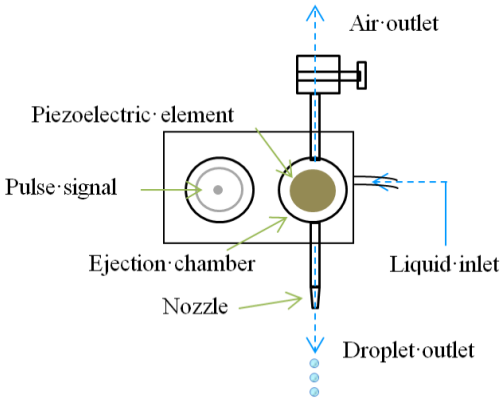

Figure 2. Schématisation globale du générateur de gouttelettes

En se basant sur les paramètres de qualité d'une image, 4 réglages pour l'acquisition des images ont été sélectionnés. Leur stabilité lumineuse et le rapport de sur-exposition ont été établis en comparant les histogrammes de valeurs d'intensité de pixels de 10 ROI (Region Of Interest) consécutives prises avec les mêmes réglages sans la présence d'une gouttelette.

L'analyse des images combine des techniques et des mesures basées sur les intensités de niveaux de gris des pixels des images qui ont été utilisées pour déterminer les caractéristiques des images obtenues pour les différents réglages envisagés. A partir des histogrammes, différentes propriétés statistiques du 1er ordre (Materka & Strzelecki, 1998) des images prises avec et sans gouttelettes ont été déterminées et utilisées pour comparaison des différents réglages des systèmes d'imagerie: la moyenne des niveaux de gris ou moyenne, le contraste moyen ou écart-type, et l'entropie (Haralick *et al.*, 1973; Gonzalez *et al.*, 2004).

Les expérimentations mises en oeuvre permettent de conclure quant à la bonne qualité des systèmes d'acquisition pour mesurer les éléments suivants :

- Caractéristiques d'un micro-jet (taille et vitesse des gouttelettes). Le système conçu consiste en une caméra rapide fonctionnant avec un temps d'exposition idéal de 6 µs, munie d'une lentille microscopique à une distance de travail de 430 mm (champ de vue de 10.5 mm x 8.4 mm), et d'une source lumineuse à Xénon utilisée en éclairage backlight sans diffuseur.

- Caractéristiques d'un macro-jet (jet réel) (angle du jet, forme …). Le système conçu consiste en une caméra rapide fonctionnant avec un temps d'exposition de 15 µs, munie

d'une lentille macro à zoom à une distance de travail de 143 mm (champ de vue de 88 mm X 110 mm), et d'une source lumineuse combinant un spot halogène et un diffuseur.

Les sytèmes d'imagerie mis en place peuvent également être utilisés pour visualiser et déterminer les caractéristiques d'un micro-jet et d'un macro-jet de pulvérisation selon des techniques non invasives. En outre, ils offrent la possibilité d'étudier les gouttes et le comportement du jet à l'impact comme indiqué par Zwertvaegher et al. (2014).

CHAPITRE 4 DEVELOPPEMENT DES ALGORITHMES D'ANALYSE ET DE TRAITEMENT DES IMAGES POUR LA CARACTERISATION D'UNE SEULE GOUTTELETTE

Le suivi et l'évaluation des tailles des gouttelettes en mode continu et mode "goutte à la demande" sont déterminés en se basant sur un algorithme de suivi d'objets (Jain & Nagel, 1979; Baek & Lee, 1996; Lecuona *et al.*, 2000; Maggio & Cavallaro, 2011; Castanet *et al.*, 2013) développés sous Matlab (2011b). Une fois que les images ont été acquises par la caméra rapide, une séquence d'étapes de pré-traitement et traitement pour l'analyse d'images été mise en place comme décrit dans la Figure 3.

Figure 3. Flow chart de l'algorithme d'analyse des images pour la caractérisation des gouttelettes

La Figure 4 fournit un exemple d'image obtenue par le système (a) ainsi que le résultat du pré-traitement (b), pour le mode «goutte à la demande».

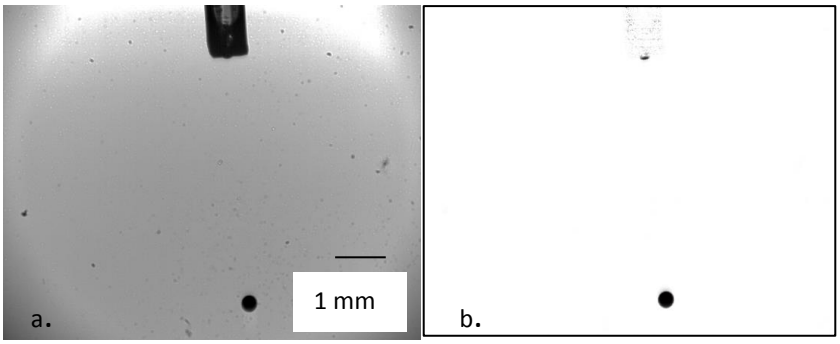

Figure 4. Image originale (a) et résultat après pré-traitement (b) pour le mode «goutte à la demande»

Les algorithmes de segmentation peuvent être classés selon deux catégories principales : seuillage et détection de contours (Gonzalez *et al.*, 2004). Une technique de segmentation basée sur le seuillage par histogramme a été utilisée pour notre projet afin de discriminer les gouttelettes du fond (chapitre 5). La seconde catégorie d'algorithmes de segmentation qui recherche les changements nets de contours a été utilisée pour la définition d'un critère de focalisation optique (chapitre 6).

Lorsque les gouttes sont extraites du fond, différentes opérations de morphologie mathématique comme la dilatation, l'érosion, l'ouverture et la fermeture ont été envisagées pour caractériser les gouttes. L'élément structurant choisit est un disque faisant écho à la sphéricité suposée des gouttelettes. Pour notre objectif, une fermeture a été utilisée: dilatation suivie par une érosion. Ceci permet de lisser les contours des objets, d'associer ensemble les coupures de contours et de remplir les zones dont la taille est inférieure à celle de l'élément structurant. Ensuite une labellisation des gouttelettes est réalisée. Finalement, l'extraction de région est effectuée en mesurant les propriétés des objets labellisés comme le diamètre, l'aire, le périmètre, l'orientation (Figure 5).

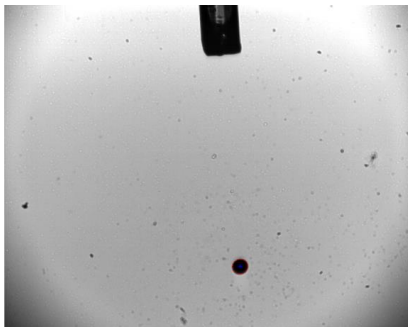

Figure 5. Résultat de l'extraction de région pour le mode "goutte à la demande" (le centre de la goutte est marqué d'une étoile bleue et les contours sont en rouge)

Dès que le centre et la localisation des gouttes sont déterminés, le tracking de ces gouttes est réalisé en recherchant la même goutte sur deux images successives ainsi que le vecteur déplacement et la vitesse. Cela est possible grâce à la large gamme de fréquences d'acquisition de la caméra rapide. Le tracking d'une goutte dans l'image *I* est étendu dans l'image suivante *J*. Chaque suivi entre deux images peut générer plusieurs résultats. La vitesse d'une goutte est calculé avec l'équation (1) (Lecuona *et al.*, 2000):

$$\vec{v}_{ij} = \frac{\vec{d}_{ij}}{\Delta t} = \frac{(X_j - X_i, Y_j - Y_i)}{\Delta t} \quad (1)$$

où $\vec{d}_{ij}$ et $\vec{v}_{ij}$ sont le vecteur déplacement et la vitesse respectivement.

La vitesse d'une goutte est calculée comme le déplacement divisé par le temps entre deux expositions (fpour le mode «goutte à la demande»: 1 image = 1 ms et pour le mode continu: 1 image = 0.1 ms). Un des résultats est fournit sur la Figure 6.

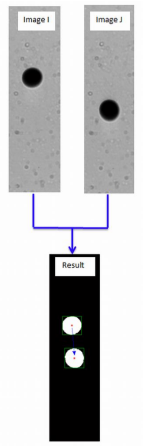

Figure 6. Tracking des gouttelettes en mode "goutte à la demande"

CHAPITRE 5 GENERATION ET CARACTERISATION DE GOUTTELETTES UNIQUES A PARTIR DE TECHNIQUES D'IMAGERIE ET D'UN GENERATEUR DE GOUTTELETTES PIEZOELECTRIQUES SELON DEUX MODES : GOUTTELETTES A LA DEMANDE ET MODE CONTINU

Les différentes mesures ont été effectuées grâce à l'utilisation d'un générateur de gouttelettes fonctionnant selon deux modes: gouttelettes à la demande ou mode continu. Les effets des paramètres de fonctionnement du générateur, incluant la largeur de pulse et son amplitude avec 4 tailles d'orifice de buses (261 µm, 123 µm, 87 µm and 67 µm) sur le diamètre des gouttes et leur vitesse ont été caractérisés. Les tailles et vitesses des gouttelettes ont mesurées avec succès par le système d'imagerie et les traitements développés dans les chapitres 3 et 4.

Le calcul de la taille des gouttelettes et leur tracking ont été réalisés en 3 étapes: 1) Détection du mouvement des gouttes en utilisant une technique de détection de contours basée sur un changement local de luminance dans l'image (Lecuona *et al.*, 2000); 2) Tracking des gouttelettes entre deux images successives et 3) Mesure des caractéristiques des gouttelettes (taille, vitesse, espacement entre gouttelettes (en mode continu)). La vitesse d'une goutte est calculée en mesurant sa position entre deux images successives, connaissant le délai entre deux images, grâce au système d'acquisition mis en œuvre. Une description détaillée des techniques d'analyse d'images est fournie au chapitre 4.

<u>Plusieurs conclusions ont été obtenues à partir des travaux de ce chapitre</u> :

- Les expérimentations en mode continu ont montré que les caractéristiques initiales des gouttelettes issues du générateur sont une fonction double de la largeur du pulse et de la taille de l'orifice. Les valeurs de largeur du pulse sont des paramètres critiques pour l'éjection des gouttes. En changeant la largeur, il est ainsi possible de contrôler la vitesse des gouttes et la taille de leur diamètre. En général, diminuer la valeur de t_a et augmenter celle de t_p induit une augmentation du diamètre de la goutte. De manière identique, si la taille de l'orifice d'une buse augmente, le diamètre de la goutte également.

- Avec le mode “goutte à la demande”, les tailles des gouttelettes se situent dans l’intervalle 134.1 µm et 461.5 µm. Principalement, les plus petites et plus grandes gouttelettes ont été mesurées avec l’orifice de buse le plus petit. Les vitesses mesurées se situent entre 0.08 m/s et 1.78 m/s. En outre, nous avons noté un effet de l’amplitude du pulse sur la vitesse et le diamètre de la goutte. En mode continu, la plus petite vitesse de 1.84 m/s a été mesurée avec l’orifice de buse le plus petit tandis que la vitesse la plus élevée (4.66 m/s) l’a été avec l’orifice le plus grand. Dans ce dernier mode, les vitesses obtenues se rapprochent des valeurs utilisées pour des pulvérisations réelles.
- Le rapport entre le diamètre d’une goutte et l’orifice d’une buse en mode “goutte à la demande” est inscrit dans l’intervalle 1.3 à 3.9.
- Le mode continu pour chaque buse a été établit pour une fréquence résultant en une génération continue de gouttelettes. Cette fréquence combinée avec des amplitudes de pulse différentes ont été utilisées pour tester l’impact sur le diamètre des gouttes, l’espacement inter-gouttes et la vitesse. En se basant sur les résultats des expérimentations l’effet de l’amplitude du pulse sur l’espacement inter-goutte est statistiquement significatif. En outre, il existe une relation globalement linéaire entre le diamètre des gouttes et la vitesse, pour le mode continu.

CHAPITRE 6 DEVELOPPEMENT D’ALGORITHMES DE TRAITEMENT DES IMAGES POUR LA CARACTERISATION DE MICRO-JETS ET COMPARAISON DES RESULTATS OBTENUS AVEC LES RESULTATS DU SYSTEME PDPA

La distribution des vitesses et tailles des gouttelettes est un paramètre important des jets de pulvérisation. L’objectif de ce chapitre est de mesurer les caractéristiques d’un micro-jet (taille et vitesse des gouttelettes) de différentes buses hydrauliques (Albuz ATR orange et rouge, TeeJet XR 110 01, XR 110 04 and Al 110 04) en utilisant le système d’acquisition d’images développés dans le chapitre 3 (Figure 7), et les méthodes de traitement d’images développées dans les chapitres 4 et 5.

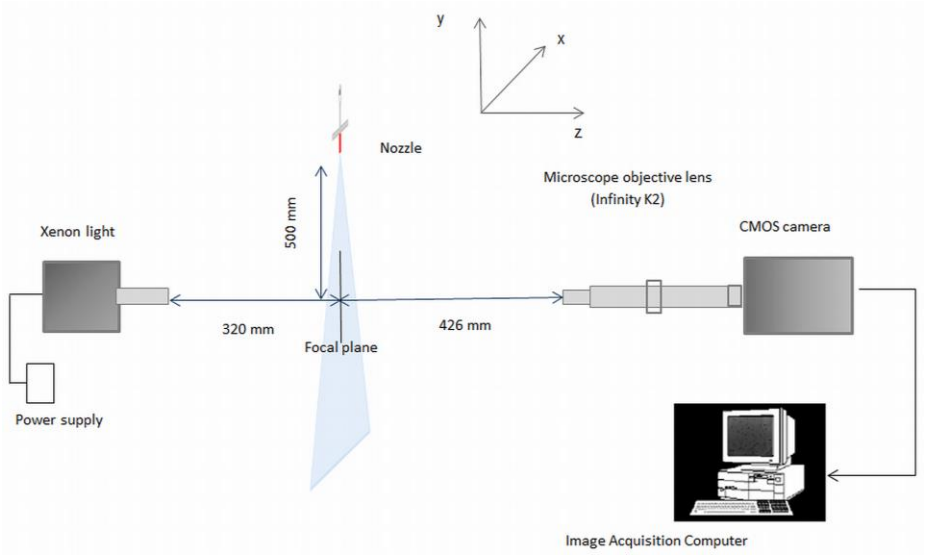

Figure 7 Système d'acquisition des images pour la caractérisation d'un jet de gouttelettes

Dans une première partie, un critère de focalisation optique des gouttelettes est présenté, basé sur le gradient de niveaux de gris, pour décider quelles sont les gouttelettes dans et en dehors du plan focal. L'analyse des images pour caractériser ce critère comporte 3 étapes (Figure 8): pré-traitement par soustraction du fond, segmentation d'image et détection de contour, calcul du paramètre de focalisation optique et du critère.

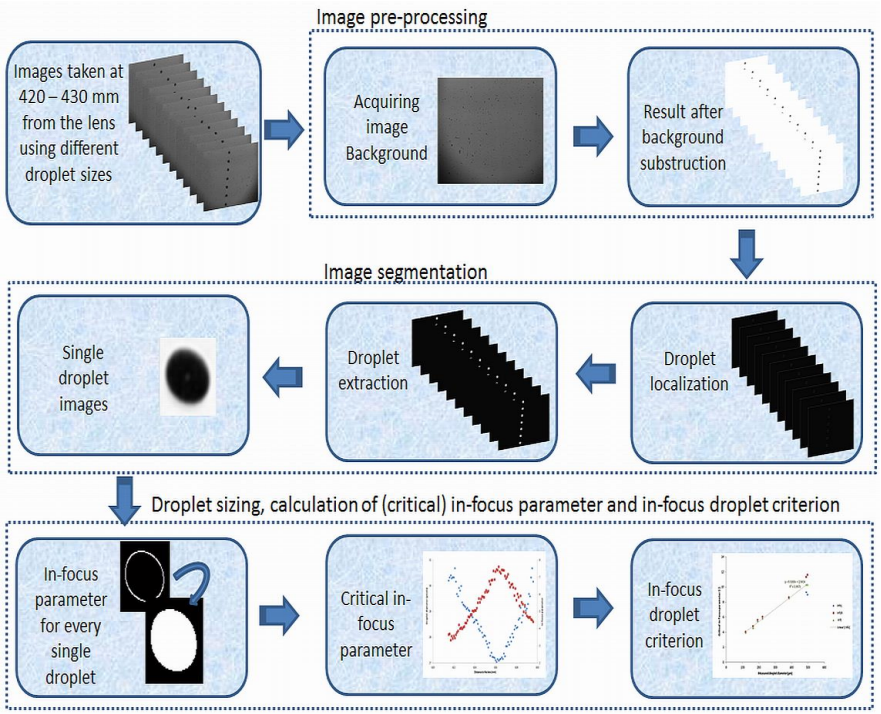

Figure 8 Flow chart de l'algorithme d'analyse des images pour l'établissement du critère de focalisation optique des gouttelettes

A partir du processus de traitement des images précèdent, un paramètre critique de focalisation (Inf_c) a été établit pour chaque taille de goutte et un critère de focalisation optique a été déduit afin de définir si une goutte est dans le plan focal ou pas. La zone de focalisation des gouttes est définie comme la zone dans laquelle une gouttelette avec un certain diamètre est dans le plan focal.

Dans une seconde partie, le critère de focalisation optique a été appliqué à différentes images de jets pour les 5 buses testées, et les caractéristiques des gouttelettes ont ensuite été déterminées. Les effets des types de buses et des tailles de buses sur la taille du jet et la vitesse des gouttelettes ont été étudiés. Les résultats ont été comparés avec le système laser PDPA (Nuyttens et al., 2007a).

Les principaux résultats de ce chapitre sont les suivants :

- Un critère de focalisation basé sur le gradient de niveaux de gris a été mis en place pour déterminer les gouttelettes qui sont dans le plan focal. Différentes tailles de gouttelettes ont été générées grâce à un générateur de gouttelettes piézoélectriques et des buses en verre en mode continu à différentes distances du plan focal en utilisant un système de micro-translation. Ceci a permis la mesure d'un gradient de niveaux de gris et d'un paramètre de focalisation optique pour chaque gouttelette. A partir de là, un paramètre de focalisation critique (Inf_c) a été établit pour chaque goutte et un critère de focalisation des gouttes en a été déduit. La zone de focalisation des gouttelettes est ensuite définie comme la zone dans laquelle une goutte avec un certain diamètre est dans le plan focal.
- Le critère définit a été appliqué aux images de jets de pulvérisation pour différentes buses hydrauliques et les caractéristiques des gouttelettes ont été calculées. Les effets du type de buse et de leur diamètre sur ces caractéristiques ont par ailleurs été étudiés.
- Les résultats sur les taille et vitesse des gouttelettes obtenus grâce au traitement des images ont montré qu'il était possible de mesurer les caractéristiques d'un jet avec un système non invasif à partir de techniques d'imagerie.
- Ces résultats ont été comparés avec ceux obtenus par la technique du PDPA laser considérée comme la référence.

CHAPITRE 7 DEVELOPPEMENT D'ALGORITHMES DE TRAITEMENT D'IMAGES POUR LA CARACTERISATION DE MACRO-JETS ET COMPARAISON DES RESULTATS AVEC CEUX OBTENUS VIA LE SYSTEME «PATTERNATOR» DE L'INSTITUT ILVO

Les jets de pesticides sont appliqués avec différents types de buses, chacune possédant ses propres caractéristiques. L'objectif de ce chapitre 7 est de mesurer les caractéristiques d'un jet global (angle de pulvérisation, longueur de la nappe liquide, forme du jet et volume de pesticides projeté) provenant de différents types de buses hydrauliques en utilisant le système d'imagerie développé dans le chapitre 3 et des traitements d'images spécifiques. Les tests inclus 5 buses différentes communément utilisées (Albuz ATR orange et rouge, TeeJet XR 110 01, XR 110 04 et Al 110 04), avec différents angles de projection et tailles. A partir des images de jet, les caractéristiques macroscopiques obtenues sont comparées à des résultats obtenus grâce au dispositif «patternator» disponibles à l'institut ILVO, en Belgique.

Les principaux résultats obtenus sont les suivants:

- Les angles des jets des combinaisons buse/pression à la sortie de l'orifice (0 cm) ont été mesurés par imagerie. Les valeurs obtenues sont plus grandes que l'angle nominal des jets, excepté pour la buse XR 110 01. Pour les buses à cône creux et à inclusion d'air, l'analyse d'images fournie une très bonne représentation des angles des jets même si les angles sont surestimés pour les deux buses standard à jet plat.
- A partir des mesures effectuées avec le système "patternator" à trois hauteurs différentes (15cm, 30 cm et 50 cm), les angles des jets actuels diminuent avec la hauteur de positionnement des buses du fait de la gravité. Cet effet est bien plus prononcé pour les jets les plus fins.
- La plus petite nappe liquide a été calculée pour la buse XR 110 01 (18.5 mm), suivie des deux buses à cône creux (27.4 et 31.3 mm). La plus longue nappe a été obtenue pour les buses XR 110 04 (38.9 mm) et AI 110 04 (43.1 mm).
- Concernant la forme du jet, les largeurs des distributions des gouttelettes à 4 hauteurs (5, 10, 15, 20 cm) pour toutes les buses et pour les angles correspondant ont été calculées et comparées aux résultats obtenus par le système «patternator». En général, le volume de gouttelettes le plus grand a été trouvé directement sous la buse et

diminue de chaque côté de la buse. En complément, plus la buse est haute, plus les pics de distribution du jet sont lissés compares à ceux obtenus à une hauteur de 15 cm. A cause de la gravité, la forme du jet est parabolique et l'angle du jet décroît généralement quand la hauteur de positionnement de la buse augmente.

La comparaison des résultats d'analyse d'images et du « patternator » a été effectuée à une hauteur de 15 cm. L'erreur relative sur l'angle du jet pour la buse XR 110 01 était de 0.5 %, et de 0.6% pour les buses XR 110 01 et AI 110 04. L'erreur sur l'angle du jet était plus grande pour la buse à cône creux, les buses ATR orange et rouge, avec 2.8% et 5.4% respectivement.

CHAPITRE 8 CONCLUSION

Dans les 50 dernières années, les avancées dans le domaine de la protection des plantes ont contribué à augmenter les rendements et à assurer une large production. Facile à utiliser et plutôt bon marché à l'époque, les pesticides ont prouvé leur efficacité. Cependant, quand ils sont appliqués aux cultures, une partie du produit n'atteint pas sa cible et est perdu dans l'air ou au sol. Par conséquent, des efforts ont été consentis pour améliorer leur efficacité et leur innocuité sanitaire, souvent grâce à des lois environnementales internationales.

Les produits sont appliqués à partir de matériels combinant type de buse/pression induisant des gammes de vitesses et de tailles de gouttelettes très diverses (Chapitre 2). Une mesure simultanée de ces vitesses et tailles est ainsi d'une grande importance dans le processus de pulvérisation. Il existe de nombreuses méthodes pour la mesure des caractéristiques des gouttelettes qui peuvent être divisées en trois catégories: *mécaniques, électriques et optiques*. Ces dernières apparaissent comme les plus pertinentes puisqu'étant non invasives et en perturbant donc pas le processus de pulvérisation.

Les améliorations récentes dans le domaine du traitement des images et la réduction du coût des systèmes d'imagerie ont ainsi accru l'intérêt des techniques d'imagerie rapide pour les applications agricoles telles que la pulvérisation de pesticides.

Cette thèse s'est donc focalisée sur le développement d'une telle technique pour la caractérisation des sprays (micro et macro). Les travaux effectués ont permis de démontrer que les caractéristiques d'un jet de pesticides peuvent être correctement et précisément

mesurées par des techniques d'imagerie non-invasives couplées à des traitements spécifiques.

Les travaux à venir consisteraient notamment en l'amélioration de la précision des mesures effectuées: précision sub-pixellique, calcul des profondeurs de champ, mesure de particules non sphériques.

Mots-clés: *Générateur de gouttelettes, imagerie rapide, traitment d'image, angle de pulvérisation, caractérisation gouttelette, buses hydrauliques*

SUMMARY

In recent years, advances in plant protection have contributed considerably to increasing crop yields in a sustainable way. Easy to apply and rather inexpensive, pesticides have proven to be very efficient. However, when pesticides are applied to crops some of the spray may not reach the target, but move outside the intended spray area. This can cause serious economic and environmental problems.

Most of the pesticides are applied using agricultural sprayers. These sprayers use hydraulic nozzles which break the liquid into droplets with a wide range of droplet sizes and velocities and determine the spray pattern. Small droplets are prone to wind drift, while large droplets can runoff from the target surface and deposit on the soil. Therefore, efforts are being undertaken to come to a more sustainable use of pesticides which is more and more regulated by international environmental laws. One of the main challenges is to reduce spray losses and maximize spray deposition and efficacy by improving the spray characteristics and the spray application process. Because mechanisms of droplets leaving a hydraulic spray nozzle are very complex and difficult to quantify or model, there is a need for accurate quantification techniques.

The recent improvements in digital image processing, sensitivity of imaging systems and cost reduction have increased the interest in high-speed (HS) imaging techniques for agricultural applications in general and for pesticide applications in specific.

This thesis focused on the development and application of high speed imaging techniques to measure micro (droplet size and velocity) and macro (spray angle and shape, liquid sheet length) spray characteristics.The general aim was to show that the spray characteristics from agricultural spray nozzles can be measured correctly with the developed imaging techniques in a non-intrusive way.

After a review of the spray application process and techniques for spray characterization (Chapter 2), two image acquisition systems were developed in Chapter 3 based on single droplet experiments using a high speed camera and a piezoelectric droplet generator. 58

combinations of lenses, light sources, diffusers, and exposure times were tested using shadowgraph (background) imaging and evaluated based on image quality parameters (signal to noise rate, entropy ratio and contrast ratio), light stability and overexposure ratio and the accuracy of the droplet size measurement. These resulted into development of two image acquisition systems for measuring the macro and micro spray characteristics. The HS camera with a macro video zoom lens at a working distance of 143 mm with a larger field of view (FOV) of 88 mm x 110 mm in combination with a halogen spotlight and a diffuser was selected for measuring the macro spray characteristics (spray angle, spray shape and liquid sheet length). The optimal set-up for measuring micro spray characteristics (droplet size and velocity) consisted of a high speed camera with a 6 µs exposure time, a microscope lens at a working distance of 430 mm resulting in a FOV of 10.5 mm x 8.4 mm, and a xenon light source used as a backlight without diffuser.

In Chapter 4 image analysis and processing algorithms were developed for measuring single droplet characteristics (size and velocity) and different approaches for image segmentation were presented.

With the set-up for micro spray characterization and using these dedicated image analysis algorithms (Chapter 4), measurements using a single droplet generator in droplet on demand (DOD) and continuous mode were performed in Chapter 5. The effects of the operating parameters, including voltage pulse width and pulse amplitude with 4 nozzle orifice sizes (261 µm, 123 µm, 87 µm and 67 µm) on droplet diameter and droplet velocity have been characterized. The experiments in DOD mode have shown that the initial droplet characteristics from the droplet generator are a function of the double pulse width (absorption time (t_a) and pulsation time (t_p)) and the orifice size. By changing pulse width, it was possible to control droplet velocity and size. In general, decrease of t_a and increase of t_p increased the droplet diameter. Similarly, increasing the nozzle orifice size increased the droplet diameter. With the DOD mode, droplet sizes ranged between 134.1 µm and 461.5 µm. Foremost, the smallest and the fastest droplets were measured with the smallest nozzle orifice. The measured droplet velocities ranged between 0.08 m/s and 1.78 m/s. Besides, an effect of the pulse amplitude on the droplet diameter and velocity was noticed. The ratio of the droplet diameter and nozzle orifice in DOD mode ranged from 1.3 to 3.5. The continuous mode for every nozzle was established for a high frequency (kHz) resulting in a continuous

droplet generation. This frequency together with different pulse amplitudes were used to test the effect on the droplet diameter, inter-droplet spacing and velocity. As for the DOD mode, the droplet diameter was mainly controlled by the nozzle orifice. The droplet size here was between 167.2 µm and 455.8 µm. Furthermore, the nozzle orifice also influenced the droplet velocity i.e., the bigger the nozzle orifice was, the higher the droplet velocity. Obviously, there was a linear trend between the droplet diameter and velocity in continuous mode. The ratios between the droplet diameter and the nozzle orifice ranged from 1.3 to 3.9. In continuous mode, the lowest droplet velocity of 1.84 m/s was measured with the smallest nozzle orifice size while the highest droplet velocity of 4.66 m/s was measured with the biggest nozzle orifice size. Based on the results in both modes, similar droplet sizes were produced in both modes but in continuous mode it was possible to achieve faster droplets which correspond better with real spray application.

In Chapter 6, the image acquisition technique for measuring micro spray characteristics was used for measuring the droplet size and velocity characteristics of agricultural hydraulic spray nozzles. This included the development of an in-focus droplet criterion based on the gray level gradient to decide whether a droplet is in focus or not. Differently sized droplets generated with a piezoelectric generator and glass nozzles in continuous mode at different distances from the focal plane and lens using a micro translation stage were measured. This enabled measurement of the gray level gradient and in-focus parameter for every droplet size at different positions. From here, a critical in-focus parameter (Inf_c) was established for every droplet size and an in-focus droplet criterion was deduced to decide whether a droplet is in focus or not depending on its diameter and in-focus parameter. In this study the focused droplet zone (FDZ) was defined as the zone in which a droplet with a certain diameter is in focus and a linear relation between droplet size and FDZ was found.

The developed in-focus droplet criterion was applied to spray images of five nozzles taken at different positions: two standard flat fan nozzles (XR 110 01 & 04 at 400 kPa), an air inclusion nozzle (AI 110 04 at 400 kPa) and two hollow cone nozzles (ATR orange at 600 kPa and red at 800 kPa). The effects of nozzle type, nozzle size and measuring position on droplet size and velocity characteristics were studied.

The droplet size and velocity results from the imaging technique have shown that it is possible to measure the spray characteristics in a nonintrusive way using an image acquisition set-up and image processing. Measured droplet sizes ranged from 24 µm to 543 µm depending on the nozzle type and size. Droplet velocities at 0.5 m below the nozzle ranged from 0.5 m/s up to 12 m/s. Spray droplet size characteristics such as $D_{V0.1}$, $D_{V0.5}$, $D_{V0.9}$ and RSF as well as spray velocity characteristics such as V_{Vol10}, V_{Vol50}, V_{Vol90} and VSF, were extracted from the images. Similar effects of nozzle type and measuring position on droplet sizes as well as on droplet velocities were found with the imaging technique as with the *Phase Doppler Particle Analyzer* (PDPA) laser technique. The developed imaging technique can be seen as an alternative to the well-established PDPA laser technique. The droplet diameter and velocity characteristics showed a relatively good comparison with the results measured with the PDPA laser. When compared with the PDPA laser, the imaging technique generally measured less small droplets and in some cases also less big droplets. Differences between both techniques can be attributed to the fact that the smallest measured droplet size with the imaging system is 24 µm while smaller droplets are measured with the PDPA. In addition, the number of droplets measured with the imaging technique was much smaller compared with the PDPA which increases the chance to miss one of the biggest droplets. This can be improved by taking more images. Differences in droplet velocity characteristics between both techniques can be attributed to the fact that the PDPA laser is only measuring droplet velocity in one dimension and hence underestimates the actual droplet velocity. In addition, the imaging technique applied did not allow the measurement of droplets faster than about 12 m/s based on FOV and the acquisition rate while some droplets with higher speeds were observed with the PDPA mainly for the XR 110 04. In future, the imaging system can be further improved to be able to measure at a higher frame rate with the same accuracy.

In Chapter 7, the image acquisition system for macro spray characterization was used to measure the spray angle, spray shape and liquid sheet length of the same nozzle-pressures combinations as mentioned above. Where possible, the results were compared with the existing non-imaging measuring techniques like a horizontal patternator. The measured spray angles were higher than the nominal spray angle except for the XR 110 01 nozzle. For the hollow cone (ATR orange and red) and air inclusion nozzle (AI 110 04), the imaging

technique gave a good comparison of the spray angle while the spray angle was underestimated for both standard flat fan nozzles (XR 110 01 & 04). The shortest liquid sheet was found for the XR 110 01 nozzle (18.5 mm), followed by the two hollow cone nozzles (27.4 and 31.3 mm). The longest liquid sheets were found for the XR 110 04 (38.9 mm) and AI 110 04 (43.1 mm). In addition, from the spray shape, the spray pattern width at four heights (5, 10, 15 and 20 cm) of all selected nozzles and the corresponding spray angles were calculated and compared with the results from the horizontal patternator. For the spray angle, a good correspondence between imaging technique and patternator was found with relative errors of 0.5% for the XR 110 01, 0.6% for the XR 110 01 and AI 110 04 and 2.8% and 5.4% for the ATR orange and ATR red, respectively.

Keywords: Piezoelectric droplet generator, high-speed imaging technique, image processing, spray angle, spray shape, droplet characterization, spray nozzles

SAMENVATTING

De voorbije jaren werd veel aandacht besteed aan innovaties in gewasbescherming vooral met het oog op het verhogen van opbrengsten op een duurzame manier. Het gebruik van chemische gewasbeschermingsmiddelen (GBM) met een hoge efficiëntie speelt hierin nog steeds een belangrijke rol. Hieraan zijn echter ook belangrijke nadelen verbonden. Tijdens hun toepassing kunnen GBM b.v. verloren gaan en op ongewenste plaatsen terechtkomen met financiële, economische en milieukundige gevolgen.

GBM worden meestal toegepast met landbouwspuiten. Deze spuittoestellen gebruiken hydraulische spuitdoppen die het spuitbeeld vormen en de spuitvloeistof omzetten in spuitdruppels met een breed spectrum van druppelgroottes en –snelheden. Kleine druppels driften echter makkelijk weg onder invloed van wind terwijl grote druppels van het gewas kunnen afrollen en de bodem contamineren. Om die redenen worden meer en meer inspanningen geleverd om tot een duurzamer gebruik van GBM te komen en is er steeds meer internationale regelgeving betreffende het gebruik van GBM. Eén van de grootste uitdagingen is om via geschikte spuittechnieken de verliezen naar de omgeving te minimaliseren in combinatie met het maximaliseren van depositie en bio-efficiëntie. Omdat het druppelvormingsproces van hydraulische spuitdoppen complex en moeilijk te kwantificeren of modelleren is, is er nood aan accurate meettechnieken. De recente ontwikkelingen in soft- en hardware openen mogelijkheden om hogesnelheidscamera's en beeldverwerking te gebruiken voor landbouwtoepassingen in het algemeen en spuittoepassingen van GBM in het bijzonder.

Dit onderzoek focust op de ontwikkeling en toepassing van technieken van snelle beeldacquisitie en –verwerking voor het niet-intrusief opmeten van de micro- (druppelgrootte en –snelheid) en macro- (spuithoek, spuitbeeld, lengte vloeistofvlies) karakteristieken van spuitnevels van GBM.

Na een review over spuittoepassingen van GBM en technieken om spuitnevels te karakteriseren (Hoofdstuk 2), werden in dit proefschrift twee snelle beeldacquisitiesystemen ontwikkeld in Hoofdstuk 3 op basis van *single-droplet* experimenten met een

snellebeeldcamera en een piëzo-electrische druppelgenerator. 58 combinaties van lenzen, lichtbronnen, diffusoren en sluitertijden werden getest en geëvalueerd op basis van beeldkwaliteitsparameters (signaal-ruisverhouding, entropieratio en contrastratio), lichtstabiliteit en hoeveelheid overbelichting en de meetnauwkeurigheid. Dit resulteerde in twee bruikbare beeldacquisitiesystemen. De hogesnelheidscamera met een macrovideozoomlens op een afstand van 143 mm met een gezichtsveld van 88 mm x 110 mm in combinatie met een halogeenspotlicht en een diffusor werd geselecteerd voor het meten van macrokarakteristieken van spuitnevels (spuithoek, spuitbeeld, lengte vloeistofvlies). De optimale opstelling voor het opmeten van de microkarakteristieken (druppelgrootte en -snelheid) bestond uit een hogesnelheidscamera met 6 µs sluitertijd, een microscopische lens op een afstand van 430 mm, resulterend in een gezichtsveld van 10,5 mm x 8,4 mm, en een Xenon tegenlicht zonder diffusor.

Met deze laatste techniek en de nodige ontwikkelde beeldverwerkingsalgoritmen (Hoofdstuk 4) werden in Hoofdstuk 5 metingen uitgevoerd met een druppelgenerator in *droplet on demand* (DOD) en continue modus. De effecten van instellingen (elektrische spanning, pulsbreedte en pulshoogte) en dopopening (261 µm, 123 µm, 87 µm and 67 µm) op druppelgrootte en –snelheid werden bepaald. De experimenten in DOD-modus toonden aan dat de initiële druppelkarakteristieken bepaald werden door de dubbele pulsbreedte (absorptietijd t_a en pulsatietijd t_p) en de grootte van de dopopening. Door te spelen met de pulsbreedte was het mogelijk om druppelgrootte- en snelheid te beïnvloeden. Algemeen leidden een daling van t_a en een stijging van t_p tot een toename van de druppelgrootte. In DOD-modus varieerden de druppelgroottes tussen 134,1 µm en 461,5 µm. De kleinste en tegelijk snelste druppels werden gegenereerd met de kleinste dopopening. De druppelsnelheden varieerden van 0,08 m/s tot 1,78 m/s. Daarnaast werd ook een effect van pulshoogte vastgesteld. De verhouding tussen druppelgrootte en grootte van de dopopening varieerde van 1,3 tot 3,5 in DOD-modus. In continue modus werd voor elke dopopening een hoogfrequent signaal (kHz) aangelegd resulterend in een continue druppelproductie. De effecten van frequentie en amplitude op druppelgrootte en –snelheid en de afstand tussen de druppels werden bepaald. Naar analogie met de DOD-modus werden druppelgroottes voornamelijk bepaald door de grootte van de dopopening. Druppelgroottes varieerden van 167,2 µm tot 455,8 µm. Daarnaast resulteerde een grotere dopopening eveneens in hogere

druppelsnelheden en was er een duidelijk lineair verband tussen druppelgroottes en -snelheden. De verhouding tussen druppelgrootte en grootte van de dopopening varieerde van 1,3 tot 3,9 in continue modus terwijl de druppelsnelheden varieerden tussen 1,84 m/s en 4,66 m/s. Zowel in DOD- als in continue modus kon een gelijkaardige range van druppelgroottes gegenereerd worden maar in continue modus waren de druppels sneller en dus representatiever voor een echte spuittoepassing.

In hoofdstuk 6 werd het beeldacquisitiesysteem voor het opmeten van de micro-karakteristieken van spuitnevels gebruikt om de druppelgroottes en –snelheden op te meten voor werkelijke spuitnevels van hydraulische spuitdoppen. In een eerste fase werd een in-focuscriterium opgesteld op basis van de grijswaarden-gradiënt om te bepalen of een druppel al dan niet in focus is. Verschillende druppelgroottes werden gegenereerd in continue modus met de druppelgenerator op verschillende afstanden van het focaal vlak met behulp van een micro-positioneersysteem. Voor elke positie en druppelgrootte werden de grijswaarden-gradiënt en de in-focusparameter bepaald. Op basis hiervan werd een kritische in-focusparameter (Inf_c) gedefinieerd voor elke druppelgrootte en een in-focus criterium dat bepaalt of een druppel al dan niet in focus is op basis van de diameter en de in-focusparameter. De *focused droplet zone* (FDZ) werd gedefinieerd als de zone waarin een druppel met een bepaalde diameter in focus is. Een lineaire correlatie tussen druppelgrootte en FDZ werd vastgesteld.

Het ontwikkelde in-focuscriterium werd toegepast op beelden genomen met vijf spuitdoppen op verschillende posities in de spuitnevel: twee standaardspleetdoppen (XR 110 01 & 04 bij 4.00 kPa), een luchtmengdop (AI 110 04 bij 400 kPa) en twee werveldoppen (ATR oranje bij 600 kPa en ATR rood bij 800 kPa). De effecten van doptype, dopgrootte en positie op druppelgroottes en –snelheden werden geëvalueerd.

De gemeten druppelgroottes en –snelheden met de beeldverwerkingstechniek toonden aan dat het mogelijk was om microkarakteristieken van spuitnevels op te meten op een niet intrusieve manier. De gemeten druppelgroottes varieerden van 24 µm tot 543 µm afhankelijk van doptype en –grootte. Druppelsnelheden op 0,5 m onder de spuitdop varieerden van 0,5 m/s tot 12 m/s. Druppelgroottekarakteristieken zoals $D_{V0.1}$, $D_{V0.5}$, $D_{V0.9}$ en RSF en druppelsnelheidskarakteristieken zoals V_{Vol10}, V_{Vol50}, V_{Vol90} and VSF werden berekend.

Gelijkaardige effecten van doptype en positie op druppelgroottes en –snelheden werden vastgesteld met de ontwikkelde beeldverwerkingstechniek als met de algemeen aanvaarde *Phase Doppler Particle Analyzer* (PDPA)--lasertechniek. Er werd een relatief goede correlatie gevonden tussen druppelkarakteristieken gemeten met de nieuw ontwikkelde techniek en de PDPA laser. In vergelijking met de PDPA-laser werden met de beeldverwerkingstechniek algemeen minder zeer kleine druppels opgemeten en in sommige gevallen ook een kleiner aantal grote druppels. Verschillen tussen beide technieken waren onder meer te wijten aan het feit dat de minimale gemeten druppelgrootte met de beeldverwerkingstechniek 24 µm is terwijl met de PDPA nog kleinere druppels kunnen worden opgemeten. Daarenboven was het aantal opgemeten druppels met de beeldverwerkingstechniek klein ten opzichte van de PDPA- techniek waardoor de kans stijgt om enkele van de zeer grote druppels te missen. Het nemen en analyseren van meer beelden kan dit verhelpen. Het verschil in druppelsnelheden tussen beide technieken is te wijten aan het feit dat de PDPA-laser slechts de verticale component van de druppelsnelheid meet, waardoor de werkelijke druppelsnelheid onderschat wordt. Daarnaast konden met de beeldverwerkingstechniek geen druppels sneller dan ongeveer 12 m/s opgemeten worden op basis van FOV en *frame rate* terwijl met de PDPA sporadisch druppels met hogere snelheden opgemeten werden voornamelijk bij de XR 110 04. In de toekomst kan de beeldverwerkingstechniek verder geoptimaliseerd worden door te meten bij een hogere *frame rate* met een zelfde nauwkeurigheid.

In hoofdstuk 7 werd het beeldacquisitiesysteem voor het opmeten van de macro-karakteristieken van spuitnevels gebruikt om de spuithoek, het spuitbeeld, en de lengte van het vloeistofvlies te bepalen voor dezelfde dop-druk–combinaties als hierboven. Waar mogelijk werden de resultaten vergeleken met die van traditionele meettechnieken zoals de verdeeltafel. De opgemeten spuithoeken bleken groter dan de nominale waarden met uitzondering van de XR 110 01. Voor de werveldoppen (ATR oranje en rood) en de luchtmengdop (AI 110 04) werd een goede overeenkomst gevonden tussen de met de beeldverwerkingstechniek gemeten spuithoeken en met de traditionele meettechniek terwijl voor beide standaardspleetdoppen (XR 110 01 en XR 110 04) een lagere waarde werd gevonden met de beeldverwerking. De kleinste lengte van het vloeistofvlies werd opgemeten voor de XR 110 01 (18.5 mm), gevolgd door beide werveldoppen (27.4 en 31.3 mm), terwijl de grootste waarden opgemeten werden voor de XR 110 04 (38.9 mm) en de AI

110 04 (43.1 mm). De spuitbreedtes op vier hoogtes (5, 10, 15 en 20 cm) werden opgemeten samen met de overeenkomstige spuithoeken en vergeleken met de resultaten van de horizontale verdeeltafel. Voor de spuithoek werd een goede overeenkomst tussen beide meettechnieken gevonden met een relatieve fout van 0.5% voor de XR 110 01, 0,6% voor de XR 110 04 en de AI 110 04 en 2,8% en 5,4% voor respectievelijk de oranje en de rode werveldop.

Trefwoorden: Piëzo-electrische druppelgenerator, snelle beeldacquisitie en –verwerking, beeldverwerking, spuithoek, spuitbeeld, druppelkarakterisatie, spuitdoppen

TABLE OF CONTENTS

LIST OF FIGURES

LIST OF TABLES

LIST OF ABBREVIATIONS

Abbreviation	Description
AI	TeeJet Air Induction flat spray nozzle
ATR	Albuz ATR Hollow cone nozzle
DOD	Droplet on Demand
FAO	Food and Agriculture Organization of the United Nations
FOV	Field of view
HS	High-Speed
IPM	Integrated Pest Management
ILVO	Institute for Agricultural and Fisheries Research
NMD	Nominal Median Diameter
NMV	Nominal Median Velocity
PDPA	Phase Doppler Particle Analyzer
PPP	Plant protection products
XR	TeeJet extended range flat spray nozzle
VC	Very coarse droplet spectrum
VF	Very fine droplet spectrum
VMD	Volume Median Diameter

1 GENERAL INTRODUCTION

1.1 INTRODUCTION

Plant protection is necessary for preventing a decline in yields, due to appearance of pests, weeds and diseases. Plant protection products (PPP) are essential tools for plant protection and disease prevention. Without pesticides a significant percentage of food and fiber crops would be lost, plant diseases would increase, and valuable native habitats would be devastated (Rice *et al.*, 2007). Unfortunately the application of PPP may cause pollution of surface- and groundwater, contamination of non-target organisms as well as human hazards. More than 80% of pesticide may be lost during spraying due to drift (up to 15%), rebound (up to 30%), run-off (up to 20%) and other processes (up to 15%) including evaporation or photolysis and thus can affect public health as well as contaminate water, soil and the atmosphere of an ecosystem (Pimentel, 1995; Knowles, 2001; Pimentel & Burgess, 2012). Therefore their safe and efficient use is a major social and economic issue which is more and more regulated by international environmental laws while they play an important role in agricultural marketing.

PPP are mainly applied as liquid solutions by using different types of sprayers equipped with hydraulic spray nozzles (Figure 1.1). These nozzles atomize the liquid to produce a broad spectrum of droplet sizes (~ 10-1000 µm) and velocities (~ 0-25 m/s) (Nuyttens *et al.*, 2007a; 2009). Droplet size as well as droplet velocity characteristics both influence the efficiency of the spray application. First, small droplets are subject to spray drift which distorts the spray pattern and causes environmental pollution (Nuyttens *et al.*, 2010). Second, large droplets have a greater kinetic energy which increases their ability to penetrate into the canopy but also the chance to rebound or shatter when the droplet impacts the plant surface (Zwertvaegher *et al.*, 2014).

Figure 1.1. Orchard (left) (www.airtecsprayers.com) and field (right) crop spray application (ILVO)

Besides droplet sizes and velocities, other important spray characteristics influencing the efficiency of the application process are droplet directions, the volume distribution pattern, the spray sheet structure and length, the structure of the individual droplets and the 3D spray dimensions (Miller & Ellis, 2000). Spray characteristics depend on nozzle type, nozzle size, liquid properties, spray pressure and sprayer settings (boom height, driving speed, etc.).

Hence, the challenge is to reduce spray losses during transport to their target and maximize spray deposition and efficacy and minimize off-target spray deposition by improving the spray application process (Zabkiewicz, 2007) by selecting and using adequate spray equipment and spray solutions at the right conditions (Dorr *et al.*, 2007).

Because mechanisms of droplets leaving a hydraulic spray nozzle are very complex and difficult to quantify or model, there is a need for accurate quantification techniques. Although techniques are available to measure some specific spray characteristics, none of them are able to fully characterize a spray application process. Therefore, adjusting sprayers is still based on practical experience and 'trial and error' as it is impossible to test any combination of sprayer type and settings, nozzle type, air support, spray pressure, crop characteristics, driving speed etc. on the application efficacy. The use of models could increase the knowledge on droplet transport processes and the effect of sprayer settings and environmental conditions. The validation of this is however difficult and cannot only be performed with traditional measuring techniques (like spray liquid distribution and air velocity measurements).

Spray characterization techniques can be classified in three broad categories: mechanical, electrical and optical. With mechanical techniques, droplets are collected and analyzed using sampling devices. However, these sampling devices may affect the spray flow behavior and can only be used to evaluate spray deposition and estimate droplet size (Rhodes, 2008). Therefore, the availability of non-intrusive systems for spray characterization is of great importance.

Quantitative (optical) non-imaging droplet characterization techniques are available but they are complex, expensive and in most cases limited to small measuring volumes. The limitations of the non-imaging techniques and the recent improvements in digital image processing, sensitivity of imaging systems and cost reductions, have increased the interest in high speed imaging techniques for agricultural applications in general and for fertilizer (Vangeyte, 2013; Cool *et al.*, 2014) and pesticide applications in specific. Imaging analyzers are spatial sampling techniques consisting of a light source, a camera and a computer with image acquisition and processing software. The small droplet size and the high velocity of the ejected spray droplets make it a challenge to use imaging techniques for spray characterization.

1.2 RESEARCH OBJECTIVES AND THESIS OUTLINE

Spray nozzles do not atomize the liquid into droplets of identical size and velocity but into a range of droplets of various sizes and velocities. These micro spray characteristics (droplet size and velocity) as well as the macro spray characteristics (spray angle, liquid sheet length, etc.) influence the efficiency of the spray application. Consequently more information on the micro and macro spray characteristics can lead to a more efficient pesticide usage.

Therefore, the general objective of this doctoral research is to develop image acquisition systems for pesticide sprays which are then used to systematically measure different micro and macro spray characteristics.

To achieve this main objective, the following sub-objectives are addressed, each corresponding with one of the following chapters:

- To review the spray application process and application techniques together with the available measuring techniques for micro and macro spray characteristics (Chapter 2);
- To develop and describe image acquisition systems for measuring the micro and macro spray characteristics (Chapter 3);
- To develop and describe image analysis and image processing algorithms for single droplet characterization (Chapter 4);
- To generate and characterize single droplets using imaging techniques and a piezoelectric droplet generator in two modes: Droplet on Demand (DOD) and continuous mode (Chapter 5);
- To develop image processing algorithms for micro-spray characterization and to compare imaging results with Phase Doppler Particle Analyzer results for different agricultural spray nozzles (Chapter 6);
- To develop image processing algorithms for macro-spray characterization and to compare these results with the horizontal spray patternator results (Chapter 7).

Finally, Chapter 8 highlights the most important conclusions and some guidelines for future research. A schematic overview of the outline of this thesis is presented in Figure 1.2.

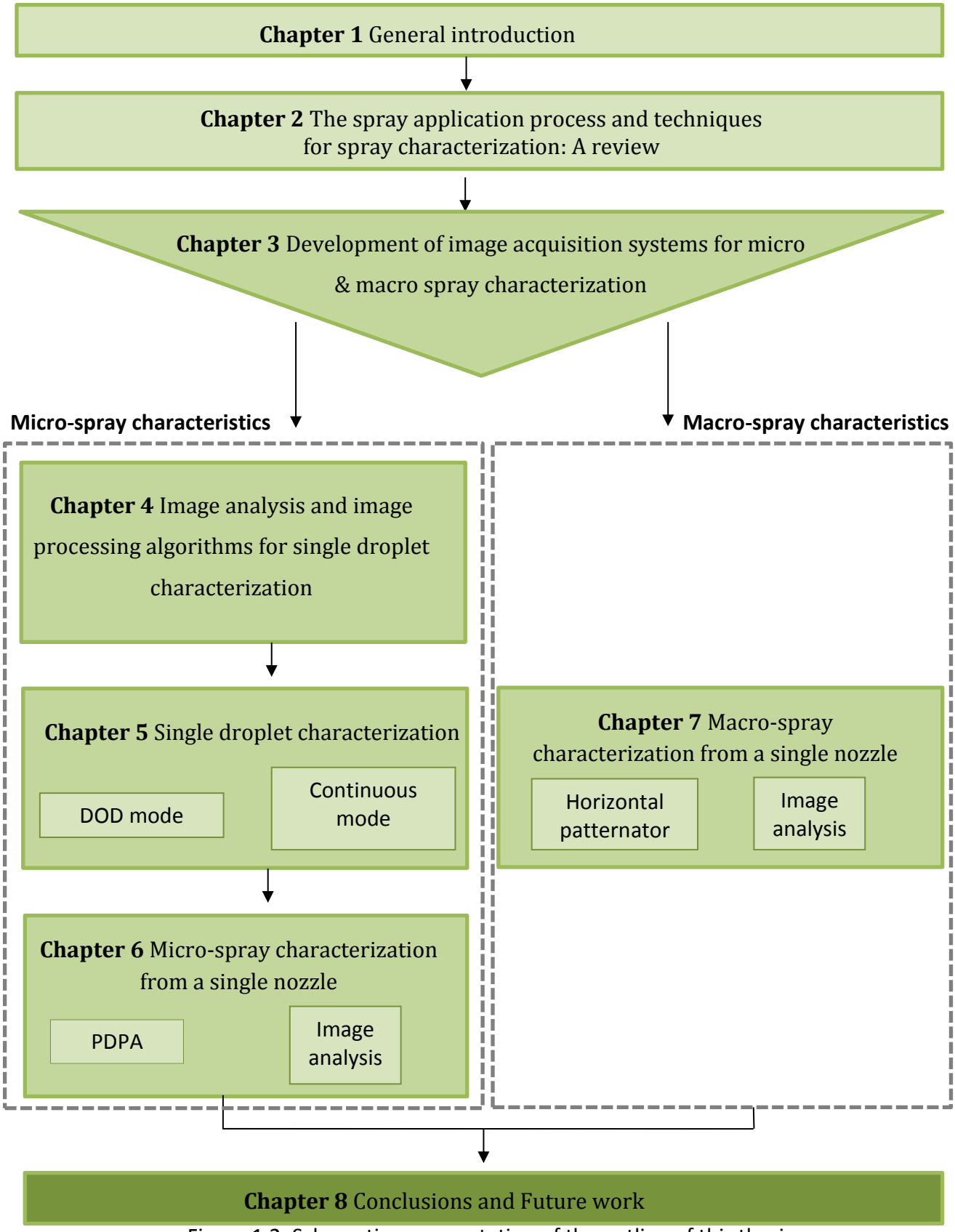

Figure 1.2. Schematic representation of the outline of this thesis

2 THE SPRAY APPLICATION PROCESS AND TECHNIQUES FOR SPRAY CHARACTERIZATION: A REVIEW[i]

A review of the use of plant protection products and the spray application process is given in this chapter. Different techniques for measuring the spray distribution and deposition are also described. Furthermore, methods for measuring spray droplet characteristics, like non-imaging and imaging and their advantages and limitations are listed here.

[i] Part of this chapter was adapted from:

Hijazi, B., Decourselle, T., **Vulgarakis Minov, S.**, Nuyttens, D., Cointault, F., Pieters, J., and Vangeyte, J. 2012. The use of high speed imaging for applications in precision agriculture. Book chapter in "New Technologies: Trends, Innovations and Research". ISBN 978-953-51-0480-3.

2.1 THE USE OF PLANT PROTECTION PRODUCTS

In the coming years, agriculture will face a 30 percent increase in the global population, intensifying competition for increasingly scarce land, water and energy resources, and the existential threat of climate change. To provide for a population projected to reach 9.3 billion in 2050 estimates are that food production will need to increase from the current 8.4 billion tons to almost 13.5 billion tons a year (FAO, 2014). Plant protection products (PPP) help farmers to grow more food on less land by protecting crops from huge losses due to pests and diseases and raising yields per hectare.

These PPP are generally chemicals used to eliminate or control a variety of agricultural pests during the growing season. The most applied PPP are insecticides (to kill insects), herbicides (to kill weeds) and fungicides (to control fungi, mold and mildew). When applying PPP the aim is always to maximize the amount reaching the target and minimize the amount reaching off-target areas. However, the use and disposal of toxic PPP by farmers and the general public provide many possible sources of PPP in the environment. This may lead to transport of PPP through the air or water, into the soil or even into living organisms.

It is estimated that about 25% of more than 2.5 million tons of PPP that are yearly applied in the world is used in the EU (Balsari & Marucco, 2011). Pesticide regulations exist to ensure the safe use of pesticides, so that farmers are equipped with the right tools for sustainable productivity so that consumers can be confident about the safety of their food and environments. Therefore, farmers and industry work together within the framework of EU Regulations and Directives to minimize any negative impacts.

In 2006, the European Commission adopted the 'Thematic Strategy on the Sustainable use of Pesticides' (European Commission, 2006). It was stated that by 2014 each country must adopt the principles of integrated pest management (IPM) and all pesticides application equipment will have to be inspected at least once by 2016 to grant a proper efficient use of any PPP (European Commission, 2009). IPM is an ecosystem strategy for crop production and protection which combines techniques to control pests and diseases and minimizes crop damage and the use of pesticides. IPM uses four approaches for pest management evaluations, decisions and controls (US Environmental Protection Agency, 2013):

- Action thresholds are set: the pest population density, at which it makes economic sense to take a control measure, is determined.
- Pest monitoring: pests are identified in the field and their population build-up is monitored to allow for sound control decisions.
- Pest prevention: if significant pest damage is expected, preventive measures are taken to avoid this damage.
- Pest control: when action thresholds are surpassed, despite the applied preventive measures, the pest control method posing the least risk to producers, consumers and the environment is chosen first. If this control method does not work, more risky methods can be applied.

Instead of only using synthetic chemical pesticides as a blanket solution, integrated pest management uses a wide array of methods for pest prevention and control. This thesis focuses on spray application techniques which is still the most used method to apply PPP. Spray application is a key component of IPM. Poor spray application can result in failure in what otherwise would be a successful IPM strategy.

2.2 SPRAY APPLICATION PROCESS

The spray application process consists of several sub-processes forming a 'delivery chain' (Matthews, 2000) (Figure 2.1). Every part of the chain can influence the spray efficiency. This thesis focuses on the droplet formation and atomization (2.2.2) and transport to the target (2.2.3). The developed image acquisition techniques can also be used to study droplet impact on the target and retention (2.2.4) as done by Zwertvaegher *et al*. (2014).

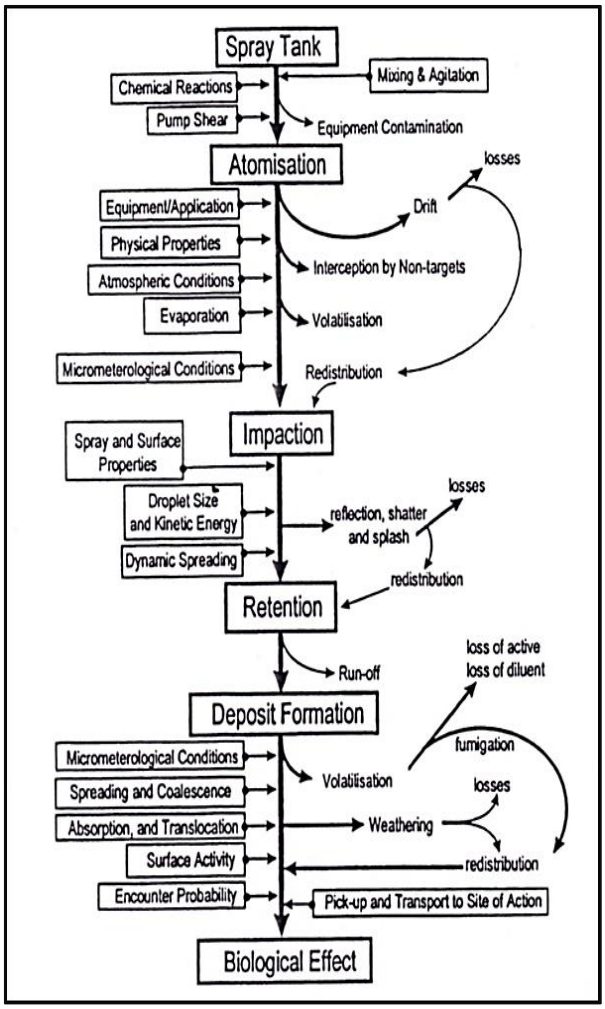

Figure 2.1. Delivery chain of the spray application process (Matthews, 2000)

2.2.1 Spray tank

The first step in the spray application process is preparing the spray tank solution. It is very important that the spray solution is mixed sufficiently before starting the application. With an inhomogeneous solution, a good and homogeneous application cannot be reached. The homogeneity of the solution is not only determined by good mixing practice, it also depends on the characteristics of the solvent. Certain products dissolve better in water than others. Compared to water, these adjuvants influence the liquid sheet formation and droplet characteristics (Wright *et al.*, 1982).

2.2.2 Droplet break-up regimes and atomization

The process of droplet ejection is not as simple as taking a fluid chamber with a small hole and pressurizing it enough for fluid to start emerging from the ejection nozzle hole (Lee, 2003). To accomplish monodisperse droplets ejected out of a nozzle, one needs the ability to produce high-speed fluid jets of approximately the diameter of the desired droplets

(Lindemann, 2006). Furthermore some terms concerning the droplet formation and ejection are necessary to be defined as they are later used in this thesis. Three breakup regimes can be distinguished as shown in Figure 2.2 of which the first two are found using a piezoelectric droplet generator (Chapters 3 to 5) while the atomization breakup is typical for hydraulic spray nozzles (Chapters 6 and 7).

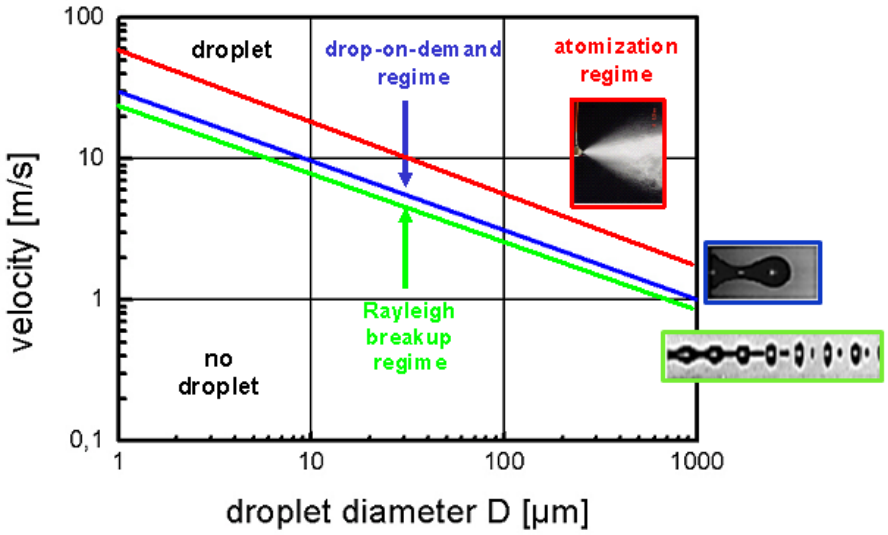

Figure 2.2. Different breakup regimes represented by the relationship of the velocity v versus the droplet diameter D for water as ejected liquid (Lindemann, 2006)

- Droplet-on-demand Breakup (DOD): characterized by ejection of a single droplet with a diameter approximately equal or slightly bigger than the nozzle diameter (Figure 5.3a) (Lindemann, 2006);
- Continuous mode: characterized by a continuous stream of uniformly sized droplets (Figure 5.3b). This continuous jet disperses into single droplets after a certain distance from the nozzle due to the source of acoustic energy causing instability and standing waves on the fluid. However, to form uniformly sized droplets, a suitable resonance frequency must be applied to it (Lee, 2003).

$$f = \frac{v}{9.016\, r_0} \qquad \text{Eq. 2.1}$$

$$d = 1.89\, d_0 \qquad \text{Eq. 2.2}$$

where f is the optimal frequency, v is liquid velocity at the nozzle exit, r_0 is the nozzle orifice radius and d_0 is the diameter of the nozzle orifice;

- Atomization Breakup: is a process in which a liquid sheet is fragmented into a fine spray of many single droplets (Figure 7.7a). This involves emitting the liquid through a small orifice at a high pressure. As a result, a wide spectrum of droplet sizes is generated by atomizers ranging from very narrow (several hundred µm) to wide (over a thousand µm) (Kirk, 2001; Teske *et al.*, 2005). Atomization breakup is typical for the application of plant protection products using hydraulic nozzles as studied in this thesis. Therefore, the atomization break up, the liquid sheet disintegration process is discussed in more detail in 2.2.2.1. Finally, the relation between the spray nozzle and the resulting spray characteristics is described in 2.2.2.2 together with the spray quality (2.2.2.3).

2.2.2.1 Liquid sheet disintegration

When the aerodynamic forces acting on the liquid sheet become larger than the surface tension, the sheet starts to disintegrate (Lefebvre, 1989). Most atomizers demonstrate three mechanisms of sheet disintegration: by perforation, by oscillation and by rim disintegration (Figure 2.3).

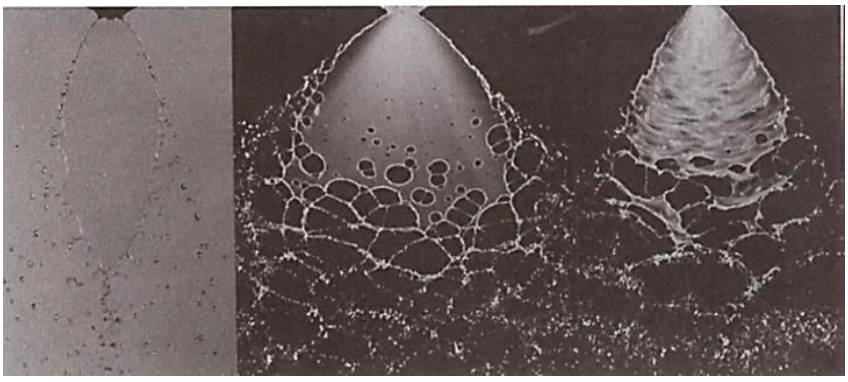

Figure 2.3. Sheet break-up by rim (left), perforated sheet (middle) and wave-sheet disintegration (right) (Matthews, 2000)

Which kind of disintegration occurs, depends on the velocity of the liquid relative to the surrounding air. A large relative velocity can be caused by fast droplets moving in still air or by droplets with a low velocity moving in high velocity airflow (Lefebvre, 1989). At relatively low liquid velocities, the liquid sheet is perforated leading to growing interruptions in the

sheet and separated droplets (disintegration by perforation) (Miller & Ellis, 2000). At higher velocities, wave phenomena occur in the sheet which leads to disintegration by oscillation. At the end of the liquid sheet, a jet-like, torus shaped structure is separated from the sheet and disintegrates into droplets (Figure 2.3) (Bayvel & Orzechowski, 1993). The last kind of sheet break-up is rim disintegration which occurs when both surface tension and viscosity are high (Lefebvre, 1989). Surface tension can act upon the edges of the liquid sheet and contract them into a rim.

The moment of sheet break-up determines the size of the droplets. A sheet breaking up early and close to the nozzle is thick and produces large droplets. A sheet breaking up at a greater distance from the nozzle orifice is thinner and produces smaller droplets (Miller & Ellis, 2000). At very high velocities, no liquid sheet is formed. Droplets are formed directly underneath the nozzle outlet and a very fine fog is produced (Bayvel & Orzechowski, 1993). In this thesis, liquid sheet length is measured using imaging techniques for different types of agricultural spray nozzles (Chapter 7). The mechanism of sheet disintegration is also influenced by fluid characteristics, like surface tension and viscosity. Increasing values of both properties lead to a longer sheet and thus smaller droplets (Kirk, 2001).

2.2.2.2 Spray nozzles and their characteristics

Each spray consists of a range of droplet sizes, referred to as the droplet size distribution. For a given formulation, the droplet size spectrum is determined by the nozzle type, the nozzle size and the spray pressure (Nuyttens *et al.*, 2007a).

The spray nozzle is the primary link between the plant protection product (PPP) and proper application to the target. The nozzle is designed to meter or regulate liquid flow rate, to form and control droplet size and to disperse and distribute the droplets in a specific pattern (Azimi *et al.*, 1985).

The nozzle type not only determines the amount of spray applied but also the uniformity of the applied spray, the coverage obtained on the sprayed surfaces and the amount of drift that might occur (Sumner, 2009).

Each nozzle type has specific characteristics and is designed to be used for different applications. Once a system is designed, selecting a nozzle based on its characteristics is

crucial. The most important nozzle parameters are: flow rate, operating pressure and pressure losses, nozzle material, nozzle spray angle, nozzle positioning, spray height, spray width, spray thickness, atomization degree or droplet size, impact, spray pattern, etc. (Lefebvre, 1989).

Selecting a nozzle based on the spray pattern and other spray characteristics that are required generally yields good results (Lipp, 2012). Different types of spray nozzles are available as shown in Figure 2.4. Air atomizing nozzles produce the smallest droplet sizes followed by fine spray, hollow cone, flat fan and full cone nozzles (Schick, 1997).

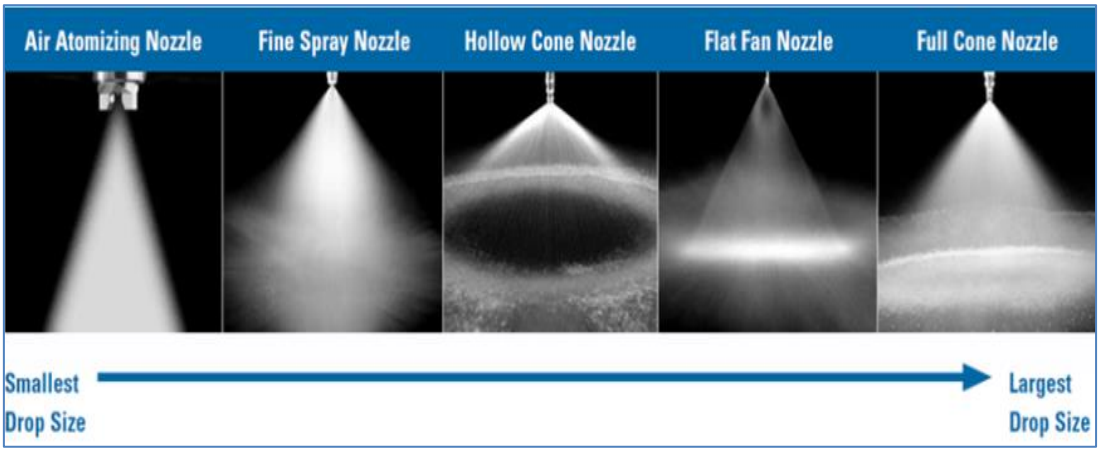

Figure 2.4. Spray patterns for different nozzle types (Schick, 1997)

The most commonly used nozzle types for ground application of PPP are the flat fan and hollow cone nozzles (Sumner, 2009). The nozzle size and corresponding color are defined by the International Organization for Standardization (2005). The higher the ISO number the larger the orifice and the flow rate and the larger the droplets in the spectrum (Lefebvre, 1989). Pressure has an inverse relationship effect on droplet size, thus, increase in pressure will generally reduce the droplet size (Schick, 1997).

In this study, hollow cone nozzles as well as standard flat fan nozzles and air inclusion flat fan nozzles are considered (Chapters 6 and 7).

a. Hollow cone nozzles: are mainly used on hand-operated sprayers and on orchard sprayers in which spray droplets are projected into the canopy by a blast of air from a fan (Nuyttens, 2007a). They produce a cone-shaped pattern with the spray

concentrated in a ring around the outer edge of the pattern (Figure 2.5). This is the most popular nozzle type for orchard and vineyard spray applications.

Figure 2.5. Liquid sheet and droplet formation from a hollow cone nozzle (www.lechler.de)

b. Flat fan nozzles: are mostly used on field crop sprayers. They can achieve a very good cross distribution under a spray boom with the correct nozzle spacing and spray height. Flat fan nozzles produce a fan-shaped spray pattern (Nuyttens *et al.*, 2007a) i.e. delivering the highest amount of spray volume in the center and lower spray volumes at the boundaries. Therefore, in practice, it is important to create a good spray overlap in order to obtain a homogeneous coverage of the field (Faqiri & Krishnan, 2005) (Figure 2.6). The most commonly used top angle is 110° generally resulting in a uniform spray distribution for a nozzle height and nozzle spacing of 0.5 m.

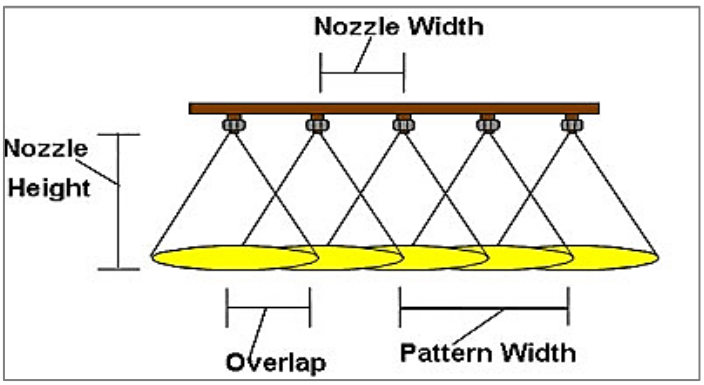

Figure 2.6. Nozzle overlap for flat fan sprayers

- *Standard flat fan nozzles* are producing the smallest droplets as compared to the other two types of flat fan nozzles (drift-reducing and air inclusion flat fan nozzles) for the same nozzle size and pressure (Figure 2.7). The small droplets secure a very effective coverage of the surface, but are very drift prone (Nuyttens, 2007b)

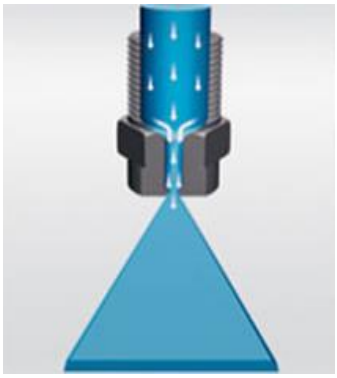

Figure 2.7. Standard flat fan nozzles

- *Air inclusion flat fan nozzles* contain a venturi insert. This venturi induces air through two holes at the side of the nozzle. The air is mixed with the liquid in the nozzle chamber (Figure 2.8). Because the liquid leaving the flat fan orifice is a mixture of air and spray liquid, the sheet becomes unstable very quickly and breaks up into large droplets, resulting in a very coarse spray (Nuyttens, 2007a). Therefore these droplets are less drift prone and explode on impact with leaves which reduces the risk of a droplet bouncing off a leaf surface.

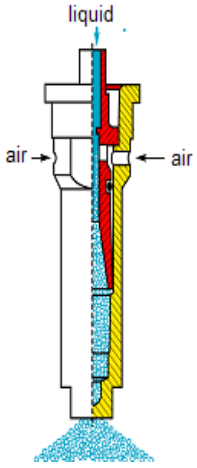

Figure 2.8. Air inclusion nozzle (Nilars, 2003)

2.2.2.3 Spray quality

The term "Spray quality" is primarily used for describing the droplet size spectra of (agricultural) sprays. The spray characteristics like droplet size, velocity and direction influence the penetration and deposition of droplets. The efficiency of pesticide distribution often depends on droplet size (Hislop, 1987) but hydraulic spray nozzles are not able to produce uniform droplets. A high coverage of the target is usually best achieved with small droplets (Cawood *et al.*, 1995) which are more subject to wind drift (Nuyttens *et al.*, 2011).

On the other hand, large droplets increase the risk of run off from target surfaces but have a higher kinetic energy which improves canopy penetration. The droplet size distribution is not homogeneous and depends on the position within the spray (Butler Ellis *et al.*, 1997).

Because of the importance of droplet size, the British Crop Protection Council (BCPC) has devised a nozzle classification scheme and also described the entire droplet spectrum generated by hydraulic spray nozzles (Southcombe *et al.*, 1997). The spray classification system divides the quality of sprays into five categories: very coarse (VC), coarse (C), medium (M), fine (F), very fine (VF) and extremely coarse (XC) (Figure 2.9).

Classification Category	Symbol	Color Code	Approximate VMD
Very Fine	VF	Red	<100
Fine	F	Orange	100-175
Medium	M	Yellow	175-250
Coarse	C	Blue	250-375
Very Coarse	VC	Green	375-450
Extremely Coarse	XC	White	>450

Figure 2.9. Spray quality standards (Southcombe *et al.*, 1997)

A comparison of the percentile volume fractions produced by a nozzle to that of specific standardized reference nozzles classifies a droplet size spectrum. The $D_{V0.5}$ or volume median diameter (VMD) is commonly used to characterize the droplet size characteristics of a spray. The VMD is the droplet diameter at which 50% of the spray volume is contained in larger droplets and the other half is contained in smaller droplets (Schick, 1997). Two nozzle-

pressure combinations with the same VMD may actually produce a quite different droplet spectrum. Droplet spectra are normally represented by a frequency histogram or a cumulative volumetric droplet size distribution (Nuyttens *et al.*, 2007a).

A summary of the main values that are used to describe the droplet size spectra is presented in Table 2.1.

Table 2.1.Overview of parameters to describe droplet size spectra

Parameter	Description	Units
VMD or $D_{v0.5}$	Volume median diameter or diameter for which a volume fraction of 50% is made up of droplets with diameters smaller than this value	µm
$D_{v0.1}$, $D_{v0.9}$	Diameter at which a volume fraction of 10, 90 percent is made up of droplets with diameter smaller than this value	µm
RSF	Relative span factor; indicating the uniformity of the droplet size distribution$= \frac{D_{v0.9}-D_{v0.1}}{VMD}$	-
NMD	Number median diameter; droplet diameter for which 50% of the number of droplets is smaller than this value	µm

Other important droplet characteristics are droplet velocity and direction (trajectory). Increasing the spray liquid pressure to the nozzle results into a finer spray and increases the droplet velocities. As the effect of making a finer spray dominates with initial increases of pressure, the risk of drift tends to increase. Further increase in pressure does not result in a further increase of drift and may even, with some nozzles designs, result in a decrease in drift at high pressure due to the dominance of the droplet velocity effect (Miller & Butler Ellis, 1997).

Sidahmed (1996) formulated a droplet-size/velocity equation based on the energy balance equation:

$$v = \left(\frac{d^3 v_a^2}{d_a^3}\right)^{1/2} \quad \text{Eq. 2.3}$$

Where d_a and v_a are the size-class median droplet diameter and velocity and *d* and *v* are the representative diameter and velocity. Hence the droplet velocity depends on its diameter at formation.

2.2.3 Transport to target

At a short distance from the nozzle the motion of droplets stops to be governed by the atomizer and becomes a function of physical phenomena in the atmosphere. The transition from motion being governed by the atomizer to being governed by the flow field is conveyed by stop distance or relaxation time (Bache & Johnstone, 1993). The stop distance (D_s) can be calculated with Eq. 2.4 (Bayvel & Orzechowski, 1993):

$$D_s = \frac{\rho_d D^2 v_0}{18 \rho_a v_a} \qquad \text{Eq. 2.4}$$

with v_0 the droplet velocity at the nozzle exit (m s^{-1}), D the droplet diameter (m), ρ_d the droplet density (kg/m^3), ρ_a the density of the air (kg/m^3) and v_a the kinematic viscosity of air (m^2/s). Relaxation time is defined as the time scale over which the movement of a particle reaches equilibrium within a flow field, subsequent to a disturbance. After some time, the aerodynamic drag forces will equal the gravitational forces and the droplet will reach a constant velocity, called the sedimentation velocity (Bayvel & Orzechowski, 1993).

Although particle movement is complex and depends on many variables, some of the basic laws of physics can be used to predict particle movement in most cases. The motion of large particles is dominated by gravity and in some cases by severe cross flows. The size and mass of these particles can be used, along with density of the flow field, to calculate gravitational forces and drag coefficients, and to determine the velocity of the particles (Galeev & Zaripov, 2003). Droplets with a diameter smaller than 100 µm are said to be buoyant because gravitational force acting on these droplets is roughly equal to their drag force (Whitney & Roth, 1985). Because movement of these droplets is governed primarily by the flow field, they require an advanced understanding of the turbulence phenomena in the field to describe their path (Shirolkar *et al.*, 1996).

2.2.4 Impact on target

Collection efficiency is the probability that a drop will deposit after impact on a surface and is dependent on the relative velocity of the drop with respect to the target, wind velocity relative to the target, the size, shape, and orientation of the target, drop size and drag

coefficient (Shirolkar *et al.*, 1996). Larger drops are collected more efficiently on horizontal surfaces while smaller drops are collected better on vertically oriented targets (Zhu *et al.*, 1996).

Generally small drops have much shorter stopping distances and remain entrained in the flow field that moves around the collecting object (Spillman, 1984). Image acquisition techniques can be used to study droplet impact characteristics (Massinon & Lebeau, 2012a; Zwertvaegher *et al.*, 2014).

Spherical and cylindrical surfaces are better collectors of droplets than flat objects because the flow field follows the cylinder over its sides and reduces the zone of dead air behind the object. Objects oriented at 90° to the flow field have greater collection efficiency than those oriented at smaller angles. Objects oriented at smaller angles generate less severe changes in the flow field, which means that the droplets are less likely going to collide with an object (Spillman, 1984).

2.3 MEASURING SPRAY DISTRIBUTION AND DEPOSITION

The spray distribution pattern and spray deposition have been used to evaluate nozzle performance in agricultural applications for many years.

These characteristics are traditionally measured using intrusive measuring techniques also called sampling techniques: spray scanner (2.3.1), vertical patternator (2.3.2) or a distribution bench (2.3.3). With these techniques, droplets are collected and analyzed using mechanical sampling devices. However, these sampling devices may affect the spray flow behavior (Rhodes, 2008).

In this thesis, these techniques are referred to as ‘traditional measuring techniques’. The results of these traditional measuring techniques are compared with the results from the developed image acquisition techniques.

2.3.1 Spray scanner

The spray volume cross flow distribution under a spray boom or a set of hydraulic nozzles mounted on a standard boom reflects the quality of the sprayer or the nozzles and the spray distribution under field conditions. It can be measured using a spray scanner. The spray

scanner available at ILVO consists of a receiver unit with 0.10 m grooves which autonomously moves along an aluminum rail installed beneath the spray boom (Figure 2.10).

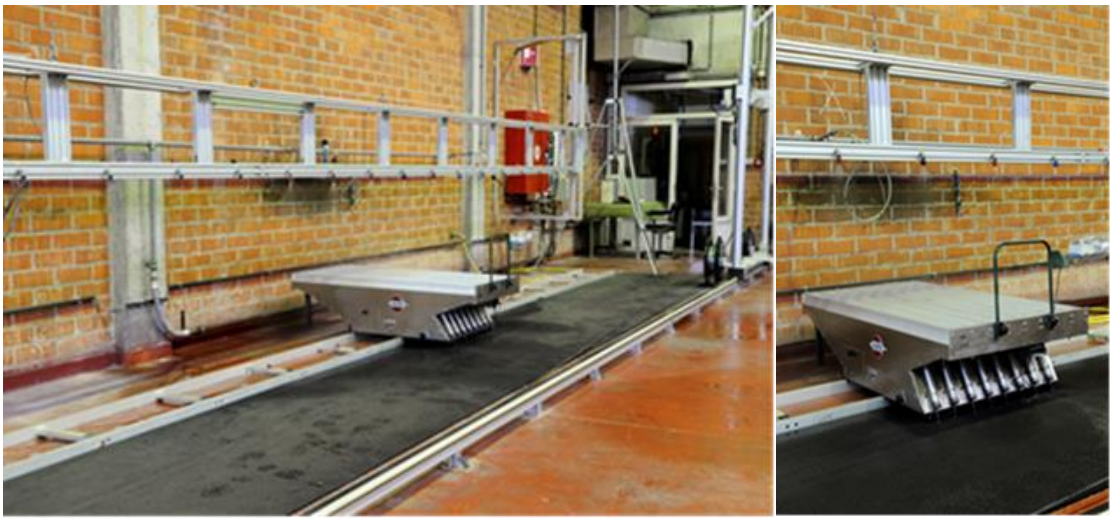

Figure 2.10. Spray scanner in Spray Tech Lab, ILVO

2.3.2 Vertical patternator

The vertical patternator is designed to measure the vertical liquid distribution of orchard, air-blast sprayers and vertical spray booms (Figure 2.11). The patternator available at ILVO with a height of 3.2 m is constructed with specially manufactured lamellae that allow the air to pass through and filter the sprayed liquid. The collected liquid between the lamellae is guided per 10 cm of height and drained off in measuring cylinders.

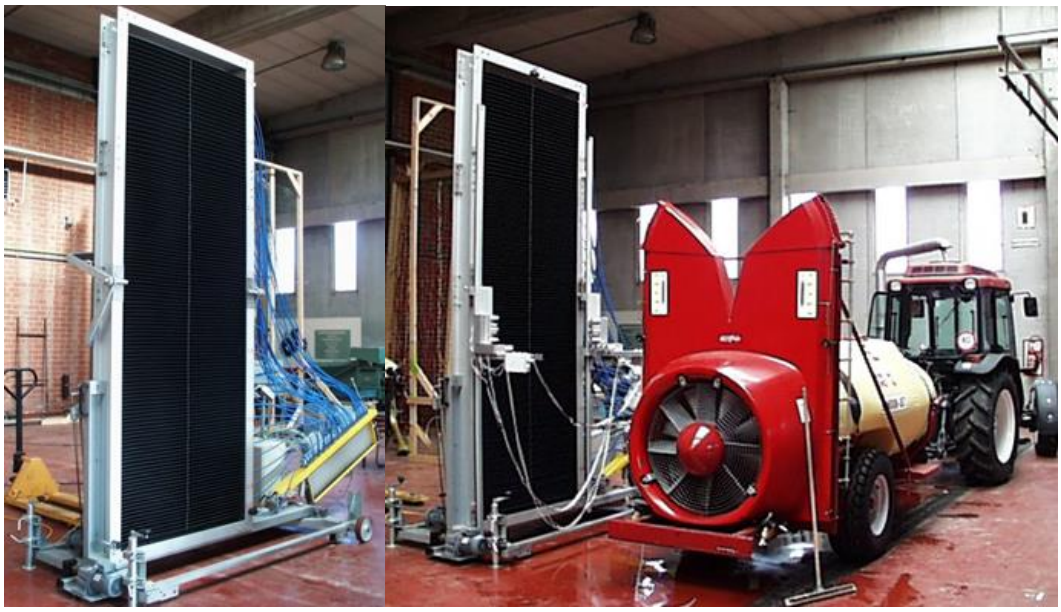

Figure 2.11. Vertical patternator from Spray Tech Lab, ILVO

2.3.3 Spray distribution bench

A spray distribution bench or horizontal patternator can be used to measure the spray distribution of a single spray nozzle or a short spray boom (Figure 2.12). It is important to have uniform spray distribution for efficient application of the pesticides. The uniformity of the spray distribution is sensitive to nozzle properties, nozzle-mounting configurations, and various nozzle-operation conditions (Wang *et al.*, 1995).

Figure 2.12. Spray distribution pattern at Spray Tech Lab, ILVO

2.3.4 Measuring spray deposition

Through the years, spray deposition data is widely used in optimizing the spray application techniques. Spray deposition in the crop can be assessed using water sensitive papers (WSP) (Foqué *et al.*, 2012a), metal chelates (Foqué *et al.*, 2012a), water-soluble food dyes (Sanchez-Hermosilla *et al.*, 2011) or fluorescent tracers (Khot *et al.*, 2011). For example, WSP can provide a qualitative and cheap evaluation of the spray distribution. Here droplets deposit on the water sensitive paper and create a stain (Figure 2.13). A more complete review on the measuring spray deposition techniques was written by Foqué (2012b).

Figure 2.13. Water sensitive paper

2.4 METHODS FOR MEASURING SPRAY DROPLET CHARACTERISTICS

There are numerous methods for measuring droplet characteristics which can be divided into three categories: *mechanical, electrical and optical methods*.

The *mechanical methods* involve the collection of a spray sample on a solid surface (2.3.4) or in a cell containing a specific liquid. *Electrical methods* measure droplet size distribution via the detection and analysis of electronic pulses produced by the spray. Charged wire and hot wire are two techniques used within this method. More information on this technique can be found in the work of Gardiner (1964). By far, the most common method is the *Optical measurement* which can be divided into non-imaging light scattering (2.4.1) and high speed imaging methods (2.4.2).

2.4.1 Optical non-imaging light scattering spray characterization techniques

Due to the development of modern technology such as powerful computers and lasers, quantitative optical non-imaging light scattering droplet characterization techniques have been developed for non-intrusive spray characterization. Although these techniques are able to measure some specific spray characteristics, none of them are able to fully characterize a spray application process. Moreover, these techniques are complex, expensive and (in most cases) limited to small measuring volumes. They are not able to accurately measure non-spherical particles. The most important types of non-imaging light scattering droplet characterization techniques are the Phase Doppler Particle Analyzers (PDPA) (Nuyttens *et al.*, 2007a; 2009) (2.4.1.1), the laser diffraction analyzers, e.g., Malvern Analyzer (Stainier *et al.*, 2006) (2.4.1.2) and the optical array probes (Teske *et al.*, 2002) (2.4.1.3). Several studies have shown a wide variation in mean droplet sizes for the same nozzle specifications while using different techniques (Nuyttens, 2007a).

2.4.1.1 Phase Doppler Particle Analyzer (PDPA)

Phase Doppler Particle Analyzers (PDPA) are flux-sampling, non-imaging instruments used to measure the droplet size and velocity. This technique has been used in this thesis to compare with the imaging results (Chapter 6). Point sampling refers to an instrument that focuses on a portion of the total spray pattern and requires targeting several test points within the spray in order to obtain a composite sample of the spray flux distribution.

The PDPA produces two low-power laser beams crossing each other at a point referred to as the probe volume. The scattered light created from a droplet passing this measuring volume forms an interference fringe pattern. The frequency of this scattered light is proportional to the droplet velocity while the spatial frequency of the interference fringe pattern is inversely proportional to the drop diameter. Depending on the optical configuration, PDPA measures sizes in the 0.5-10.000 µm range. This measuring technique is best suited for complete spray evaluation where droplet velocities are required for a wide range of nozzle types (Nuyttens *et al.*, 2007a).

The measuring set-up is composed of a spray unit, a three-dimensional automated positioning system, a controlled climate room, and a PDPA laser system (Figure 2.14).

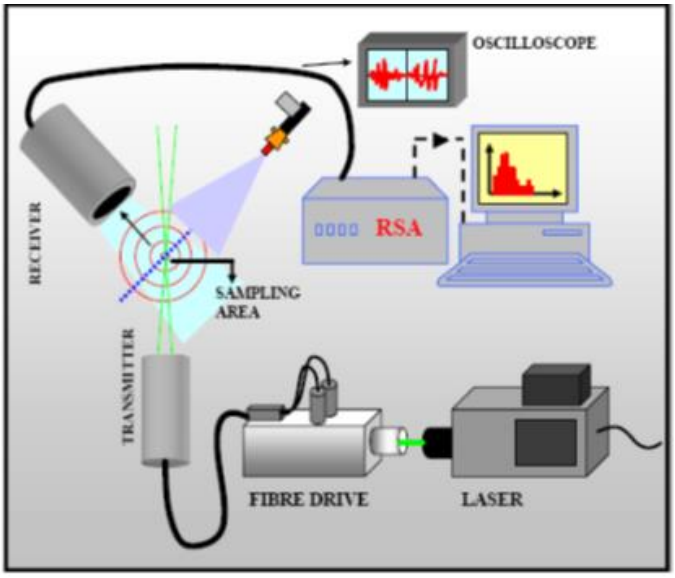

Figure 2.14. Schematic overview of the PDPA optical laser instrument (Nuyttens, 2007a)

With the PDPA laser set-up available at ILVO, different scan patterns can be carried out (Figure 2.15), each one with the start and end position of the spray nozzle in the center of the XY-rectangle straight above the measuring point (Figure 2.15).

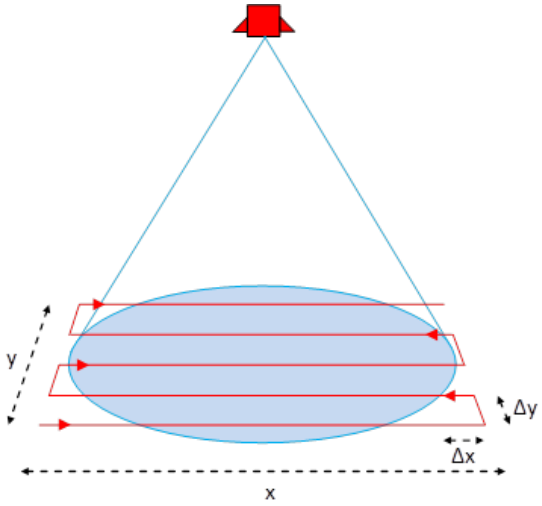

Figure 2.15. Scan pattern of the total scan of the spray cloud (Nuyttens, 2007a)

However, the PDPA measuring system has some limitations. It requires a higher cost and results may differ significantly between different researchers depending on the measuring protocol, the settings and the type of measuring equipment (Nuyttens, 2007a).

2.4.1.2 Laser diffraction analyzers

Laser diffraction analyzers are spatial, non-imaging sampling devices which operate by directing a laser beam through a spray cloud. These analyzers consist of a transmitter, a receiver and a computer. Spray droplets diffract the light at different angles according to droplet size as they pass through the analyzer sampling area. The technique is based on measuring the scattered light intensity caused by the droplets using semicircular photodiodes. From the light intensity distribution, the droplet size spectrum of an entire spray cloud is computed (Nuyttens, 2007a). Droplet velocities are not measured with this technique.

The most common laser diffraction instrument today is the Malvern analyzer (Teske *et al.*, 2002; Stainier *et al.*, 2006). A schematic overview of the Malvern analyzer is shown in Figure 2.16.

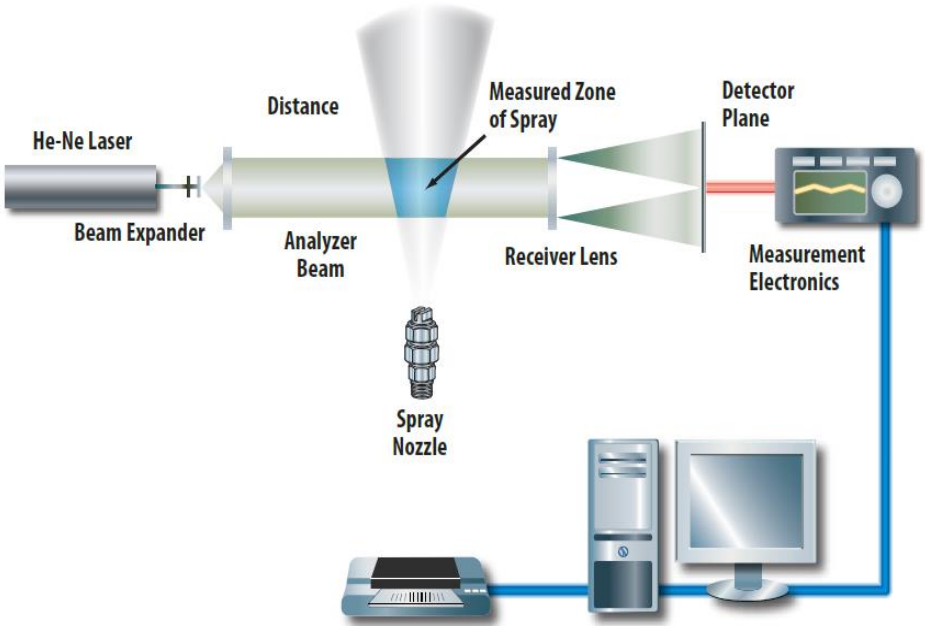

Figure 2.16. Schematic overview of the laser diffraction analyzer (Schick, 1997)

Nevertheless, the most serious limitation of this technique is known as multiple scattering which occurs when spray densities are too high resulting in the light being scattered by multiple droplets before reaching the detector. This may introduce errors in computing the droplet size distribution (Schick, 1997).

2.4.1.3 Optical array probes

Optical array probes are flux-sampling instruments and also fall into the non-imaging category. These devices consist of a light source (low-power laser beam), photo-diode array and computer. With this type of instruments, droplets passing a sampling plane, created by the laser beam, are sized and counted by measuring the amount of laser light shadowed by the droplets. Moreover, information is provided that can be used to determine droplet velocities. The measurement range for these probes can vary from 100-12 400 µm and they are best suited for large capacity nozzles (Schick, 1997; Teske *et al.*, 2002).

A schematic overview of one optical array probe device is given in Figure 2.17.

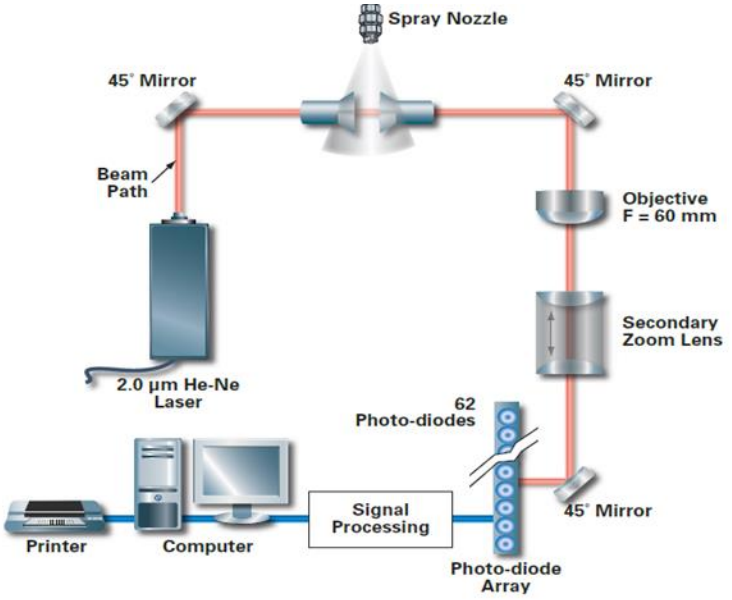

Figure 2.17. Schematic overview of optical array probe device (Schick, 1997)

2.4.2 High-speed imaging spray analyzers

The limitations of the non-imaging techniques and the recent improvements in digital image processing, sensitivity of imaging systems and cost reduction have increased the interest in high-speed imaging techniques for agricultural applications in general, specifically for pesticide applications. Another major advantage is that a visual record of the spray under investigation is available, providing a simple means to verify what is being measured, and perhaps more importantly, what is not being measured (Kashdan *et al.*, 2004a). Furthermore, another fundamental limitation of light scattering techniques is the inability to accurately measure non-spherical droplets. For this reason, measurements must be obtained sufficiently far downstream from the primary sheet or jet break-up region where ligaments and initially large and often non-spherical droplets are formed. This is an unfortunate limitation, since the near-orifice region is where the process of atomization is occurring and the initial droplets are formed (Kashdan *et al.*, 2004a).

Recent developments in nozzle technology produce sprays with droplets containing air inclusions. Because these internal structures can cause uncertainty with techniques that rely on diffraction or scattering, interest has been renewed in droplet sizing using imaging techniques. Moreover, imaging techniques offer greater simplicity over light scattering techniques. One of the main issues using imaging techniques is not only the need for

automated processing routines but also the problem of resolving the depth-of-field (DOF) effect and its inherent influence on measurement accuracy (Kashdan *et al.*, 2004b).

High-speed imaging analyzers are spatial sampling techniques consisting of a (strobe) light source, a (high-speed) camera and a computer with image acquisition and processing software. The image frames from the video are analyzed using various image processing algorithms to determine spray droplet characteristics. The imaging techniques have the potential to determine the droplets velocity and droplet distribution. Several industrial imaging techniques (PDIA, PIV, LIF) are used for droplet characterization. They have the potential to fully characterize spray characteristics in a non-intrusive way. For pesticide applications, however, technical and financial challenges make this impossible to put into practice. These techniques are currently mainly used for the characterization of small sprays, e.g., paints, medical applications, fuel injectors, etc.

Some of the available imaging techniques mainly used for industrial spray characterization are discussed below (2.4.2.1– 2.4.2.3).

Other interesting techniques were proposed to characterize pesticide sprays using either a high-speed camera with a high-power light source (2.4.2.4) or a high-resolution standard camera with a strobe light (2.4.2.5). These techniques can give additional information about the droplets' trajectory, which is needed to predict the droplet impact outcome.

2.4.2.1 Particle/droplet imaging analyzers (PDIA)

Particle Droplet Imaging Analyzers (PDIA) automatically analyzes digital images of a spray (Figure 2.18). A very short flash of light illuminates a diffusing screen to back-illuminate the subject. A digital camera with a microscope lens captures images of the subject. Different magnification settings can be used to measure a very wide range of droplet sizes. Image analysis software analyses the images to find droplet size. Shape data for the particles can also be measured and recorded. By using dual laser flashes in short succession and measuring the movement of the particle, it is possible to measure the particle velocity. Information on spray geometry can be provided by switching to light sheet illumination. The most common PDIA in use is the VisiSizer software developed by Oxford Laser and used among others by Kashdan et al. (2007). This system measures cone angle, drop size and drop

velocity and other key parameters of the spray. Kashdan *et al*. (2004a; 2004b) found a good correlation between PDIA, PDPA and Laser Diffraction results.

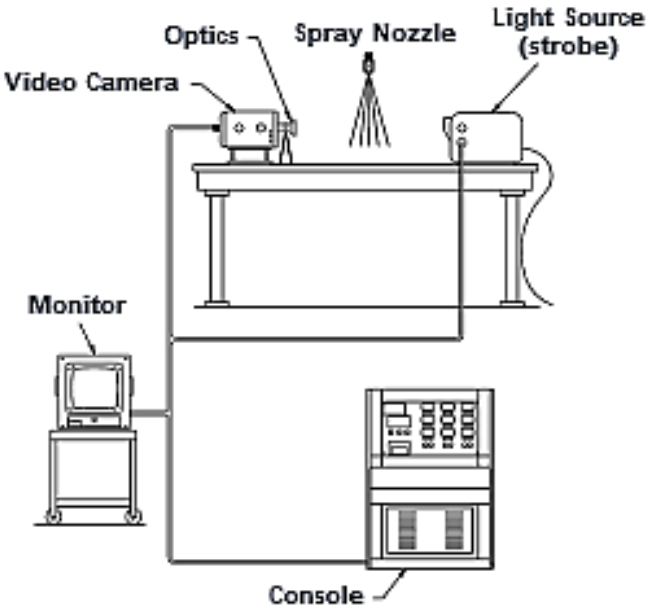

Figure 2.18. Typical Particle droplet imaging analyzer (Schick, 1997)

2.4.2.2 Particle Image Velocimetry (PIV)

Particle Image Velocimetry (PIV) is an optical method used to obtain velocity vector measurements in a cross-section of a flow and related properties of particles (Grant, 1997; Dorr *et al.*, 2013) (Figure 2.19). It produces two-dimensional vector fields, whereas other techniques measure the velocity at a point. In PIV, the particle size and density make it possible to identify individual particles in an image, but not with enough certainty to track it between images. This technique uses laser light and it is well adapted to laboratory conditions but cannot be used in the field. It is rather used as a reference method and not for pesticide spray characterization under practical conditions. Particle Tracking Velocimetry (PTV) (Hatem, 1997; Kreizer *et al.*, 2010) is a variant which is more appropriate with low seeding density experiments, and Laser Speckle Velocimetry (LSV) with high seeding density. Like PIV, PTV and LSV measure instantaneous flow fields by recording images of suspended seeding particles at successive instants in time (Kowalczyk, 1996). Hence, LSV, PTV and PIV are essentially the same technique, but are used with different seeding densities of particles (Paul *et al.*, 2004).

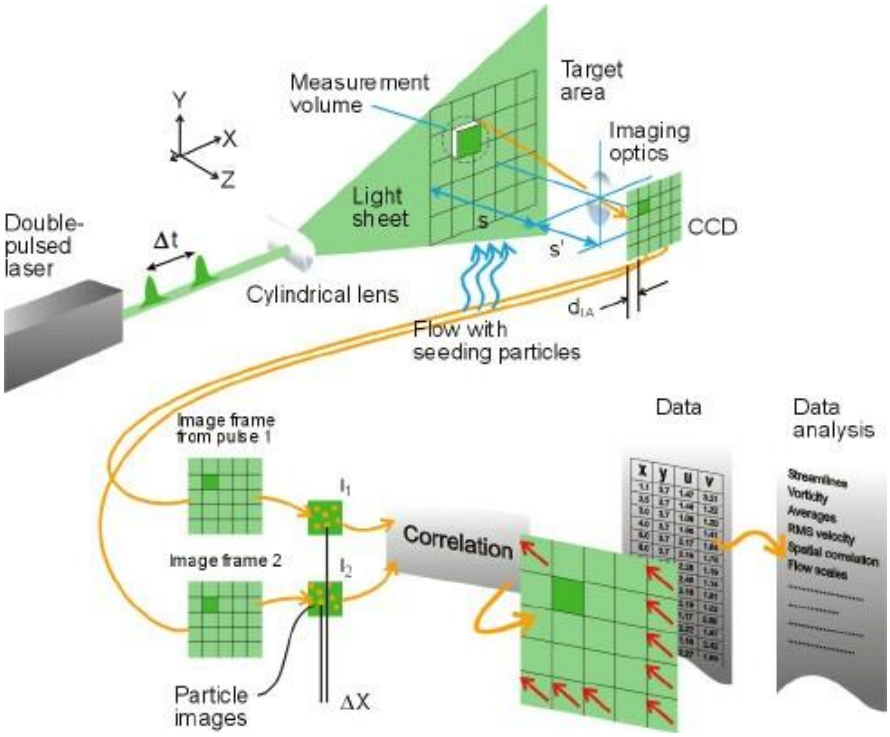

Figure 2.19. Measurement principals of PIV (Dantec Dynamics Inc.)

2.4.2.3 Laser Induced Fluorescence (LIF)

Laser Induced Fluorescence (LIF) is a spectroscopic method used to study the structure of molecules, detect selective species, and to perform flow visualization and measurements (Cloeter *et al.*, 2010). The particles to be examined are excited with a laser. The excited particles will, after a few nanoseconds to microseconds, de-excite and emit light at a wavelength larger than the excitation wavelength. This light (fluorescence) is then measured. One advantage that LIF has over absorption spectroscopy is that LIF can produce two- and three-dimensional images, as fluorescence takes place in all directions (i.e., the fluorescence signal is isotropic). By following the movement of the dye spot using high speed camera and image processing, the particle velocity can be determined (Mavros, 2001). LIF can minimize the effect of multiple scattering found with laser diffraction analysers and can minimize the interference between the reflection and refraction lights (Hill & Inaba, 1989). The drawback of this method is that the particles reflect the LIF signal of the tracers, which can cause error in the measurement signal of the liquid flow.

2.4.2.4 High resolution camera with a strobe light

This technique combines a high resolution standard (slow speed) camera with a strobe light for tracking high-speed particles (Cointault *et al.*, 2002; Kuang-Chao *et al.*, 2008; Hijazi *et al.*,

2010; Li *et al.*, 2010; Vangeyte, 2013). The principle is that a series of light flashes is triggered one after the other over a single camera exposure. The number of flashes determines the maximum number of particle positions that can be recorded on each image.

Cointault et al. (2002) proposed a system combining a monochrome camera (1008x1018 pixels) with a strobe light consisting of photograph flashes to determine the trajectories and velocities of fertilizer grains in a FOV of 1 m x 1 m. Vangeyte and Sonck (2005) also used a similar system but with a LED stroboscope and a small field of view (0.1m x 0.1m) to capture the fertilizer grain flow.

This technique was already used by Reichard et al. (1998) to analyze single droplet behavior combining a monochrome video camera (60 fields per second) with a single backlight stroboscope (Type 1538-A, Genrad, Concord, MA 01742) at a flash rate of about seven times the field-sequential rate used to drive the camera. This produced multiple images of the same droplet.

Lad et al. (2011) used a high-intensity pulsed laser (200 mJ, 532 nm) as a backlight source which was synchronized with a firewire type of digital camera (1280 x 960 pixels) to analyze a spray atomizer. The laser beam was converted to a laser cone using a concave lens, and then it was diffused by a diffuser. A 200 mm micro-lens equipped with a spacer was used to get a magnification of 2.6 of the image resulting in a field of view of 1.82 x 1.36 mm for a working distance of 250 mm. The digital camera captured shadow images which were analyzed to determine droplet sizes. The system is capable of performing an online characterization of spray droplets and an image calibration was performed using graph paper. A calibration method of an imaging system in the diameter range 4 to 72 µm has been reported by Kim and Kim (1994).

Malot and Blaisot (2000) developed a particle sizing method based on incoherent backlight images using a stroboscope with two fibers synchronized with two cameras. This technique was used to project 2D images of drops on a video camera, which led to two-dimensional images.

2.4.2.5 High-speed camera with high-power light source

An alternative method to analyze spray characteristics is to use a high-speed camera combining high resolution images with a high frame rate (1000 fps and more) (Kim *et al.*, 2011). This technique was further investigated in this thesis. Because of the short exposure time inherent to high-speed imaging, very high illumination intensities are needed. The usual method to illuminate the spray is a powerful background illumination either with a xenon light (Kashdan *et al.*, 2007) or with powerful LEDs (Massinon & Lebeau, 2012b). The advantage of this system is the possibility to be adapted to the application condition, the frame rate and the resolution of the image.

Massinon and Lebeau (2012b) and Zwertvaegher *et al*. (2014) used a high-speed camera (Y4 CMOS, Integrated Design Tools) with a high magnification lens (12 x zoom Navitar, 341 mm working distance) coupled with high-power LED lighting and image processing to study droplet impact and spray retention of a real spray application. Camera resolution was reduced to 1016 x 185 pixels to acquire 20.000 images per second with a spatial resolution of 10.58 µm.pixel^{-1}. A background correction was performed with Motion Studio embedded camera software to get a homogeneous image. Nineteen-LED backlighting (Integrated Design Tools) with a beam angle of 12.5° was placed 0.50 m behind the focus area to provide high illumination and a uniform background to the images. Based on the pixel size of the droplet as determined manually from the pictures with Motion Studio software, together with the spatial resolution, the diameter of the droplets was calculated. Similarly, droplet velocities were calculated in a very-time consuming and visual way, based on the distance between the position of the droplet between two consecutive frames and the frame rate. In this way, only the 2-dimensional velocity was calculated.

Many others, like Šikalo et al. (2005) also studied the impact of droplets with a high-speed CCD camera but in these studies, single droplets were produced using a microdrop generator in DOD or continuous mode.

In conclusion, a number of studies based on shadowgraphy have been used to measure the droplet size and velocity in a spray application using a standard camera/stroboscopic light and HS camera/coherent light. These studies are well adopted to low density sprays where

droplet sizes are bigger than 100 µm. In addition, in a high dense spray, the problem of DOF is more pronounced than in a low dense spray.

2.5 CONCLUSION

The majority of pesticides used in agricultural production are delivered in the form of droplets produced from different types of hydraulic spray nozzles. To maximize spray efficiency, spray droplets must be uniformly distributed on a target surface with minimum losses due to drift, evaporation or run-off. More information on spray characteristics will help manufacturers and spray operators to get the best possible results.

However, the mechanisms of atomization and how the droplets leave the nozzle and impact the leaves are very complex and difficult to quantify or model. Existing measuring techniques are not able to fully characterize the spray application process. Besides, imaging techniques are non-intrusive and have proven to be an effective tool for analysis in various domains and applications. Imaging techniques in combination with image processing can help manufacturers and users to better understand and evaluate the spray application process at an affordable cost. This thesis focuses on the development and application of high speed imaging techniques for spray characterization.

3 DEVELOPMENT OF HIGH SPEED IMAGE ACQUISITION SYSTEMS BASED ON SINGLE DROPLET EXPERIMENTS[ii]

The goal of this Chapter was to develop two image acquisition systems based on single droplet experiments using a piezoelectric single droplet generator and a high speed imaging technique which were used in this study to evaluate single droplet characteristics (Chapter 5) as well as micro (Chapter 6) and macro (Chapter 7) spray characteristics of different spray nozzles. This Chapter presents experiments done with different camera settings, lenses, diffusers and light sources. Different image acquisition techniques were evaluated based on the resulting image quality parameters.

[ii] This chapter has been compiled from:

Vulgarakis Minov, S., Cointault, F., Vangeyte, J., Pieters, J.G., and Nuyttens, D., 2015. Development of high speed image acquisition systems for spray characterization based on single droplet experiments. Transactions of ASABE 58 (1): 27-37.

3.1 INTRODUCTION

The characteristics of pesticide sprays generated by agricultural nozzles play an important role in the application accuracy and efficiency of plant protection products in precision agriculture (Stafford, 2000). Poor accuracy and spray losses may reduce the effectiveness of the application and increase environmental contamination and operator risk. The challenge is to reduce spray losses during the transport to the target and maximize spray deposition and efficacy, thus improving the spray application process (Zabkiewicz, 2007). The most important spray characteristics influencing the pesticide application process are droplet size and velocity, spray volume distribution pattern, liquid sheet length and thickness, structure of individual droplets and 3D spray dimensions (Miller & Ellis, 2000; Nuyttens *et al.*, 2009).

An overview of existing non-imaging (2.4.1) and HS imaging (2.4.2) spray characterization techniques was presented in Chapter 2. From this review, a high speed (HS) camera with a high–power light source technique seems a promising technique to measure spray and spray droplet characteristics combining high resolution images with a high frame rate (1000 fps and more) (Kim *et al.*, 2011). Because of the short exposure time inherent to high-speed imaging, high illumination intensities are needed. The usual method to illuminate the spray is a powerful background illumination either with a xenon light (Kashdan *et al.*, 2007) or with power LEDs (Massinon & Lebeau, 2012b). The advantages of using this method are the possibility of modifying the number of frames per second and the high resolution of the images. Massinon and Lebeau (2012a) and Zwertvaegher *et al*. (2014) used a high-speed camera to study droplet impact and spray retention of a real spray application. Many others, including Šikalo (2005) studied the impact of droplets with a high-speed CCD camera but in these studies, single droplets were produced using a microdrop generator in an on-demand or continuous mode. Because spray droplets are fast, translucent and their diameters cover a wide range (from 10 to 1000 µm), droplet measurement accuracy strongly depends on the imaging and optical set-up.

The aim of this Chapter was to develop two image acquisition systems based on images with single droplets generated with a piezoelectric droplet generator in the on-demand mode (Switzer, 1991; Yang *et al.*, 1997; Lee, 2003). Different high-speed camera settings, illuminations, diffusers and lenses were tested using shadowgraph (background) imaging

(Lecuona *et al.*, 2000; Castanet *et al.*, 2013) and evaluated based on three defined image quality parameters (entropy ratio, contrast ratio, signal to noise ratio), the light stability and overexposure ratio, and the measuring accuracy. The developed image acquisition systems were used to characterize single droplet characteristics (Chapter 5) using adequate image processing algorithms (Chapter 4) and the micro (droplet size, velocity) (Chapter 6) and macro (spray angle, liquid sheet length, droplet trajectory) (Chapter 7) spray characteristics of real pesticide sprays.

This chapter comprises four sections. Section 3.2 introduces the piezoelectric droplet generator, the image acquisition system and eventually the steps of image analysis based on a) the image quality parameters (3.3.1), b) the light stability and overexposure ratio (3.3.2) and c) the accuracy of the droplet size measurement (3.3.3). Section 3.3 contains the results and discussions from the image analysis. Section 0 concludes the chapter.

3.2 MATERIALS AND METHODS

3.2.1 Piezoelectric Droplet Generator

The development of HS image acquisition systems was done using uniformly size controlled and on-demand droplets. For this purpose, a piezoelectric droplet generator (Université de Liége, Gembloux, Agro-Bio-Tech, Belgium) (Figure 3.1 top) was used in this study consisting of a liquid filled chamber with a piezoelectric element that can be driven with voltages up to 60V (Figure 3.1 top). It is able to form uniform droplets in 2 modes, i.e.: Droplet-On-Demand (DOD) and Continuous mode, which are described in more detail in Chapter 5.

In this chapter, the single droplet formation was done in DOD mode (Yang *et al.*, 1997) which relays on the double pulse width values (absorption time: ta (ms) and pulsation time: tp (ms)) and voltage pulse amplitude (±Vp (V)) (Figure 3.1 bottom) which were applied using LabView software (National Instruments, Austin, Tex.). Applying a double voltage pulse to the piezoelectric element, it compresses the fluid inside the nozzle. This compression creates a complex acoustic wave within the fluid chamber that leads to a pressure gradient field. As a result, liquid is pushed out of the nozzle at the nozzle fluid-air interface (Riefler & Wriedt, 2008) and a droplet (µm) is created.

In fact, a positive voltage sent to the piezoelectric element results in absorption (Lam *et al.*, 2009) and a negative voltage results in pressure in the ejection chamber. In this chapter, droplets were generated in DOD mode using a glass nozzle (Figure 3.1 top) with a 123 µm orifice size at ta = 0.4 ms, tp= 50 ms and Vp = ± 4.5 V. In Chapter 5, the effect of different nozzles and settings on droplet characteristics is discussed.

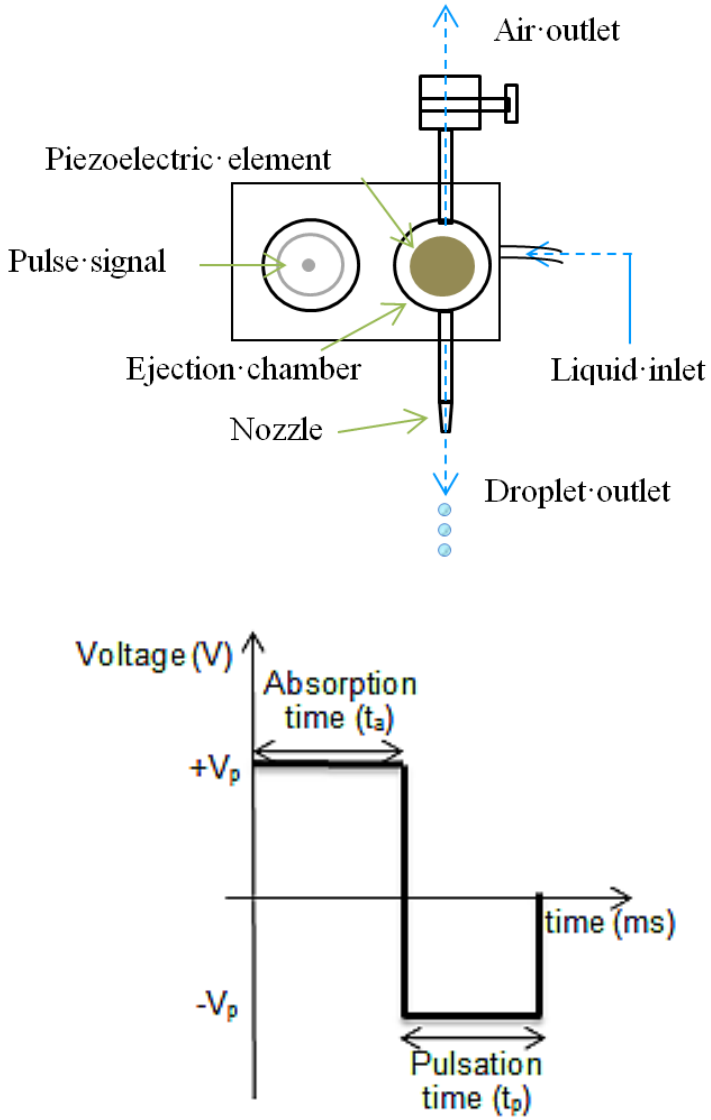

Figure 3.1. Schematic overview of the droplet generator (top) and block diagram of the driving rectangular double pulse used to generate on-demand droplets where: ta is absorption time, tp is pulsation time and ± Vp is the pulse amplitude voltage set in LabView (bottom)

The piezoelectric set-up consists of an electronic part, including amplifier, a pulse generator (digital-to-analogue converter (DAC) (National Instruments, Austin, USA)), a pressure

supplier (Furness Controls FCO 502, East Sussex, UK), and a software part (LabView) installed on a conventional PC (Figure 3.2 top).

The pulse generator drives the piezoelectric element. The signal from the pulse generator was amplified 10 times before it was sent to the piezoelectric element via an RG-58 coaxial cable and the LabView software enabled specific pulse forms to be generated.

3.2.2 Image acquisition system

The imaging acquisition system consisted of a high-speed (HS) camera and a high power backlight (Figure 3.2). An overview of the different lenses, illumination systems and exposure times tested is given in Table 3.1. The software package Motion Studio (IDT, Lommel, Belgium, version: 2.09, 2011) was used as a frame capture device for choosing the settings of the HS camera like frame rate, record mode, sensor gain, image resolution and exposure mode.

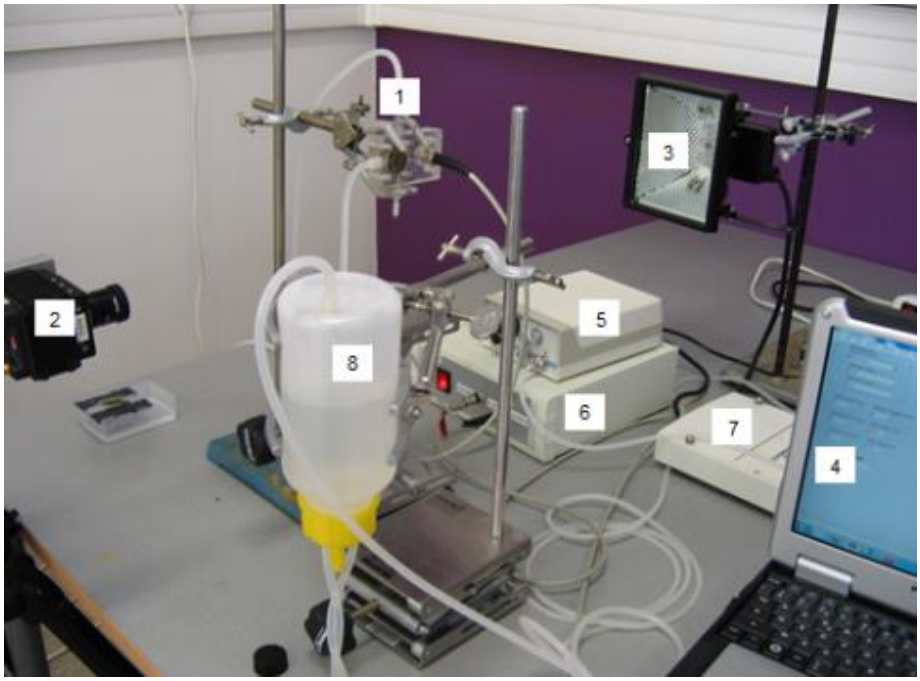

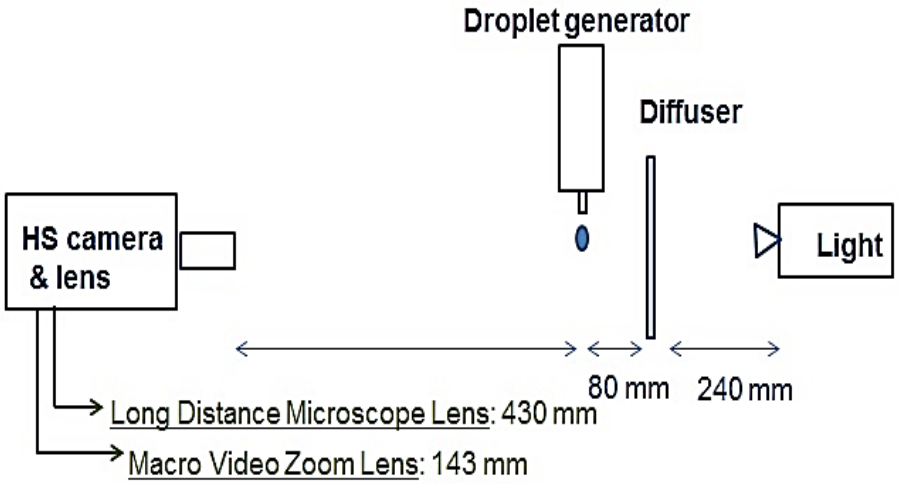

Figure 3.2. Image acquisition system (top) with (1=droplet generator with piezoelectric element, 2=high-speed camera and lens, 3=light source, 4=computer with frame software, 5-pressure supply, 6=signal amplifier, 7=pulse generator, and 8- liquid tank) and schematic of the system (bottom)

An N3 HS camera (IDT, Lommel, Belgium) with a 25.4 mm (1 in.) CMOS sensor and 12 µm pixel resolution set to 1000 Hz with a +3 dB sensor gain was used (Massinon & Lebeau, 2012b). Exposure times were set at 5, 10 and 15 µs and additionally at 6, 7, 8 and 9 µs for the xenon light in combination with the K2/SC long-distance microscope lens without diffuser (Table 3.1). In order to image a droplet, the droplet ejection was triggered with the camera.

For each of the 58 combinations of lens, light source, diffuser, and exposure time (Table 3.1), droplet ejection videos with 100 images were taken. When a droplet could be detected visually in these videos, ten consecutive images with a droplet were selected for image analysis. Similarly, 10 consecutive images without a droplet were also selected from these videos for further image analysis.

Two types of lenses were evaluated. A macro video zoom lens (18 to 108 mm focal length, F/2.5to closed, 2/3 in. format, Thales Optem, Fairport, N.Y.) with a close-up lens was used (Kim *et al.*, 2011) at a working distance of 143 mm, resulting in a FOV of 88 mm x 110 mm. To achieve a small FOV, and to measure droplet characteristics in an accurate way, a K2/SC long-distance microscope lens (Infinity Photo-Optical Co., Boulder, Colo.) (Riefler & Wriedt,

2008) was used with a CF1 objective attached directly to its front. At a working distance of 430 mm, a FOV of 10.5 mm x 8.4 mm (Infinity Photo-Optical Company, 2009) was obtained. For all tests, the distances between the nozzle and light, between nozzle and diffuser glass, and between the diffuser and the illumination source were 320, 80 and 240 mm, respectively (Figure 3.2 bottom).

Knowing that spray droplet velocities can be in the range of 1 to 15 m s^{-1} (Nuyttens *et al.*, 2007a), the exposure time should be in the time range of microseconds, thus requiring high illumination intensities (Ju *et al.*, 2012). Moreover the illumination should be stable, which requires a precisely controlled supply voltage. Therefore, three types of light source were tested with and without two types of diffusers (Table 3.1). First, a Seven-Star power LED assembly (40 mm round, 5650 K, 14W, Philips, Lumileds, San Jose, Cal.) with a polymer 264 lens and DC power supply delivering 1645 lm at 700 mA (Sunrise Power Transformers GmbH, Hamburg, Germany, 10x3 LSD) was tested. Second, a halogen spotlight (350 W, EcoHalo, Koninklijke Philips Amsterdam, The Netherlands) (Ulmke *et al.*, 2001) with a maximum power of 500 W and a working temperature of 3200 K was included in the tests. The spotlight is the least expensive light source, but care must be taken not to overheat any object in the recorded zone. Finally, a xenon short arc lamp (model 5132, 300 W, Richard Wolf GmbH, Knittlingen, Germany) fed to the head by a flexible light conductor was selected for the purpose of achieving a clear image even at a very short exposure time (Kim *et al.*, 2011). This type of light source is easy to handle and capable of providing instant high-power white light and a high-intensity continuous spectrum with low heat buildup.

A simple and effective way of reducing light inhomogeneity involves the use of a diffuser placed between the light and the lens (Kashdan *et al.*, 2007; Lad *et al.*, 2011) (Figure 3.2 bottom). Two types of ground glass diffusers (TECHSPEC, Edmund Optics, Barrington, N.J. USA) were used: 120 grit and 220 grit sandblast, both with a thickness of 1.6 mm and a size of 250 mm x 250 mm.

Table 3.1. Summary of the tested image acquisition set-ups

Lens	Light	Diffuser	Exposure time (µs)
Macro Video Zoom Lens	Seven-Star LED	120 grit	5, 10, and 15
		220 grit	
		none	
	Halogen spotlight	120 grit	5, 10, and 15
		220 grit	
		none	
	Xenon light	120 grit	5, 10, and 15
		220 grit	
		none	
K2/SC long-distance microscope system	Seven-Star LED	120 grit	5, 10, and 15
		220 grit	
		none	
	Halogen spotlight	120 grit	5, 10, and 15
		220 grit	
		none	
	Xenon light	120 grit	5, 10, and 15
		220 grit	
		none*	

* Additional tests at 6, 7, 8, and 9 µs exposure times.

3.2.3 Image analysis

Image analysis combines techniques and measurements based on the gray-level intensities of the image pixels and were used here to determine the imaging characteristics of the different image acquisition set-ups using image histograms. From the histograms, different first -order statistical properties (Materka & Strzelecki, 1998) of images taken with and without droplets were determined and used for comparison of the different image acquisition set-ups.

As the *N x M* image (region) is a function *f(x,y)* of two variables *x* and *y*, *x*=0,1,…,*N*-1 and *y*=0,1,..,*M*-1, the function *f(x,y)* can take discrete values *i*=0,1,…,*L*-1, where *L* is the total number of intensity levels in the image. Furthermore, an intensity level histogram shows the the number of pixels in the image (region) that have a given intensity level:

$$h(i) = \sum_{x=0}^{N-1} \sum_{y=0}^{M-1} \delta(f(x,y), i) \quad \text{Eq. 3.1}$$

where $\delta(j,i)$ is the Kronecker delta function:

$$\delta(j,i) = \begin{cases} 1, & j = i \\ 0, & j \neq i \end{cases} \quad \text{Eq. 3.2}$$

Dividing the values *h(i)* by the total number of pixels in the image (region), we obtain the approximate probability density of occurrence of the intensity levels (Tuceryan & Jain, 1998):

$$p(i) = \frac{h(i)}{NxM}, i = 0,1,....,L-1. \quad \text{Eq. 3.3}$$

The first-order statistical properties used to assess the image characteristics of the image acquisition set-ups were the average gray level or mean, the average contrast or standard deviation and the entropy (Haralick *et al.*, 1973; Gonzalez *et al.*, 2004) (Table 3.2). These values were calculated for a defined region of interest (ROI) for all the images with a droplet as well as for all the images without a droplet using an image processing program developed in Matlab (MathWorks, Inc., Natick, Mass) that is divided into three steps: (1) selecting the ROI in an image, (2) showing the ROI image histogram, and (3) calculating the first-order statistical properties of the chosen ROI. The flowchart in Figure 3.3 shows the process for determining the first-order statistical properties. For the macro video zoom lens, the ROI was defined as a region starting 5.0 mm below the nozzle with a size of 17.5 mm x 45 mm (Figure 3.4a). For the K2/SC long- distance microscope lens, the ROI started at 0.8 mm below the nozzle with a size of 2.5 mm x 8.0 mm (Figure 3.4b). In both cases, the ROI was large enough to capture the same droplet in at least ten consecutive images.

Table 3.2. First-order statistical equations

Parameter	Expression[*]	Description
Mean (average gray level)	$f_1 = \mu = \sum_{i=0}^{L-1} ip(i)$	A measure of the average gray level of an image and indicating the brightness
Standard Deviation (average contrast)	$f_2 = \sigma = \sqrt{\sum_{i=0}^{L-1} p(i)(i-\mu)^2}$	A measure of how much the gray level of pixels differs from the mean value to detect if there are any substantial light or dark spots in the image
Entropy	$f_3 = e = -\sum_{i=0}^{L-1} p(i)\log_2 p(i)$	A measure of disorder. A high entropy value indicates the presence of an object, whereas a 0 value corresponds with a constant image

[*] L is the number of quantized gray levels, $L=2^B$, where B is the number of bits.

For the specific purpose of comparing the different image acquisition set-ups, three image quality parameters for the ROI were defined and calculated from the first-order statistical properties:

Entropy Ratio

Defined as the ratio of the entropy values from images with a droplet and without a droplet taken with the same image acquisition set-up, the entropy ratio should be maximized, as we are aiming for maximal entropy in images with a droplet and minimal entropy in images without a droplet.

Contrast Ratio

Defined as the ratio of the average contrast values from images with a droplet and without a droplet taken with the same image acquisition set-up, the contrast ratio should be maximized, as we are aiming for maximal contrast in images with a droplet and minimal contrast in images without a droplet.

Signal-to-Noise Ratio (SNR)

SNR is defined as the ratio between the mean (signal) and the standard deviation (or average contrast). For images with a droplet, the SNR should be maximized, as we are aiming for a large signal value and a small noise value in images with a droplet.

Based on the image quality parameters, four image acquisition set-ups were selected, and their light stability and overexposure ratio was assessed by comparing histograms of pixel intensity values of ten consecutive ROI images taken at the same settings without a droplet. An overexposed or saturated image contains a large number of pixels with maximum gray level values resulting in a loss of information.

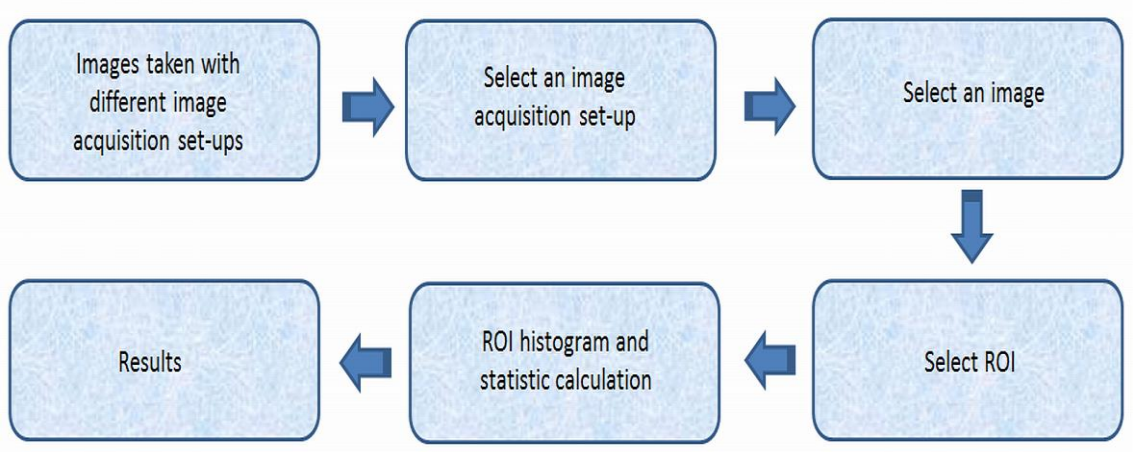

Figure 3.3. Flowchart of the first-order statistics algorithm

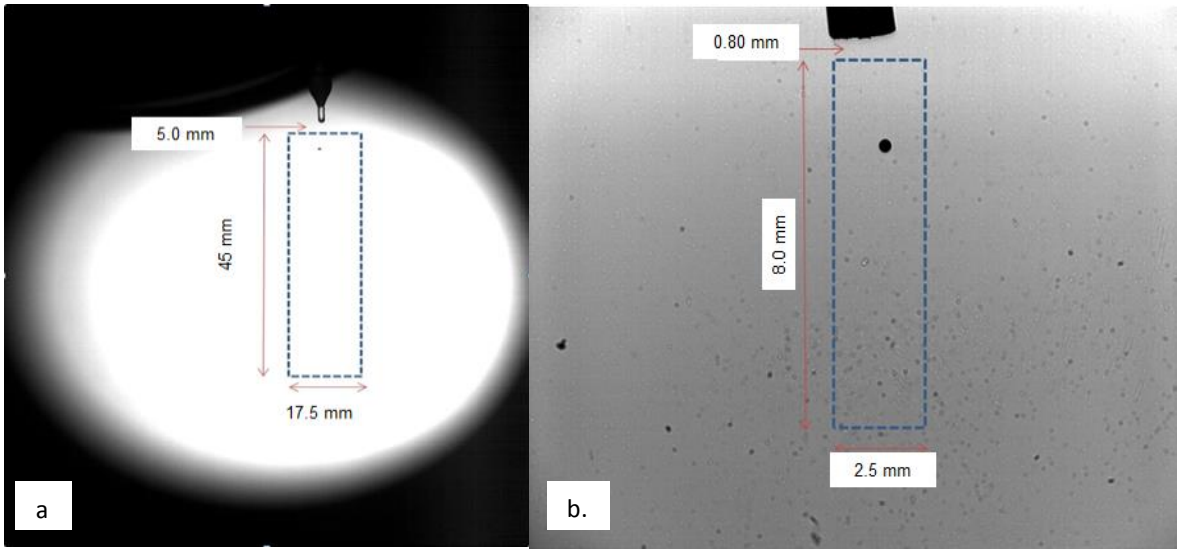

Figure 3.4. Region of interest (ROI) (blue dotted rectangle) (a) with the macro video zoom lens and xenon light with 120 grit diffuser at 15 µs exposure time, and (b) with the K2/SC long-distance microscope lens and xenon light without a diffuser at 5 µs exposure time

3.2.4 Accuracy of the droplet size measurement

In order to determine the correct droplet size and ensure measuring accuracy, the exact pixel size must be known for both lenses. For the macro video zoom lens, the focal length and pixel size were calculated with the following equations:

$$Focal\ length\ = \frac{Working\ distancex\ CMOS\ width}{Object\ width + CMOS\ width} \quad \text{Eq. 3.4}$$

$$Pixel\ size = \frac{Camera\ pixel\ resolution\ x\ Working\ distance}{Focal\ length} \quad \text{Eq. 3.5}$$

where the CMOS width for this 25.4 mm (1 in.) camera sensor was 12.8 mm (www.idtvision.com).

For the K2/SC long-distance microscope lens, multiple images of a Halcon ceramic calibration plate (2.5 mm x 2.5 mm) were taken to ensure coverage of the whole FOV using the xenon light as a front light. The resulting images were processed with HDevelop software (version 8.0, GmbH, MVTec Software GmbH, München, Germany) to determine the actual pixel size.

The size of the droplets produced in the DOD mode with the droplet generator was measured using the image processing algorithms, discussed in detail in Chapter 4. To validate the droplet size measurement accuracy of the imaging system, the measured value was compared with the actual droplet size by collecting and weighing 100 droplets at the same nozzle settings in a Petri dish. This Petri dish was covered with Parafilm during this test to prevent evaporation. The test was performed in a climate controlled room at 20°C and 47% RH. The measurement was repeated 5 times.

3.2.5 Statistical analysis

The statistical analysis was carried out separately for each of the two lenses. To test the effects of the different combinations of the two diffusers and no diffuser, the exposure times, and the three lighting systems (independent variables) on the entropy ratio, contrast ratio and SNR ratio (dependent variables), an analysis of variance (ANOVA) was performed. In addition to the main effects, all two-way and three-way interactions were tested. A p-value of 0.05 was considered statistically significant. Non-significant interactions were removed from the model. The test was performed in SPSS Statistics 19 (IBM, Armonk, USA).

Significant differences were assessed using the Scheffé and Student–Newman-Keuls (SNK) post hoc tests.

3.3 RESULTS AND DISCUSSION

The different image acquisition systems were evaluated based on the following criteria: image quality parameters (including entropy ratio, contrast ratio, and SNR), light stability and overexposure ratio, and accuracy of the droplet size measurement.

3.3.1 Image quality parameters

Entropy ratio, contrast ratio, and SNR for the different image acquisition systems are presented in Figure 3.5 for the macro video zoom lens and in Figure 3.6 for the K2/SC long-distance microscope lens. For the macro video zoom lens (Figure 3.5, Table A1), no significant effect on the entropy ratio of the three-way interaction light x diffuser x exposure time ($p=0.077$) was found, but the two-way interactions light x diffuser ($p=0.019$) and light x exposure time ($p<0.001$) did have significant effect. For the two-way interaction diffuser x exposure time, a p value of 0.06 was found. Post hoc test revealed that, at 15 µs exposure time, the combinations spotlight x 120 grit diffuser and spotlight x 220 grit diffuser had significantly higher entropy ratios than the other combinations. For these two image acquisition set-ups, no significant difference in entropy ratio was found.

For the contrast ratio, the three-way interaction light x diffuser x exposure time was significant ($p<0.001$). Similar to the entropy ratio, the combinations spotlight x 120 grit diffuser x 15 µs exposure time ($p<0.001$) and spotlight x 220 grit diffuser x 15 µs exposure time ($p<0.001$) had significantly higher contrast ratios than all other combinations. The same conclusion was found for SNR: the combinations spotlight x 120 grit diffuser x 15 µs exposure time ($p<0.001$) and spotlight x 220 grit diffuser x 15 µs exposure time ($p<0.001$) had significantly higher SNR than all other combinations.

These results show that for all three image quality parameters, the best results for the macro video zoom lens were found when using the spotlight in combination with a diffuser and an exposure time of 15 µs. No significant differences were found between the two types of diffusers. Therefore, the combinations spotlight x 120 grit diffuser x 15 µs exposure time and spotlight x 220 grit diffuser x 15 µs exposure time were selected for further analysis.

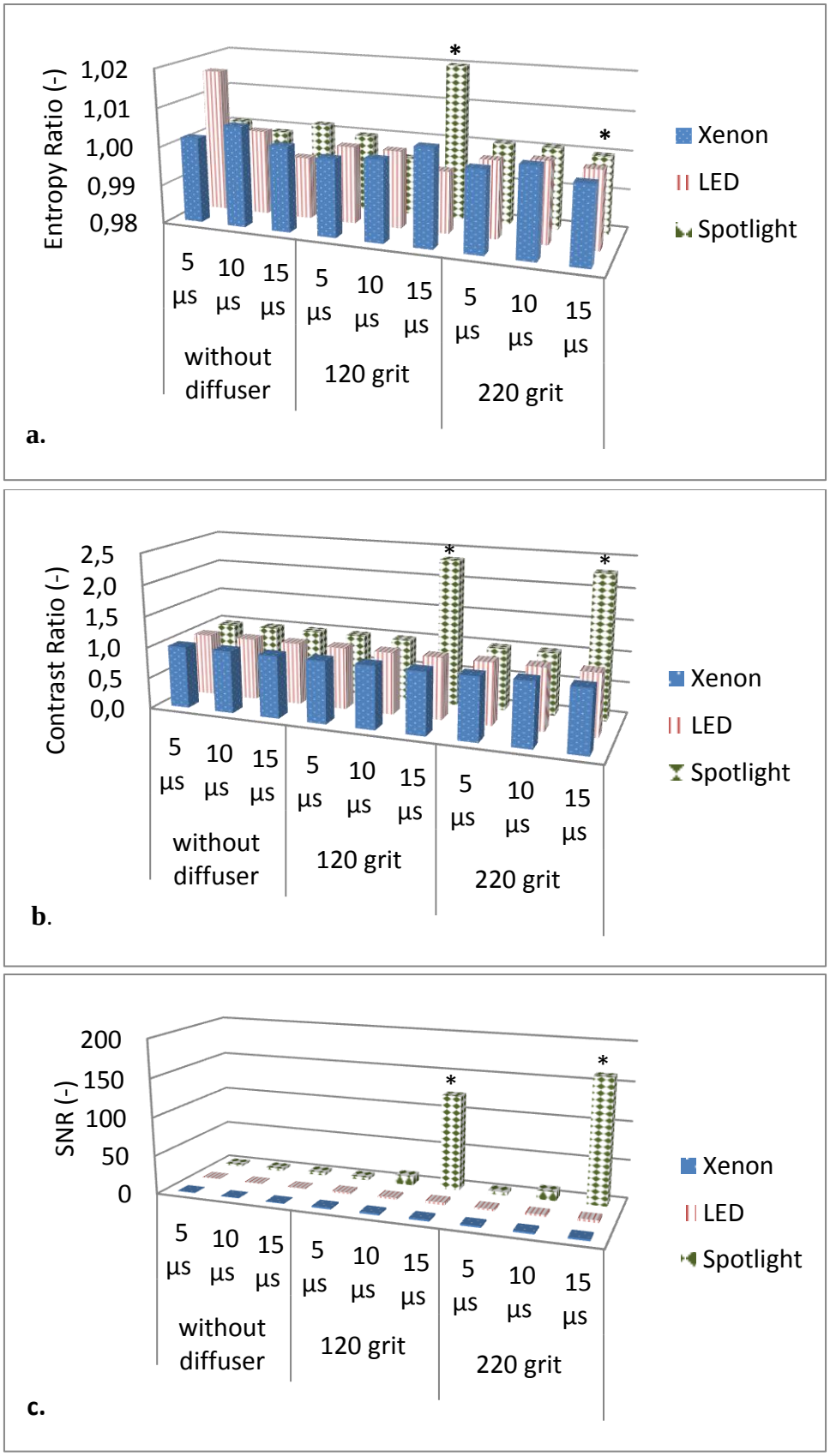

Figure 3.5. Image quality parameters (entropy ratio (a), contrast ratio (b) and SNR (c)) for the macro video zoom lens for different exposure times and lighting systems. Bars with asterisks Mean values are statistically different: * = $p<0.05$ (Scheffé test).

For the K2/SC long -distance microscope lens (Figure 3.6, Table A2), the three-way interaction *light x diffuser x exposure time* was significant for the entropy ratio ($p<0.001$) as well as for the contrast ratio ($p<0.001$). In both cases, the Scheffé post hoc tests revealed that the combination *xenon x no diffuser x 15 µs exposure time* ($p<0.001$) had significantly higher ratios than all other combinations. For the SNR, the Scheffé test confirmed that the combination *xenon x no diffuser x 15 µs exposure time* ($p< 0.001$) had higher values than all other combinations, while the SNK test showed that the combination *xenon x no diffuser x 10 µs exposure time* ($p< 0.001$) outperformed all others.

These results show that the best results with the K2/SC long-distance microscope lens were always obtained with the xenon light source without a diffuser. For this set-up and depending on the statistical test used, the best exposure time was 10 or 15 µs based on the image quality parameters. With the combination x*enon x no diffuser x 10 µs exposure time* was selected for further analysis because images taken with the 15 µs exposure time were visually found to be partly overexposed, which might affect the accuracy of the droplet size measurement. Additionally, the combination *LED x no diffuser x 5 µs* was selected as the best low cost alternative for the expensive xenon light based on the relatively good image quality parameters, although it was not statistically significant.

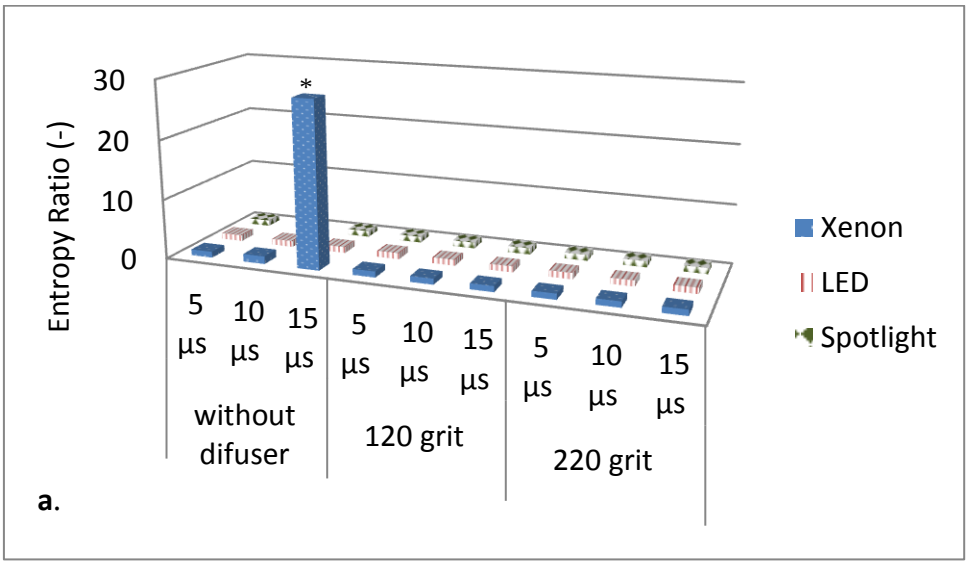

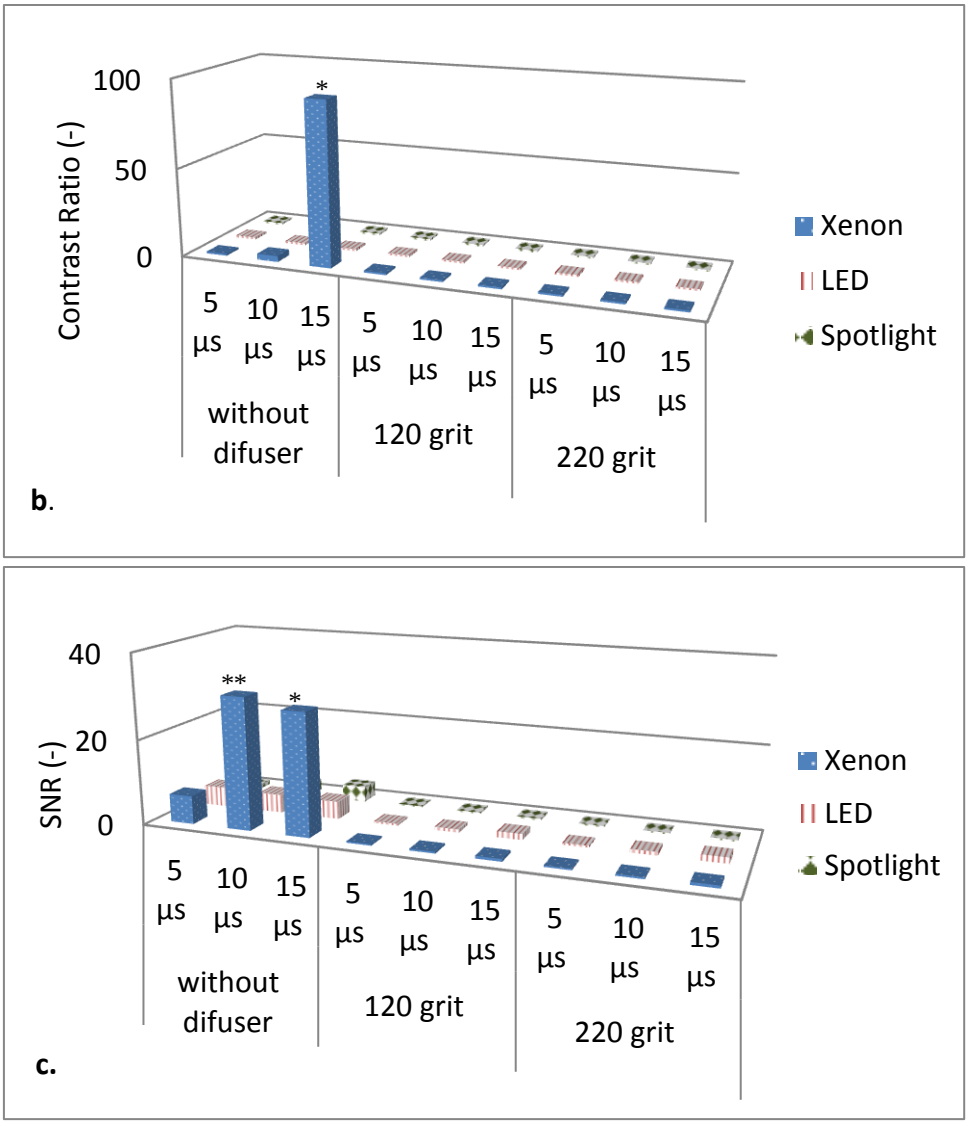

Figure 3.6. Image quality parameters (entropy ratio (a), contrast ratio (b) and SNR (c)) for the K2/SC long-distance microscope lens for different exposure times and lighting systems. Bars with asterisk are statistically different: * = $p<0.05$ (Scheffé test) and ** = $p<0.05$ (SNK test)

3.3.2 Light stability and overexposure ratio

An appropriate image acquisition set-up for droplet characterization must be capable of delivering an adequate, even and stable illumination without over- or under-exposed areas. In order to achieve this, the previously selected image acquisition techniques were tested for their light stability and overexposure ratio based on image histograms of ten consecutive images without a droplet (Figure 3.7). The histograms of both spotlight configurations at 15 µs exposure time (Figure 3.7a and b) showed light instability, as the curves of different frames did not overlap and were partially overexposed. Because the spotlight was used without AC/DC converter, light instability was also present for the shorter exposure times of

5 and 10 µs; however, reducing the exposure time reduced the overexposure ratio (results not shown).

On the other hand, the use of the LED lighting with the K2/SC long-distance microscope lens at 5 µs gave rise to a clear and stable peak around a gray level of 40 but with relatively dark images (Figure 3.7c). The xenon light at 10 µs exposure time appeared stable but the images were overexposed (Figure 3.7d; note the different scale of the *y*-axis in this figure).

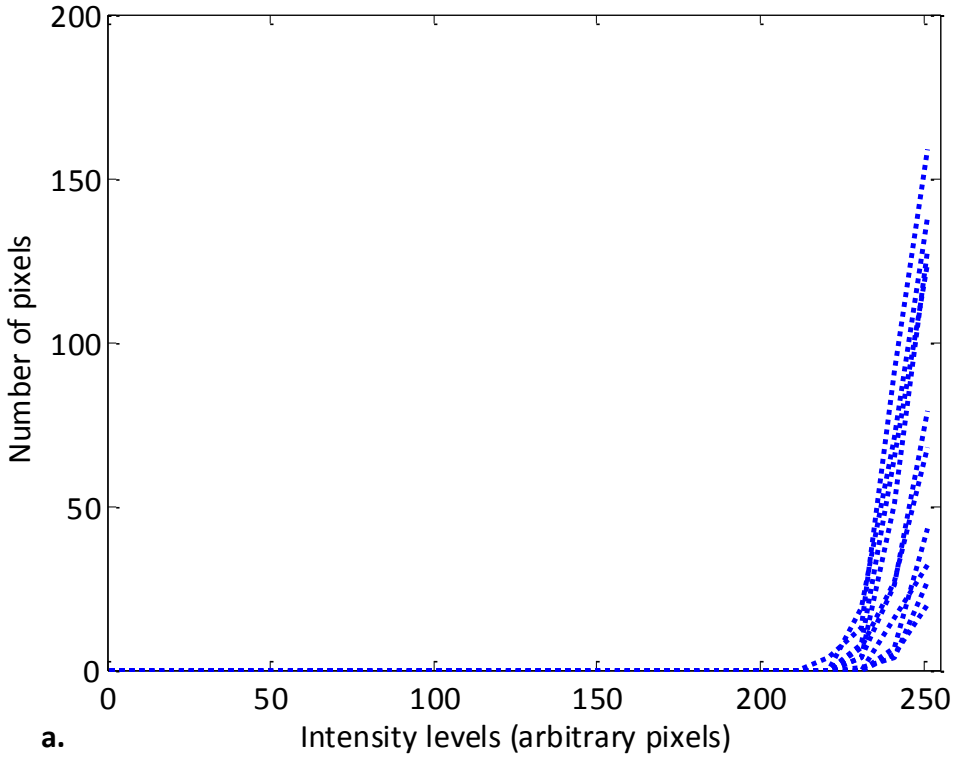

a.

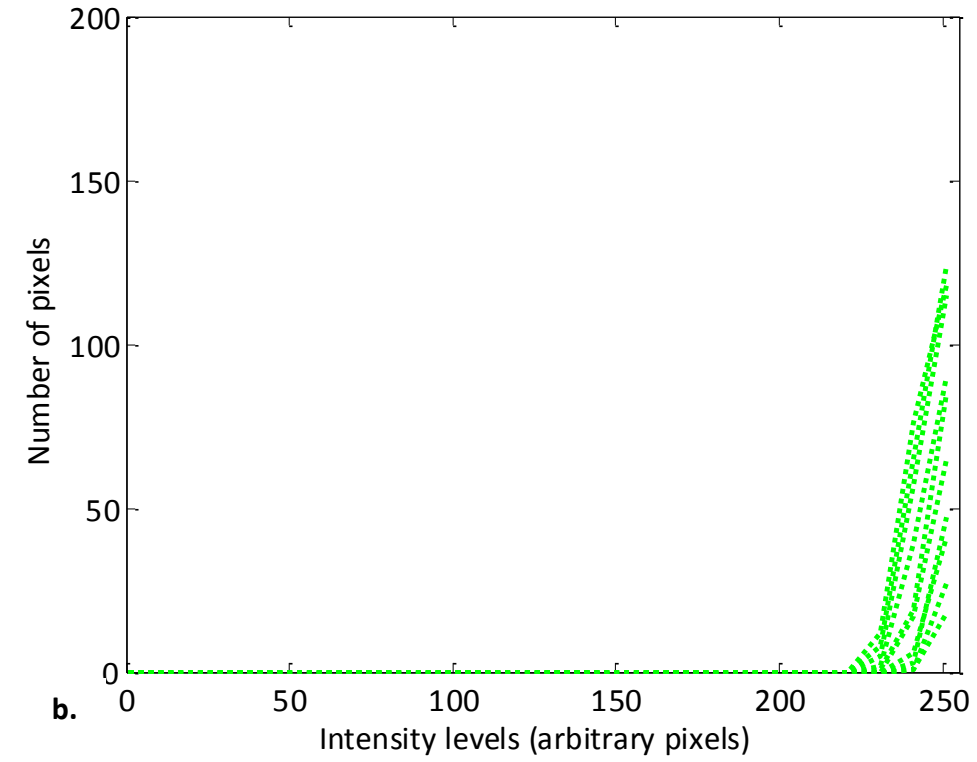
200
150
100
50
0
Number of pixels
0
50
100
150
200
250
Intensity levels (arbitrary pixels)

b.

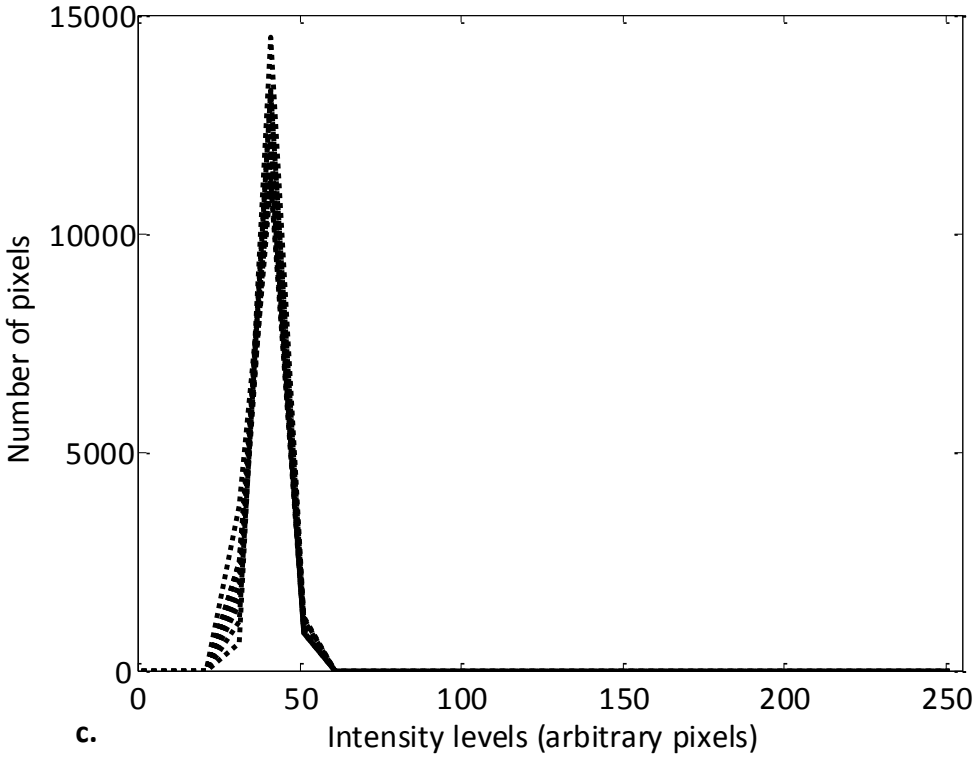
15000
10000
5000
0
Number of pixels
0
50
100
150
200
250
Intensity levels (arbitrary pixels)

c.

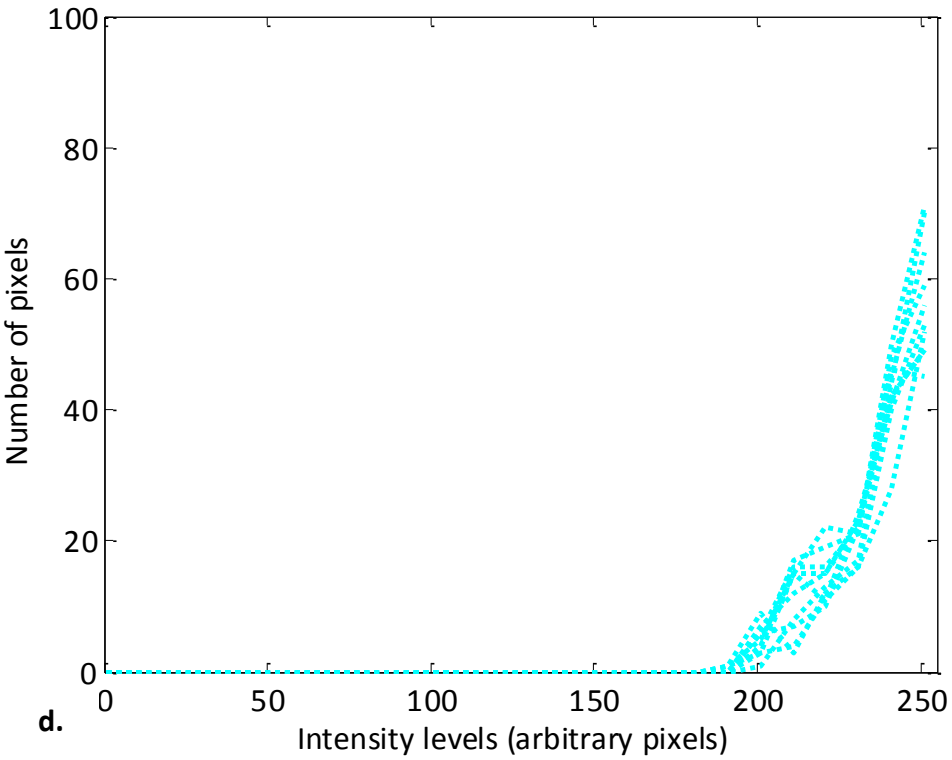

Figure 3.7. Histograms of ten consecutive images for four imaging set-ups: (a) macro video zoom lens x spotlight x 120 grit diffuser x 15 µs, (b) macro video zoom lens x spotlight x 220 grit diffuser x 15 µs, (c) K2/SC long distance microscope lens x LED x no diffuser x 5 µs and (d) K2/SC long distance microscope lens x xenon x no diffuser x 10 µs

Therefore, additional experiments were included to calculate the image quality parameters with reduced exposure times of 6, 7, 8 and 9 µs using the xenon light (Figure 3.8a). Increasing the exposure time considerably increased the SNR and contrast ratio. No correlation was found between the exposure time and the entropy ratio. At the same time and for droplets produced at the same settings, increasing the exposure time reduced the measured droplet size and increased the variation in measured droplet size (Figure 3.8b) because of the effect of overexposure. To find the optimal exposure time, image histograms were taken with the K2/SC long-distance microscope lens and xenon light at different exposure times and are presented in Figure 3.9. This figure shows that a 6 µs exposure time is optimal as it gives the brightest images without any overexposure, and the complete histogram is in-between the 256 intensity levels. In addition, because of the absence of overexposure, no reduction of measured droplet size was observed at 6 µs (Figure 3.8b).

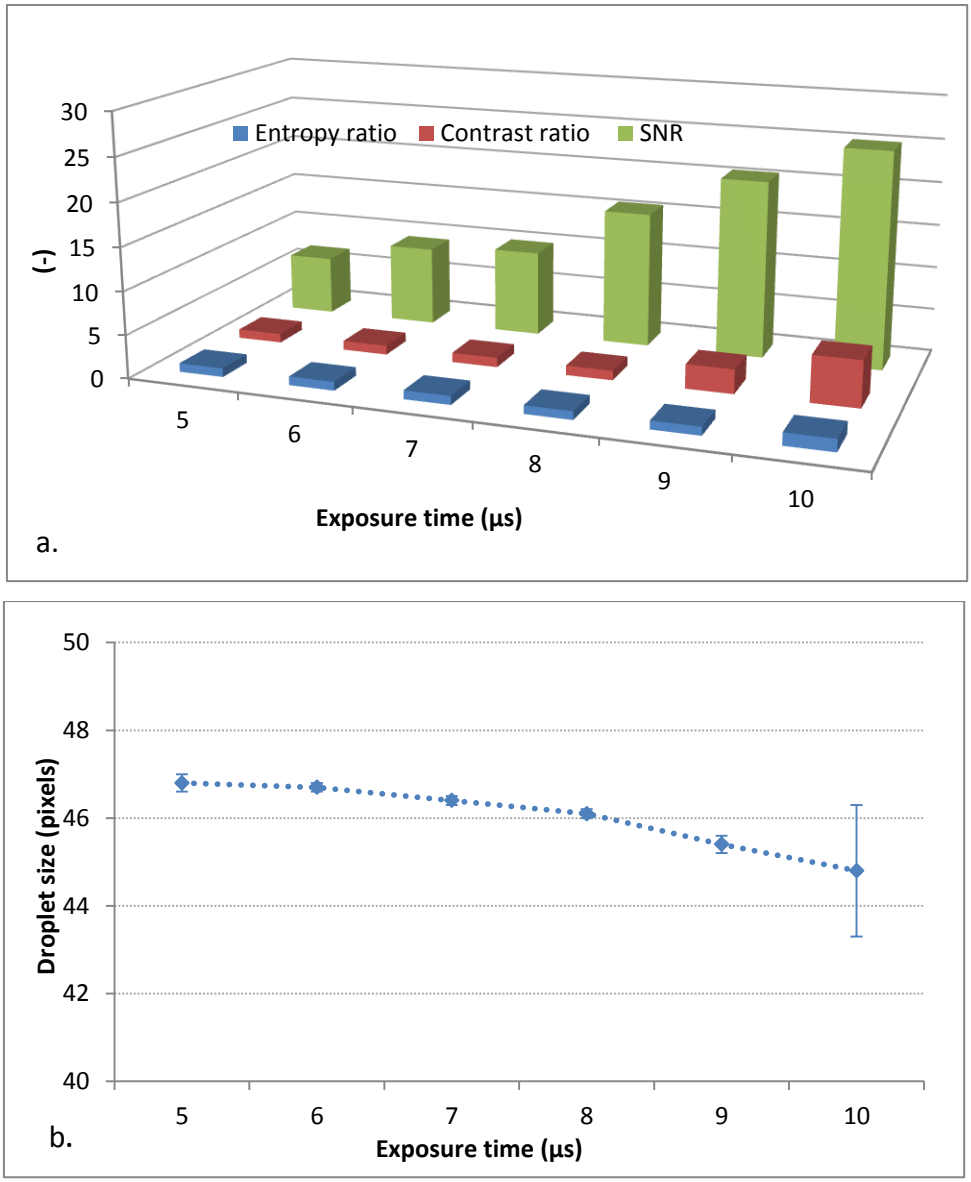

Figure 3.8. (a) Image quality parameters for K2/SC long-distance microscope lens, xenon light, without diffuser at 5, 6, 7, 8, 9 and 10 µs exposure time and (b) effect of exposure time on droplet diameter measurement

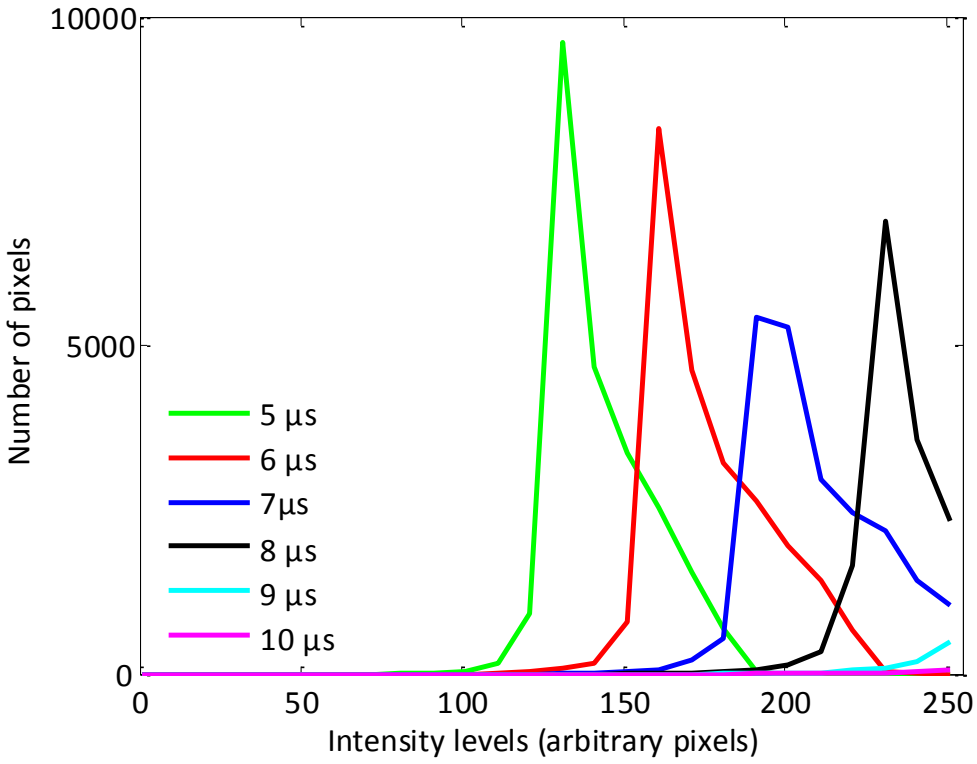

Figure 3.9. Image histograms using the K2/SC long-distance microscope lens and xenon light with no diffuser at 5, 6, 7, 8, 9 and 10 µs

3.3.3 Accuracy of the droplet size measurement

From the camera calibration, the calculated pixel size for the set-up with the macro video zoom lens was 85.8 µm. This is too big to measure droplet size accurately, knowing that droplet sizes in a pesticide spray might vary from only a few micrometres up to 1000 µm. Hence, this set-up cannot be used for accurate droplet size measurements, but it can be useful for tracking droplets over longer distances and for measuring macro-spray characteristics, as it is done in Chapter 7.

For the K2/SC long distance microscope lens, the output of the HDevelop software gave a focal length of 67.1 mm, corresponding to a pixel size of 8.2 µm and an image size of 10.5 mm x 8.4 mm for the 1280 x 1024 pixel images. Moreover, at 6 µs exposure time, the droplets moved less than a pixel between frames, which ensured the absence of blurring effects (Ju *et al.*, 2012).

The actual average droplet diameter based on weighing 100 droplets was 386.2 ± 6.7 µm, while a value of 390.2 ± 4.0 µm was found from the image analysis. Hence, the overall precision of the measurements was satisfactory, with a relative measurement error of about 1% and an absolute error of about 4 µm (1/2 pixel). This droplet size was big enough to be measured with both image acquisition set-ups. Assuming a constant absolute error, the relative error will be larger while measuring smaller droplet sizes and smaller for bigger droplet sizes.

3.4 CONCLUSION

The development of an imaging system based on single droplet experiments was presented using a high speed camera and a piezoelectric droplet generator. Different lenses, light sources, diffusers, and exposure times were tested. The different imaging systems were evaluated based on image quality parameters (SNR, entropy ratio and contrast ratio), light stability and overexposure ratio and the accuracy of the droplet size measurement. The experiments resulted in a good image acquisition and processing system for accurate spray characterization.

The optimal set-up for measuring micro spray characteristics (droplet size and velocity) consisted of a high speed camera with a 6 µs exposure time, a microscope lens at a working distance of 430 mm resulting in a FOV of 10.5 mm x 8.4 mm, and a xenon light source used as a backlight without diffuser. This set-up is used in Chapter 5 for single droplet characterization and in Chapter 6 for measuring micro spray characteristics.

The HS camera with a macro video zoom lens at a working distance of 143 mm with a larger FOV of 88 mm x 110 mm in combination with a halogen spotlight and a diffuser was found to have the best potential for measuring macro spray characteristics, such as droplet trajectory, spray angle, and spray shape. With this system, attention should be paid to the light stability. This set-up is used in Chapter 7 to measure macro spray characteristics.

The developed image acquisition systems can be used to visualize and determine the micro and macro spray characteristics of real pesticide sprays in an accurate and non-intrusive way as shown in next chapters. In addition, they offer the possibility of studying droplet and spray impact behavior as done by Zwertvaegher et al. (2014). Future work should focus on

further improving the droplet measuring accuracy (e.g., sub-pixel accuracy, calculating depth of field, non-spherical particles, etc.) because of the small, fast droplets in real spray.

4 IMAGE ANALYSIS ALGORITHMS FOR SINGLE DROPLET CHARACTERIZATION[iii]

This chapter presents the development of image analysis and image processing algorithms to evaluate the characteristics of a single droplet like droplet diameter and velocity as it is done in Chapter 5. The image acquisition system for micro-spray characteristics presented in Chapter 3 was used. Droplets were generated by a piezoelectric droplet generator in two modes: droplet on demand (DOD) and continuous mode. The presented algorithms also serve as a basis for the image based spray characterization presented in Chapter 6.

[iii] This chapter has been partially compiled from:

Vulgarakis Minov S, Cointault F, Vangeyte J, Pieters J G, Nuyttens D. 2013. Measurement of single droplet characteristics using high speed imaging techniques. Proceedings of the IASTED International Conference on Signal Processing, Pattern recognition and Applications (SPPRA). February 12-14, Innsbruck, Austria. 321-326. DOI: 10.2316/P.2013.798-058 (*Awarded as a Best Student Paper*).

4.1 INTRODUCTION

As described in Chapter 2, both spray droplet size and velocity affect the efficiency of pesticide spray applications. Better knowledge and control of spray droplet characteristics may lead to reduction of pesticide usage and so reduce the environmental impact. For this reason, accurate spray droplet quantification techniques are needed. However, spray droplet diameters are small and cover a wide range of diameters (10-1000 µm). Consequently, it is necessary to magnify the images of the droplets in order to measure their size accurately. As droplets are translucent, a backlight must be used and because of the specific characteristics of this technique and application, a high power light source is needed. Additionally, spray droplets are fast (from 1 to 15 m/s and even faster) which means that high-speed cameras with a frame rate between 500 and 1000 frames/s are needed to capture the droplet movement. An exposure time of only a few µs is allowed, to record a small droplet at a considerable velocity with sufficient sharpness and contrast. This can be realized with a suitable shutter time of the camera. An image acquisition set-up fulfilling the above requirements was developed in Chapter 3 consisting of a high speed camera with a 6 µs exposure time, a microscope lens at a working distance of 430 mm resulting in a field of view (FOV) of 10.5 mm x 8.4 mm and a xenon light source without diffuser used as a backlight. A second requirement to come to an accurate droplet characterization is the use of dedicated image analysis algorithms.

This chapter presents the developed image analysis and processing algorithms for measuring the single droplet characteristics (size and velocity). Droplets were generated by a droplet generator, as described in detail in 3.2.1, in 2 modes: DOD and continuous mode.

4.2 DROPLET CHARACTERIZATION WITH IMAGE ANALYSIS

Tracking and sizing the droplets in DOD and continuous mode were based on the object tracking algorithm (Jain & Nagel, 1979; Baek & Lee, 1996; Lecuona *et al.*, 2000; Maggio & Cavallaro, 2011; Castanet *et al.*, 2013) using image processing algorithms developed in Matlab (2011b). Once the images were acquired by the HS camera, a sequence of steps were employed to process and analyze these images, i.e. image pre-processing (4.2.1), image segmentation (4.2.2), droplet extraction and sizing (4.2.3), droplet tracking

(4.2.4) and saving the results (4.2.5). The flow chart of the image analysis algorithm is shown in Figure 4.1.

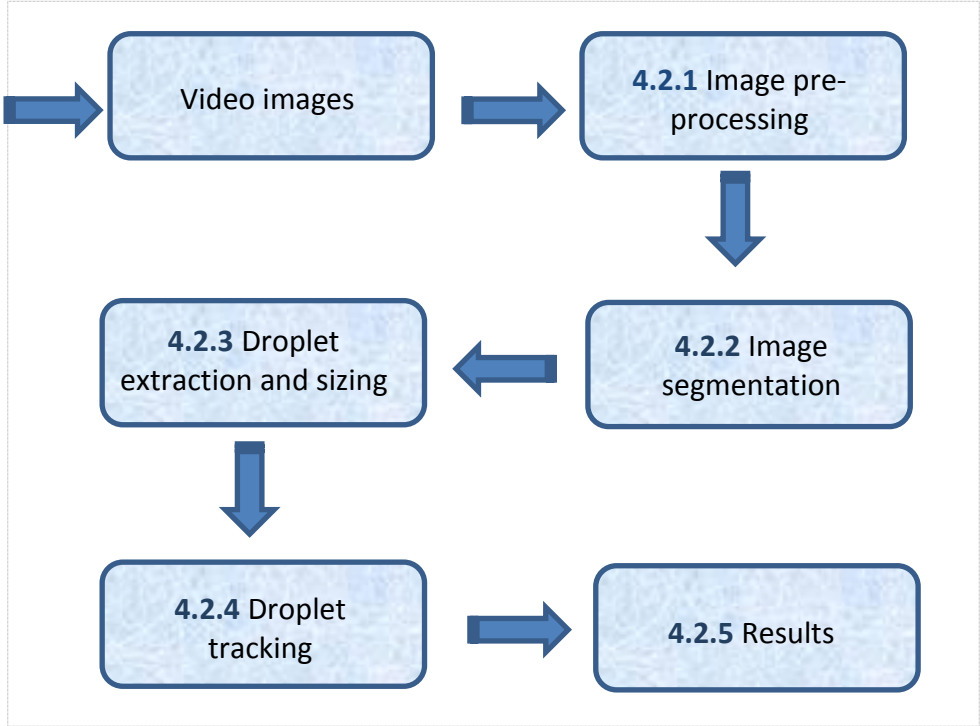

Figure 4.1. Flow chart of the image analysis algorithm for droplet(s) characterization

Images obtained with the image acquisition system presented in Figure 3.2 include droplets generated in DOD (Figure 4.2a) or continuous mode (Figure 4.3a). The nozzle was always kept in the center of the image.

For the DOD images, the complete FOV of 10.5 mm x 8.4 mm (1280 × 1024 pixels) was used at a frame rate of 1000 frames/s. Due to the bigger droplet velocities in continuous mode, a smaller FOV of 3.95 mm x 0.79 mm (480 x 96 pixels) was used in order to be able to increase the frame rate up to 10.000 frames/s. This did not have an influence on the droplet size measurements.

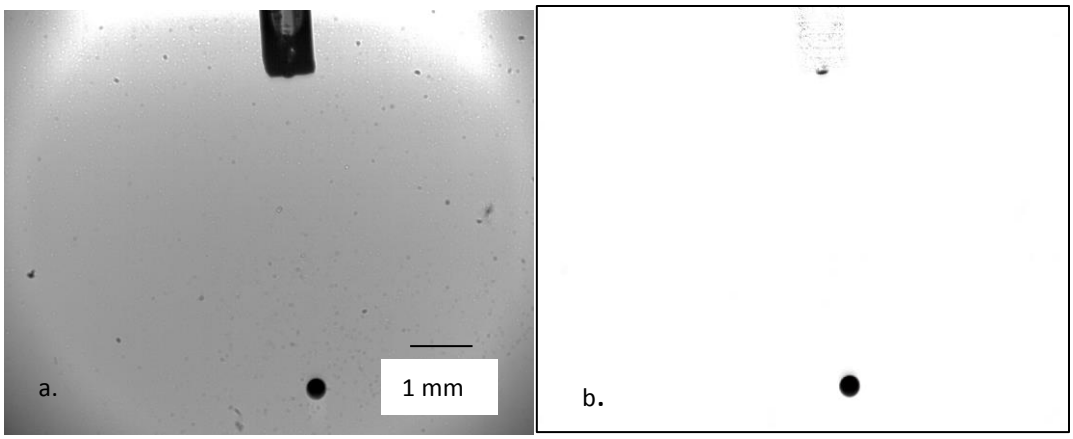

Figure 4.2. Original image (a) and image after pre-processing (b) in DOD

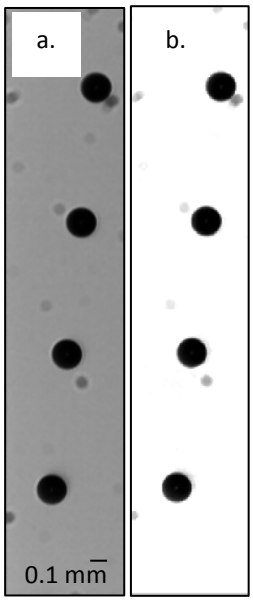

Figure 4.3. Original image (a) and image after pre-processing (b) in continuous mode

4.2.1 Pre-processing the images to enable analysis

The quality of the images obtained by the image acquisition system influences the success of the image processing (Yan *et al.*, 2009). Therefore, image pre-processing techniques are used to improve the quality of an image before further processing, i.e., droplet detection. In literature these techniques are also referred to as filtering and enhancement (Gonzalez *et al.*, 2004). Images with droplets were pre-filtered to remove irrelevant and misleading image information like lighting patterns or dirt on the lens (Figure 4.2 and Figure 4.3).

In order to detect, segment and track droplets automatically in videos, several approaches exist. For images obtained using the single droplet generator, a background subtraction

algorithm was used which compares a static background image without droplet(s) with the images with droplet(s), pixel by pixel. The purpose of this algorithm is to distinguish moving droplets from the static parts of the scene, i.e., nozzle, dust, etc. by differencing (Barnich & Droogenbroeck, 2011; Evangelio, 2014). In addition, after background subtraction, the image contrast is adjusted by mapping the values of the pixels to new values such that 1% of the pixels are saturated (Gonzalez *et al.*, 2004). Examples of images before (Figure 4.2a and Figure 4.3a) and after pre-processing (filtering and background subtraction) (Figure 4.2b and Figure 4.3b) are shown..

4.2.2 Image segmentation

The purpose of using image segmentation was to subdivide the image into its background and into connected pixels for further analysis, i.e., droplet(s).

Segmentation algorithms can be categorized among two important types: gray level similarity detection among pixels (thresholding) and discontinuity or edge detection (Gonzalez *et al.*, 2004). A histogram-based thresholding segmentation technique was used for segmenting images from the single droplet generator into droplets and background (4.2.2.1) and is used in Chapter 5. The second category of segmentation algorithms, involved finding abrupt changes in gray level in order to detect droplet edges in real spray images (4.2.2.2). This edge detection technique was therefore used in Chapter 6.

4.2.2.1 Histogram-based thresholding

The histogram is a graph showing the number of pixels in an image at each different intensity value found in that image. For an 8-bit grayscale image there are 256 different possible intensities. Hence, the histogram will graphically display 256 numbers showing the distribution of pixels amongst those grayscale values.

Here a bi-modal thresholding was applied to extract the droplet from its image background. The histogram was clearly bimodal: two peaks corresponding with the droplet and background regions and a valley in between (Figure 4.4). The valley point is usually chosen as the threshold. In bimodal thresholding all gray values greater than threshold *T* are assigned to the *background* and all other gray values are assigned to the foreground (*droplet),* thus separating the droplet pixels from the background pixels (Acharya & Ray, 2005).

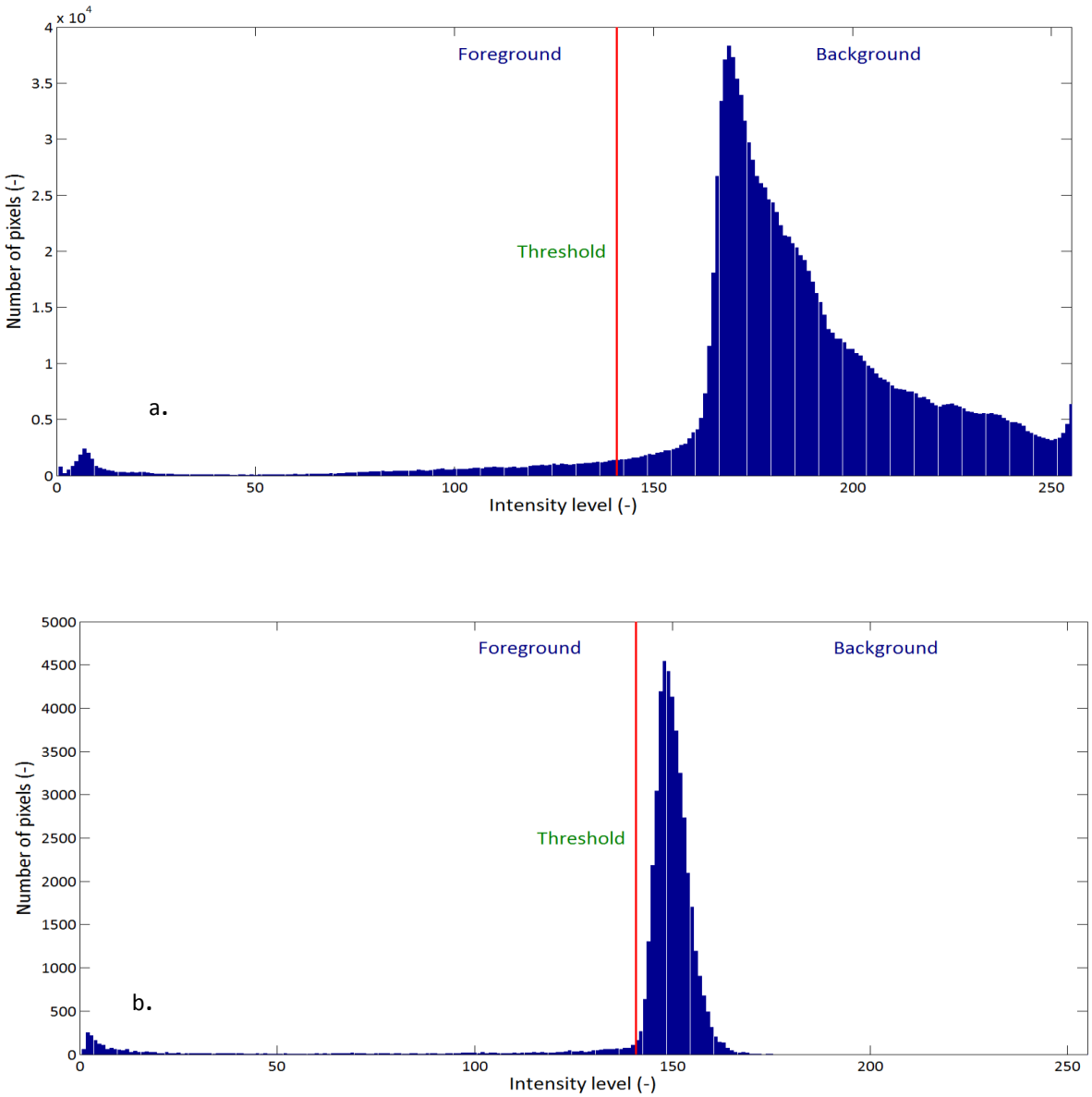

Figure 4.4. Bi-modal histogram for image in (a) DOD mode and (b) continuous mode both with a threshold value of 55%

The threshold value is expressed in % of the maximum intensity level value as shown in Figure 4.4. There have been many thresholding methods that used the criterion-based concept to select the most suitable gray scale as a threshold value (Gonzalez *et al.*, 2004). However, in order to apply a good segmentation, the optimal static threshold value in this study (Figure 4.4) was selected based on droplet size measurements in DOD mode. Threshold values ranging from 30 to 60% (in step of 5%) were tested as shown in Table 4.1.

Table 4.1.Droplet size measurements in DOD mode with nozzle 2 for t_a =0.4 ms, t_p =50 ms, $V_{p=}$ ± 4.5 V applying different threshold values

Threshold value (%)	Droplet size (µm)
30	382.3
35	388.0
40	393.8
45	399.4
50	407.6
55	415.5
60	418.1

A static threshold T of 55 % of the intensity image value was selected to binarize the images. A bigger threshold value did not separate the droplet from the background (Figure 4.5c, Figure 4.6c). A smaller value underestimated the droplet size (Figure 4.5a, Figure 4.6a, Table 4.1). Furthermore; examples with different threshold values for both modes are given in Figure 4.5 and Figure 4.6.

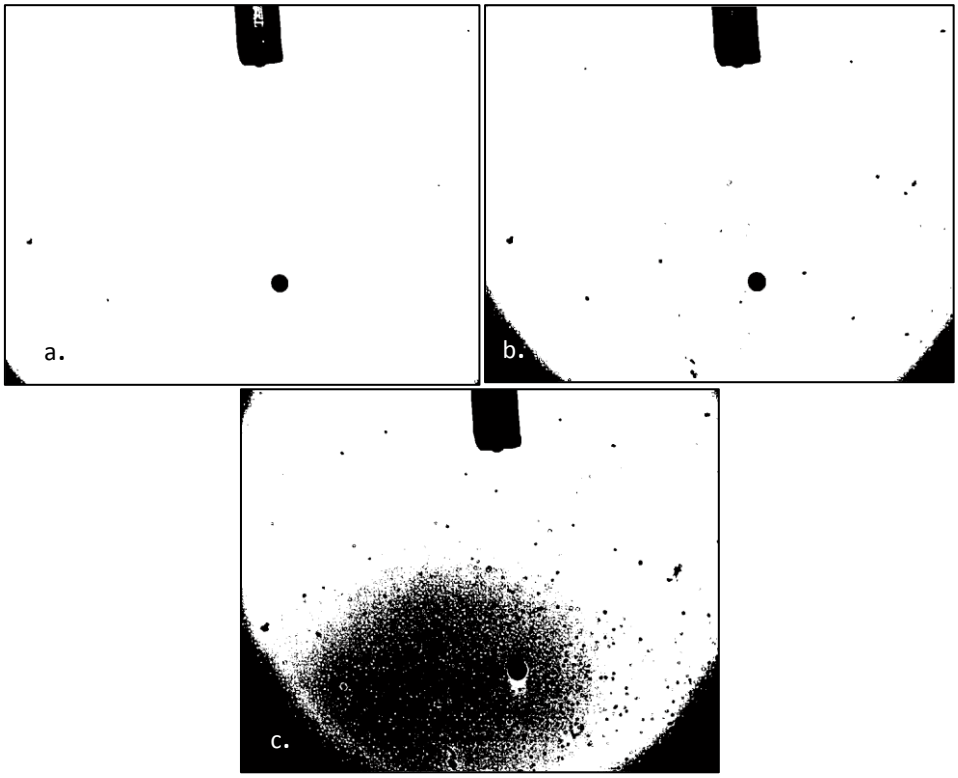

Figure 4.5. DOD droplet images after thresholding at a) 30 %, b) 55% and 60% of the mean intensity value

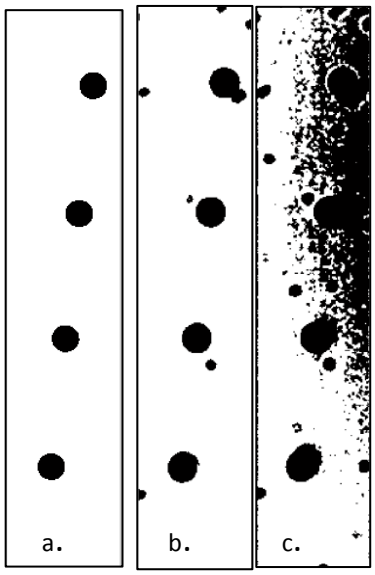

Figure 4.6. Continuous mode droplet images after thresholding of a) 30 %, b) 55% and c) 60% of the of the mean intensity value

4.2.2.2 Edge detection technique

The edge detection approach is a technique to detect significant local changes in the intensity level in an image. The change in intensity level is measured by the gradient of the image (Acharya & Ray, 2005). Since an image *f(x, y)* is a two dimensional function, its gradient is a vector:

$$\nabla f = \begin{bmatrix} G_x \\ G_y \end{bmatrix} = \begin{bmatrix} \frac{\partial f}{\partial x} \\ \frac{\partial f}{\partial y} \end{bmatrix} \quad \text{Eq. 4.1}$$

where G_x and G_y are the partial derivatives in the horizontal and vertical directions of the image. The magnitude of this vector provides information about the strength of the edge:

$$|\nabla f| = \left(G_x^2 + G_y^2\right)^{1/2} \quad \text{Eq. 4.2}$$

The direction of the gradient is:

$$\Theta(\mathrm{x},\mathrm{y}) = \tan^{-1}\left(G_y \Big/ G_x\right) \qquad \text{Eq. 4.3}$$

where the angle *Θ* is measured with respect to the X-axis. Gradient operators compute the change in gray level intensities and also the direction in which the change occurs. This is calculated by the difference in values of the neighboring pixels, i.e., the derivatives along the X-axis and the Y-axis (Acharya & Ray, 2005). For a two-dimensional image the gradients are calculated as:

$$\begin{aligned} G_x &= f(i+1,j) - f(i,j) \\ G_y &= f(i,j+1) - f(i,j) \end{aligned} \qquad \text{Eq. 4.4}$$

Gradient operators require two masks, one for the X-direction gradient and one for the Y-direction gradient. These two gradients are combined to obtain a vector quantity whose magnitude represents the strength of the edge gradient at a point in the image and whose angle represents the gradient angle (Acharya & Ray, 2005). An alternative approach for calculating edge gradients involves convolving the image with a set of edge masks (kernels) (Figure 4.7). A mask is a small matrix useful for blurring, sharpening, edge detection and etc.

Each mask corresponds to the edges in the X or Y direction. Thus, the process consists of moving the filter mask from point to point in an image and multiplying each pixel in the image by a corresponding coefficient from the mask and then summing the result to obtain the response at each point (*x, y*) (Eq. 4.5). In Figure 4.7 an example is given with a 3 x 3 mask and the image section directly under it.

$$\begin{aligned} f(i,j) = {} & m_{11}\, I(i-1,j-1) + m_{12}\, I(i-1,j) + m_{13}\, I(i-1,j+1) \\ & + m_{21}\, I(i,j-1) + m_{22}\, I(i,j) + m_{23}\, I(i,j+1) \\ & + m_{3\,1}\, I(i+1,j-1) + m_{32}\, I(i+1,j) + m_{33}\, I(i+1,j+1) \end{aligned} \qquad \text{Eq. 4.5}$$

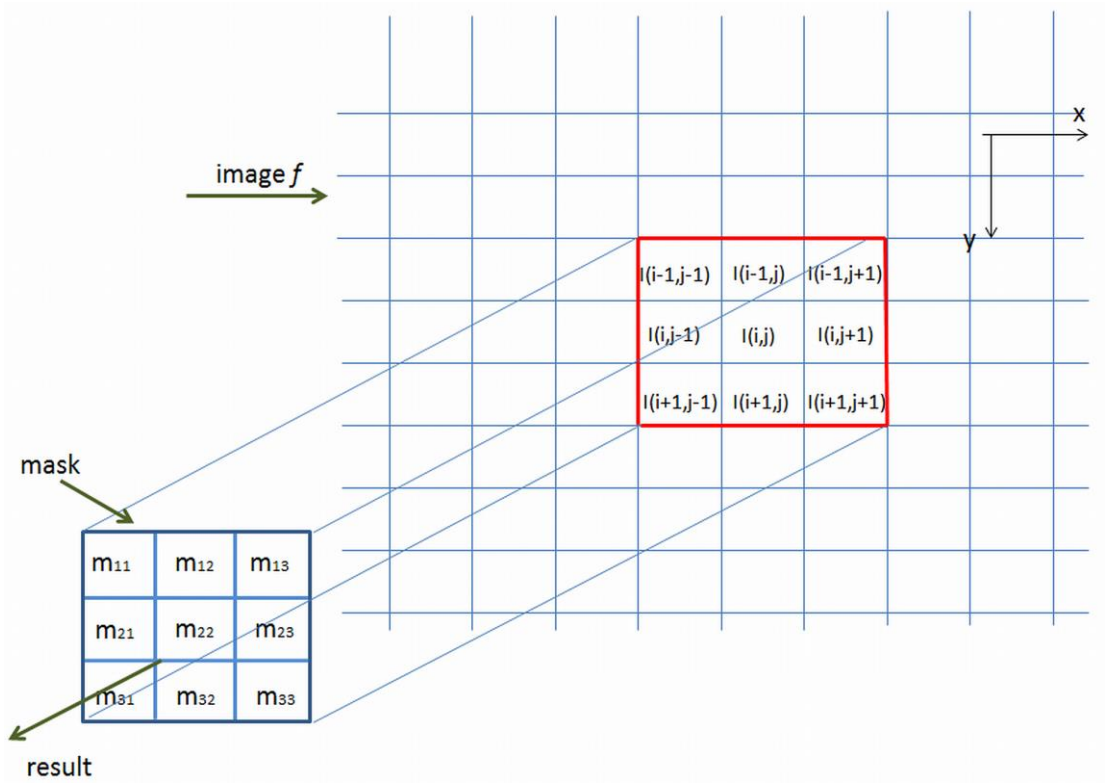

Figure 4.7. Concept approach for calculating the edge gradient of pixel I(i,j) from image f using a 3 x 3 mask

An ideal edge detector is needed to detect an edge point precisely. The decision regarding the existence of an edge point is based on a threshold. Hence, if the magnitude of the gradient is above a threshold, then an edge point exists at that point, else, there is no edge point. The goal of an ideal edge detector is to choose the threshold appropriately (Acharya & Ray, 2005).

There are numerous edge-finding algorithms based on a single derivative with different masks (Ziou & Tabbone, 1998; Gonzalez *et al.*, 2004; Umbaugh, 2010). Amongst them most important operators are the Robert operator, Sobel operator, Prewitt operator, Canny operator, etc. However, here only those that are used for droplet detection are explained, i.e., Sobel edge detector and Canny edge detector.

- Sobel edge detector

The Sobel edge detector uses two different masks to approximate digitally the first derivatives G_x *and* G_y (Figure 4.8). The left mask is responsible for horizontal edges and the right mask for vertical edges. Typically it is used to find the approximate absolute gradient

magnitude at each point in a grayscale image. The result of using the Sobel edge detector on a droplet image (Figure 4.9a) is shown in Figure 4.9b.

-1	0	+1
-2	0	+2
-1	0	+1

G_x

+1	+2	+1
0	0	0
-1	-2	-1

G_y

Figure 4.8.Filter masks used by Sobel edge detector

- Canny edge detector

Canny edge detector is one of the standard edge detection methods (Canny, 1983) known as the optimal edge detector. The algorithm consists of five separate steps that can detect edges with noise suppression at the same time:

- Smoothing: Blurring of the image to remove noise;
- Finding gradients: The edges should be marked where the gradients (Eq. 4.2) of the image have large magnitudes;
- Non-maximum suppression: Only local maxima should be marked as edges;
- Double-tresholding: Potential edges are determined by thresholding;
- Edge tracking by hysteresis: Final edges are determined by suppressing all edges that are not connected to a very certain edge. A result of using the Canny edge detector is shown in Figure 4.9c.

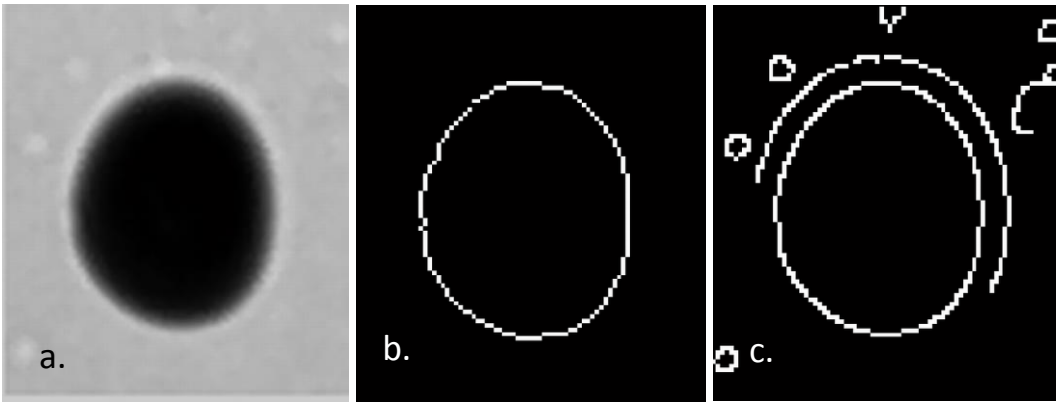

Figure 4.9. Results on droplet edge detection (b) using Sobel edge detector and (c) Canny edge detector

It can be seen that the Canny edge detection (Figure 4.9c) yielded better results than Sobel edge detection (Figure 4.9b). This is because Canny is more robust to noise and accounts for regions in the image. As well, thin lines for its edges by using non maximal suppression and hysteresis with thresholding (Gonzalez *et al.*, 2004).

4.2.3 Droplet extraction and size measurement

Several morphological operations may be applied to the binary images obtained after the image segmentation. Here only the ones that are used for droplet characterization are discussed.

The operations of dilation and erosion are fundamental to morphological image processing. Dilation is an operation that "grows" or "thickens" while erosion "shrinks" or "thins" objects in an image (Gonzalez *et al.*, 2004). The specific manner is controlled by a shape referred to as a structuring element. For droplet characterization a disk structuring element was used. Combining dilation and erosion results into opening, closing and hit-or-miss transformation. For the droplet characterization, a closing transformation was used. The morphological closing is dilation followed by erosion. It tends to smooth the contour of the objects. Also, it joins narrow breaks, fills long thin gulfs, and fills holes smaller than the structuring element. Subsequently, it was possible to apply droplet labelling.

Afterwards, region extraction was performed measuring the properties of the labelled object like: diameter, area, perimeter, orientation and so forth. The droplet area was calculated as the sum of the pixel components and the position of its center was found as the mass center

of the droplet (Figure 4.10, Figure 4.11). Because the droplets were not perfectly spherical when in motion, they were considered as elliptical shapes for the droplet diameter. Their long and short axes were measured to calculate the equivalent droplet diameter from the area (Dong *et al.*, 2013).

The circularity of an object can range from 0 (line) to 1 (circle) and is calculated as follows:

$$circularity = \frac{4 * \pi * area}{perimeter^2} \qquad \text{Eq. 4.6}$$

The calculated circularity based on Eq. 4.6 of the droplets in Figure 4.3 was between 0.93 and 0.95. However, droplets generated by a real spray can be much more elliptical (Lefebvre, 1989). Therefore a lower circularity value of 0.8 was chosen to eliminate objects that are not droplets.

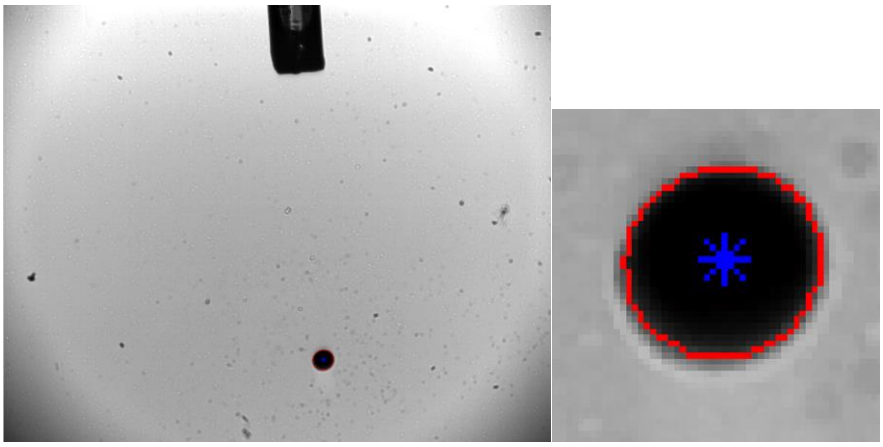

Figure 4.10. Result after droplet extraction, sizing and locating the droplet center in DOD mode (The droplet center is marked with a blue star and the droplet edge is in red)

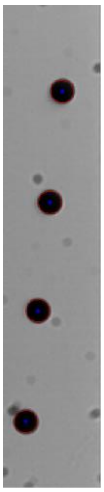

Figure 4.11. Result after droplet extraction, sizing and locating the droplet centers in continuous mode (The droplet centers are marked with a blue star and the droplet edges are in red)

4.2.4 Droplet tracking algorithm

Once the droplet center and position were determined, the next step involved droplet tracking to find the same droplet in two consecutive images, as well as the displacement vector and velocity (Figure 4.12). This is possible because of the large acquisition rate of the HS camera.

The tracking of a droplet begins in image *I* and is extended to the next image by association with a droplet in image *J*. Each track at image *I* can generate few possible ending tracks in image *J*. The droplet velocity can be calculated as (Lecuona *et al.*, 2000):

$$\vec{v}_{ij} = \frac{\vec{d}_{ij}}{\Delta t} = \frac{(X_j - X_i, Y_j - Y_i)}{\Delta t} \qquad \text{Eq. 4.7}$$

where $\vec{d}_{ij}$ and $\vec{v}_{ij}$ are the droplet displacement vector and velocity, respectively. The droplet velocity is calculated as the displacement divided by the time between two exposures (for DOD: 1 frame = 1 ms and for continuous mode: 1 frame = 0.1 ms).

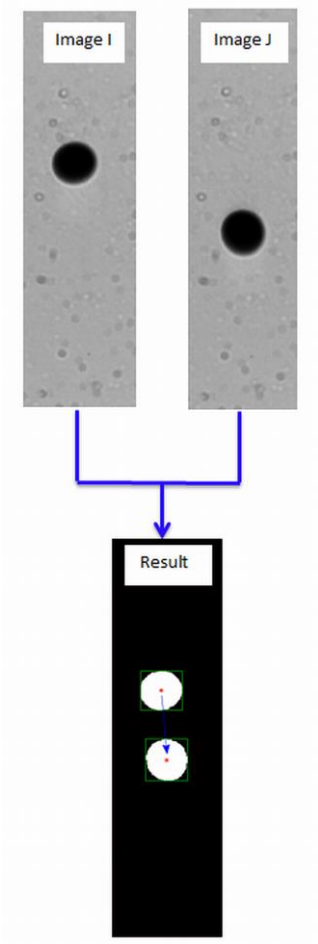

Figure 4.12 Droplet tracking result from two consecutive images in DOD mode.

4.2.5 Results

In the last stage, the algorithm displays the actual droplet diameter by multiplying the droplet size in pixels with the actual pixel size (1 pixel = 8.23 µm). In continuous mode, besides the droplet diameter, it was possible based on the droplet center positions to calculate the inter-droplet spacing. Finally, the droplet velocity was plotted as a function of time as shown in Figure 4.13. In this example, the droplet appeared in the tenth frame and the droplet velocity was increasing with every following frame until the moment when it disappeared from our FOV.

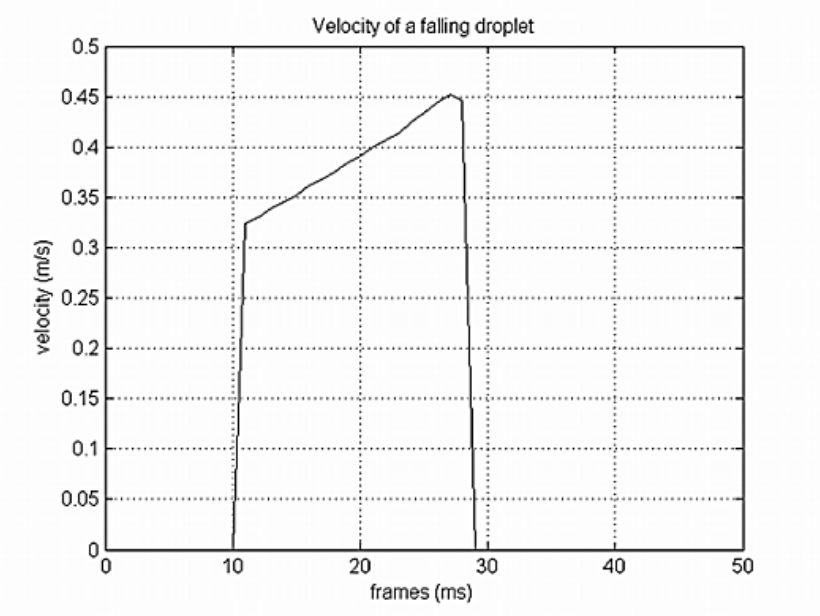

Figure 4.13. Droplet velocity diagram

4.3 CONCLUSION

Image analysis and image processing algorithms in Matlab were developed to evaluate the characteristics of a single droplet. These algorithms are further used in Chapter 5 for droplet characterization in DOD and continuous mode. Furthermore, they are also used as a basis for developing the algorithms for micro-spray characterization of real spray nozzles (Chapter 6).

5 DROPLET GENERATION AND CHARACTERIZATION USING A PIEZOELECTRIC DROPLET GENERATOR AND IMAGING TECHNIQUES[iv]

Accurate spray (droplet) characterization helps in better understanding the pesticide spray application process. The goal of this chapter was to evaluate the characteristics of a single droplet generated using a piezoelectric single droplet generator in 2 modes: Droplet-On-Demand (DOD) and continuous with 4 different orifice sizes. The image acquisition system and the image analysis algorithms developed in Chapters 3 and 4 were used.

[iv] This chapter has been compiled from:

Vulgarakis Minov, S., Cointault, F., Vangeyte, J., Pieters, J.G., and Nuyttens, D., 2015. Droplet generation and characterization using piezoelectric droplet generator and high speed imaging techniques. Crop Protection 69, 18-27.

5.1 INTRODUCTION

The process of generating and controlling small droplets of constant size, form and velocity is necessary to study the behavior of spray droplets before, during and after impact in a controlled and repeatable way (Reichard, 1990). A better understanding of spray droplet behavior and of the complex spray application process can lead to more efficient pesticide usage and a reduction of the environmental impact. Poor accuracy and spray losses may reduce the effectiveness of the application and increase environmental contamination and operator risk (Matthews, 2000). Droplet sizes and velocities are important characteristics in the spray application process, because of their strong influence on droplet impact behavior (Massinon & Lebeau, 2012a; Zwertvaegher *et al.*, 2014), crop coverage (Dorr *et al.*, 2008), biological efficacy of the applied pesticide (Permin *et al.*, 1992; Whisenant *et al.*, 1993) and spray drift risk (Nuyttens et al., 2007a; 2009; 2011).

In general, spray droplet characteristics depend on nozzle type and orifice size (Nuyttens *et al.*, 2007a), liquid properties (De Schampheleire *et al.*, 2009) and spray pressure (Etheridge *et al.*, 1999). In practice, a pesticide spray produced by hydraulic nozzles is characterized by a wide range of droplet sizes (~10–1000 µm) and velocities (~0–25 m/s). To evaluate the behavior of such droplets in a realistic way, a droplet generation method that produces uniform droplets within these size and velocity ranges in a controlled and repeatable way is needed, while the combination with an imaging technique allows for the reliable and automated evaluation of droplet characteristics and behavior.

Droplet generation can be accomplished by making one short duration fluid jet which condenses into a single droplet of desired diameter (Droplet-On-Demand (DOD) mode) or by breaking up a continuous fluid jet into uniformly sized droplets with a source of acoustic energy (Continuous mode) as described in detail by Lee (2003). The first mode, DOD mode, has been used in many technical, industrial and scientific applications because only a small amount of fluid is needed to form droplets e.g.: inkjet printing (Li *et al.*, 2010), calibration of particle sizing instruments (Ulmke *et al.*, 1999; Ulmke *et al.*, 2001), one–drop-fill technology (Kuang-Chao *et al.*, 2008), biotechnology and medicine (Saunders *et al.*, 2008). Continuous mode has also been used in applications like fabrication of metal parts (Luo *et al.*, 2011) and inkjet printing (Castrejon-Pita *et al.*, 2008). Basi et al. (2012) used a pneumatic droplet generator in DOD mode for pesticide applications to crops and weeds. In addition, a

piezoelectric droplet generator producing highly stable water droplets in the size range of a few µm over long time periods was developed by Riefler and Wriedt (2008).

The aim of this chapter was to determine the range of droplet sizes and velocities that can be obtained and the corresponding settings using distilled water and a droplet generator in two modes, DOD and continuous mode, for different nozzle orifice sizes, using the image acquisition system developed in Chapter 3 consisting of a high speed (HS) camera with microscope lens and xenon backlight and the image processing algorithms described in Chapter 4. This droplet generation system may be useful for various fundamental researches using single and uniform size droplets such as droplet–target interactions (Reichard *et al.*, 1998), droplet formation and ejection (Castrejon-Pita *et al.*, 2008) and validation of droplet size measuring equipment (Nuyttens *et al.*, 2007a).

5.2 MATERIALS AND METHODS

5.2.1 Droplet generator set-up

The droplet generator set-up (Université de Liège, Gembloux, Agro-Bio-Tech, Belgium) (Figure 5.1) used in this study was described in more detail in 3.2.1.

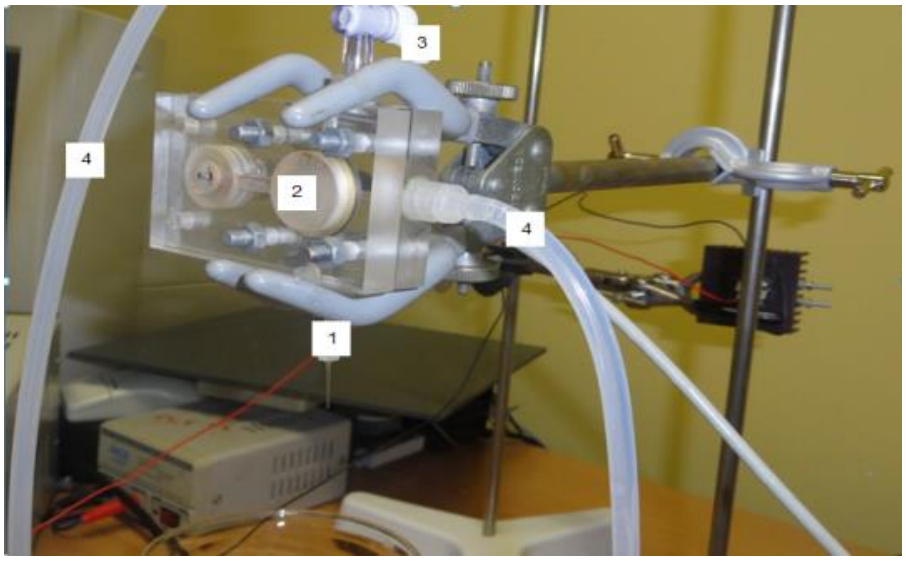

Figure 5.1. Piezoelectric droplet generator: 1-Glass nozzle, 2-Piezoelectric element, 3-Clamp, 4-Tubes

Different glass nozzles (Université de Liège, Gembloux, Agro-Bio-Tech, Belgium) were placed on the outlet of the droplet generator (Figure 5.1). In contrast with hydraulic spray nozzles, such nozzles can be used to produce single or a continuous stream of droplets with a uniform size in a controlled way.

Tests were done with 4 glass nozzles with orifice sizes of 261.6 ± 3.3 µm (nozzle 1), 123.4 ± 5.2 µm (nozzle 2), 87.2 ± 4.0 µm (nozzle 3) and 67.4 ± 3.3 µm (nozzle 4). These orifice diameters were determined by producing a continuous fluid jet through every nozzle which was filmed using the image acquisition set-up described below. By measuring the jet diameters at the orifice exit (in number of pixels) and multiplying with the 8.23 µm pixel size, (Vulgarakis Minov *et al.*, 2015a) the actual orifice sizes were determined. The measurements were repeated 5 times.

The droplet generator is able to form uniform droplets in 2 modes: DOD, generating single droplets using double square–edged pressure pulses (Switzer, 1991) (Figure 5.2a) and continuous, generating a continuous stream of uniformly spaced and sized droplets using a continuous square signal (Figure 5.2b).

The following paragraphs contain a description of the steps involved in both modes.

5.2.1.1 Droplet on demand (DOD) generation

The principle of DOD mode is based on two closely timed pulses (double pulse) that are fed to the droplet generator to eject a single droplet (Switzer, 1991; Yang *et al.*, 1997; Lee, 2003; Hsuan-Chung & Huey-Jiuan, 2010).

The single droplet breakup (Figure 5.3a) is characterized by an ejection of a single droplet. A pulse width that is too large may lead to droplet ejection followed by satellite droplets of different sizes (jet on demand) (Riefler & Wriedt, 2008; Li *et al.*, 2010). These satellite droplets and the settings at which they are formed (Figure 5.4) were not desired and not analyzed in this study. To avoid satellite droplets, small pulse widths should be applied. The surface tension of the fluid is then strong enough to absorb the fluid back to the nozzle (Riefler & Wriedt, 2008).

Droplet formation in DOD-mode requires some conditions in order to generate uniform and single droplets in a repeatable way (Lee, 2003). Air bubbles are detrimental to the operation

of the droplet generation and should be removed. To prevent fluid from dripping out and air bubbles from entering the system via the nozzle orifice, the fluid pressure should be controlled until a meniscus is just visible at the tip of the nozzle. This can be achieved by changing the liquid column height in the fluid tank (Yang *et al.*, 1997). After that, droplets can be generated by pressure pulses delivered by the actuator to the piezoelectric element (Castrejon-Pita *et al.*, 2008).

During the positive pressure period of the double pulse or the absorption time (t_a) (Figure 5.2a), the meniscus at the nozzle exit is formed and a droplet is created. Once the pressure reaches a negative value the droplet is ejected from the nozzle. This process occurs during the pulsation time (t_p). More information on the droplet formation and ejection can be found in the study of Li et al. (2010).

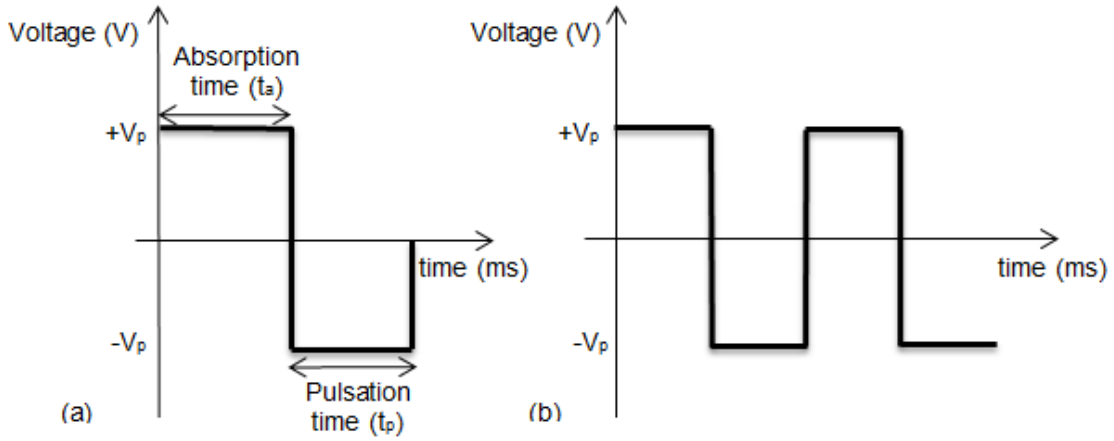

Figure 5.2. (a) Block diagram of the double pressure pulse for DOD mode and (b) continuous square signal for continuous mode

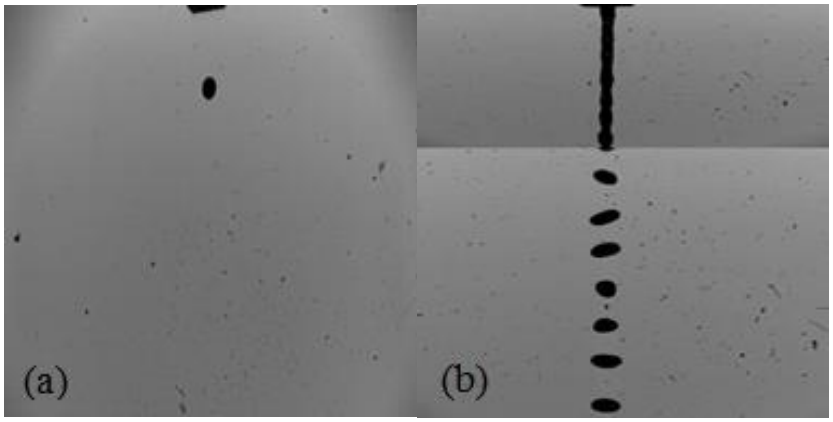

Figure 5.3. (a) Examples of single droplet ejection in DOD mode and (b) uniformly sized droplets in continuous mode

The effects of the following pressure pulse parameters on droplet formation and droplet diameter and velocity were tested: absorption time (t_a (ms)), pulsation time (t_p (ms)) and pulse amplitude ($\pm V_p$ (V)) (Figure 5.2a).

In a first stage, determination of the appropriate pressure pulse settings resulting in single droplet breakup was done for each of the four nozzles. These preliminary tests were done at t_a values of 0.01, 0.02, 0.05, 0.1, 0.2, 0.3, 0.4, 0.5, 0.6, 0.7, 0.8, 0.9, 1, 2 and 5 ms, all combined with t_p values of 0.01, 0.05, 0.1, 1, 5, 10, 25 and 50 ms. All 135 combinations were tested at a V_p value of ±4.5 V. The combinations of pulse width values resulting in a repeatable single droplet ejection were selected for the actual single droplet characterization (Figure 5.4, Table 5.1). These combinations differed considerably between the nozzles. For one and the same nozzle, increasing t_a values were associated with decreasing t_p values in order to produce single droplets. In addition, the effect of the pulse height from 3.0 V to 6.0 V at incremental steps of 0.5 V using nozzle 1 at t_a = 5 ms and t_p = 0.01 ms was also evaluated.

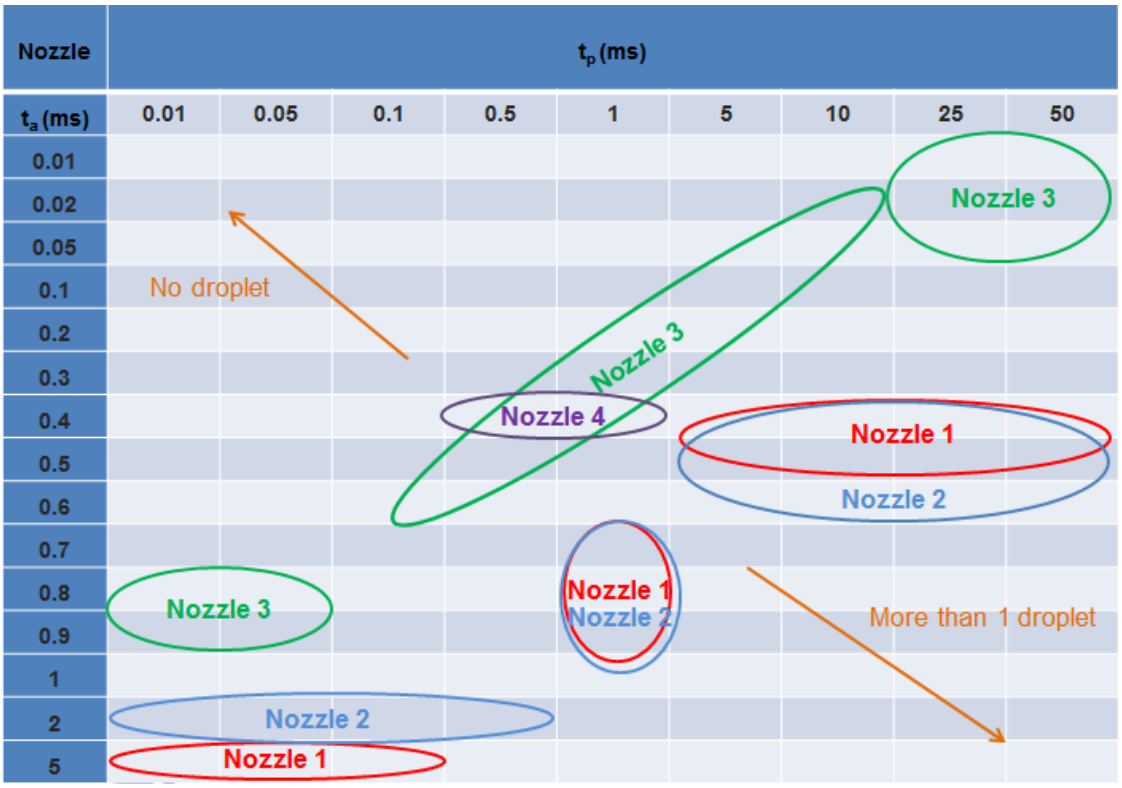

Figure 5.4. Selected pulse width values for the single droplet characterization at V_p = ± 4.5V for the 4 different sized nozzles which resulted in a single droplet ejection

Table 5.1. Selected pulse width values for the single droplet characterization for the 4 nozzles at V_p = ±4.5 V which resulted in a single droplet ejection

nozzle 1		**nozzle 2**	
t_a(ms)	**t_p (ms)**	**t_a (ms)**	**t_p (ms)**
5	0.01	2	0.01
5	0.05	2	0.1
5	0.1	0.7	1
0.7	1	0.9	1
0.9	1	0.4	10
0.4	5	0.4	50
0.5	50		
nozzle 3		**nozzle 4**	
t_a (ms)	**t_p (ms)**	**t_a (ms)**	**t_p (ms)**
0.8	0.01	0.4	0.6
0.6	0.1	0.4	0.8
0.3	1	0.4	0.9
0.2	5		
0.01	50		
0.1	25		

The DOD measurements were repeated 5 times for every setting. After breakup from the nozzle exit, the falling droplet was recorded using an HS image acquisition system (5.2.3), and the droplet diameter and droplet ejection velocity were determined using image analysis (5.2.4). All measurements were done using distilled water in a climate control room at an ambient temperature of 20°C and a relative humidity of 47%.

5.2.1.2 Continuous mode droplet generation

In the continuous mode, a continuous stream of uniformly sized droplets is produced with the piezoelectric droplet generator. Using the LabVIEW software, a square acoustic signal was sent to the piezoelectric element causing instability and standing waves on the fluid stream as it emerges from the orifice (Lee, 2003) (Figure 5.3b). In order to form uniformly sized droplets (Figure 5.3b), a suitable frequency must be applied (Switzer, 1991). In contrast with the DOD mode where a liquid column was used, a pressure supplier was used to create a liquid pressure of around 2 kPa in order to create a continuous jet.

Preliminary tests were done at frequency values from 7.5 to 8.5 kHz at incremental steps of 0.1 kHz and amplitudes of 1.0–9.0 V at steps of 1.0 V. All combinations were tested for the 4 nozzles resulting in 99 frequency/pulse amplitude combinations. These preliminary tests

showed that 8 kHz was a suitable frequency for generating uniformly sized droplets for every nozzle. At this frequency and for each nozzle, the effects of pulse amplitude on the droplet diameter, droplet velocity and inter-droplet spacing were examined using image analysis (5.2.4). The experiments were repeated 5 times.

5.2.2 Statistics

Per nozzle for DOD mode, a one-way ANOVA with technique, which is a combination of t_a and t_p, was performed on the droplet diameter and droplet velocity (dependent variables). In addition, per nozzle for continuous mode, a one-way ANOVA with voltage height (independent variable) was performed on droplet diameter, droplet velocity and inter-droplet spacing (dependent variables). Significant differences were assessed by Tukey's *post hoc* test. The experiments were statistically analyzed using IBM SPSS statistics 21 (SPSS Inc. 2012, IBM corporation, New York, USA). Statistical significance was considered at $P < 0.05$.

5.2.3 Image acquisition system

The image acquisition system to characterize droplets developed in Chapter 3 was used. The system consisted of a powerful xenon light (WOLF 5132, Knittlingen, Germany, 300 W) used as a background illumination against the droplet generator combined with an N3 HS (high speed) camera (IDT, Lommel, Belgium) with a 6 µs exposure time, a K2/SC Long-Distance Microscope System Lens (Infinity, USA) and a frame capture device Motion studio (IDT, Lommel, Belgium). In order to successfully record the single droplets in DOD mode, the piezoelectric generator was connected to the HS camera via a trigger.

The set-up resulted in a pixel size of 8.23 µm. In DOD mode the images were taken at full resolution (1280 × 1024 pixels) with a field of view (FOV) of 10.5 mm × 8.4 mm at 1000 fps. In continuous mode the frame rate was set to 10.000 fps due to the bigger droplet velocities with an image size of 480 × 96 pixels corresponding with an FOV of 3.95 mm × 0.79 mm.

An example of the captured droplet formation in DOD mode with the described image acquisition system is shown in Figure 5.5.

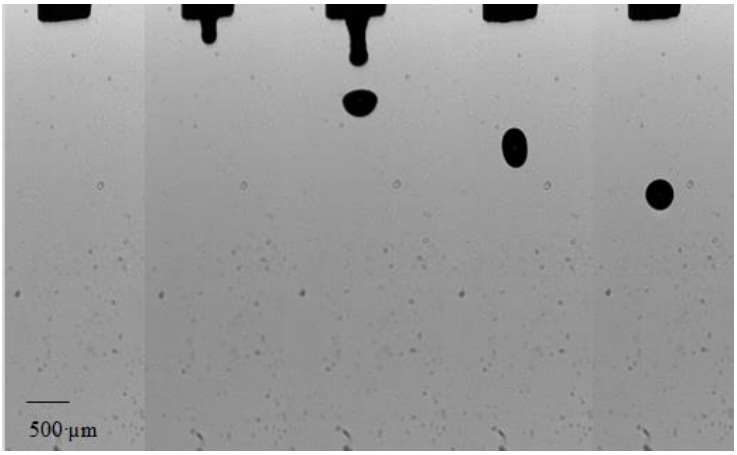

Figure 5.5. Image sequence showing the formation of a 461.5 µm droplet in DOD mode with nozzle 1 with an ejection droplet velocity of 0.59 m/s. The different frames correspond with times of 0, 3, 6, 9, 12 ms after the first frame

5.2.4 Droplets(s) characterization with image analysis

Image processing algorithms were developed in Matlab (2011b, MathWorks Company, Massachusetts, USA) to characterize the single droplets (Chapter 4). Tracking and sizing of the droplet(s) were done in 3 steps:

1) Detection of the moving droplet(s) using edge detection based on local changes in the image brightness (Lecuona *et al.*, 2000); 2) Tracking of the droplet between frames and 3) Measurement of the droplet characteristics (size, velocity, inter-droplet spacing (continuous mode)).

The velocity of a droplet is calculated based on its position in two consecutive frames and the time between two frames. A detailed description of the image analysis is given in Chapter 4.

5.2.5 Validation

The droplet size measuring method was validated by a droplet weight method (Li *et al.*, 2010) for DOD as well as for continuous mode. For the DOD mode, 100 droplets were collected and weighed for one test condition (nozzle 2 at t_a=0.7 ms; t_p=1.0 ms; V_p= ± 4.5 V). The total mass of droplets generated was determined using an analytical scale (Sartorius M-Pact AX224, S.A. Sartorius Mechatronics Belgium N.V., accuracy: 0.0001 g). Droplet diameters were calculated from the weight and density of the collected water and compared to the image analysis results. For the continuous mode, validation was done using nozzle 2 at

a frequency of 8.0 kHz and a pulse amplitude of 8.0 V. The liquid emitted by the nozzle over a period of 30 s was collected, weighed and the total volume was calculated. The volume of one droplet was calculated by dividing the total volume by the number of droplets generated during the 30 s period based on the breaking frequency and compared with the droplet diameter resulting from the image analysis.

Finally, to test the effect of the measuring method (image analysis vs. droplet weight) on the droplet diameter (dependent variable) an ANOVA was performed. A p-value <0.05 was considered statistically significant. The test was performed in SPSS Statistics 21 (IBM, USA). The significant differences were assessed using SNK (Student – Newman - Keuls) post hoc tests.

5.3 RESULTS AND DISCUSSION

5.3.1 Droplet on demand generation

5.3.1.1 Effects of pulse width and nozzle orifice size

The effects of the selected pulse width values (Table 5.1) on droplet diameter and droplet velocity were investigated by keeping the pulse amplitude constant at ±4.5 V for all nozzles. The results are presented inThe mean droplet diameters for the different nozzles and pulse width combinations are given in Figure 5.6. For nozzle 1, pulse width values significantly affected the droplet diameter (P = 0.000). Of all tested combinations, these were the biggest droplets produced in DOD mode. Diameters ranged from 351.2 ± 1.2 µm up to 461.5 ± 3.3 µm corresponding with about 1.3 and 1.8 times the orifice size, respectively.

For other glass nozzles, the combination of pulse width values also significantly affected droplet diameters (P < 0.001). Droplet diameters ranged from 312.7 ± 1.5 - 416.5 ± 0.2 µm (nozzle 2), 242.9 ± 1.5 - 310.1 ± 0.3 µm (nozzle 3), 134.1 ± 3.7 - 207.2 ± 16.4 µm (nozzle 4), corresponding with 2.53 - 3.37 (nozzle 2), 2.78 - 3.55 (nozzle 3), 1.99 - 3.07 (nozzle 4) times the orifice size (**Error! Not a valid bookmark self-reference.**).

In general, a decrease of *ta* in combination with an increase of *tp* tended to increase the droplet diameter (Riefler & Wriedt, 2008). This effect was most pronounced for larger nozzle orifices (nozzle 1 and nozzle 2).

Table 5.2, Figure 5.6 and

Figure 5.8.

The mean droplet diameters for the different nozzles and pulse width combinations are given in Figure 5.6. For nozzle 1, pulse width values significantly affected the droplet diameter (P = 0.000). Of all tested combinations, these were the biggest droplets produced in DOD mode. Diameters ranged from 351.2 ± 1.2 µm up to 461.5 ± 3.3 µm corresponding with about 1.3 and 1.8 times the orifice size, respectively.

For other glass nozzles, the combination of pulse width values also significantly affected droplet diameters (P < 0.001). Droplet diameters ranged from 312.7 ± 1.5 - 416.5 ± 0.2 µm (nozzle 2), 242.9 ± 1.5 - 310.1 ± 0.3 µm (nozzle 3), 134.1 ± 3.7 - 207.2 ± 16.4 µm (nozzle 4), corresponding with 2.53 - 3.37 (nozzle 2), 2.78 - 3.55 (nozzle 3), 1.99 - 3.07 (nozzle 4) times the orifice size (**Error! Not a valid bookmark self-reference.**).

In general, a decrease of t_a in combination with an increase of t_p tended to increase the droplet diameter (Riefler & Wriedt, 2008). This effect was most pronounced for larger nozzle orifices (nozzle 1 and nozzle 2).

Table 5.2. Effect of the pulse width values (ms) on the droplet diameter (µm) and droplet velocity (m/s) produced with nozzles 1 to 4 (mean ± std)

Nozzle	Pulse width combination t_a (ms) / t_p (ms)	Droplet diameter (µm)	Droplet velocity (m/s)
1	5 / 0.01	389.2 ± 2.4 b	0.33 ± 0.02 e
	5 / 0.05	360.9 ± 2.2 d	0.65 ± 0.05 b
	5 / 0.1	351.2 ± 1.2 e	0.81 ± 0.03 a
	0.7 / 1	383.4 ± 1.2 c	0.10 ± 0.01 f
	0.9 / 1	385.7 ± 3.0 bc	0.48 ± 0.02 d
	0.4 / 5	458.7 ± 3.5 a	0.34 ± 0.01 e
	0.5 / 50	461.5 ± 3.3 a	0.59 ± 0.01 c
2	2 / 0.01	330.1 ± 1.3 d	0.66 ± 0.03 c
	2 / 0.1	333.2 ± 1.2 c	0.72 ± 0.01 b
	0.7 / 1	390.2 ± 4.6 b	0.49 ± 0.01 d
	0.9 / 1	312.7 ± 1.5 e	0.86 ± 0.01 a
	0.4 / 10	416.5 ± 0.2 a	0.26 ± 0.01 e
	0.4 / 50	415.5 ± 0.4 a	0.26 ± 0.01 e
3	0.8 / 0.01	242.9 ± 1.5 d	0.30 ± 0.06 e
	0.6 / 0.1	249.1 ± 8.4 d	0.68 ± 0.10 a

	0.3 / 1	284.6 ± 2.9 c	0.52 ± 0.09 b
	0.2 /5	310.1 ± 0.3a	0.53 ± 0.01 b
	0.01 / 50	293.0 ± 0.4 b	0.08 ± 0.01 d
	0.1 / 25	303.9 ± 0.8 a	0.19 ± 0.01 cd
	0.4 / 0.6	134.1 ± 3.7 a	0.76 ± 0.12 b
4	0.4 / 0.7	207.2 ± 16.4 c	1.78 ± 0.12 a
	0.4 / 0.8	171.8 ± 4.6 b	0.77 ± 0.12 b

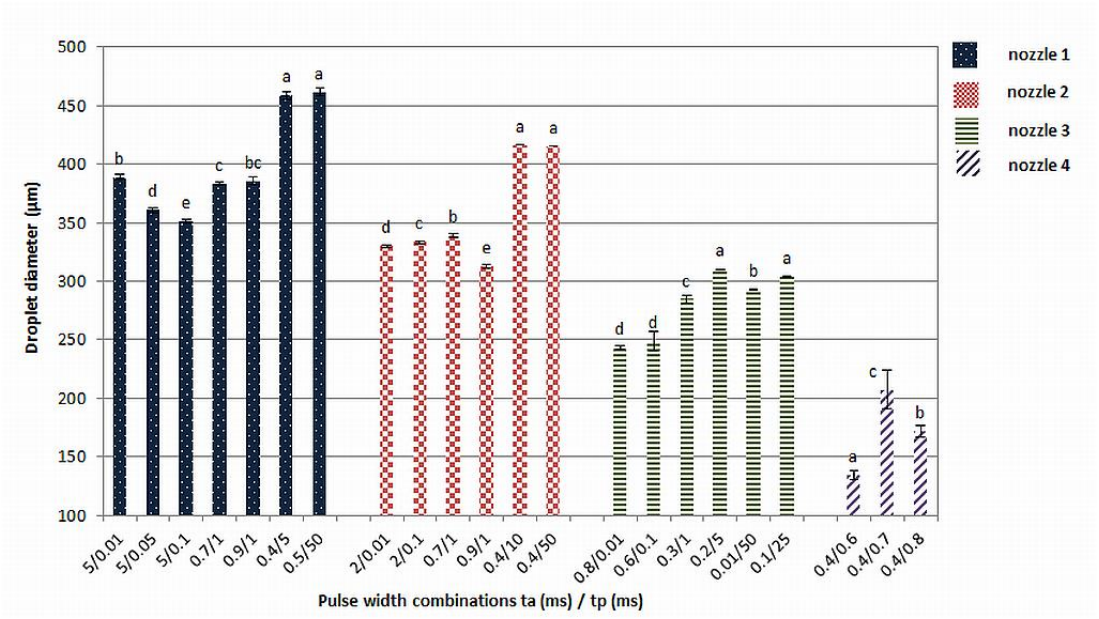

Figure 5.6. Droplet diameter (µm, mean ± std.) for different nozzles and pulse width combinations. Different letters indicate statistical differences within the same nozzle ($P < 0.05$)

Increasing the nozzle orifice increased the measured droplet diameter as it was also found by Kuang-Chao et al. (2008) and Basi et al. (2012). By selecting nozzle and pulse width values, droplets ranging from 134.1 ± 3.7 up to 461.5 ± 3.3 µm could be generated which is a realistic size range for real pesticide sprays (Nuyttens *et al.*, 2007a).

The smaller the nozzle orifice size, the more difficult it was to produce droplets. This comes from the fact that if the pressure (pulse width and voltage amplitude) is not high enough to overcome surface tension, a droplet is not ejected. Therefore, only 3 different droplet sizes could be generated with nozzle 4 (The mean droplet diameters for the different nozzles and pulse width combinations are given in Figure 5.6. For nozzle 1, pulse width values

significantly affected the droplet diameter (P = 0.000). Of all tested combinations, these were the biggest droplets produced in DOD mode. Diameters ranged from 351.2 ± 1.2 µm up to 461.5 ± 3.3 µm corresponding with about 1.3 and 1.8 times the orifice size, respectively.

For other glass nozzles, the combination of pulse width values also significantly affected droplet diameters (P < 0.001). Droplet diameters ranged from 312.7 ± 1.5 - 416.5 ± 0.2 µm (nozzle 2), 242.9 ± 1.5 - 310.1 ± 0.3 µm (nozzle 3), 134.1 ± 3.7 - 207.2 ± 16.4 µm (nozzle 4), corresponding with 2.53 - 3.37 (nozzle 2), 2.78 - 3.55 (nozzle 3), 1.99 - 3.07 (nozzle 4) times the orifice size (**Error! Not a valid bookmark self-reference.**).

In general, a decrease of t_a in combination with an increase of t_p tended to increase the droplet diameter (Riefler & Wriedt, 2008). This effect was most pronounced for larger nozzle orifices (nozzle 1 and nozzle 2).

Table 5.2 and Figure 5.7).

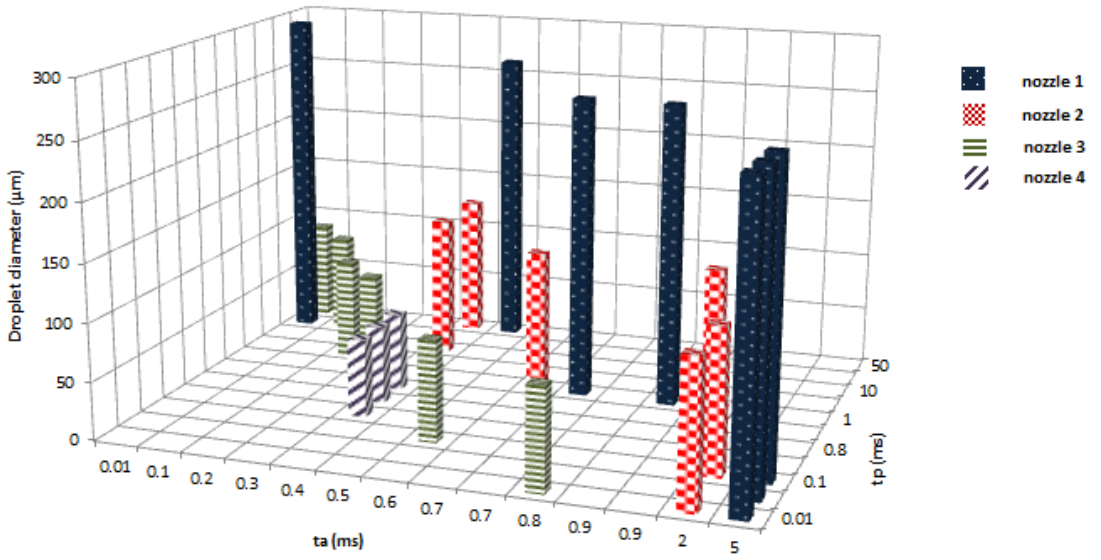

Figure 5.7. Mean droplet diameter results for the selected pulse width values for the 4 nozzles with Vp = ± 4.5 V

Figure 5.8 presents the mean droplet velocity for the different nozzles and pulse width combinations.

Pulse width combinations significantly affected droplet velocities at nozzle 1 (P < 0.001), nozzle 2 (P < 0.001), nozzle 3 (P < 0.001) and nozzle 4 (P < 0.001).

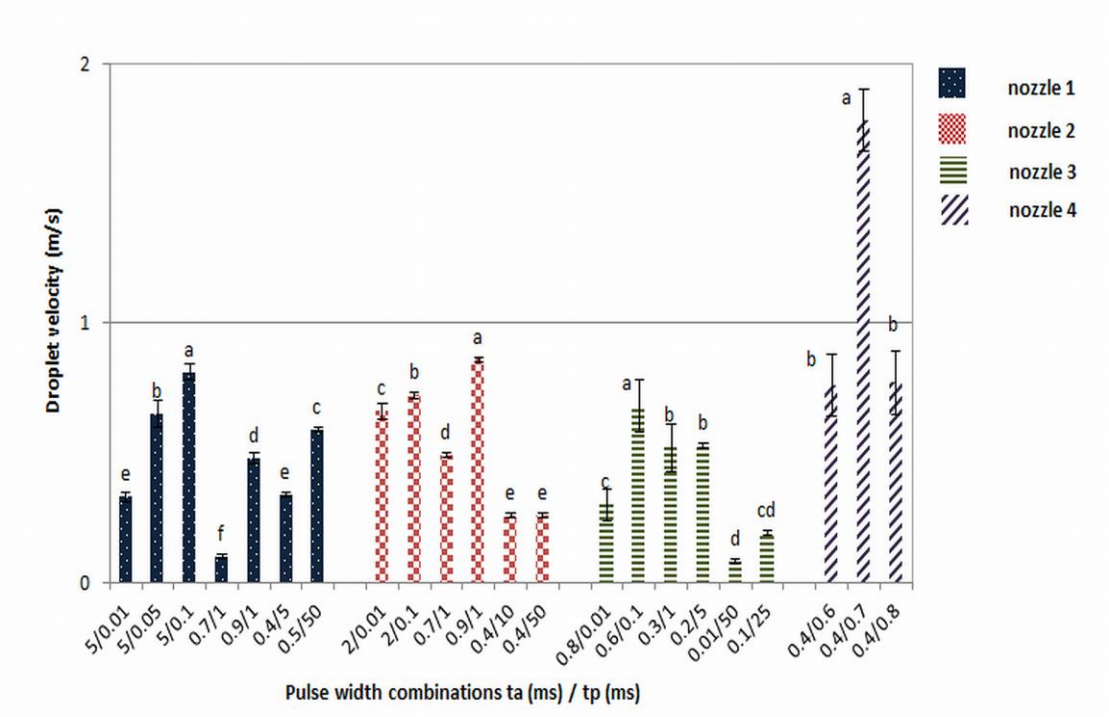

Figure 5.8. Droplet velocity (m/s, mean ± std.) for different nozzles and pulse width combinations. Different letters indicate statistical differences within the same nozzle ($P < 0.05$)

Furthermore, it can be observed in The mean droplet diameters for the different nozzles and pulse width combinations are given in Figure 5.6. For nozzle 1, pulse width values significantly affected the droplet diameter (P = 0.000). Of all tested combinations, these were the biggest droplets produced in DOD mode. Diameters ranged from 351.2 ± 1.2 µm up to 461.5 ± 3.3 µm corresponding with about 1.3 and 1.8 times the orifice size, respectively.

For other glass nozzles, the combination of pulse width values also significantly affected droplet diameters ($P < 0.001$). Droplet diameters ranged from 312.7 ± 1.5 - 416.5 ± 0.2 µm (nozzle 2), 242.9 ± 1.5 - 310.1 ± 0.3 µm (nozzle 3), 134.1 ± 3.7 - 207.2 ± 16.4 µm (nozzle 4), corresponding with 2.53 - 3.37 (nozzle 2), 2.78 - 3.55 (nozzle 3), 1.99 - 3.07 (nozzle 4) times the orifice size (**Error! Not a valid bookmark self-reference.**).

In general, a decrease of *ta* in combination with an increase of *tp* tended to increase the droplet diameter (Riefler & Wriedt, 2008). This effect was most pronounced for larger nozzle orifices (nozzle 1 and nozzle 2).

Table 5.2 that the smallest droplet velocity (0.08 ± 0.01 m/s) was measured for nozzle 3 whilst the biggest droplet velocity of 1.78 ± 0.12 (m/s) for the smallest nozzle orifice (nozzle 4). The data showed no clear relation between pulse width values on droplet velocity at

constant pulse amplitude. Similarly, no clear correlation between droplet size and droplet ejection velocity was detected for nozzle 1 and nozzle 3 (Figure 5.9). However, a strong correlation (R^2 = 0.96) using nozzle 2 was observed i.e. increasing the droplet diameter led to decreasing the droplet velocity while the opposite effect was observed for nozzle 4 (R^2 = 0.74) (Figure 5.9). The generated droplet velocities were lower than the ones of hydraulic spray nozzles used for pesticide applications in practice (Nuyttens *et al.*, 2007a) indicating the difference in droplet formation mechanisms between DOD mode and hydraulic spray nozzles.

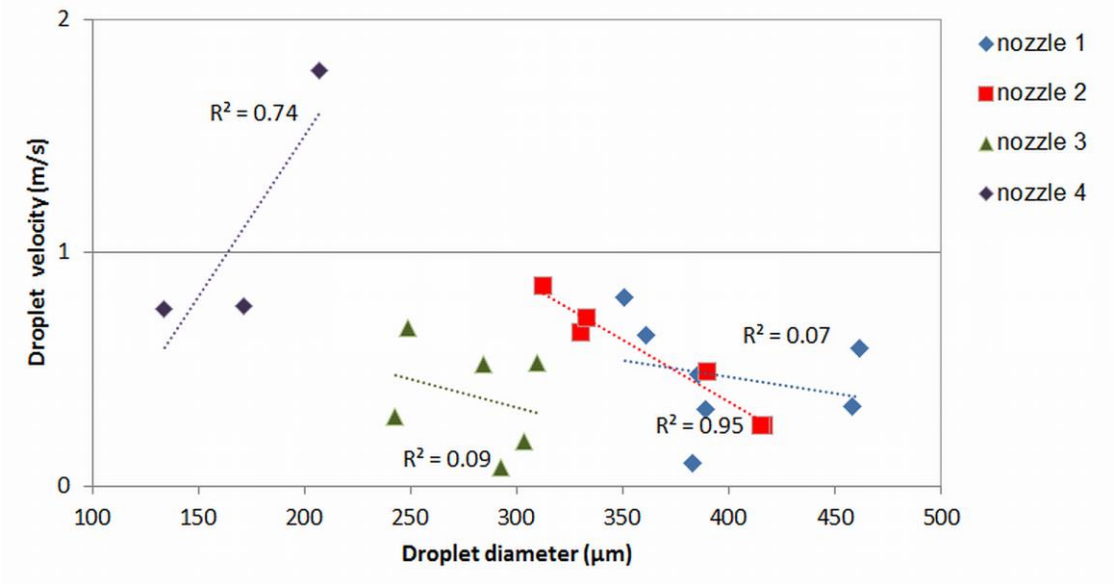

Figure 5.9. Correlation between droplet diameter and velocity in DOD mode for 4 different nozzles at pulse amplitude of ±4.5 V

5.3.1.2 Effect of pulse amplitude

The effects of pulse amplitude (Vp) on droplet diameter and droplet velocities were investigated by keeping the pulse widths constant at t_a = 5 ms and t_p = 0.01 ms for nozzle 1. Pulse amplitude significantly affected droplet diameter (P < 0.001) as well as droplet velocity (P < 0.001) as shown in Figure 5.10.

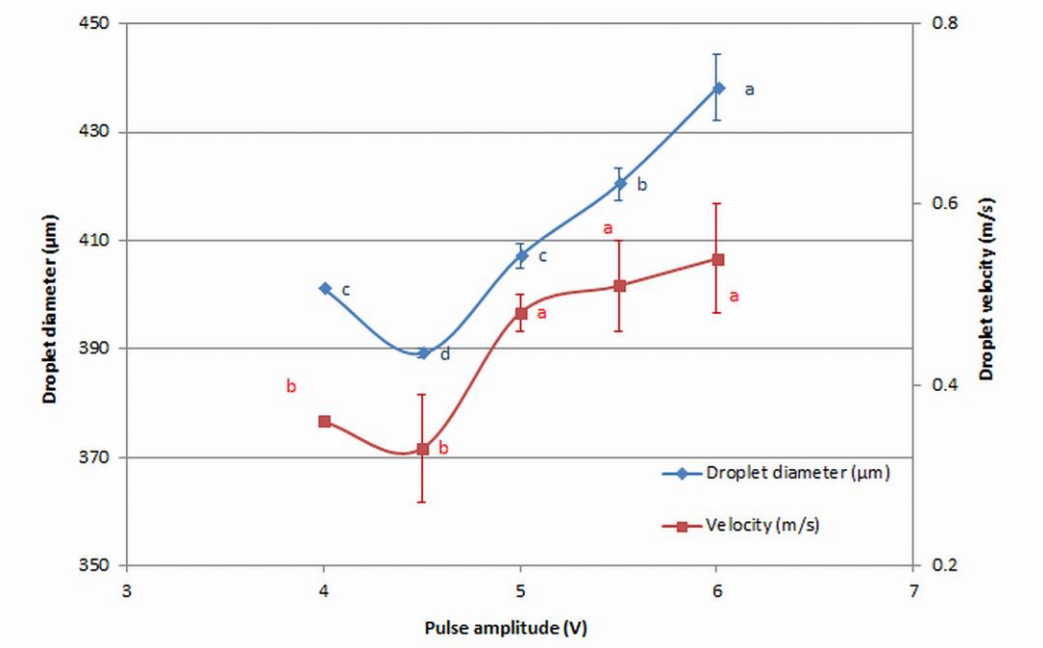

Figure 5.10. Droplet diameter (µm, mean ± std.) and velocity (m/s, mean ± std.) for nozzle 1 at different pulse amplitudes and t_a = 5 ms and t_p = 0.01 ms. Different letters indicate statistical differences between data points within the same curve ($P < 0.05$)

By increasing pulse amplitude from ±4.0 V up to ±4.5 V, both droplet diameter and velocity decreased, although not significantly for droplet velocity, and the minimum droplet diameter of 389.1 ± 2.4 µm and minimum velocity of 0.3 ± 0.0 m/s were obtained.

A further increase of V_p resulted in a significant increase of both droplet diameter and velocity as previously found by (Sadeghian *et al.*, 2014), although with little change thereafter for droplet velocity, eventually reaching a value of 438.1 ± 7.1 µm and 0.54 ± 0.0 m/s at V_p of ±6.0 V, respectively. In contrast with the effect of pulse widths, there was a clear correlation between droplet diameter and velocity (Figure 5.11). Further increasing V_p above ±6.0 V resulted into ejection of satellite droplets. Decreasing pulse amplitudes below ±4.0 V resulted into no ejection of droplets.

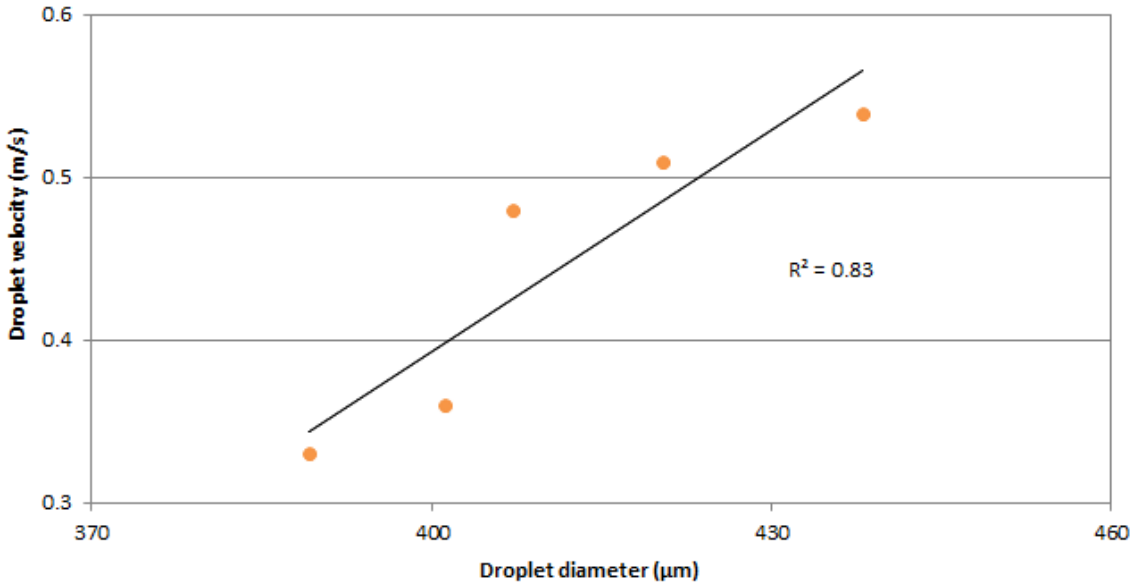

Figure 5.11. Correlation between droplet diameter and velocity in DOD mode for nozzle 1 at different pulse amplitudes and t_a = 5 ms and t_p = 0.01 ms

5.3.1.3 Validation

The actual mean droplet diameter based on weighing 100 droplets was 346.4 ± 9.5 µm while a value of 339.5 ± 1.6 µm was found with image analysis. Hence, the overall accuracy of the measurement was satisfactory with a relative measurement error of about 2% and an absolute error of about 7 µm (~1 pixel). No significant differences in droplet diameter between the two techniques were observed ($P > 0.05$).

5.3.2 Continuous mode droplet generation

The effects of pulse amplitude on droplet diameter, droplet velocity and inter-droplet spacing at the optimal frequency of 8.0 kHz for the different nozzles is shown in Figure 5.12, Figure 5.13 and Figure 5.14.

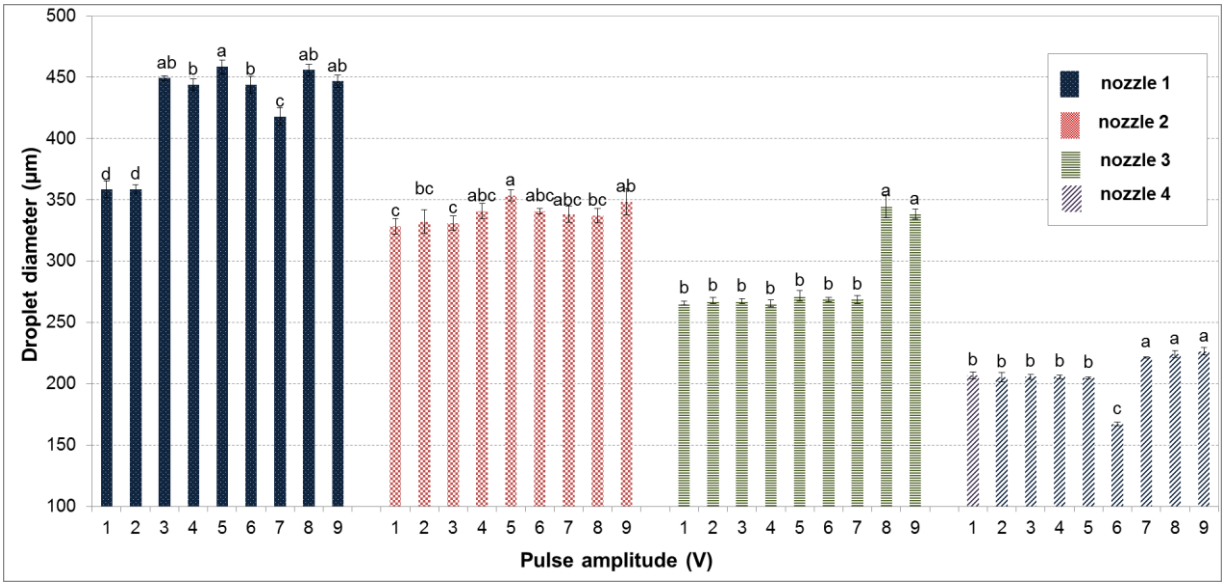

Figure 5.12. Droplet diameter (µm, mean±std.) in continuous mode for different nozzles and pulse amplitudes at a frequency of 8.0 kHz. Different letters indicate statistical differences within the same nozzle (P<0.05)

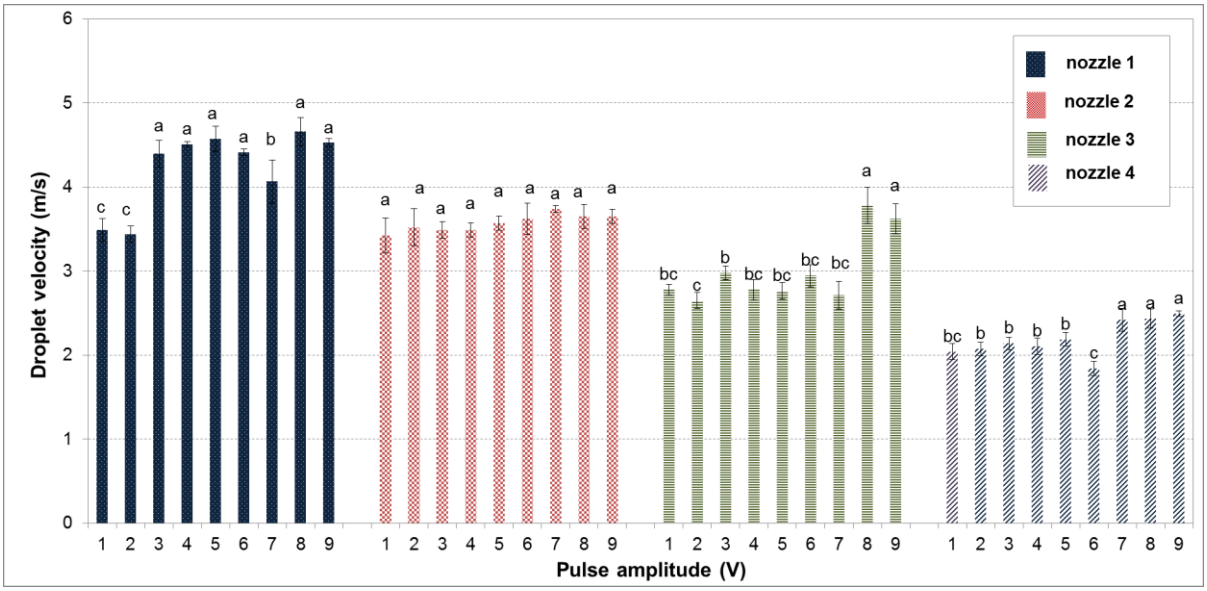

Figure 5.13. Droplet velocity (m/s, mean±std.) in continuous mode for different nozzles and pulse amplitudes at a frequency of 8.0 kHz. Different letters indicate statistical differences within the same nozzle (P<0.05)

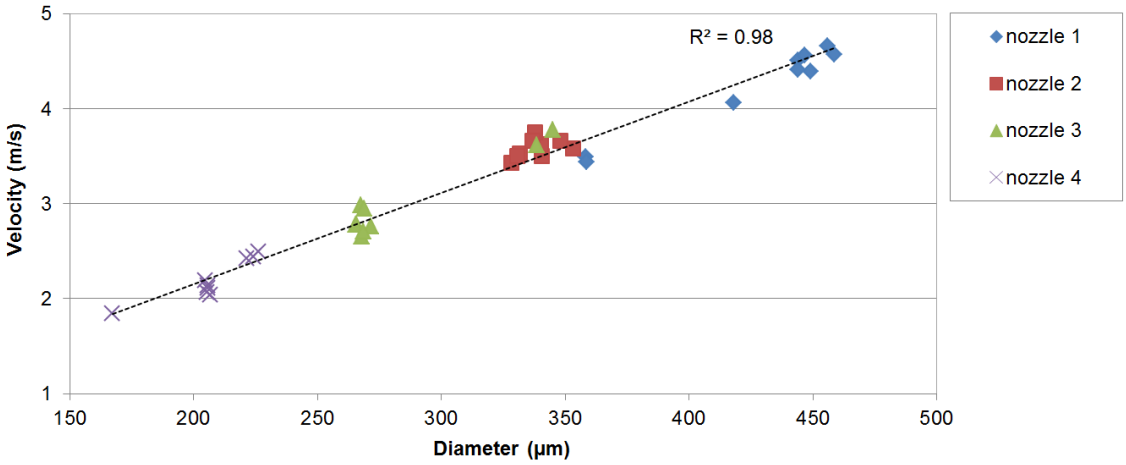

Figure 5.14. Correlation between droplet diameter and velocity in continuous mode for different nozzles and pulse amplitudes at a frequency of 8.0 kHz

For nozzle 1, the droplet diameter was significantly affected by the pulse amplitude values ($P < 0.001$) (Figure 5.12). Generally larger droplet diameters were found for pulse amplitude values of 3.0, 4.0, 5.0, 6.0, 8.0 and 9.0 V followed by 7.0 V pulse amplitude. Smallest droplets were generated at 1.0 and 2.0 V pulse amplitude. Droplet diameters with nozzle 1 ranged from 358.3 ± 6.9 to 455.8 ± 4.8 mm corresponding with 1.37-1.75 times the orifice size. The biggest droplet diameter produced in continuous mode was 455.6 mm (at 5.0 V). Using nozzle 2 ($P < 0.001$), the droplet diameter ranged between 328.4 ± 6.2 and 353.5 ± 4.6 mm. The effect of pulse amplitude was limited but significant with biggest droplets at 5.0 V and smallest droplets at 1.0 V. For nozzle 3, no significant effect of pulse amplitude was observed within the range from 1.0 to 7.0 V, while significantly bigger droplets were produced at pulse amplitudes of 8.0 and 9.0 V. ($P < 0.001$). With nozzle 4, smallest droplets were generated with a pulse amplitude of 6.0 V ($P < 0.001$). This was also the smallest droplet produced in continuous mode with a size of 167.2 ± 1.4 mm. With nozzle 4, the biggest droplets were produced at 7.0 up to 9.0 V. In general, no clear correlation between pulse amplitude and droplet diameter was found although there was a trend for bigger droplets at bigger pulse amplitudes.

The influence of the nozzle size and pulse amplitude on the droplet velocity is shown in Figure 5.13 with velocities ranging from 2.42 ± 0.1 m/s up to 4.57 ± 0.0 m/s. These higher velocities relate much better with velocities of droplets generated with hydraulic spray nozzles at a distance of 0.50 m below the nozzle where they generally impact the target

(Nuyttens *et al.*, 2007a). A positive correlation was found between the droplet diameter and velocity generated with different nozzles and pulse amplitudes at a constant frequency of 8.0 kHz (R^2= 0.98) (Figure 5.14). With nozzle 1 (P < 0.001), the lowest velocities were produced at amplitudes of 1.0 and 2.0 V. These velocities were comparable with droplet velocities produced with nozzle 2 ($P = 0.068$) at all amplitudes. With nozzle 2, no significant effect of amplitude on velocity was found, but the tendency of an increase in velocity with an increase in amplitude was confirmed. Considering nozzle 3 (P < 0.001) and nozzle 4 (P < 0.001), the highest velocities were obtained with the highest amplitudes of 8.0 and 9.0 V. For these nozzles, the effect of amplitude on velocity was limited within the range from 1.0 to 7.0 V.

A significant effect of pulse amplitude on inter-droplet spacing was found for every nozzle (Figure 5.15). For nozzle 1 (P < 0.001) a significant increase in inter-droplet spacing was observed with increasing pulse amplitudes with the smallest inter-droplet spacing at 1.0 V and the biggest inter-droplet spacing at 9.0 V. Similar as for droplet velocities, the effect of amplitude on inter-droplet spacing in case of nozzle 2 was limited and in most cases not significant with nozzle 2 (P < 0.001). There was also a significant effect of the pulse amplitude on the inter-droplet spacing using nozzle 3(P < 0.001) and nozzle 4 (P < 0.001). With nozzle 3, highest values were found at amplitudes of 5.0 and 6.0 V, with nozzle 4 at amplitudes from 7.0 up to 9.0 V. For these nozzles, the smallest inter-droplet spacing was found at 3.0 V and 6.0 V, respectively.

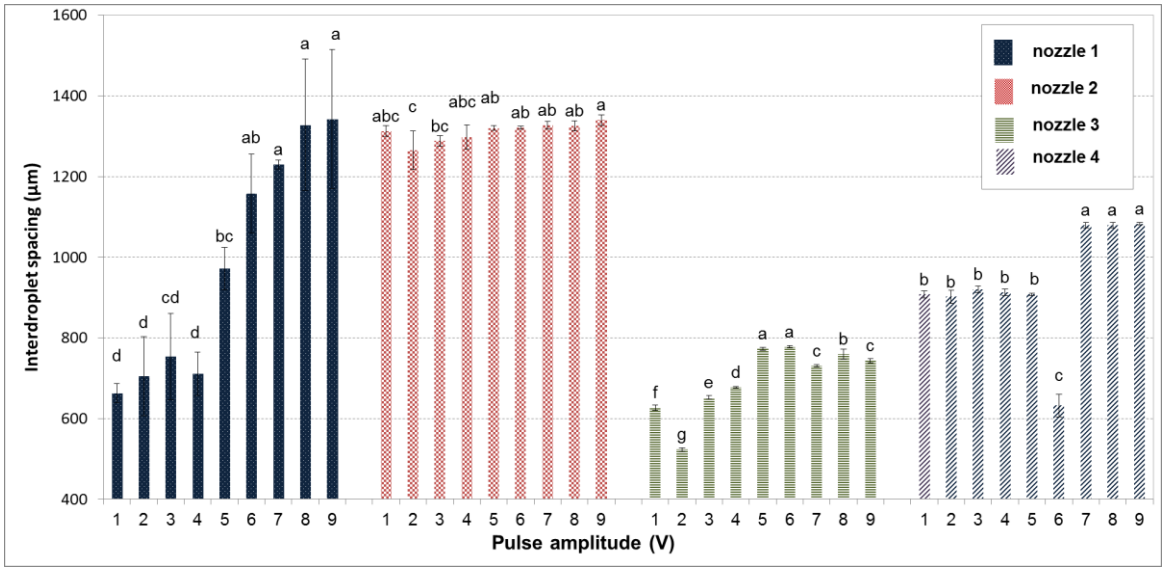

Figure 5.15. Inter-droplet spacing (µm, mean ± std.) in continuous mode for different nozzles and pulse amplitudes at a frequency of 8.0kHz. Different letters indicate statistical differences within the same nozzle (P<0.05)

5.3.2.1 Validation

The actual droplet diameter based on collecting droplets over a period of 30 s and weighing them was 320.0 ± 9.4 mm while a value of 337.1 ± 5.8 mm was found using the image analysis. Hence, the overall accuracy of the measurement was satisfactory with a relative measurement error of 5.3%. No significant differences in droplet diameter between the two techniques were observed (P > 0.05).

5.3.3 Comparison between DOD and continuous mode

The presented experiments with the DOD and continuous mode have shown comparable values for the biggest and smallest droplet diameters achieved with these glass nozzles. The smallest droplet diameters measured with image analysis in DOD and continuous mode were 134.1 ± 3.7 mm and 167.2 ± 1.4 mm, respectively. The biggest droplet diameters in DOD and continuous mode were 461.6 ± 3.3 mm and 458.6 ± 4.8 mm.

The smallest achieved droplet diameter ratio within both modes was found using nozzle 1, i.e. 1.34 for DOD and 1.37 for continuous mode. The biggest ratio between the droplet diameter and nozzle orifice size was measured with nozzle 3 in DOD (3.55) as well as in continuous mode (3.95) (Table 5.3). Previous studies were generally dealing with smaller droplet sizes and pulse widths. Riefler and Wriedt (2008) generated droplets in DOD mode ranging from 8 to 70 µm with a 40 µm orifice size. Kung et al. (1999) achieved a ratio up to 4

between droplet and orifice diameter using a very small 1 mm orifice size. Lee (2003) mentioned that droplet generators can produce drops of half the nozzle diameters to twice the whole diameter.

On the contrary, a big difference in droplet velocity results between the modes was noticed, i.e. droplets fell faster in continuous mode than in DOD mode. The droplet generator developed droplet velocities in DOD and continuous mode in the range of 0.08 ± 0.01 to 1.78 ± 0.12 m/s and 1.84 ± 0.08 to 4.66 ± 0.17 m/s, respectively.

Table 5.3. Ratio between nozzle orifice opening and minimal-maximal mean droplet diameters and minimal and maximal droplet diameters in DOD and continuous mode

Nozzle	DOD mode		continuous mode	
	ratio (mean droplet diameter / nozzle orifice size)	minimal / maximal droplet diameter (µm)	ratio (mean droplet diameter / nozzle orifice size)	minimal / maximal droplet diameter (µm)
1	1.34 ÷ 1.76	351.2 ÷ 461.5	1.37 ÷ 1.75	358.2 ÷ 458.6
2	2.53 ÷ 3.37	312.7 ÷ 416.5	2.66 ÷ 2.86	328.5 ÷ 353.5
3	2.78 ÷ 3.55	242.9 ÷ 310.1	3.04 ÷ 3.95	265.4 ÷ 344.8
4	1.99 ÷ 3.07	134.1 ÷ 207.2	2.48 ÷ 3.35	167.2 ÷ 226.3

5.4 CONCLUSION

Measurements using a single droplet generator in DOD and continuous mode were performed. The effects of the operating parameters, including voltage pulse width and pulse amplitude with 4 nozzle orifice sizes (261 µm, 123 µm, 87 µm and 67 µm) on droplet diameter and droplet velocity have been characterized. These different droplet sizes and velocities were successfully measured with the image acquisition and image processing system developed in Chapter 3 and 4. The experiments in DOD mode have shown that the initial droplet characteristics from the droplet generator are a function of the double pulse width and the orifice size. The pulse width values are critical parameters for droplet ejection. By changing pulse width, it was possible to control droplet velocity and droplet size diameter. In general, decrease of t_a and increase of t_p increased the droplet diameter. Similarly, increasing the nozzle orifice size increased the droplet diameter. With the DOD mode, droplet sizes ranged between 134.1 µm and 461.5 µm. Foremost, the smallest and the fastest droplets were measured with the smallest nozzle orifice. The measured droplet

velocities ranged between 0.08 m/s and 1.78 m/s. Besides, we noticed an effect of the pulse amplitude on the droplet diameter and velocity.

The ratio of the droplet diameter and nozzle orifice in DOD mode ranged from 1.3 to 3.5.

The continuous mode for every nozzle was established for a frequency resulting in a continuous droplet generation. This frequency together with different pulse amplitudes were used to test the effect on the droplet diameter, inter-droplet spacing and velocity. As for the DOD mode, the droplet diameter was mainly controlled by the nozzle orifice. The droplet size here was between 167.2 µm and 455.8 µm. Furthermore, the nozzle orifice also influenced the droplet velocity i.e., the bigger the nozzle orifice was, the higher droplet velocity was measured. Obviously, there was a linear trend between the droplet diameter and velocity in continuous mode. Based on the results from the experiments, the effect of the pulse amplitude on the inter-droplet spacing was statistically significant. The ratios between the nozzle orifice and droplet diameter ranged from 1.3 to 3.9. In continuous mode, the lowest droplet velocity of 1.84 m/s was measured with the smallest nozzle orifice size while the highest droplet velocity of 4.66 m/s was measured with the biggest nozzle orifice size.

Based on the results in both modes, similar droplet diameter sizes were produced. However, in continuous mode it was possible to achieve faster droplets which correspond better with real spray application.

Finally, the size and velocity range of the ejected droplets in both modes are valid for the system, nozzles and conditions (liquid properties, temperature and etc.) at which they are determined.

6 MICRO-SPRAY CHARACTERIZATION FROM A SINGLE NOZZLE[v]

Droplet size and velocity distribution are important features of an agricultural spray. The objective of this chapter was to measure the micro-spray characteristics (droplet size and velocity) for different types of hydraulic spray nozzles using the backlight image acquisition system developed in Chapter 3 and image processing based on image processing algorithms developed in Chapter 4 and Chapter 5. Tests have been done with five different commonly used agricultural spray nozzles (Albuz ATR orange and red, TeeJet XR 110 01, XR 110 04 and Al 110 04).

[v] This chapter has been compiled from:

Vulgarakis Minov S, Cointault F, Vangeyte J, Pieters J G, Nuyttens D. 2015. Spray droplet size distribution measured using high speed imaging techniques (*in preparation*).

6.1 INTRODUCTION

In the past, various measuring techniques (Rhodes, 2008) have been employed in the research on spray and atomization to investigate spray characteristics including droplet sizes and velocities. However, there are few optical measurement techniques that are able to perform simultaneous non-intrusive measurements of the droplet size and velocity.

Due to the development of modern technology such as powerful computers and lasers, quantitative *optical non-imaging light scattering spray characterization techniques* have been developed for non-intrusive spray characterization: Phase Doppler Particle Analyzers (PDPA)(Nuyttens *et al.*, 2007a; Nuyttens *et al.*, 2009), laser diffraction analyzers, e.g., Malvern Analyzer (Stainier et al., 2006) and optical array probes (Teske et al., 2002). Among them, the PDPA has widely been tested and recognized for spray characterization. The major drawback of the PDPA is that it can only measure a spherical droplet which is not always the case. In addition, it is a point–measurement technique and information on overall spray structure is beyond the capability of this laser device.

Moreover, the limitations of the non-imaging techniques and the recent improvements in digital image processing, sensitivity of imaging systems and cost reductions have increased the interest in high speed imaging techniques for agricultural applications (Hijazi et al., 2012) in general and pesticide applications (Lecuona et al., 2000) in particular.

Imaging analyzers are spatial sampling techniques consisting of a light source, a camera and a computer with image acquisition and processing software. The small droplet size and high velocity of the ejected spray droplets make it a challenge to use imaging techniques for spray characterization. Most imaging techniques use backlight for the illumination of the droplets to acquire their shadowgraphs, from which droplet characteristics are extracted. They allow one plane at a time to be imaged with exposure times down to a micro-second (Ju et al., 2012).

However, the imaging techniques have some disadvantages and their data-acquisition rates are generally lower than those of the laser-based techniques. In particular, the use of backlight can impose limitations to the measurement accuracy which is related to the depth-of-field (DOF) effect. Chigier (1991) indicated two possible sources of measurement errors caused by the DOF, i.e., the ambiguity in defining the edge of an individual droplet when the

droplet is located at some distance from the focal plane but still in the range of the DOF and the dependence of the DOF on the droplet size itself.

As droplets are scattered in the spray, not all droplet images are in-focus. DOF is the region in which the droplets are 'acceptably' sharp or 'in focus' and can thus be measured accurately. An in-focus droplet criterion is needed to select and further analyze these 'in focus' droplets.

In literature, there are two major categories for the in-focus droplet identification: the first one uses the gray level gradient at the droplet boundaries (Lecuona *et al.*, 2000; Kashdan *et al.*, 2007) while the second uses the contrast value between the droplet and the image background based on point spread function (Kim & Kim, 1994; Malot & Blaisot, 2000). The gray level gradient techniques provide information on the relation between droplet size and DOF. Kashdan *et al.* (2007) used the thickness of blurred 'halo' area at the edge of the droplet to determine the degree of droplet defocus. The gray level gradient at the droplet edges in the study of Lecuona *et al* (2000) is found by means of Sobel masks. Large droplets have a higher image contrast and thus can be measured over a greater distance to the lens than small droplets. Kashdan *et al.* (2007) and Lecuona *et al.* (2000) observed a linear relation between DOF and droplet diameter.

This chapter presents a technique based on image processing for measuring the droplet size and velocity characteristics of agricultural hydraulic spray nozzles using an image acquisition system developed in Chapter 3. The chapter is constituted of two parts. In the first part (6.2.1), an in-focus droplet criterion based on the gray level gradient was introduced to decide whether a droplet is considered to be in focus or not. A calibration system was devised using differently sized droplets generated with a piezoelectric droplet generator and glass nozzles in continuous mode, developed in Chapter 5 (Lee, 2003; Vulgarakis Minov *et al.*, 2015b), at different distances from the focal plane and lens using a micro translation stage (Kashdan et al., 2007). This enabled measurement of the gray level gradient and the in-focus parameter for every droplet size at various distances from the focal plane (Lecuona et al., 2000). From here, a critical in-focus parameter (Inf_c) was established for every droplet size and an in-focus droplet criterion was deduced to decide whether a droplet is in focus or

not depending on its diameter and in-focus parameter. The focused droplet zone (FDZ) is defined in this study as the zone in which a droplet with a certain diameter is in focus.

In the second part (6.2.2), the in-focus droplet criterion was applied to spray images of different hydraulic spray nozzles and the droplet characteristics were calculated. The effects of the nozzle type and nozzle size on spray droplet size and velocity characteristics were studied.

Droplet size and velocity results were compared with an existing non-imaging droplet measuring technique, the PDPA laser (Nuyttens *et al.*, 2007a).

6.2 MATERIALS AND METHODS

As already stated, this chapter is divided in two main parts: development of the in-focus droplet criterion (6.2.1) and spray droplet characterization using the in-focus droplet criterion (6.2.2).

6.2.1 Development of the in-focus droplet criterion

6.2.1.1 Image acquisition system and measuring set-up

The image acquisition system for the development of the in-focus droplet criterion is shown in Figure 6.1 and has been described in detail in Chapter 3.

A piezoelectric droplet generator (Université de Liège, Gembloux, Agro-Bio-Tech, Belgium) was positioned at 320 mm from the xenon backlight illumination (model 5132, 300 W, Richard Wolf GmbH, Knittlingen, Germany) and at a distance ranging between 420 and 430 mm from the lens. The camera, lens and illumination were aligned horizontally. A precision linear micro translation stage (Edmund Optics, 0-25 mm) with a straight line accuracy of 10 µm moveable in the Z direction was attached to the lens. The droplet generator was implemented in continuous mode (Chapter 5) using glass nozzles with orifice sizes of 261, 123, 67, 50, and 40 µm. These nozzle orifice sizes were chosen in order to produce a range of droplet sizes from around 100 µm up to 500 µm which is typical of most agricultural hydraulic spray nozzles. The applied settings of the droplet generator and the actual droplet sizes at the focal plane are given in Table 6.1 (Chapter 5).

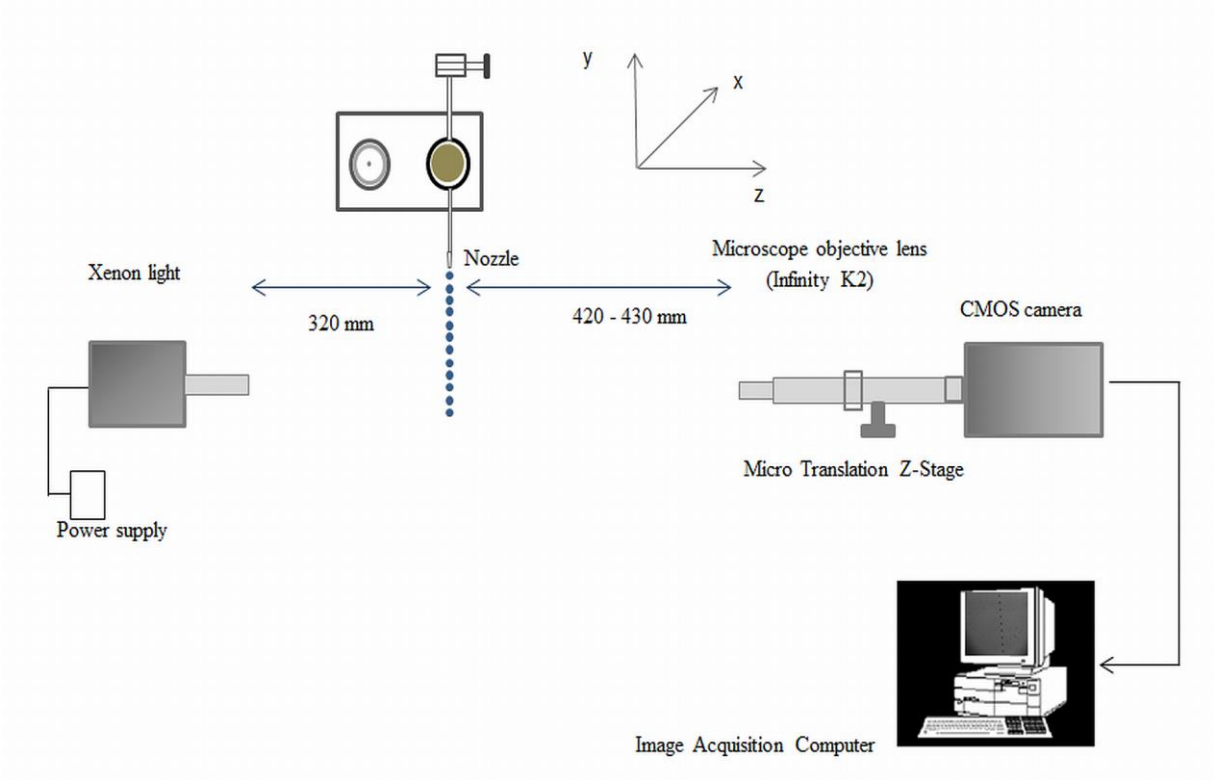

Figure 6.1. Image acquisition system for establishing the in-focus droplet criterion

Table 6.1 Actual droplet diameters in continuous mode for the different nozzle orifice sizes and continuous mode settings

Nozzle orifice size (µm)	**Settings in cont. mode A (V) / *f* (kHz)**	**Actual droplet diameter (µm) ± std.**
40	5.0/8.0	119.3± 2.6
50	5.0/8.0	164.6± 1.9
65	2.0/8.0	192.6± 1.3
65	5.0/8.0	222.9 ± 1.6
123	5.0/8.0	384.3 ± 0.8
261	5.0/8.0	489.7 ± 1.9
261	7.0/8.0	497.1± 2.0

A: Amplitude, *f*: frequency

6.2.1.2 Image acquisition for setting up the in-focus droplet criterion

For establishing the in-focus droplet criterion, images were taken at different distances from the focal plane using all nozzles and settings given in Table 6.1. This was done by moving the translation stage (lens) towards and away from the focal plane in the range between 420 mm and 430 mm in steps of 50 µm (Figure 6.1). Thus, in this manner sequences of 200 'out-in-out of focus' images were taken with every nozzle/setting combination (Table 6.1). An

example of images in continuous mode taken with the nozzle orifice size of 65 µm at 5.0 V and 8.0 kHz, generating 222.9 µm droplets, at three distances from the focal plane is shown in Figure 6.2.

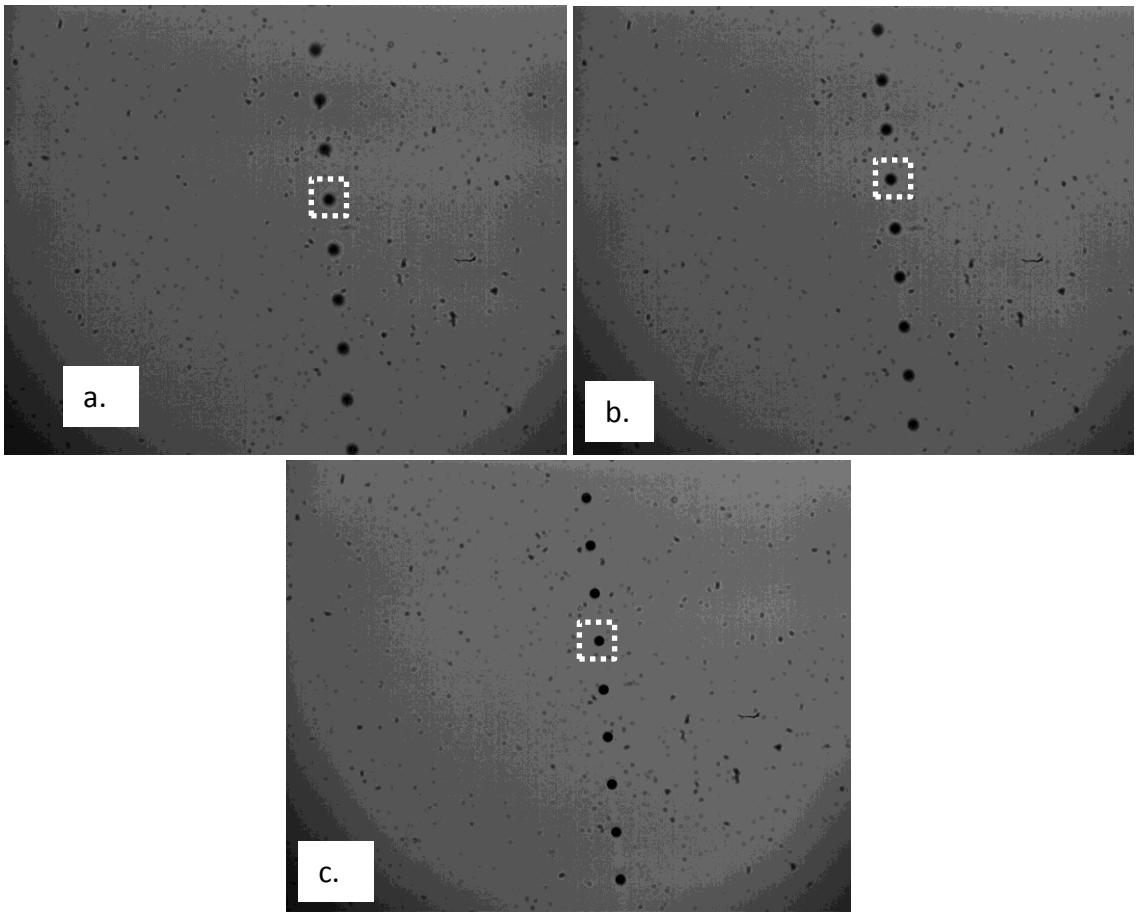

Figure 6.2. Droplet images in continuous mode using a nozzle with 65 µm orifice size at 5.0 V and 8.0 kHz at different distances from the lens: a) 420 mm; b) 423 mm c) 426 mm

Once the images were acquired, a sequence of steps was employed to process and analyze them using Matlab and its image processing toolbox (Figure 6.3).

6.2.1.3 Image analysis for setting up the in-focus droplet criterion

The image analysis for setting up the in-focus criterion consisted of 3 steps: image pre-processing (6.2.1.3.1), image segmentation (6.2.1.3.2) and droplet sizing, calculation of (critical) in-focus parameter and in-focus droplet criterion (6.2.1.3.3) (Figure 6.3).

6.2.1.3.1 Image pre-processing

Image pre-processing aims at resolving problems due to lighting patterns or dirt on the lens, given that the light source can be non-homogeneous (Castanet et al., 2013). A background subtraction was performed from every single droplet image. The image background was reconstructed from a set of 70 images with droplets. For each of these images, the background was selected based on its intensity histogram with a threshold value of 80% of the maximal pixel intensity of 255. These 70 background images were averaged and resulted in the final image background.

However, in general the image contrast was low and the droplet boundaries are uncertain. Therefore, to increase the contrast and highlight the intensity variation across the droplet boundaries, illumination normalization was performed by rescaling the gray values.

such that exactly 1% of the pixels were saturated in order to maximize image contrast (Gonzalez et al., 2004).

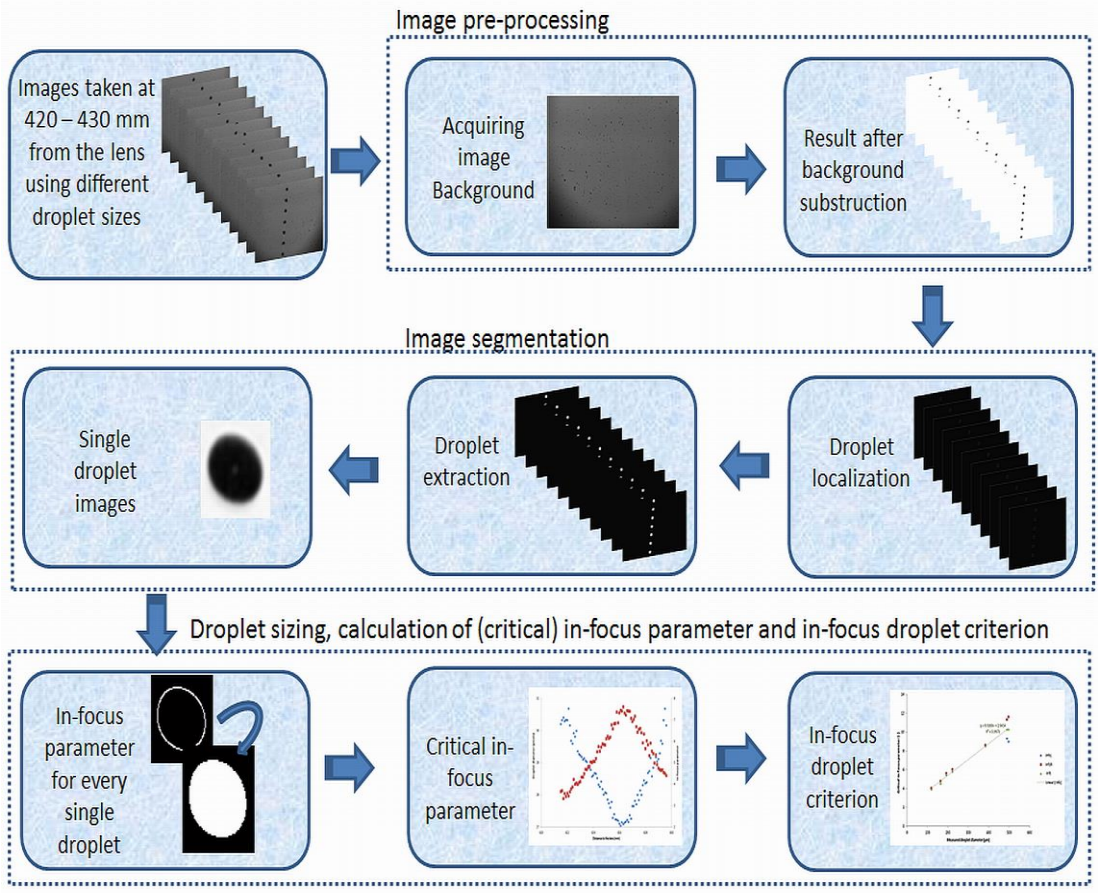

Figure 6.3. Flow chart of the image analysis algorithm for establishing the in-focus droplet criterion

6.2.1.3.2 Image segmentation

Image segmentation was introduced to divide the image into sub-images of all individual droplets. The localization of droplets was performed by searching for sudden changes in the pixel intensity corresponding with the boundaries between a droplet and background. This was done by computing the intensity gradient at each point giving the direction of the large possible increase from light to dark and the rate of change in that direction using the Sobel filter (Gonzalez et al., 2004) (Figure 6.3).

Further, the highlighted droplet contours were filled. Then, the image was binarized, i.e., image pixels were distinguished amongst two classes: droplets and background. The intensity threshold value was set to 85% of the maximum which was high enough to detect and maintain all the droplets even those out of focus. The droplet area was calculated as the sum of the component pixels, and the droplet center as the center of the droplet mass. Using the droplet area and assuming that the droplets can be elliptical, the droplet diameter was estimated as described in 4.2.3. Finally, sub-images of each detected droplet were constructed using the coordinates of the droplet center and the corresponding diameter. The size of the sub-images was equal to 1.5 times the droplet diameter, which was enough to capture the whole droplet and region of interest (Figure 6.3).

6.2.1.3.3 Droplet sizing, calculation of (critical) in-focus parameter and in-focus droplet criterion

This step consisted of two main parts. The size of each detected droplet was calculated together with the corresponding in-focus parameter. In the second part, the critical in-focus parameter was calculated for each droplet size and the in-focus droplet criterion was established. The critical-in focus parameters and the resulting in-focus droplet criterion were used to select in-focus droplets.

a) Droplet sizing and calculation of in-focus parameters

The droplet contours in the single droplet sub-images were extracted using a Canny edge detector (Canny, 1983) (Figure 6.3). When the contours were found, the droplet edge gradients, the gray level intensities of the droplet and background and the droplet size were calculated.

However, the extracted droplets did not have the same gray level intensities and edge gradients because of their different positions relative to the focal plane (Figure 6.3). In addition, droplets further from the focal plane had a bigger halo area than the droplets that are close to the focal plane (Figure 6.4). Figure 6.5 a, b & c shows three single droplet images (taken from Figure 6.2 a, b & c) and their corresponding gray level intensity profiles across their centers. Ideally a droplet in focus has a flat intensity profile at the bottom close to 0 intensity level with steep edge gradients (Figure 6.5 c). In this case, the droplet edges and size can be determined in an accurate way. In contrast, when a droplet is situated at some distance from the focal plane and is out of focus (Figure 6.5 a & b), there is an ambiguity in defining the droplet edges (Kashdan et al., 2007).

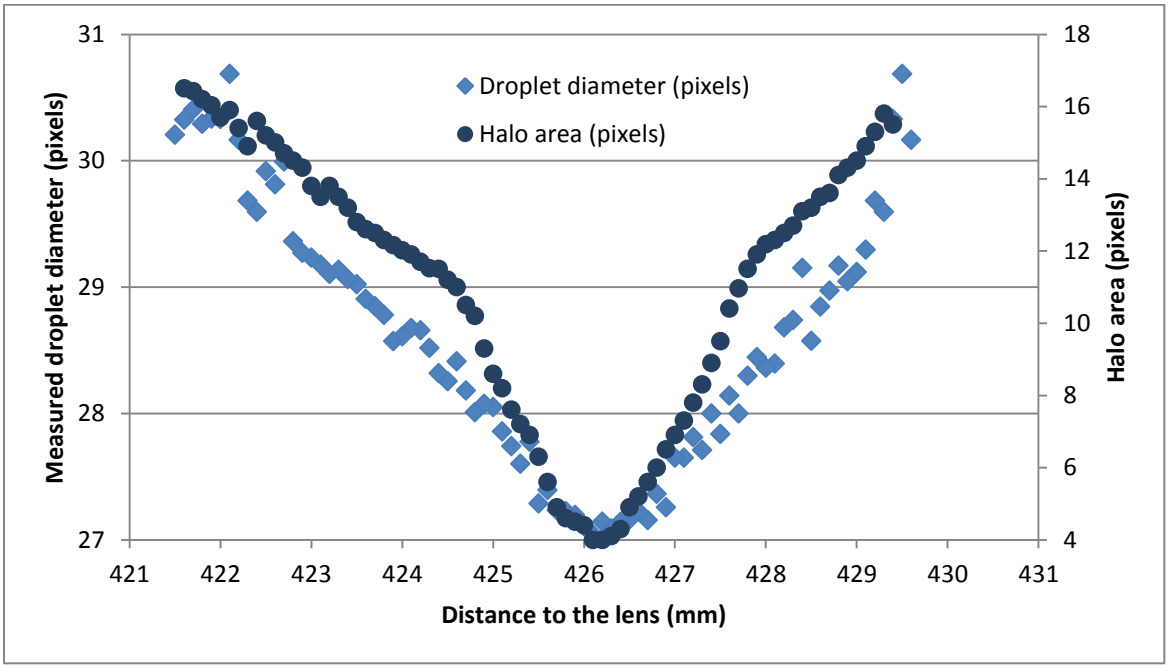

Figure 6.4. Measured droplet diameter and corresponding halo area for pictures taken of the 222.9 µm droplet diameter at various distances from the lens

The gradients at the edges of the droplets reflect their degree of focus and can be used as a criterion based on which the droplets are chosen for measurement (Yule, 1978). Therefore, the concept of the in-focus parameter was introduced to select the in-focus droplets based on the gray level gradient, droplet diameter and gray level intensities of the background and droplet (Eq. 6.1) (Lecuona et al., 2000):

$$In-focus\ parameter\ = \frac{grad_{edge}}{I_{back}-I_{droplet}} * d \qquad \text{Eq. 6.1}$$

where I_{back} (-) and $I_{droplet}$ (-) are image background and droplet gray level values, respectively, d is the droplet diameter (µm) and $grad_{edge}$ (-) is the gray level gradient at the droplet edge. The in-focus parameter (-) was calculated for every detected droplet.

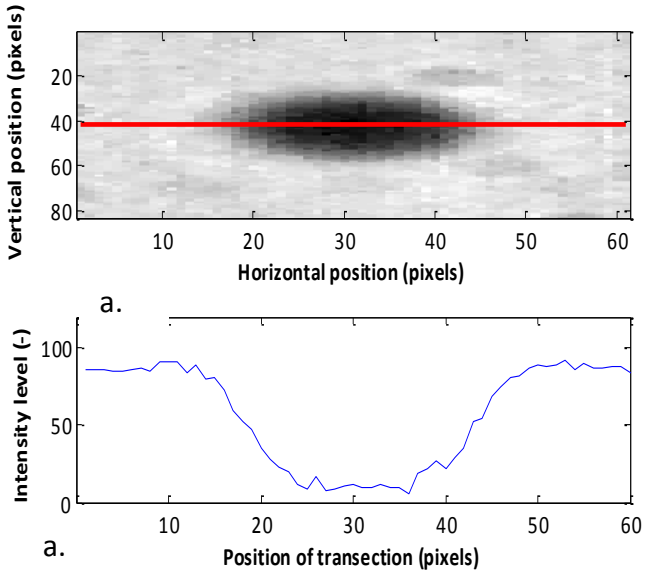

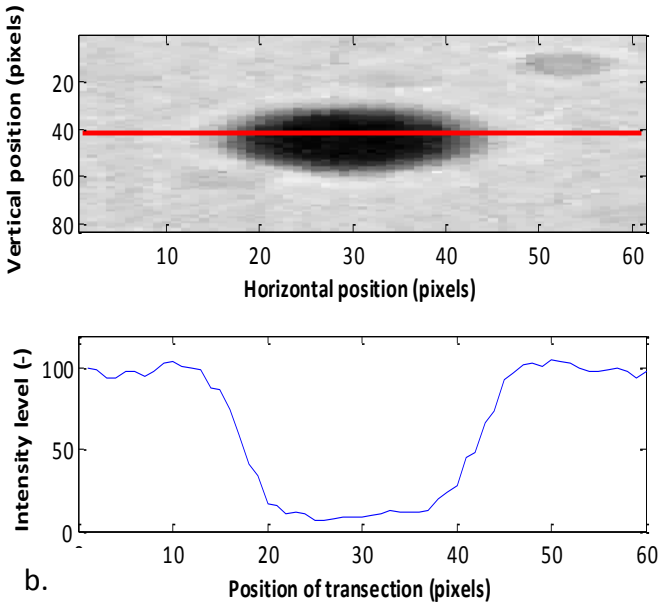

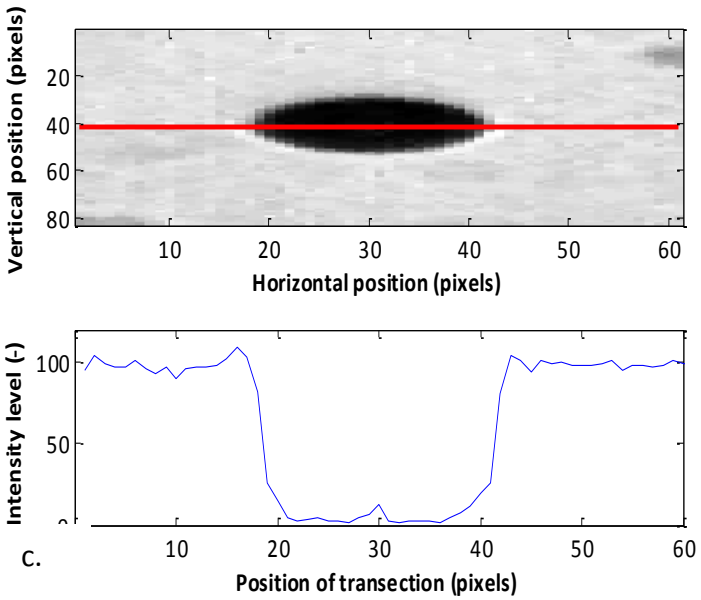

Figure 6.5. Detail and gray level intensity profiles from the marked droplets shown in Figure 6.2 a, b & c, respectively

For example, Figure 6.6 presents the measured droplet diameters and the corresponding in-focus parameters for the experiments with a 222.9 µm (27.1 pixels) droplet at various distances from the lens. It can be seen that the in-focus parameter has a maximum at or near the position where the measured droplet diameter is minimal and corresponds with the actual droplet diameter. The further the distance from the focal plane the lower the in-focus parameter and the bigger the measured droplet diameter and the deviation with the actual droplet diameter. Similar graphs were found for the other droplet diameters as shown in Figure 6.9. and Figure 6.10

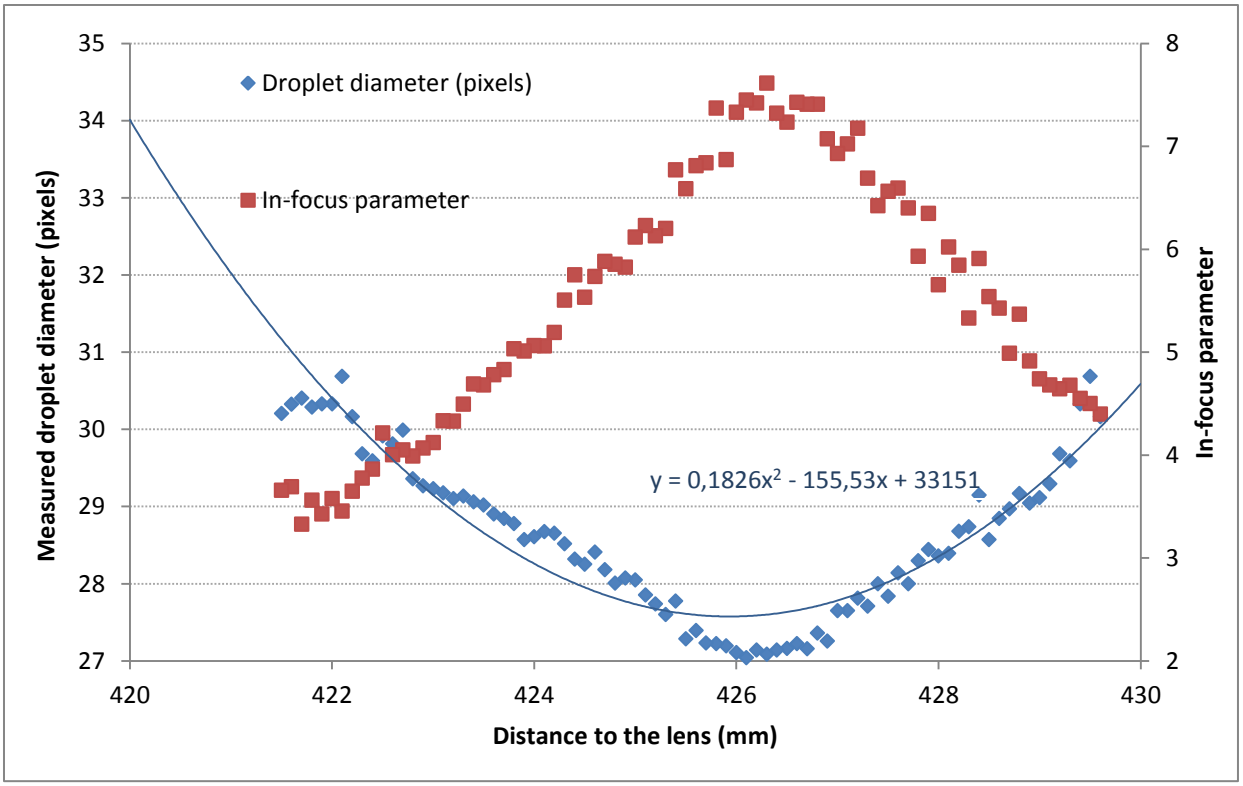

Figure 6.6. Measured droplet diameter and corresponding in-focus parameter for pictures taken of the 222.9 µm (27.1 pixels)droplet diameter at various distances from the lens

b) Calculation of critical in-focus parameters and the in-focus droplet criterion

To separate the droplets that are in-focus from the ones out of focus, a critical in-focus parameter (Inf_c) was calculated for each of the seven droplet sizes (Table 6.1). The determination of Inf_c was done in several steps and is here illustrated again for the 222.9 µm droplet size. Firstly, the minimal droplet diameter was estimated from the polynomial trend line of second order using all measured droplet diameters (27.6 pixels, Figure 6.6). Then, an acceptable one pixel error value to this minimal droplet diameter was set corresponding with 28.6 pixels (Figure 6.7.) meaning that we accept a deviation of up to 1 pixel between measured and actual droplet diameter. Hence, all droplets with a measured diameter below 28.6 pixels were considered to be in-focus, all others out of focus.

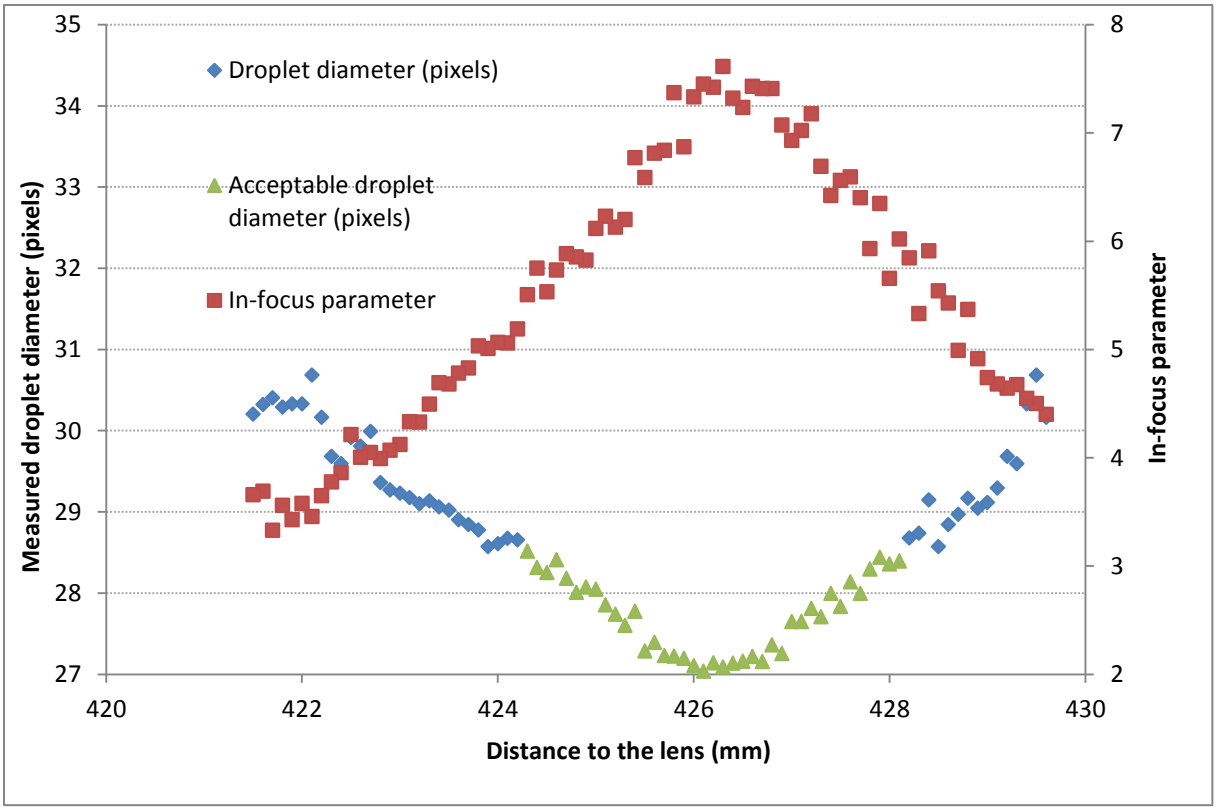

Figure 6.7. Acceptable measured droplet diameters for pictures taken of the 222.9 µm droplet diameter at various distances from the lens

Next, another second order polynomial curve was fit only through these droplets considered in focus with an acceptable measured droplet diameter (Figure 6.8.). From this equation ($y = 0.3953.x^2-336.95.x+71835$) and the droplet diameter of 28.6 pixels the corresponding distances to the lens were calculated (424.4 mm and 428.1 mm). Combining these distances to the lens with the second order polynomial curve through the in-focus parameters, resulted into two values for the critical in-focus parameter, one on the left side, Inf_{cL} (6.0), and one on the right side, Inf_{cR} (6.1).The average of both values was considered the critical in-focus parameter Inf_c (6.0). All droplets with an in-focus parameter above Inf_c were considered in-focus. Besides, based on the distances from the lens at which the droplets were considered in focus, a focused droplet zone (FDZ) was defined. This is the zone around the focal plane in which droplets of a certain size are considered in-focus (Figure 6.8.). For the 222.9 µm droplet size, the FDZ was 3.7 mm.

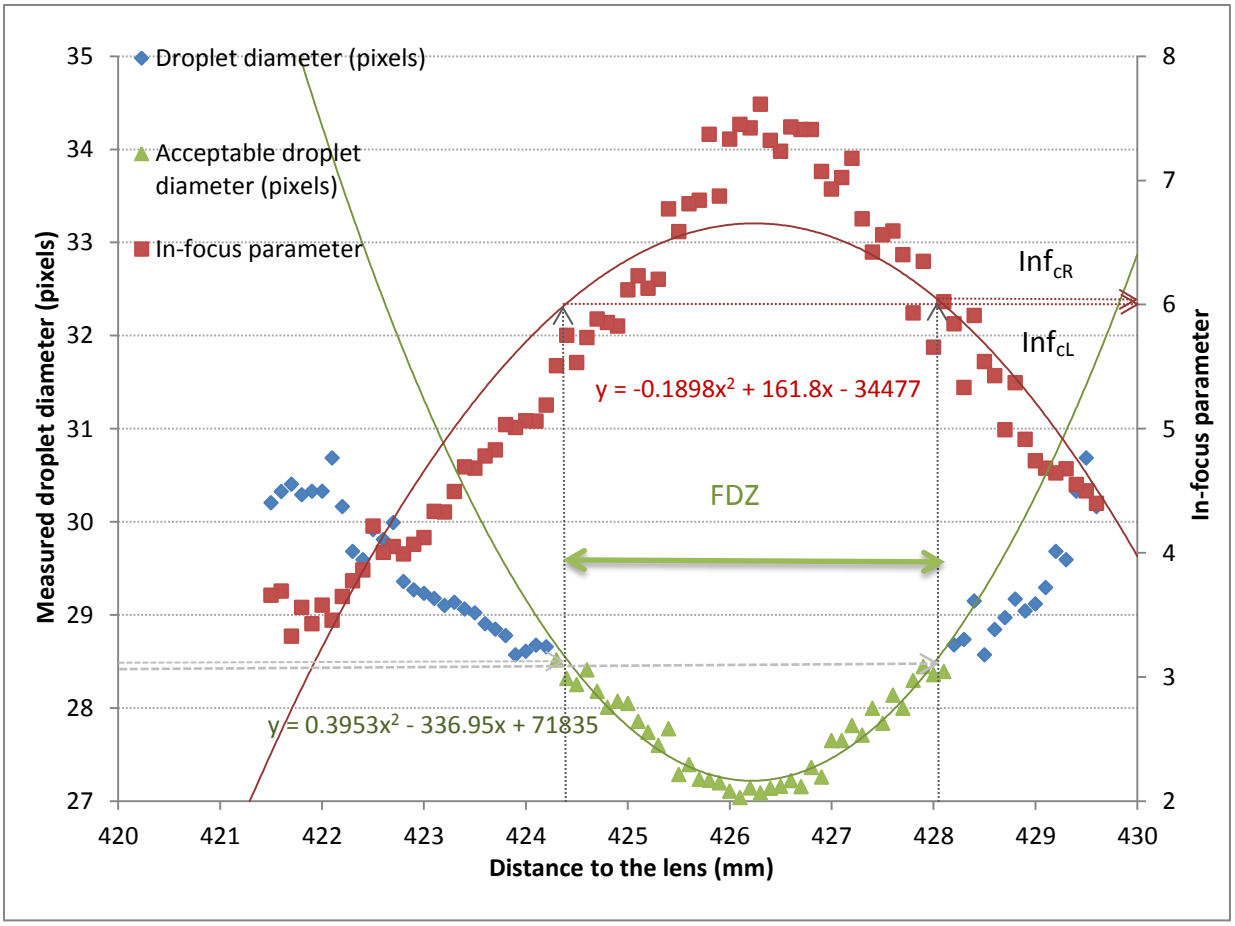

Figure 6.8. Critical in-focus parameters and FDZ for pictures taken of the 222.9 µm droplet diameter

In order to evaluate the relations between Inf_c, FDZ and droplet size, the procedure above was followed for all droplet sizes mentioned in Table 6.1. Results from these tests are shown in Figure 6.9. and Figure 6.10. and Table 6.2.

Table 6.2 Actual droplet diameters and their corresponding Inf_c and FDZ

Actual droplet diameter (µm)	**Inf_c (-)**	**FDZ (mm)**
119.3	3.95	2.1
164.6	4.62	2.6
192.6	5.50	3.2
222.9	6.05	3.7
384.3	8.55	4.1
489.7	10.30	5.0
497.1	10.30	5.0

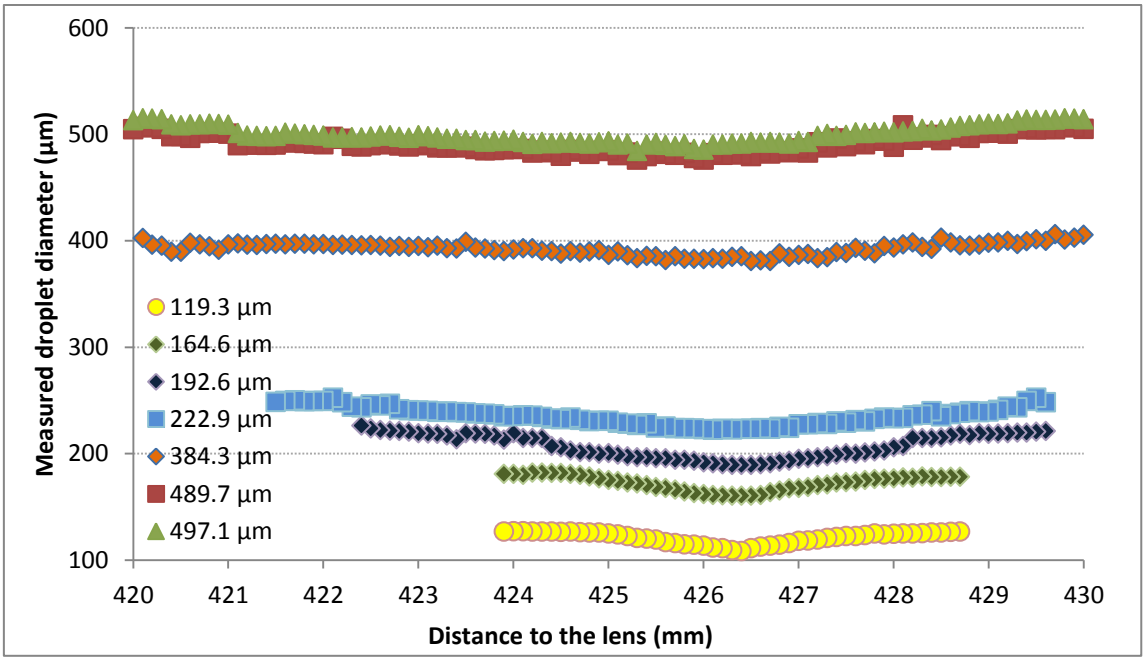

Figure 6.9. Relation between the measured droplet diameter and distance to the lens for droplet sizes ranging from 119.3 µm up to 497.1 µm

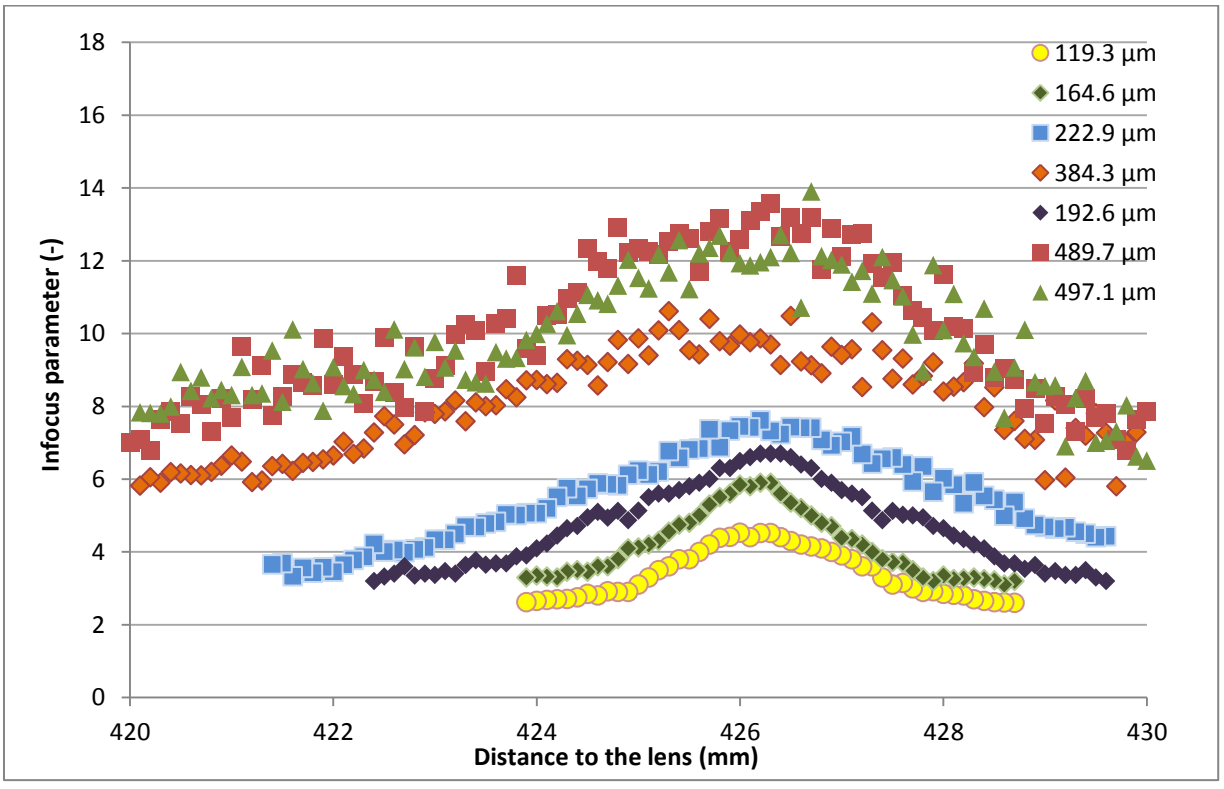

Figure 6.10. Relation between the in-focus parameter and distance to the lens for droplet sizes ranging from 119.3 µm up to 497.1 µm

Measured droplet size was lowest at or near the focal plane (Figure 6.9.). For each droplet size, the in-focus parameter was the biggest at or near the focal plane and mostly quickly drops with increasing/decreasing the distance to the focus plane (Lecuona *et al.*, 2000; Lee & Kim, 2004) (Figure 6.9., Figure 6.10.). Besides, the smaller the droplet diameters, the narrower the corresponding curves in Figure 6.9. and Figure 6.10. meaning that smaller droplets completely disappeared closer to the focal plane than bigger droplets.

Figure 6.11. and Table 6.2 show the relation between the critical in-focus parameter and the actual droplet diameter. It can be noted that the critical in-focus parameter increased almost linearly with the measured droplet diameter. In addition, this first order relation between droplet diameter (d) and Inf_c (Eq. 6.2) is defined as the in-focus droplet criterion and used for selecting only the focused droplets in a real spray application.

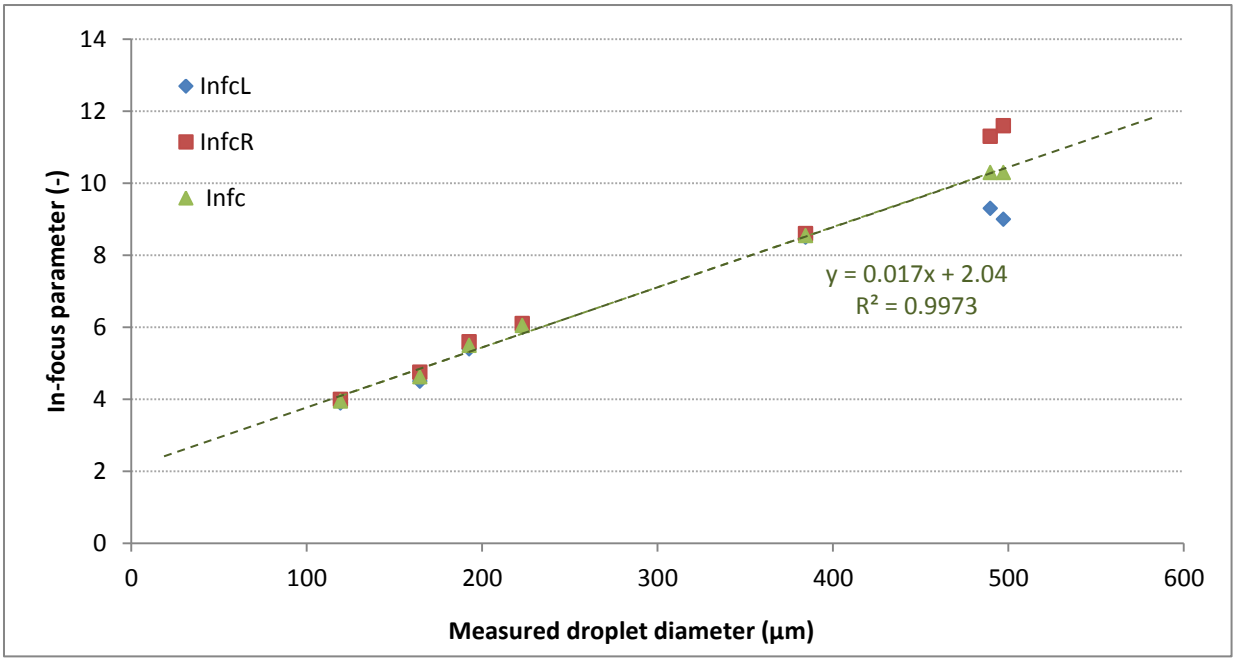

Figure 6.11. Relation between the critical in-focus parameter and measured droplet diameter

$$Inf_c = 0.017 * d + 2.04 \qquad \text{Eq. 6.2}$$

Moreover, the FDZ increased linearly with measured droplet diameter (Figure 6.12.). Droplets beyond this zone were considered defocused and thus not measured.

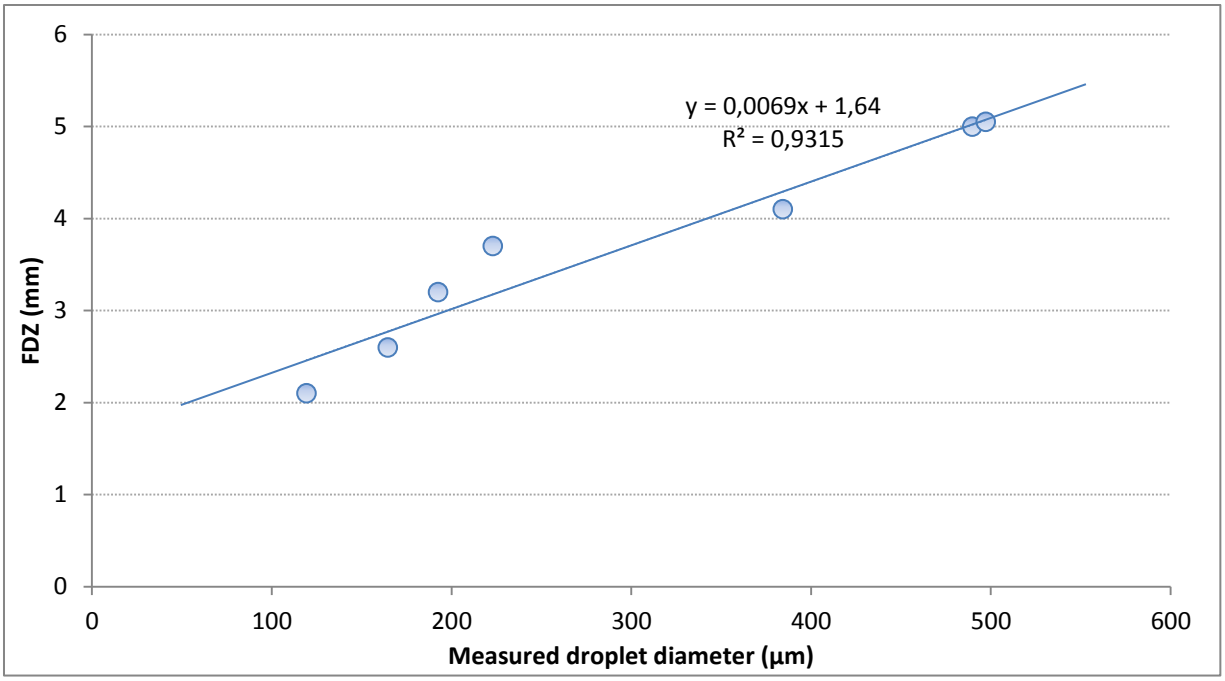

Figure 6.12. Relation between FDZ and measured droplet diameter

6.2.2 Spray droplet characterization using the in-focus droplet criterion

6.2.2.1 Measuring set-up and protocol

A similar set-up as described in 6.2.1 and Chapter 3 was used for the real spray characterization as shown in Figure 6.13.. Droplets dispersed in the spray were illuminated by a xenon light used as backlight. Spray droplet images were acquired by the HS CMOS camera.

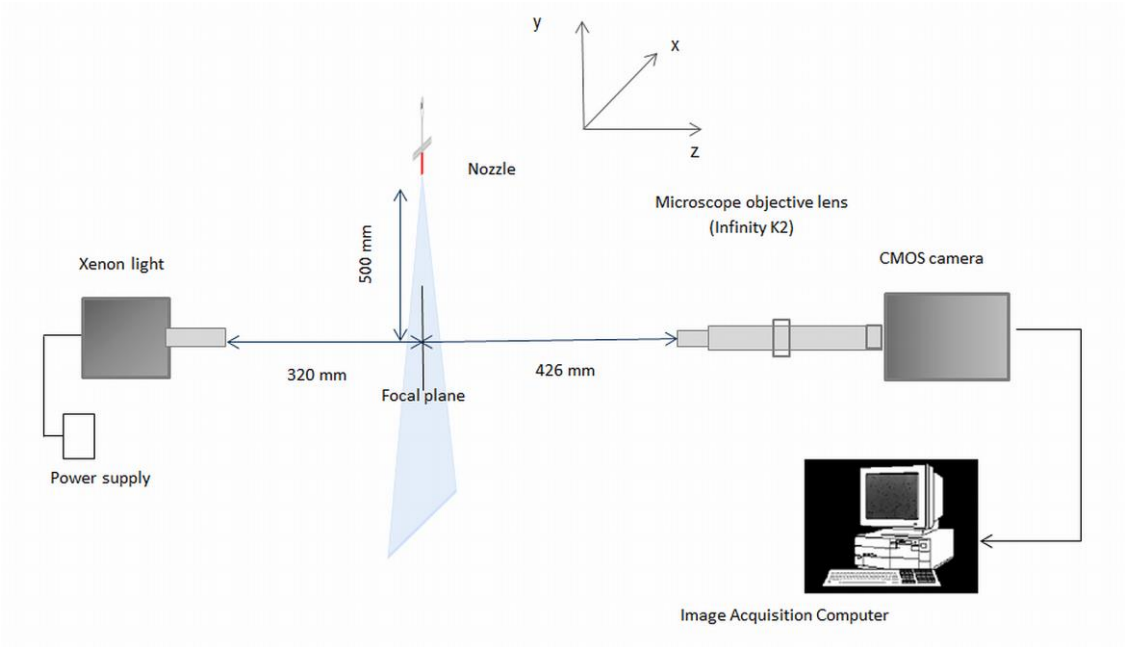

Figure 6.13. Image acquisition system for real spray droplet characterization

In this study, five different hydraulic spray nozzles were selected: two hollow cone (Figure 7.1), two standard flat fan (Figure 7.2) and one air inclusion flat fan (Figure 7.3) nozzle. The selected nozzle-pressure combinations are presented in Table 6.3. The nozzle was always set between the lens and light source with the longest axis of the spray fan (in case of flat fan nozzles) parallel to the focal plane on an automated XYZ-transporter with a traverse range of 2.0 m by 2.2 m (Nuyttens *et al.*, 2007a). Images were acquired at 500 mm below the nozzle at three different positions: in the center, at 200 mm and at the edge of the spray (Figure 6.14.). Based on the spray angles, the zone of the edge of the spray was defined at 400 mm for the flat fan nozzles and at 300 mm for the hollow cone nozzles. A schematic overview of the selected measurement points for every spray nozzle is given in Figure 6.14.. For every nozzle and position combination, 500 images were taken at 1000 fps corresponding with a total time of 0.5s.

The results measured with the imaging system at every point were compared with the results measured at the same points with the PDPA laser. Measurement set-up, protocol (2.4.1.1) and results have been described in detail by Nuyttens et al. (2007a).

Table 6.3 Manufacture specifications of the tested hydraulic spray nozzles

Nozzle type	Nozzle	Pressure (kPa)	Spray angle (°)	Nominal flow rate (l min^{-1})
Hollow cone	Albuz[a] ATR orange	600	80	1.08
Hollow cone	Albuz[a] ATR red	800	80	1.73
Standard flat fan	TeeJet[b] XR 110 01	400	110	0.45
Standard flat fan	TeeJet[b] XR 110 04	400	110	1.82
Air inclusion flat fan	TeeJet[b] AI 110 04	400	110	1.82

[a] Saint – Gobain Solcera, Evreux Cedex, France. [b] TeeJet Technologies, Wheaton, U.S.

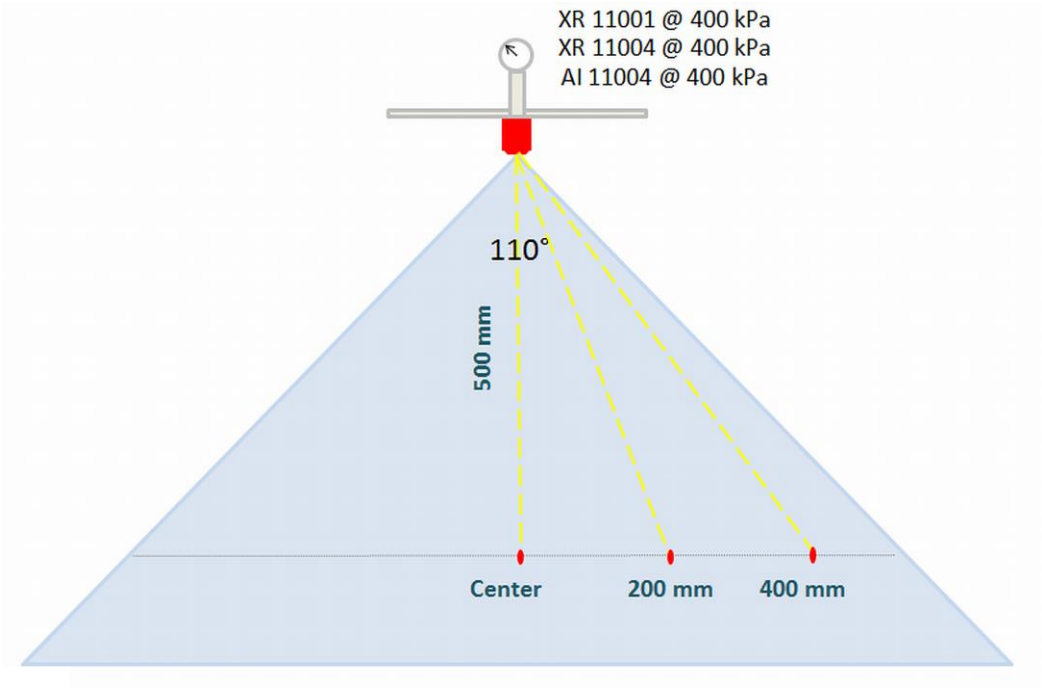

a.

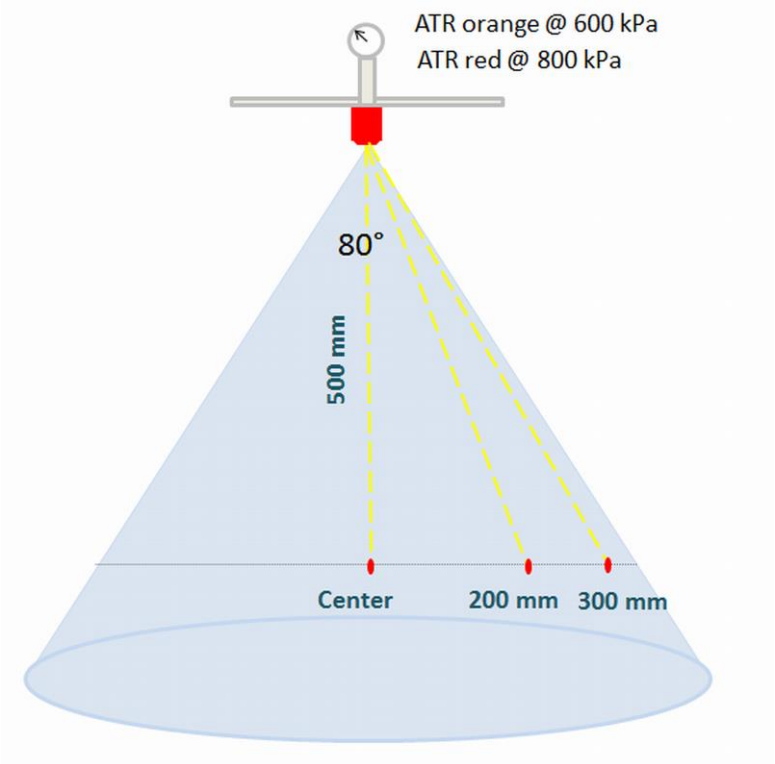

b.

Figure 6.14. Spray measurement points for: a) flat fan and b) hollow cone nozzle

6.2.3 Image analysis for spray droplet characterization

Bigger droplets generally have a higher velocity than small droplets at 500 mm below the nozzle (Nuyttens *et al.*, 2007a). Therefore, small droplets remain longer in the FOV than large droplets. This means that one and the same droplet can be captured in several consecutive pictures and that the probability to measure a droplet more than once is bigger

for smaller droplets than for bigger droplets. Therefore, not every consecutive image was analyzed but every ninth image resulting in a total number of 55 images for each nozzle at each position. This corresponds with a 9 ms time difference between analyzed images. This time difference was enough to ensure that one and the same droplet was not measured twice for the FOV of 10.5 mm x 8.4 mm and a minimal droplet velocity of 1 m/s (Nuyttens *et al.*, 2007a).

The image analysis for the selected images consisted of different steps: image pre-processing, image segmentation and droplet sizing and selection based on the in-focus criterion and droplet velocity calculation.

6.2.3.1 Image pre-processing

Figure 6.15. shows an example of a typical spray image obtained with the XR110 04 nozzle in the center (Figure 6.14.a). The image contains artefacts which have to be rejected, since they would represent a source of error.

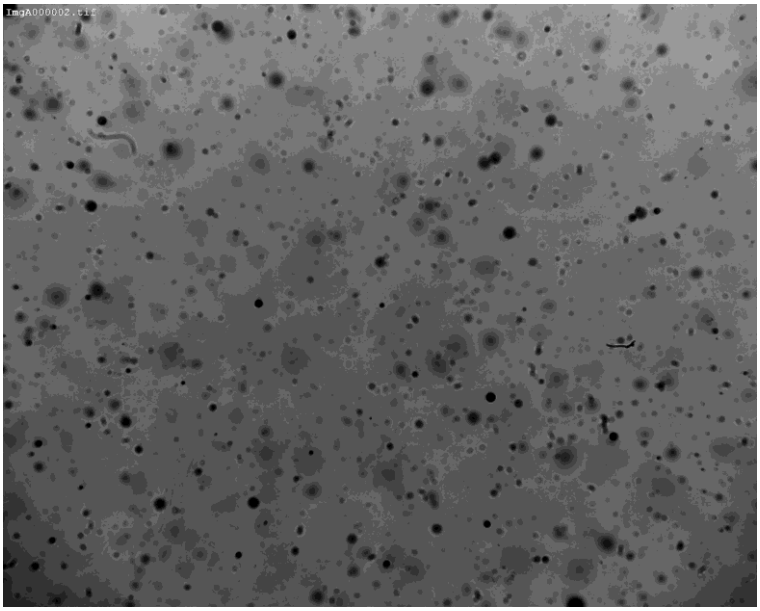

Figure 6.15. Example of spray droplet image with XR110 04 nozzle at 400 kPa in the center

The first step as in 6.2.1.3 was image pre-processing in order to improve the image quality which is essential for further image analysis. The image analysis was the same as for the droplet images in continuous mode described in 6.2.1.3. The result is shown in Figure 6.16..

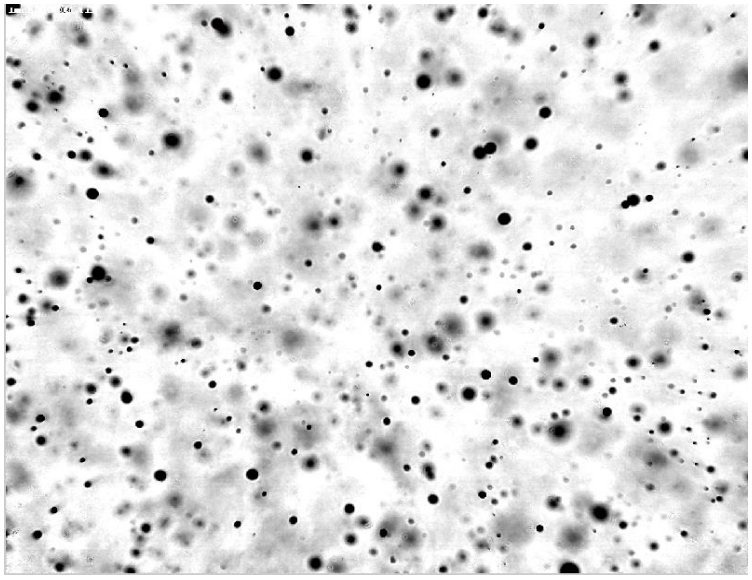

Figure 6.16. Spray droplet image shown in Figure 6.15. after image pre-processing

6.2.3.2 Image segmentation

Every spray droplet has a different gray level and sharpness due to differences in the degree of focus and illumination (Figure 6.16.). Furthermore, blurred droplets can locally modify the background around droplets that are more in-focus. Therefore, each droplet was separately analyzed by making sub-images. This image segmentation consisted of droplet localization and droplet extraction into single droplet sub-images. Droplet localization was achieved as described in 6.2.1.3 (Figure 6.17.). Each image was segmented into droplet and background regions by assigning pixels inside the droplet edge to the droplet and remaining pixels to the background (Gonzalez *et al.*, 2004; Lee *et al.*, 2009). Afterwards, the spray image was binarized for droplet detection. Morphological operations like opening, closing and filling the holes were applied (Figure 6.18.). Assuming the droplets are spherical, the next step included locating the center, calculating the area and estimating the diameter of every droplet. As in 6.2.1.3, single droplet images could be extracted. In addition, spray droplets touching the image border were rejected for reasons of measurement accuracy.

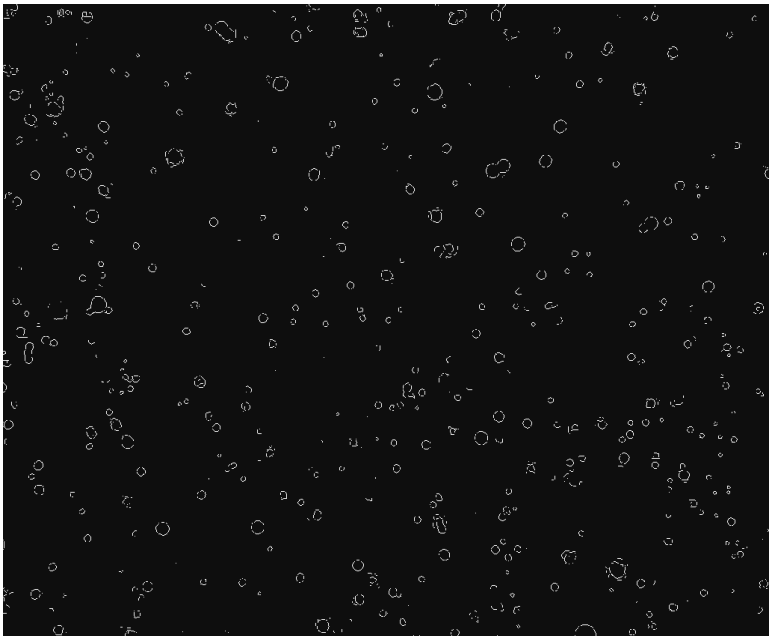

Figure 6.17. Spray droplet image shown in Figure 6.15. after droplet localization

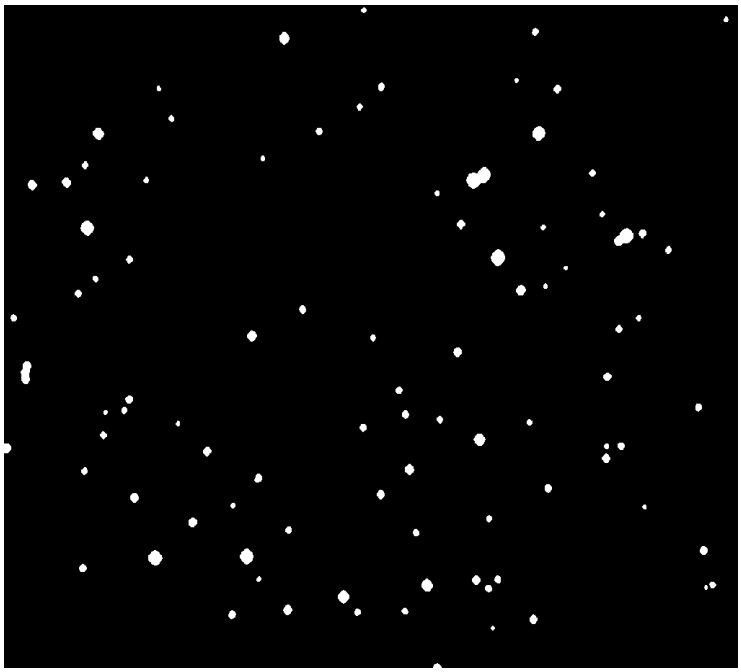

Figure 6.18. Spray droplet image shown in Figure 6.15. after applying morphological operations

6.2.3.3 Droplet sizing and selection based on in-focus criterion

Once the single droplet sub-images were extracted, a Canny edge detector was applied (Figure 6.19.). The next step consisted of calculating the droplet edge gradients, the gray level intensities of droplet and background, and the droplet size , similarly as in 6.2.1.3.

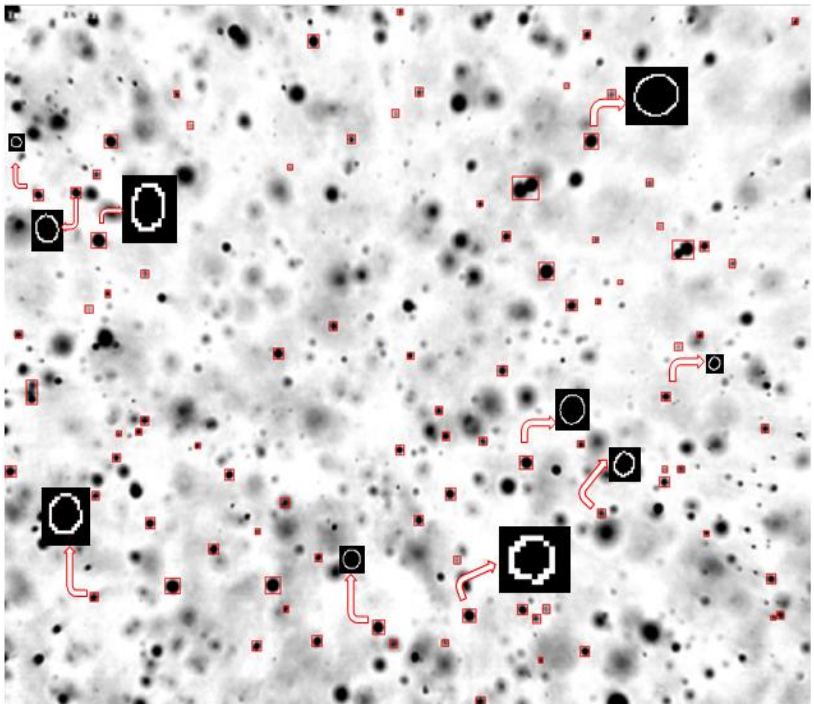

Figure 6.19. Examples of single spray droplet images after Canny edge detection

In the final step the droplet in-focus criterion (Eq. 6.2) was applied to every spray droplet that satisfies the circularity criteria (4.2.3). Overlapping droplets are not circular and therefore were not considered in the measurements.

Droplets having an in-focus parameter bigger than the corresponding Inf_c (based on the measured diameter and Eq. 6.2) were considered in focus and included in the spray droplet distribution results. All other droplets were rejected and not further used in the analysis.

6.2.3.4 Droplet velocity

Once the droplet center and position were determined, the next step involved droplet tracking to find the same droplet in two consecutive images, as well as the displacement vector and velocity. This was possible because of the large acquisition rate of the HS camera. The used droplet tracking principle is well explained in 4.2.4.

However, few conditions related to the droplet diameter, droplet displacement and droplet velocity in a real spray application exist and are necessary in order to identify the same droplet on two successive images (Baek & Lee, 1996; Castanet *et al.*, 2013). First is the condition of conservation of droplet diameter i.e. the diameter of the candidate droplet on the consecutive image should not differ more than 2 pixel (16.5 µm) from the droplet on the

first image (Baek & Lee, 1996). The second criterion is the expected droplet direction based on the direction of the flow (Figure 6.20). An angle of confidence Θ of ± 40° was considered to define the search area (circle sector) to find the same droplet in the consecutive image. The existing of a search area is important for the proper functioning of the droplet tracking algorithm. If the area is too big, this will result into droplet mismatches and velocity errors. On the other hand, if this area is too strictly defined, it will limit the detection of the fast droplets.

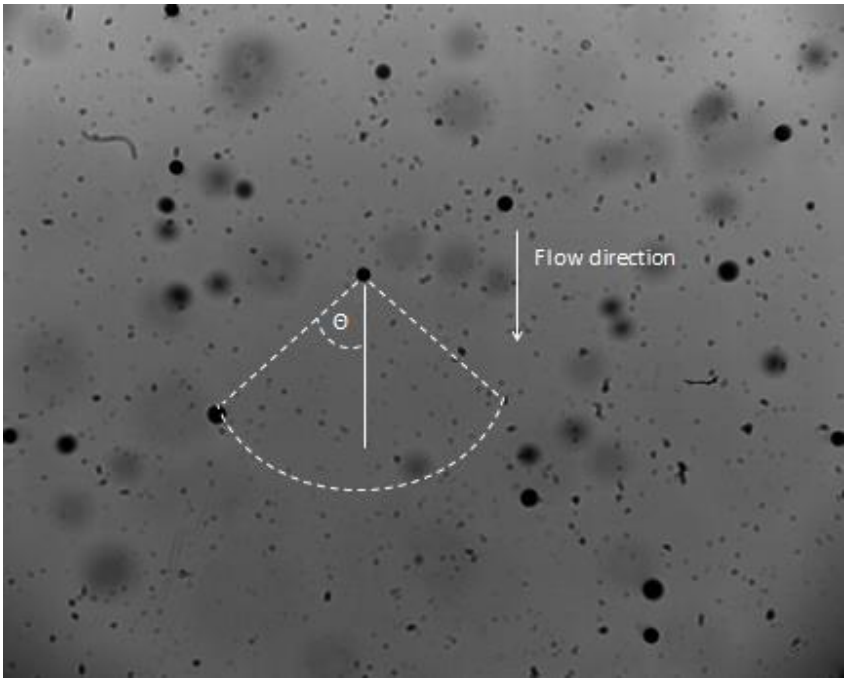

Figure 6.20. Droplet tracking principle in the center of the spray

6.3 RESULTS AND DISCUSSION

6.3.1 Spray droplet size distribution

Figure 6.21. shows a typical histogram of a droplet size distribution measurement resulting from 430 droplet size measurements using the XR110 04 at 400 kPa at 500 mm in the center of the spray which is obtained from the imaging system. The vertical, blue-colored, bars are “bins” of droplet sizes. Each “bin” has a width of 10 µm. The relative frequency of droplet size occurrence is on the left horizontal axis. For instance, about 3% of the droplets were counted in the 100 µm bin consisting of droplets from 95 µm up to 105 µm.

The red colored curve is the corresponding cumulative droplet size distribution. This graph shows, for example, that 50% of the droplets were smaller than about 130 µm.

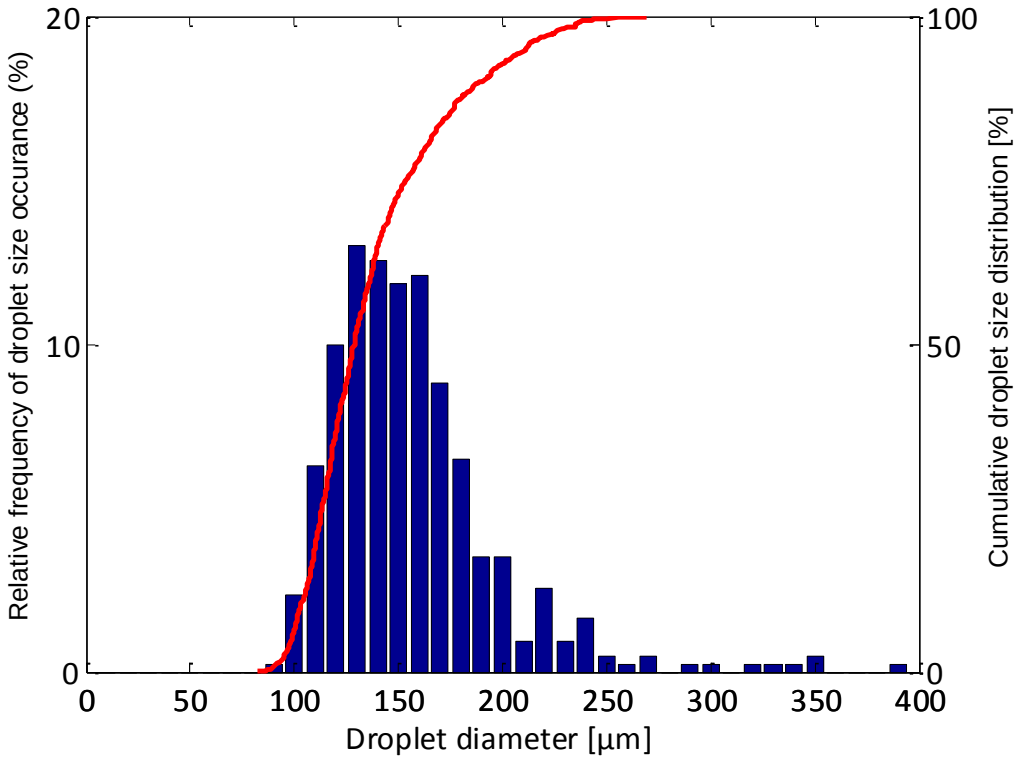

Figure 6.21. Relative frequency of droplet size occurrence (blue) and cumulative droplet size distribution (red) for the XR 110 04 at 400 kPa at 500 mm below the nozzle in the center of the spray. This data is obtained from the imaging system

6.3.1.1 Effect of the measurement point for every nozzle

Figure 6.22. presents the cumulative droplet size distributions for the five nozzle-pressure combinations (Table 6.3) at the three different measurement points always at 500 mm below the nozzle i.e. center, at 200 mm and at the edge of the spray (Figure 6.14.). In general, droplet sizes ranged from 24 µm up to 543 µm depending on nozzle type, size and measuring position.

For the flat fan nozzle pressure combinations (XR 110 01, XR 110 04, AI 110 04), the finest droplet size spectrum was measured in the center of the spray and at 200 mm, while the coarsest droplet size distribution was found at the edge of the spray (Figure 6.22.). No clear differences in droplet size distribution between the center of the spray and at 200 mm were observed.

For the hollow cone nozzles (ATR orange, ATR red), the effect of the position in the spray was even more pronounced. Again, the finest droplet size spectrum was observed in the center of the spray followed by the 200 mm position and the 300 mm position.

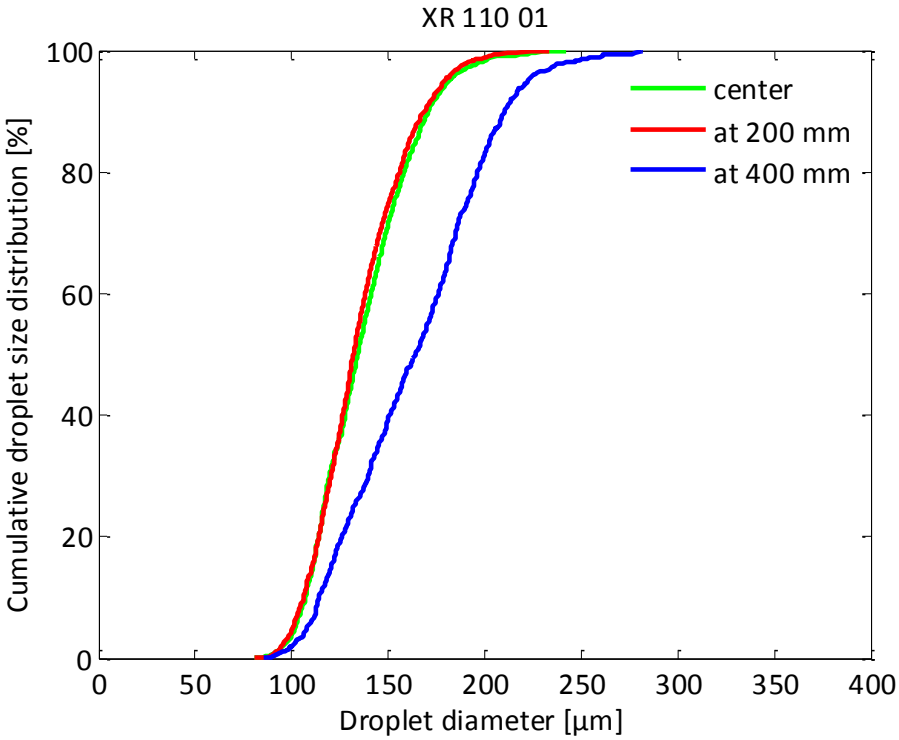

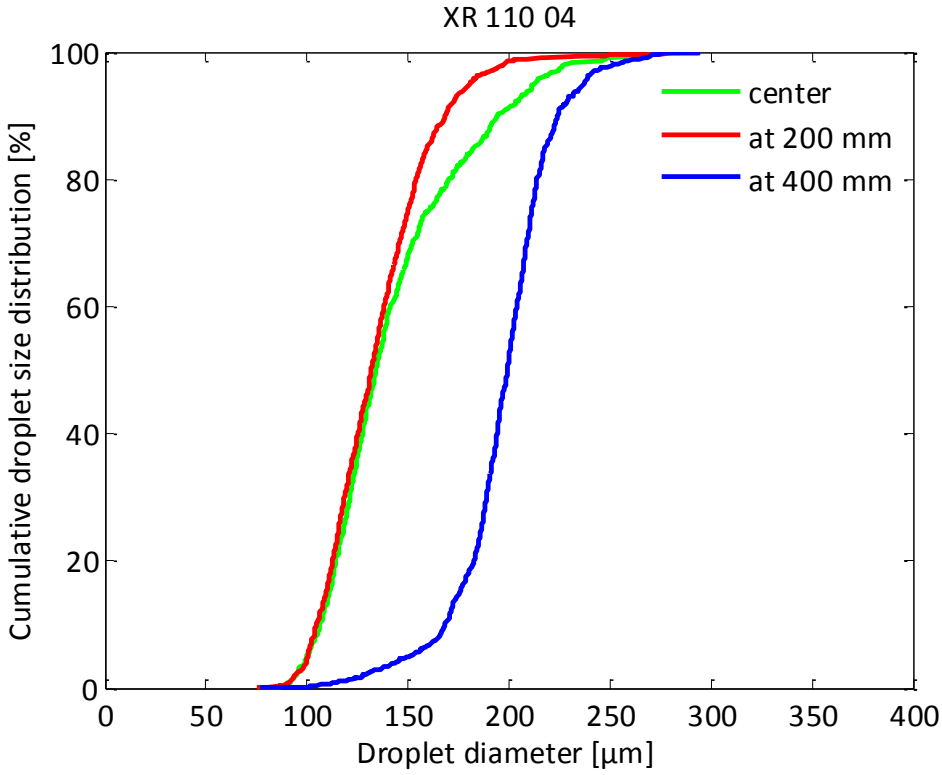

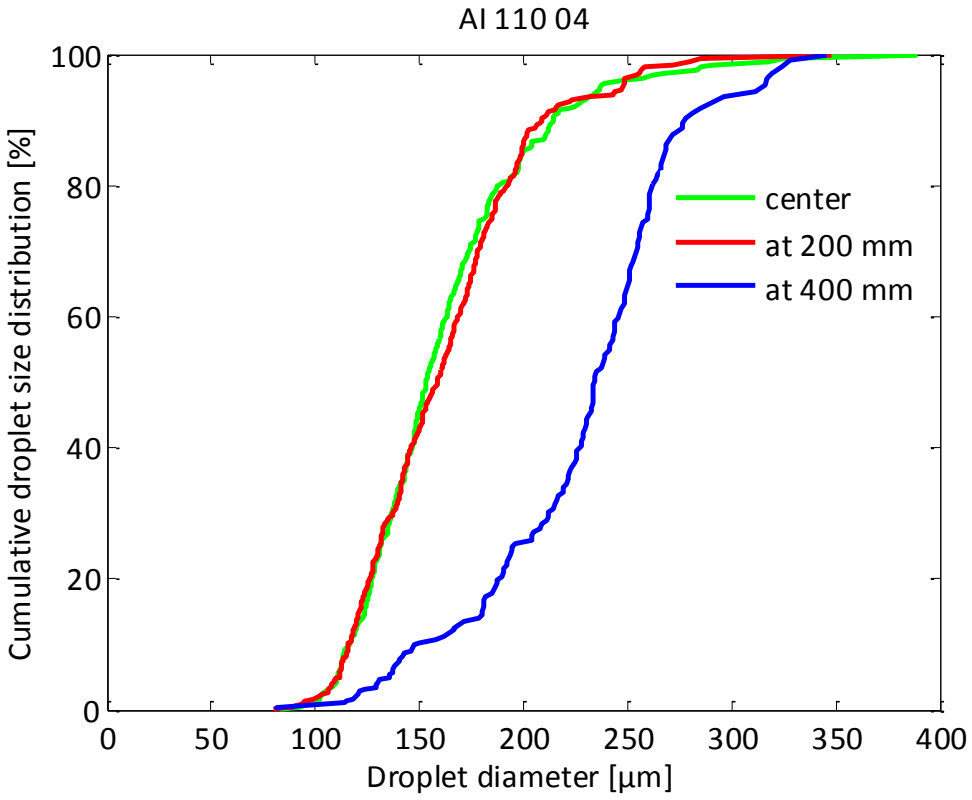
AI 110 04
Cumulative droplet size distribution [%]
Droplet diameter [µm]
center
at 200 mm
at 400 mm
0
20
40
60
80
100
0
50
100
150
200
250
300
350
400

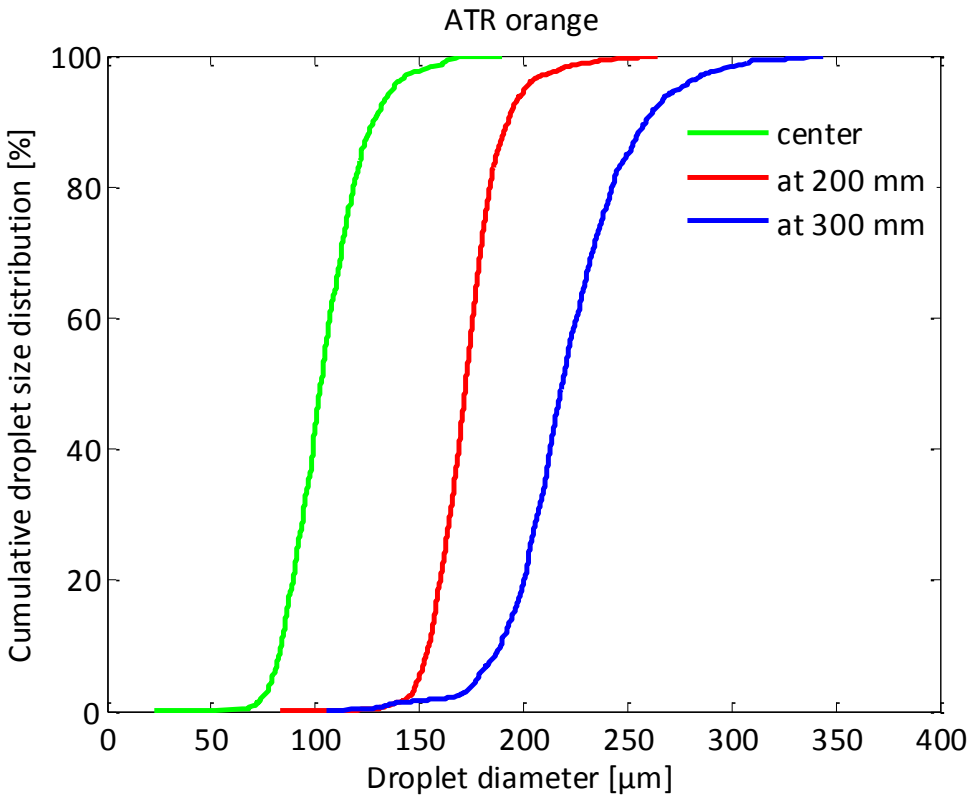
ATR orange
Cumulative droplet size distribution [%]
Droplet diameter [µm]
center
at 200 mm
at 300 mm
0
20
40
60
80
100
0
50
100
150
200
250
300
350
400

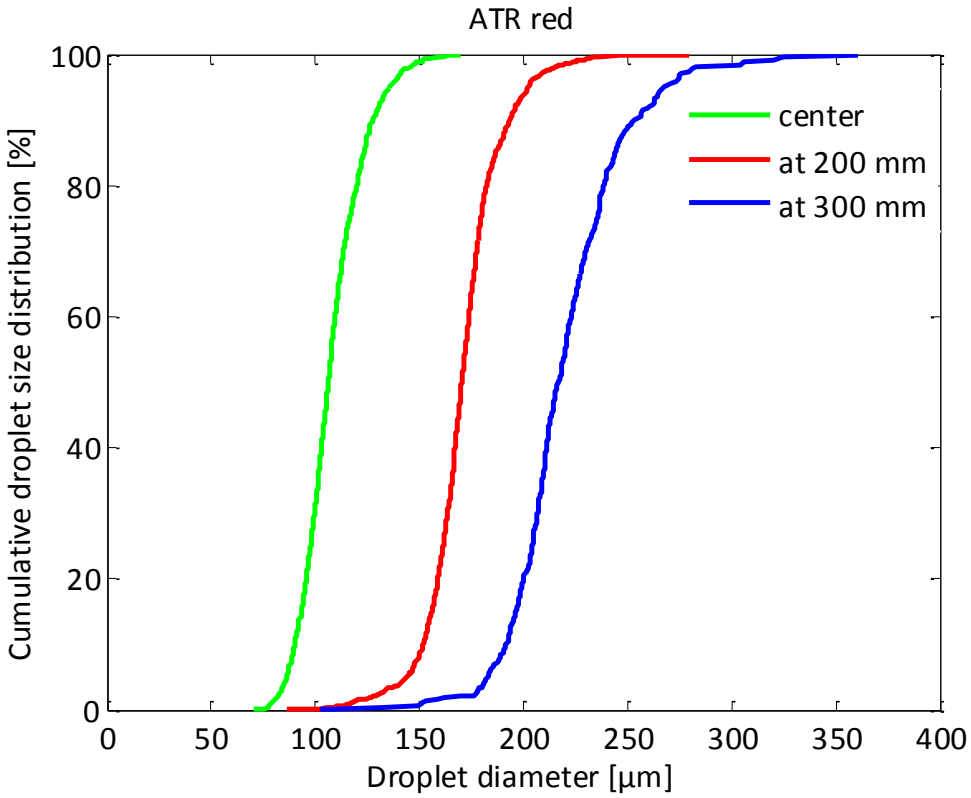

Figure 6.22. Cumulative droplet size distributions for the five nozzle pressure combinations (XR 110 01, XR 110 04, AI 110 04, ATR orange, ATR red) at 0.5 m below the nozzle in the center, at 200 mm and at the edge of the spray

6.3.1.2 Effect of the nozzle type at each measurement point

Figure 6.23. presents the cumulative droplet size distributions at the three different measurement points for the five nozzle-pressure combinations.

In the center of the spray, finest droplet size spectra were found for the hollow cone nozzles (ATR orange and red) followed by the standard flat fan nozzles (XR 110 01 and 110 04) while the coarsest droplets were found for the air inclusion flat fan nozzle (AI 110 04) which confirms previous results from, among others, Nuyttens *et al*. (2007a; 2009). The difference between the ATR orange at 600 kPa and the ATR Red at 800 kPa was limited which confirms the PDPA results published by Dekeyser *et al*. (2013). Similarly, no differences were found in measured droplet sizes between the XR 110 01 and the XR 110 04 nozzle at this position.

Because of the effect of measuring position described above, at 200 mm both standard flat fan nozzles (XR 110 01 and 110 04) produced finer droplets compared with both hollow cone nozzles (ATR orange and red). These hollow cone nozzles had a steeper cumulative droplet size distribution curve indicating a more uniform droplet size distribution compared with the

air inclusion nozzle (AI 110 04). This last one had a wider droplet size distribution with more smaller as well as bigger droplets. As expected, biggest droplets were produced with the air inclusion nozzle at the three measuring positions.

Only at the edge of the spray, a clear difference in droplet size distribution was observed between XR 110 01 and XR 110 04. The XR 110 01 produced much more small droplets resulting in a finer and wider droplet size distribution.

The presented results are point measurements. The entire spray fan should be scanned in order to measure the overall droplet size characteristics.

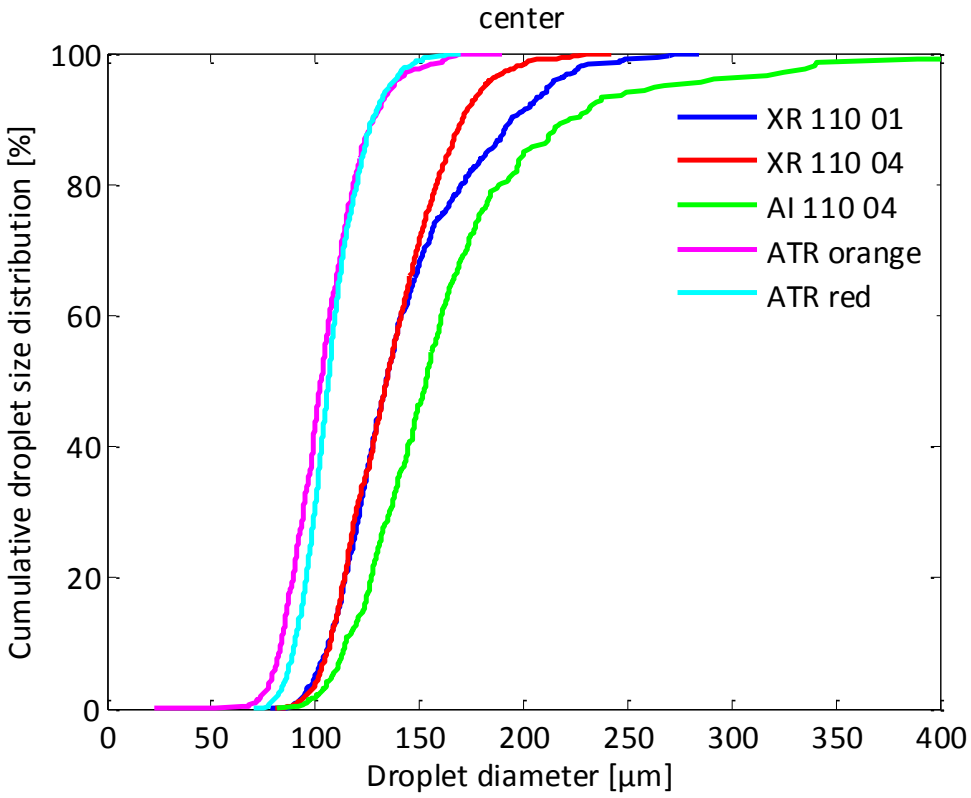

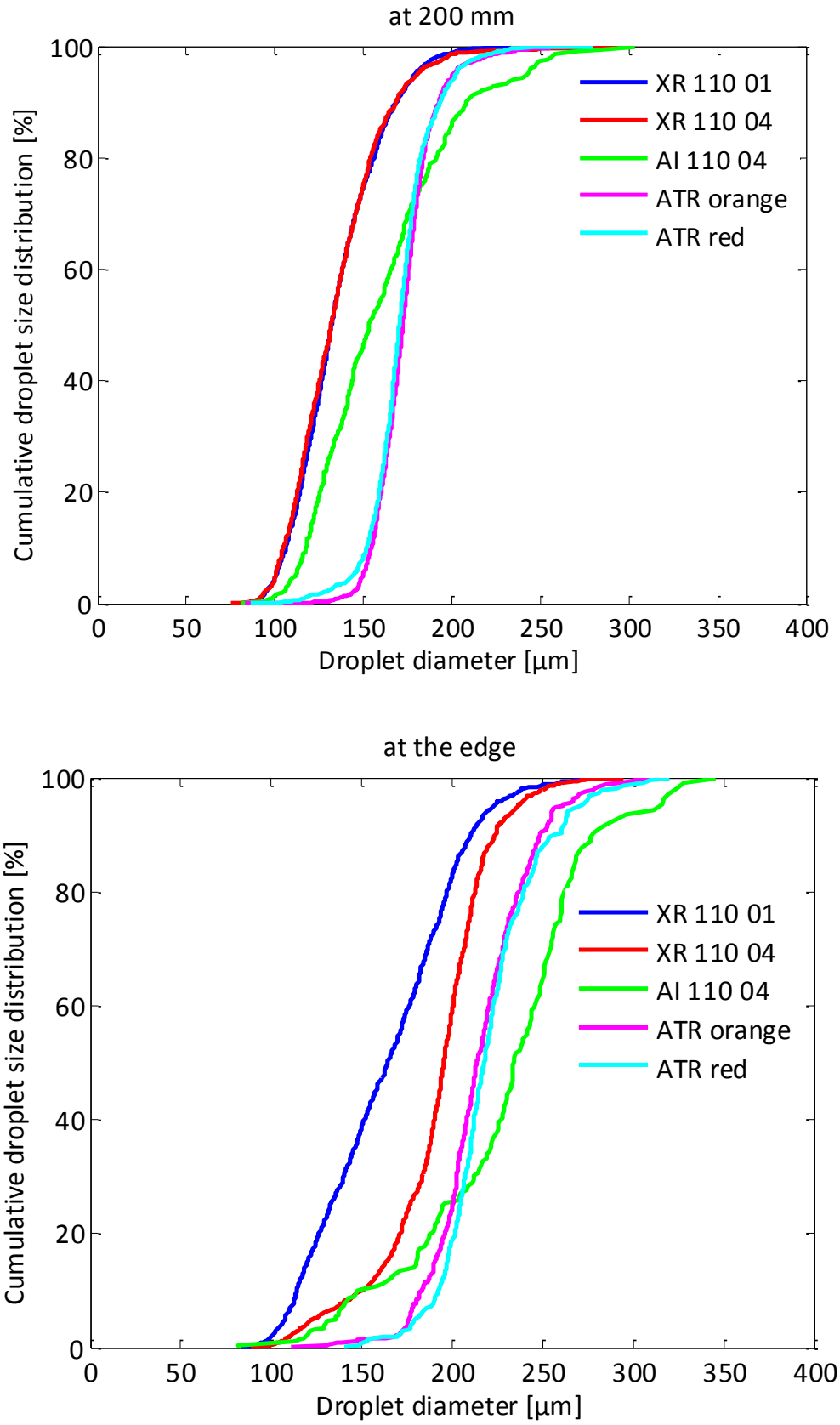

Figure 6.23. Effect of the nozzle type and size on the cumulative droplet size distribution at each measurement point

6.3.1.3 Droplet size distribution parameters

In most spray application studies, droplet size characteristics are expressed in volumetric terms as presented in Table 2.1. Droplet size characteristics $D_{v0.1}$, $D_{v0.5}$, $D_{v0.9}$ and the relative span factor (RSF), defined as $(D_{v0.9} - D_{v0.1})/D_{v0.5}$, for the five nozzle pressure combinations are presented in Figure 6.24 and Figure 6.25., respectively. $D_{v0.5}$ is the most commonly used descriptor of droplet size of a spray. $D_{v0.5}$ values ranged from 105.2 µm for the ATR orange nozzle at the center up to 250.8 µm for the air inclusion nozzle at the edge. The smallest $D_{v0.5}$ was measured with both hollow cone nozzles in the center of the spray. The $D_{v0.1}$, $D_{v0.5}$, $D_{v0.9}$ values were the biggest at the edge for all nozzles. In general, similar trends were found as from the cumulative droplet size distributions.

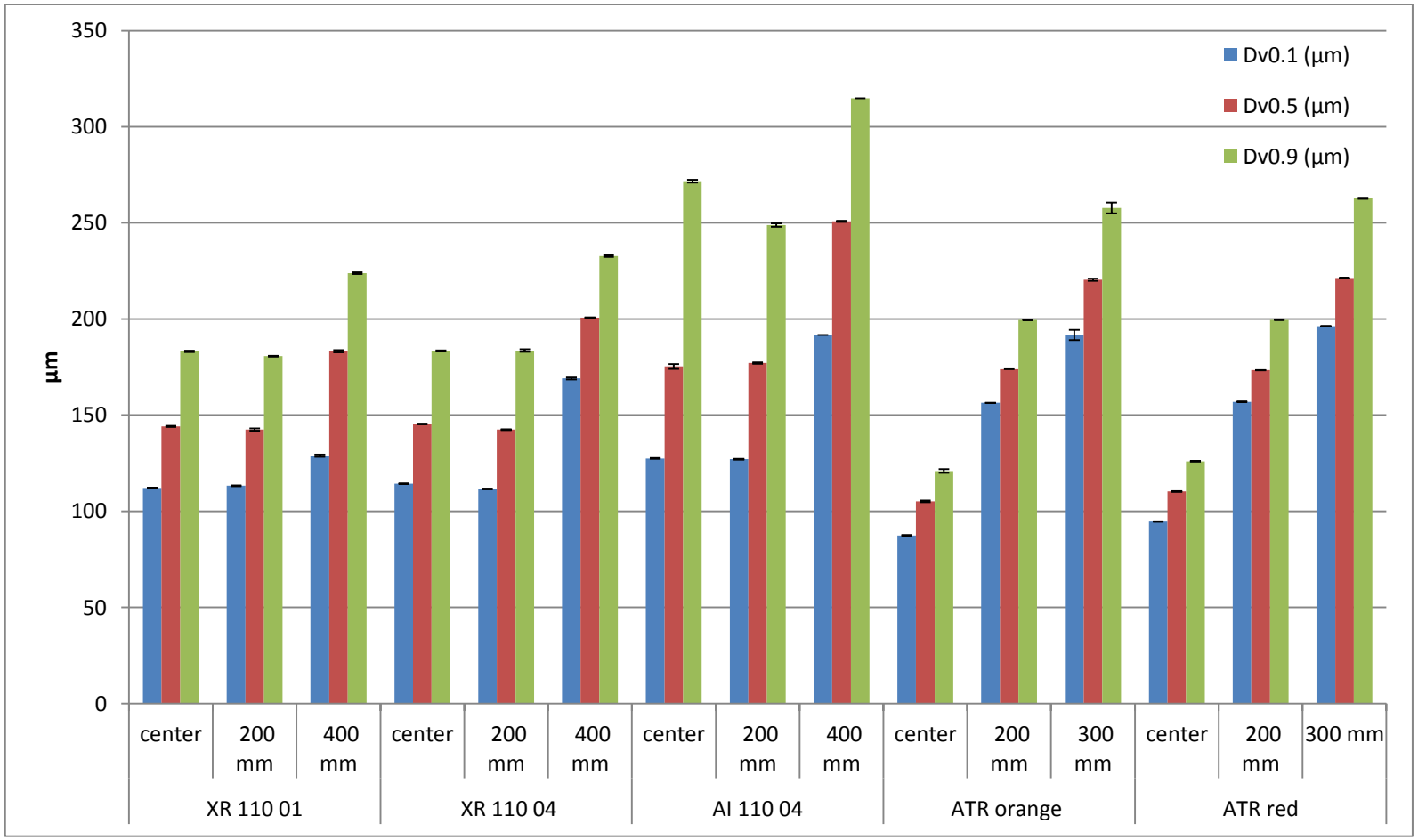

Figure 6.24. Droplet size distriubution parameters $D_{v0.1}$, $D_{v0.5}$ and $D_{v0.9}$ (µm, mean ± std.) for five nozzle pressure combinations (Table 6.3) at 0.5 m below the nozzle at three measurement points (center, 200mm, edge of the spray)

The relative span factor (RSF) indicates the range or spread of droplet sizes in a spray (Table 2.1). It is a dimensionless parameter indicative of the uniformity of the droplet size distribution. RSF values were the smallest for ATR orange (ranging from 0.25 up to 0.32 depending on the position) followed by ATR red (ranging from 0.25 up to 0.30) and XR 110 04 (ranging from 0.49 to 0.82). The highest RSF value was found with the AI 110 04 at the center of the spray (0.82).

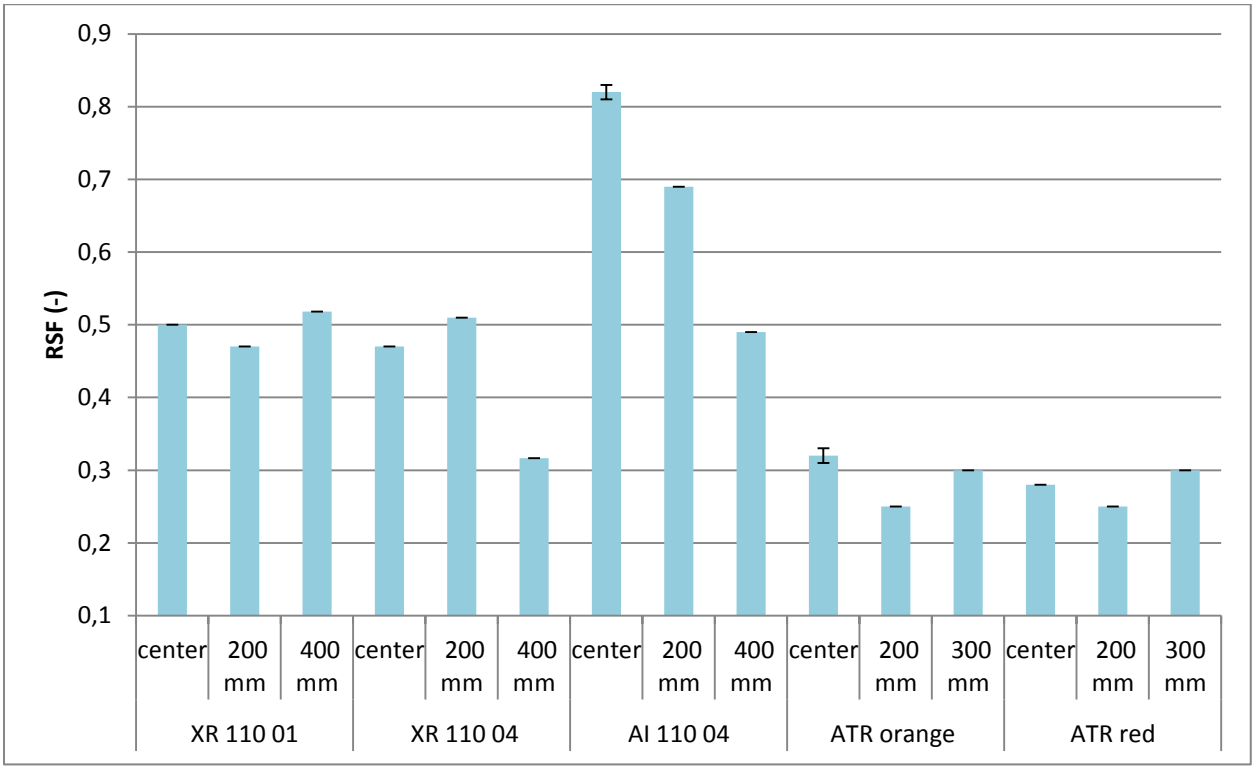

Figure 6.25. RSF (mean ± std.) for the different nozzle pressure combinations at different positions

6.3.2 Spray droplet velocity distribution

6.3.2.1 Effect of the measurement point for each nozzle

As for the droplet diameters, cumulative droplet velocity distributions were always measured at a distance of 500 mm from the nozzle in three measurement positions, i.e. center, at 200 mm and at the edge of the spray (Figure 6.14.). A complete overview of the cumulative droplet velocity distributions for the selected nozzle pressure combinations at three measurement points is presented in Figure 6.26..

Similar as for to the droplet size distributions, each nozzle produced a droplet velocity distribution with velocities ranging from about 0.5 m/s up to 12 m/s. From Figure 6.26., it can be seen that droplet velocities at the edge of the spray were lower than the droplet velocities in the center and at 200 mm for the hollow cone as well as for the flat fan nozzles. This is probably caused by the effect of the entrained air flow in the center of the spray (Farooq *et al.*, 2001) in combination with the longer distance droplets have travelled from the nozzle orifice to the edge of the spray compared with the center of the spray and a friction effect at the edges. In general, no significant differences in droplet velocities were observed between the center of the spray and at 200 mm.

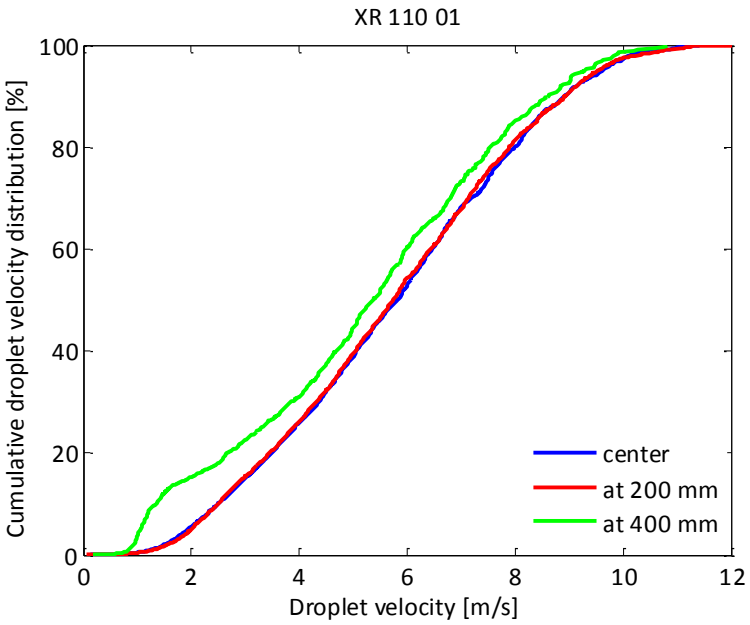

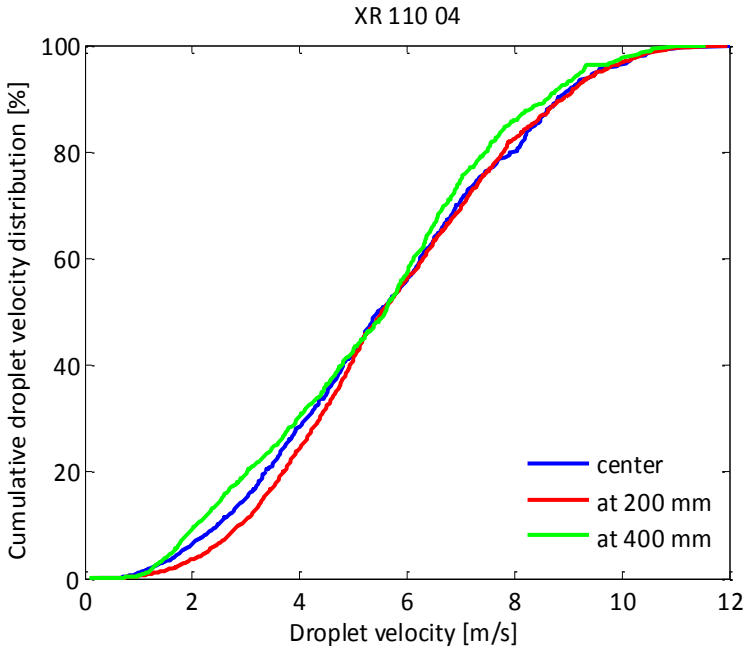

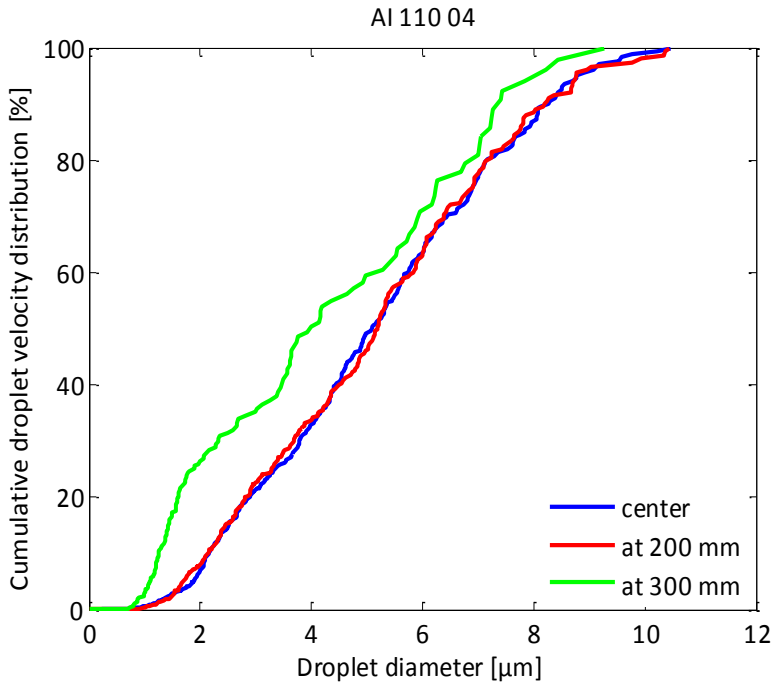
Al 110 04
Cumulative droplet velocity distribution [%]
Droplet diameter [µm]
center
at 200 mm
at 300 mm
0
20
40
60
80
100
0
2
4
6
8
10
12

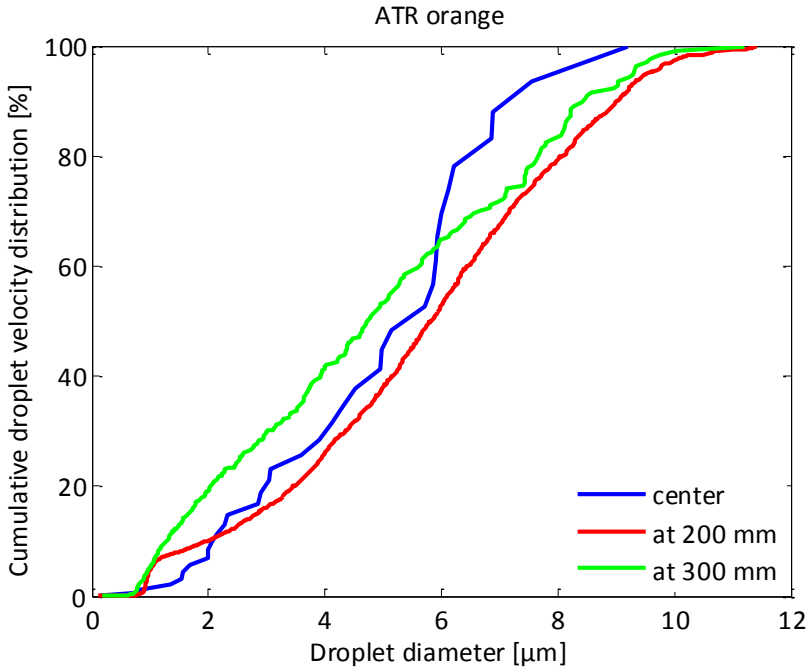
ATR orange
Cumulative droplet velocity distribution [%]
Droplet diameter [µm]
center
at 200 mm
at 300 mm
0
20
40
60
80
100
0
2
4
6
8
10
12

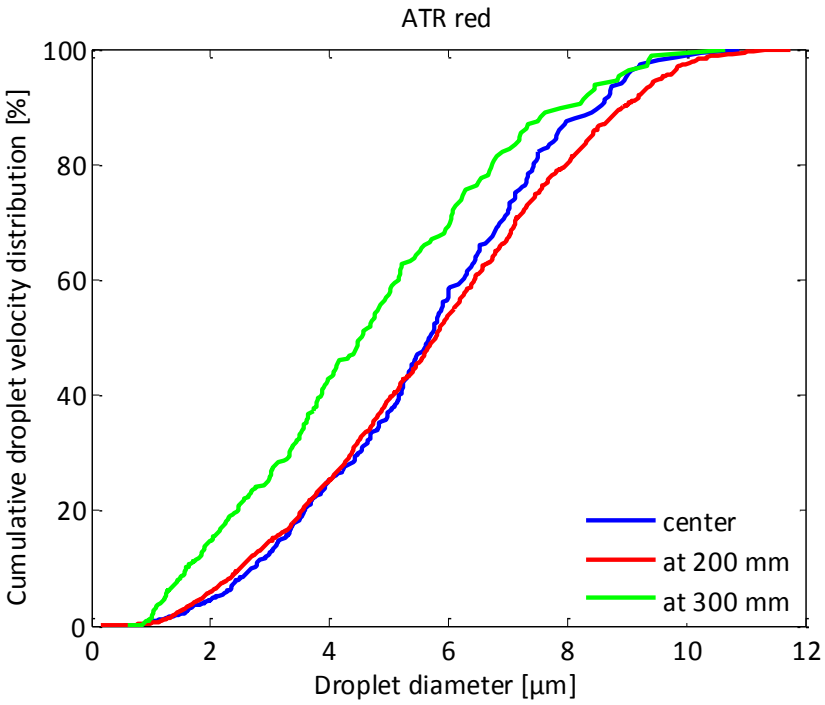

Figure 6.26. Cumulative droplet velocity distributions for the five nozzle pressure combinations in three measurement points (Table 6.3)

6.3.2.2 Effect of nozzle type at each measurement point

Figure 6.27. shows the cumulative droplet velocity distributions for the five nozzle pressure combinations in three different measurement points always at 500 mm below the nozzle, i.e., center, at 200 mm and, at the edge of the spray.

In the center of the spray, no clear differences in droplet velocity distribution were observed for the different nozzles. The air inclusion nozzle tended to produce the slowest droplets at this position which was even more pronounced at the other positions. As a result, the steepest velocity distribution was measured for the air inclusion nozzle at all positions. Differences between nozzles were most pronounced at the edge of the spray with the slowest droplets for the air inclusion nozzle followed by both hollow cone nozzles. Highest velocities were here observed with both standard flat fan nozzles (XR 110 01 and XR 110 04).

Again, the presented results relate to point measurements. The entire spray fan should be scanned in order to measure the overall droplet velocity characteristics.

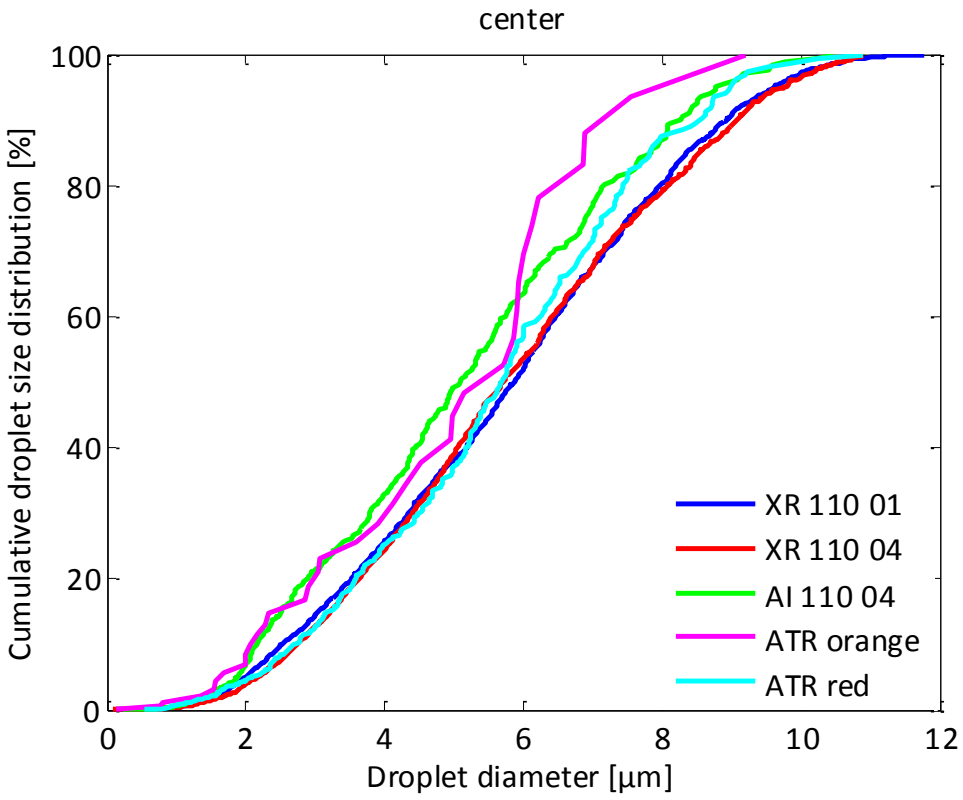
center
Cumulative droplet size distribution [%]
Droplet diameter [µm]
XR 110 01
XR 110 04
AI 110 04
ATR orange
ATR red

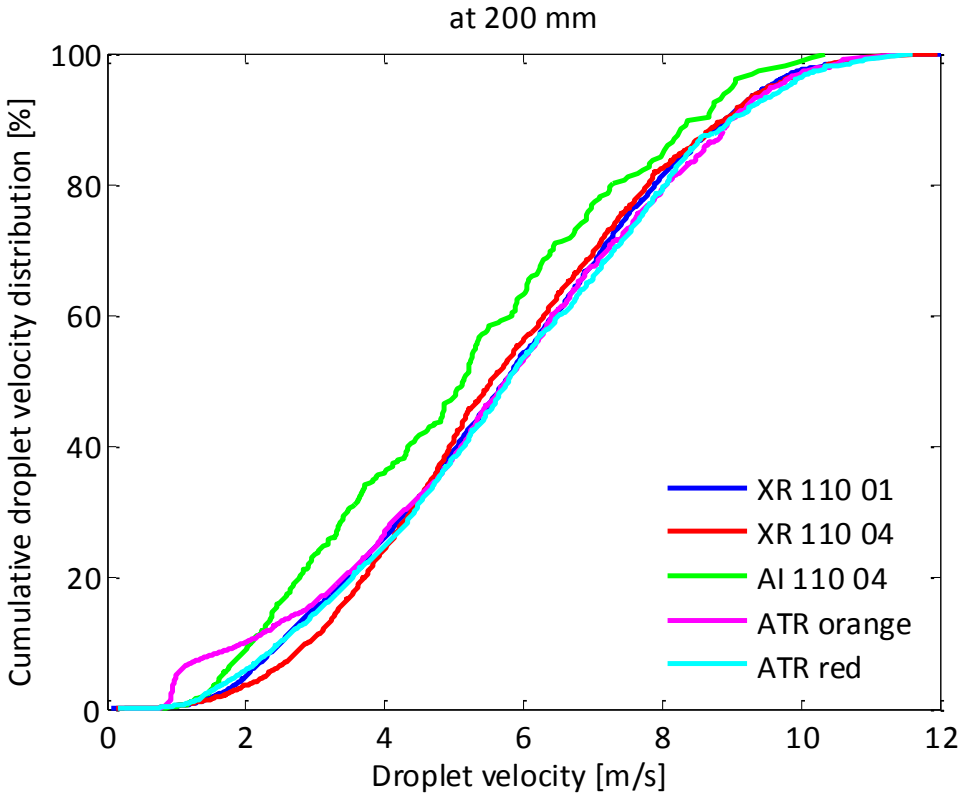
at 200 mm
Cumulative droplet velocity distribution [%]
Droplet velocity [m/s]
XR 110 01
XR 110 04
AI 110 04
ATR orange
ATR red

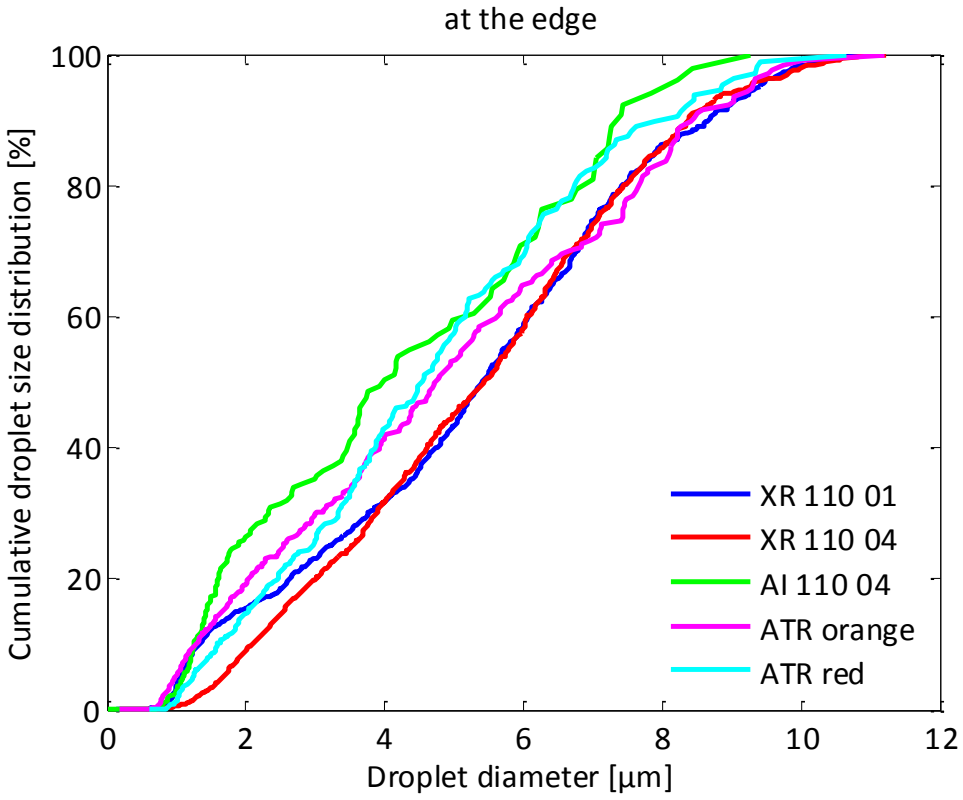

Figure 6.27. Effect of the nozzle-pressure combination on the droplet velocity distribution at each measurement point

6.3.2.3 Droplet velocity parameters

Apart from the droplet velocity distribution, the following volumetric droplet velocity parameters were also calculated:

- V_{vol10}, V_{vol50}, V_{vol90} –droplet velocity in m/s below which slower droplets constitute 10, 50, 90% of the total spray volume;
- *VSF*-velocity span factor, a dimensionless parameter indicative of the uniformity of the droplet size velocity distribution, defined as: $\frac{V_{vol90}-V_{vol10}}{V_{vol50}}$;
- *NMV*- number median velocity, droplet velocity for which 50% of the number of droplets is slower than this value.

The results are presented in Figure 6.28. and Figure 6.29..For the flat fan nozzles as well the hollow cone nozzles, lowest V_{vol10} values are generally lower at the spray edge than in the center or middle of the spray. Similar trend also is noticed for the V_{vol50} values. Highest V_{vol90} values were found for the XR 110 04 directly below the nozzle.

. In general, similar conclusions can be drawn as from the cumulative droplet velocity distributions.

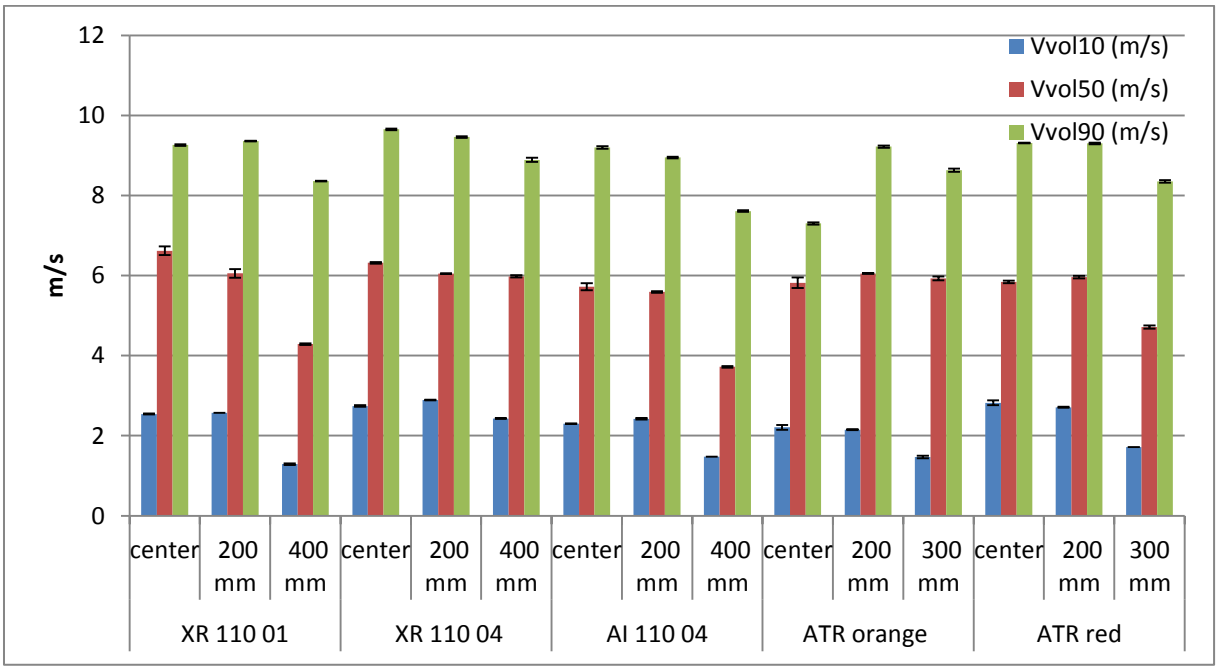

Figure 6.28. Volumetric droplet velocity parameters for every nozzle pressure combination from Table 6.3 at three measurement points at 500 mm below the nozzle

The differences in droplet velocity characteristics depending on the nozzle type, size and pressure are reflected in the VSF values. Highest VSF value was found at the edge for the air inclusion nozzle (3.31). This nozzle type also showed the highest RSF based on droplet sizes. Lowest VSF value was found for the ATR red below the nozzle.

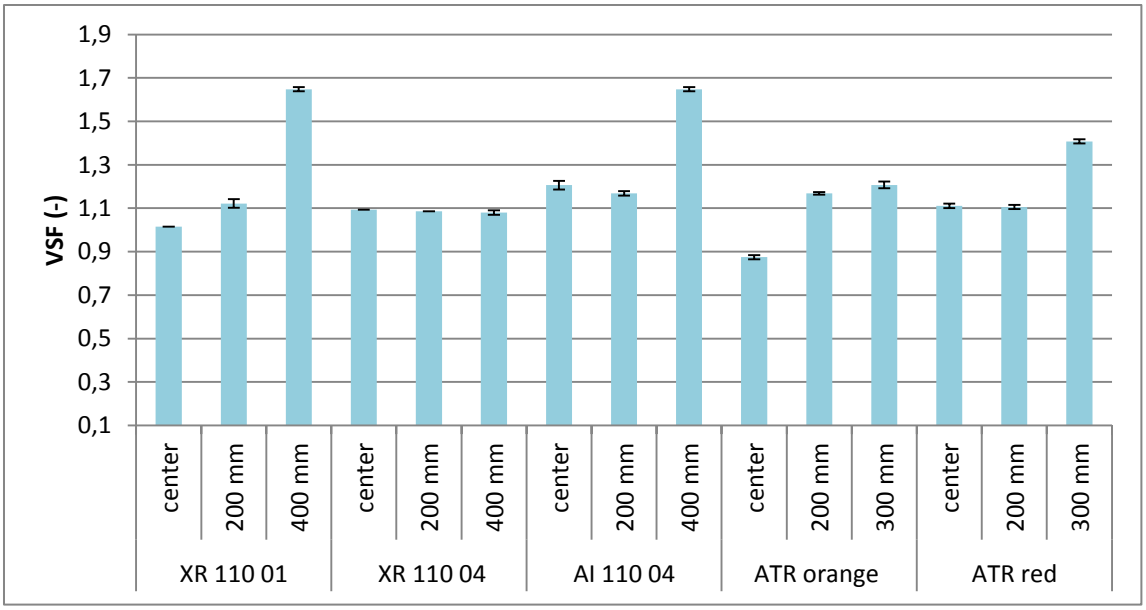

Figure 6.29. Velocity span factor for the different nozzle pressure combinations

6.3.3 Comparison between imaging and PDPA measuring technique

In Figure 6.30., the cumulative droplet size distributions measured with two techniques, i.e., imaging technique and PDPA laser at different measurement points for each selected nozzle pressure combination are presented.

In general, similar effects of nozzle type and measuring position were found with the PDPA technique as with the imaging technique although cumulative droplet size distributions curves gained with the imaging technique were steeper than those with the PDPA laser corresponding with lower RSF values. This is explained in Figure 6.32. in which RSF values measured with both techniques are compared. This is caused by the fact that compared with the PDPA laser, the imaging technique generally measures a smaller number of small droplets and in some cases also a smaller number of big droplets. Differences between both techniques can be attributed to the smaller amount of droplets measured with the imaging technique which increases the chance to miss one of the big droplets. In addition, no droplets below 24 µm were measured with the imaging technique while smaller droplets were measured with the PDPA.

For the XR 110 01 nozzle, a very good correlation between PDPA and imaging results was found at all the measurement points. Only at the edge of the spray, the imaging technique

resulted in a slightly coarser droplet distribution compared with the PDPA technique. The good correlation can be attributed to the small droplet size distribution of this nozzle and the absence of droplets > 250-300 µm.

In addition, for the ATR orange and red nozzle, a good correlation between PDPA and imaging results was found at the center although the imaging curves were a bit steeper for the reasons mentioned above. Biggest differences between imaging and PDPA results were observed for the air inclusion nozzle. Mainly a very limited amount of droplets above 350 µm is measured with the imaging technique compared with the PDPA. On the other hand, there is still no consensus about the fact whether the PDPA, which is based on light scattering principles, is capable of measuring air including droplets in an accurate way.

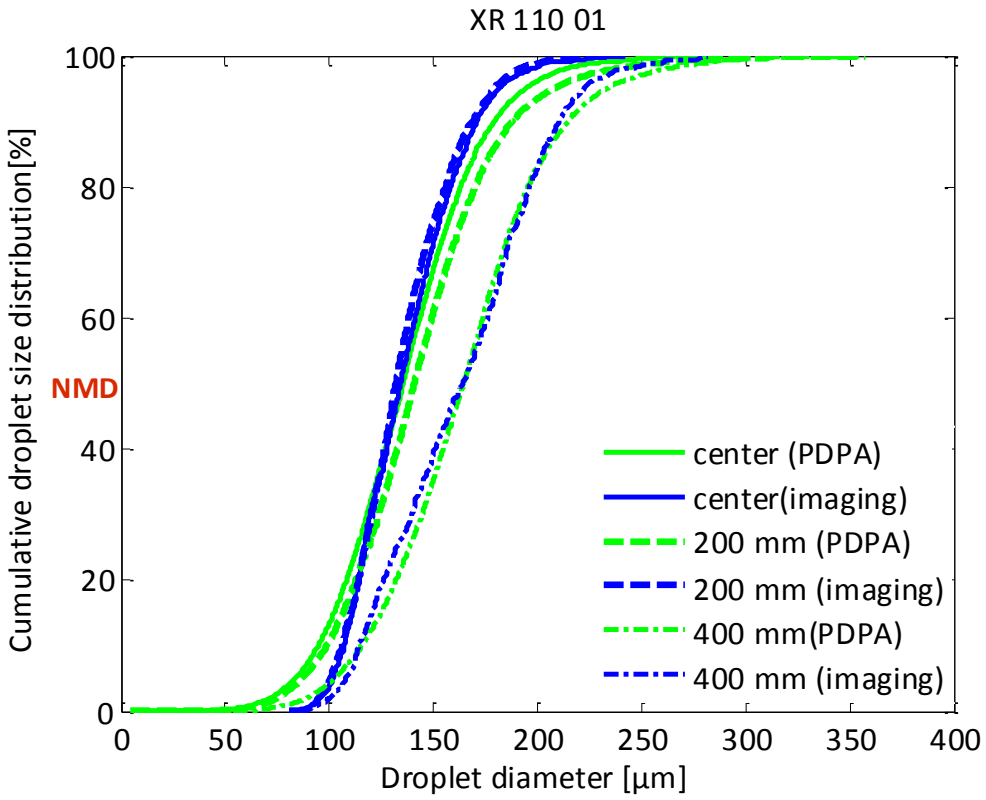

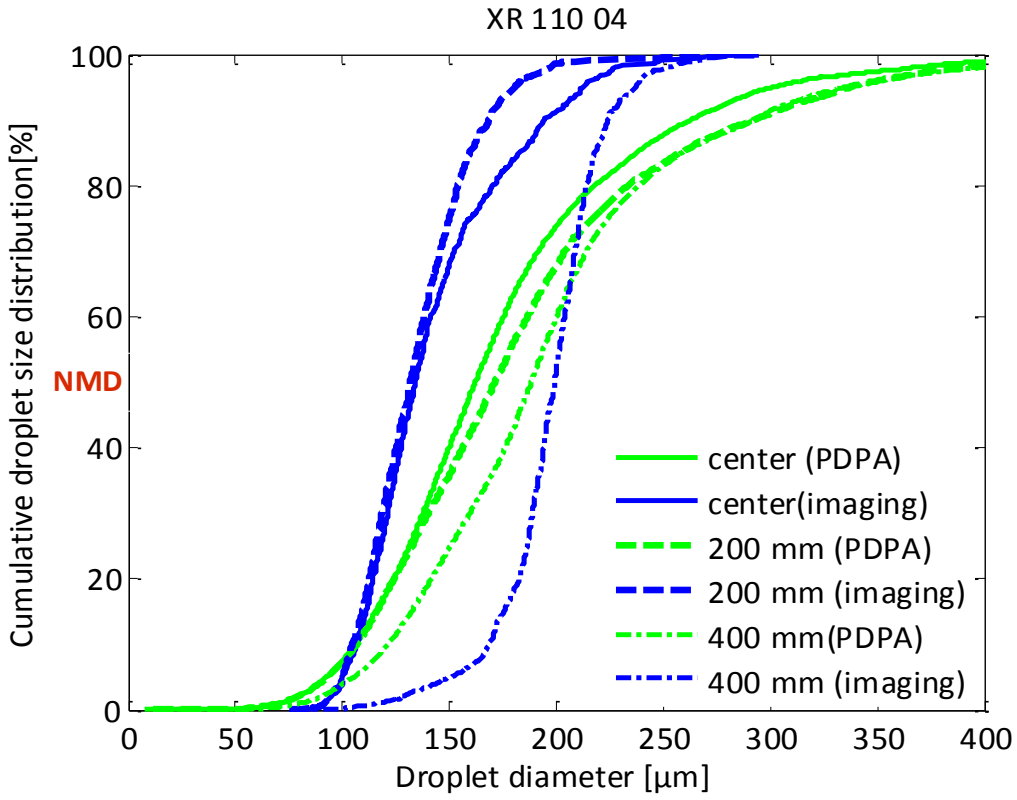
XR 110 04
Cumulative droplet size distribution[%]
NMD
Droplet diameter [µm]
center (PDPA)
center(imaging)
200 mm (PDPA)
200 mm (imaging)
400 mm(PDPA)
400 mm (imaging)

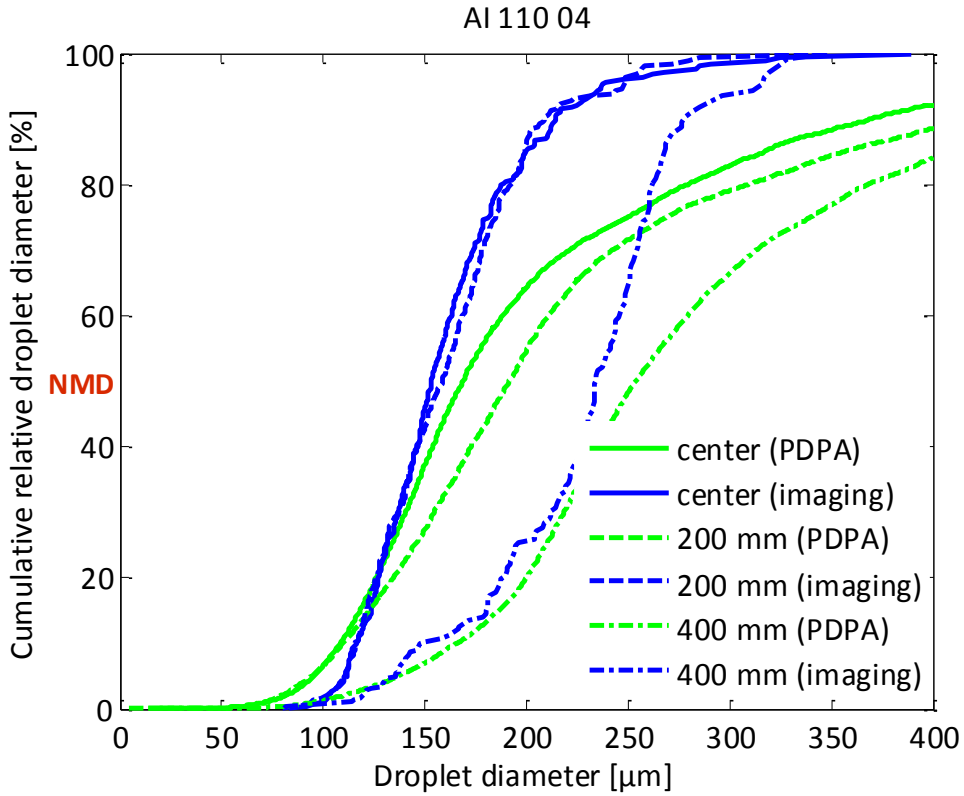
AI 110 04
Cumulative relative droplet diameter [%]
NMD
Droplet diameter [µm]
center (PDPA)
center (imaging)
200 mm (PDPA)
200 mm (imaging)
400 mm (PDPA)
400 mm (imaging)

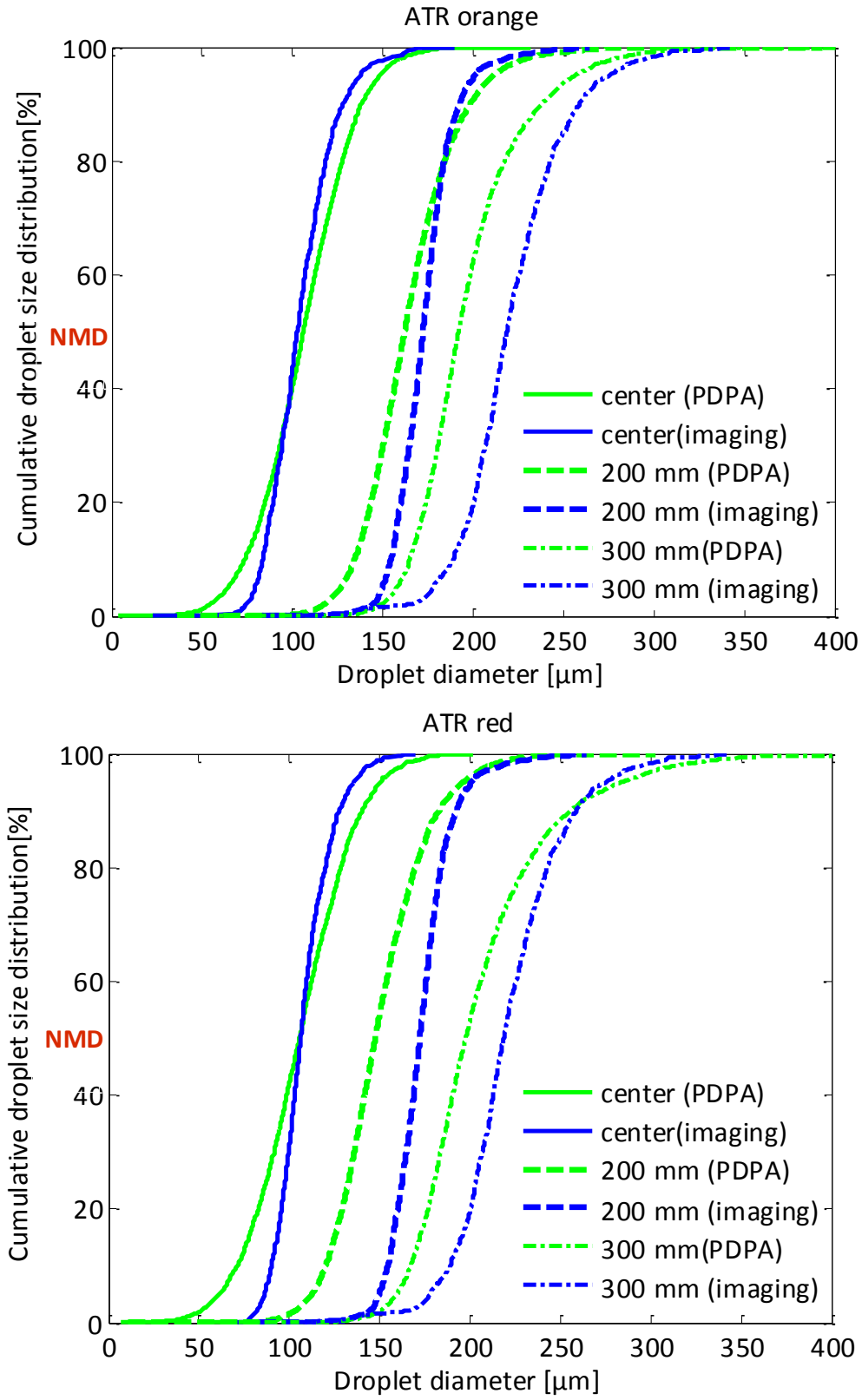

Figure 6.30. Cumulative droplet size distribution results using the imaging technique and PDPA laser for the five nozzle pressure combinations in three measurement point

In Figure 6.31., both techniques are compared in terms of the nominal median diameter (NMD) values. The smallest difference of the NMD values was found for the XR 110 01 and both hollow cone nozzles (ATR orange and red). However, a difference in the NMD values can be seen using the XR 110 04 and the air inclusion nozzle AI 110 04 where generally smaller NMD values were measured with the imaging technique. This is because bigger droplets were measured with these nozzles using the PDPA laser. In addition, a positive correlation was found between the NMD values from the imaging technique and NMD values from the PDPA laser (R^2= 0.77).

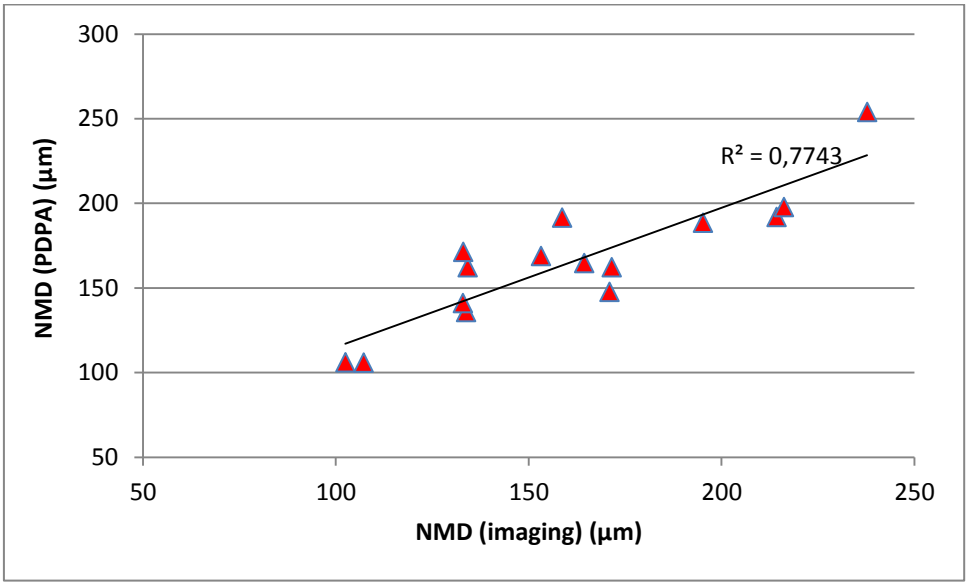

Figure 6.31. Comparison between NMD measured values with the imaging technique and NMD values with the PDPA laser for all the five nozzle pressure combinations

Figure 6.32. presents a comparison between RSF values measured with the imaging technique and the PDPA laser for all five nozzle pressure combinations at different positions. It can be observed that the measured RSF values with the PDPA laser were always higher that the RSF values gained from the imaging technique (Table 6.4).

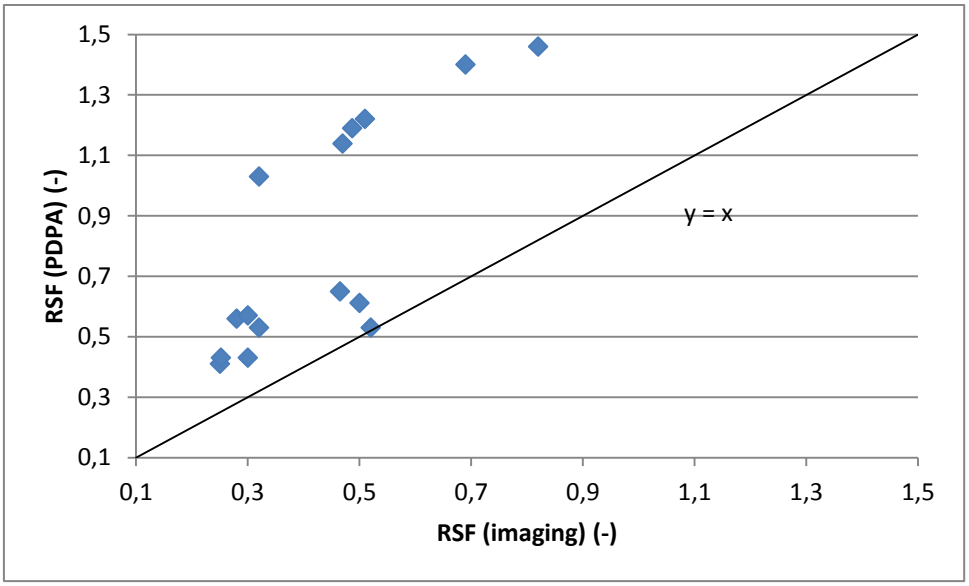

Figure 6.32. Comparison between RSF measured values with the imaging technique and RSF values with the PDPA laser for all the five nozzle pressure combinations

A complete overview of the different droplet size distribution parameters obtained with the imaging technique and the PDPA laser for the five nozzle pressure combinations can be found in Table 6.4. Average values and standard deviations with the imaging technique are based on five repetitions. Standard deviations are small, indicating a good repeatability of the measurements.

Table 6.4 Comparison between droplet size distribution parameters obtained with the imaging techniques and PDPA laser for the five nozzle pressure combinations

		$D_{v0.1}$ (µm)		$D_{v0.5}$ (µm)		$D_{v0.9}$ (µm)		RSF (-)	
		Imaging	**PDPA**	**Imaging**	**PDPA**	**Imaging**	**PDPA**	**Imaging**	**PDPA**
XR 110 01	**center**	112.2 ± 0.2	110.8	144.1 ± 0.3	151.5	183.2 ± 0.4	203.5	0. 50 ± 0.00	0.61
	200 mm	113.3 ± 0.3	114.4	142.6 ± 0.6	156.0	180.7 ± 0.2	215.3	0.47 ±0.00	0.65
	400 mm	128.9 ± 0.5	140.2	183.3 ± 0.6	185.5	223.9 ± 0.5	239.1	0.52 ± 0.01	0.53
XR 110 04	**center**	114.3 ± 0.1	134.7	145.4 ± 0.2	212.0	183.4 ± 0.3	376.1	0.47 ± 0.00	1.14
	200 mm	111.6 ± 0.2	135.2	142.5 ± 0.2	223.2	183.6 ± 0.6	407.3	0.50 ± 0.00	1.22
	400 mm	169.2 ± 0.5	148.2	200.8 ± 0.1	217.5	232.7 ± 0.2	373.0	0.30 ± 0.0	1.03
AI 110 04	**center**	127.5 ± 0.2	154.1	175.4 ± 1.3	331.9	271.7 ± 0.7	638.8	0.82 ± 0.01	1.46
	200 mm	127.1 ± 0.2	168.5	177.1 ± 0.4	358.8	248.9 ± 0.9	670.8	0.69 ± 0.00	1.40
	400 mm	191.7 ± 0.0	204.4	250.8 ± 0.3	360.0	314.8 ± 0.0	634.0	0.49 ±0.00	1.19
ATR orange	**center**	87.4 ± 0.3	87.0	105.2 ± 0.4	117.6	120.9 ± 0.9	149.7	0.3 ± 0.0	0.53
	200 mm	156.4 ± 0.1	139.2	173.0 ± 0.1	167.9	199.5 ± 0.1	208.1	0.25 ± 0.00	0.41
	300 mm	191.7 ± 2.6	170.1	220.4 ± 0.61	199.5	257.8 ±2.86	256.2	0.30 ± 0.00	0.43
ATR red	**center**	94.6 ± 0.17	85.9	110.3 ± 0.3	118.5	125.9 ± 0.1	151.7	0.28 ± 0.00	0.56
	200 mm	156.9 ± 0.1	128.9	173.0 ± 0.1	157.0	199.7 ± 0.3	196.2	0.25 ± 0.00	0.43
	300 mm	196.3 ± 0.1	174.2	221.3 ± 0.1	197.9	262.8 ± 0.3	294.6	0.30 ± 0.00	0.57

Figure 6.33. presents the comparison of the cumulative velocity distributions measured with the imaging technique and the PDPA laser at different measurement points for every selected nozzle-pressure combination. It can be observed that the droplet velocity distributions curves obtained with the imaging technique were shifted to higher values than the ones measured with the PDPA laser. This was most obvious with the standard flat fan XR 110 01 and the two hollow cone nozzles. This can partly be explained by the fact that the PDPA laser is only measuring droplet velocitities in one dimension (vertically) and hence underestimates the actual droplet velocity. That is why differences between imaging and PDPA are generally most pronounced at the edge of the spray. In addition, the imaging technique applied did not allow the measurement of droplets faster than about 12 m/s based on the dimensions of the FOV and the acquisition rate while some droplets with higher speeds were observed with the PDPA mainly for the XR 110 04. In future, the imaging system can be further improved to be able to measure at a higher frame rate with the same accuracy.

The comparison between imaging technique and PDPA can also be assessed from the nominal median velocities (NMV). The best correspondence was found for the AI 110 04 value.

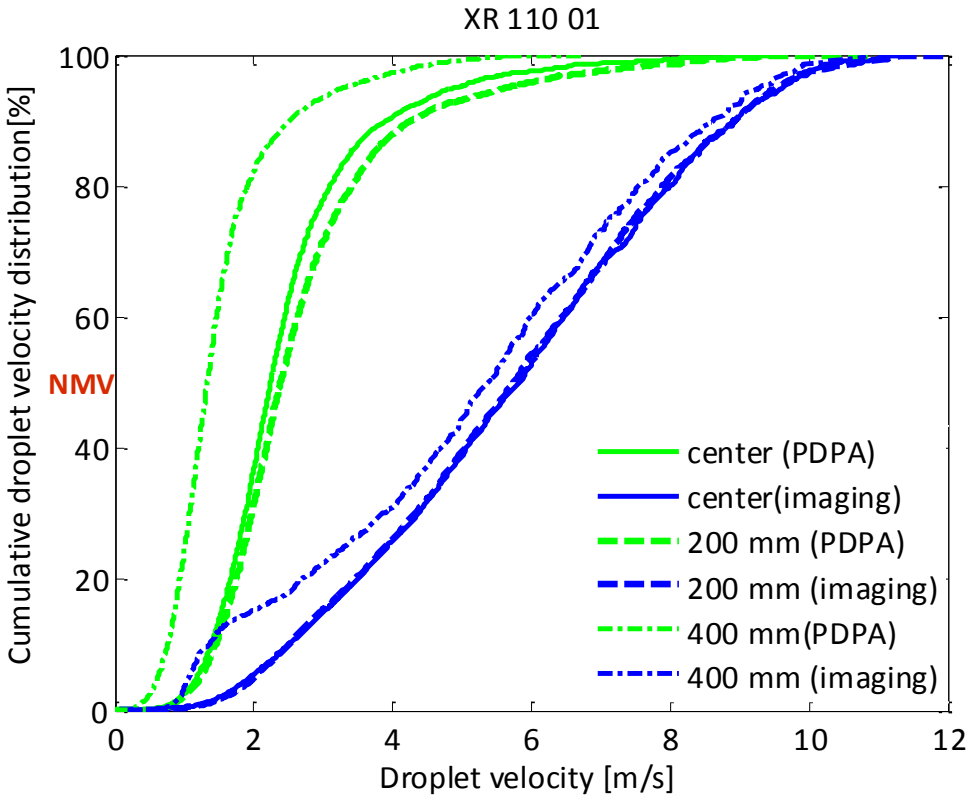

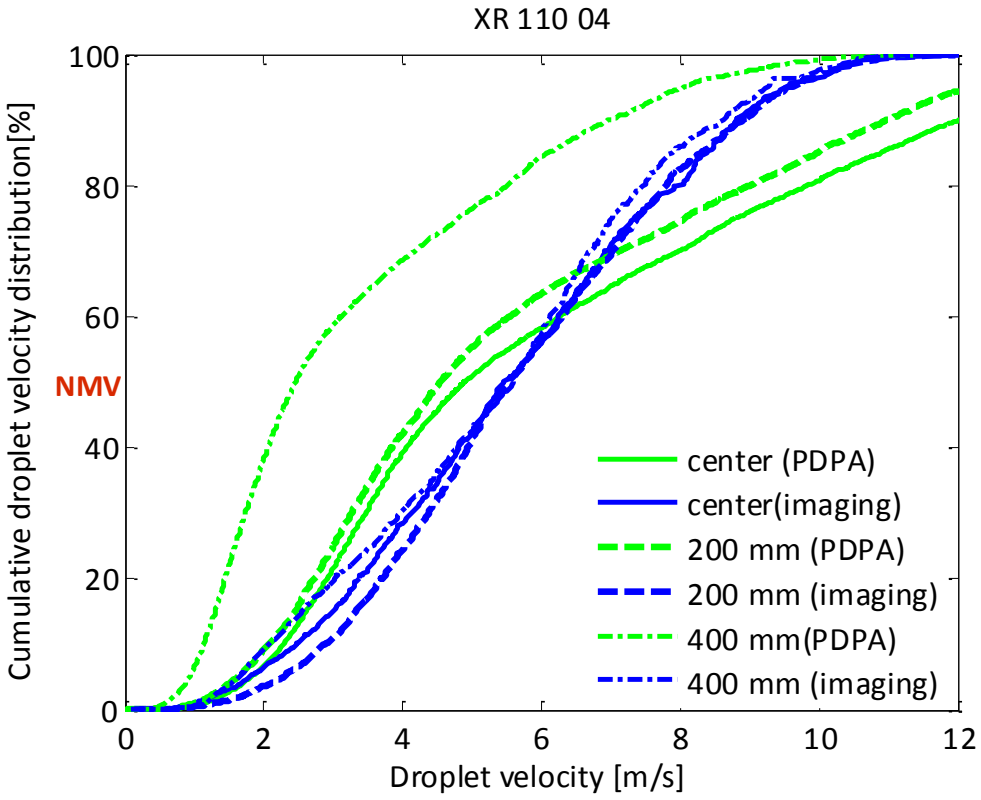
XR 110 04
Cumulative droplet velocity distribution[%]
NMV
Droplet velocity [m/s]
center (PDPA)
center(imaging)
200 mm (PDPA)
200 mm (imaging)
400 mm(PDPA)
400 mm (imaging)

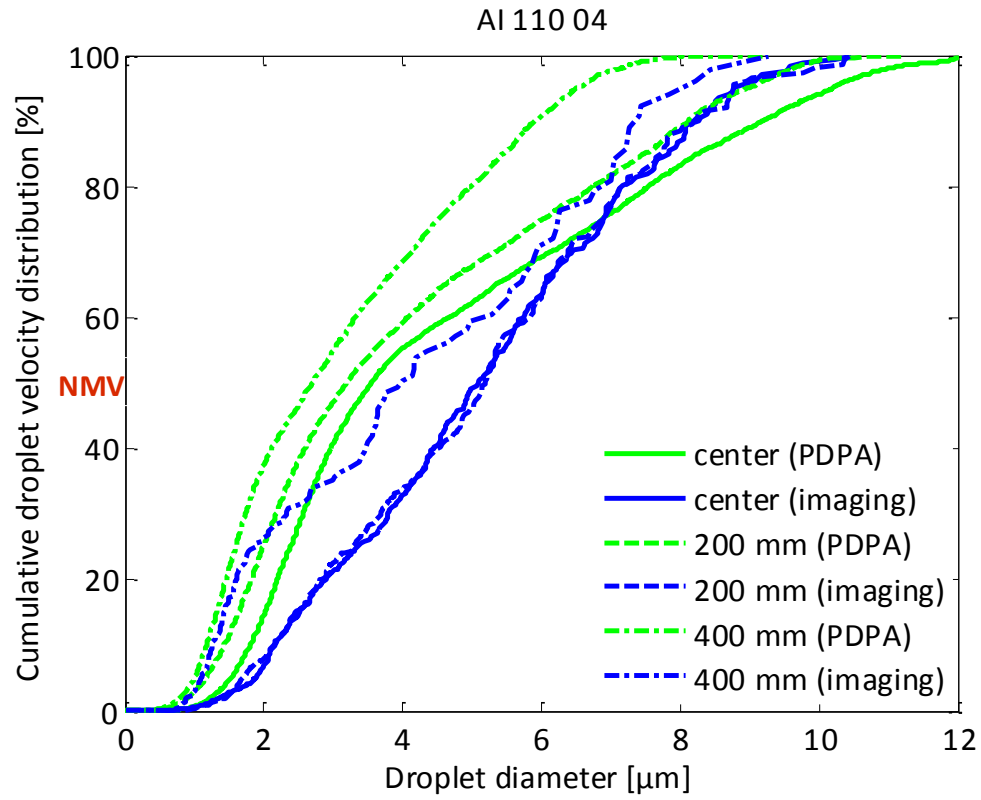
AI 110 04
Cumulative droplet velocity distribution [%]
NMV
Droplet diameter [µm]
center (PDPA)
center (imaging)
200 mm (PDPA)
200 mm (imaging)
400 mm (PDPA)
400 mm (imaging)

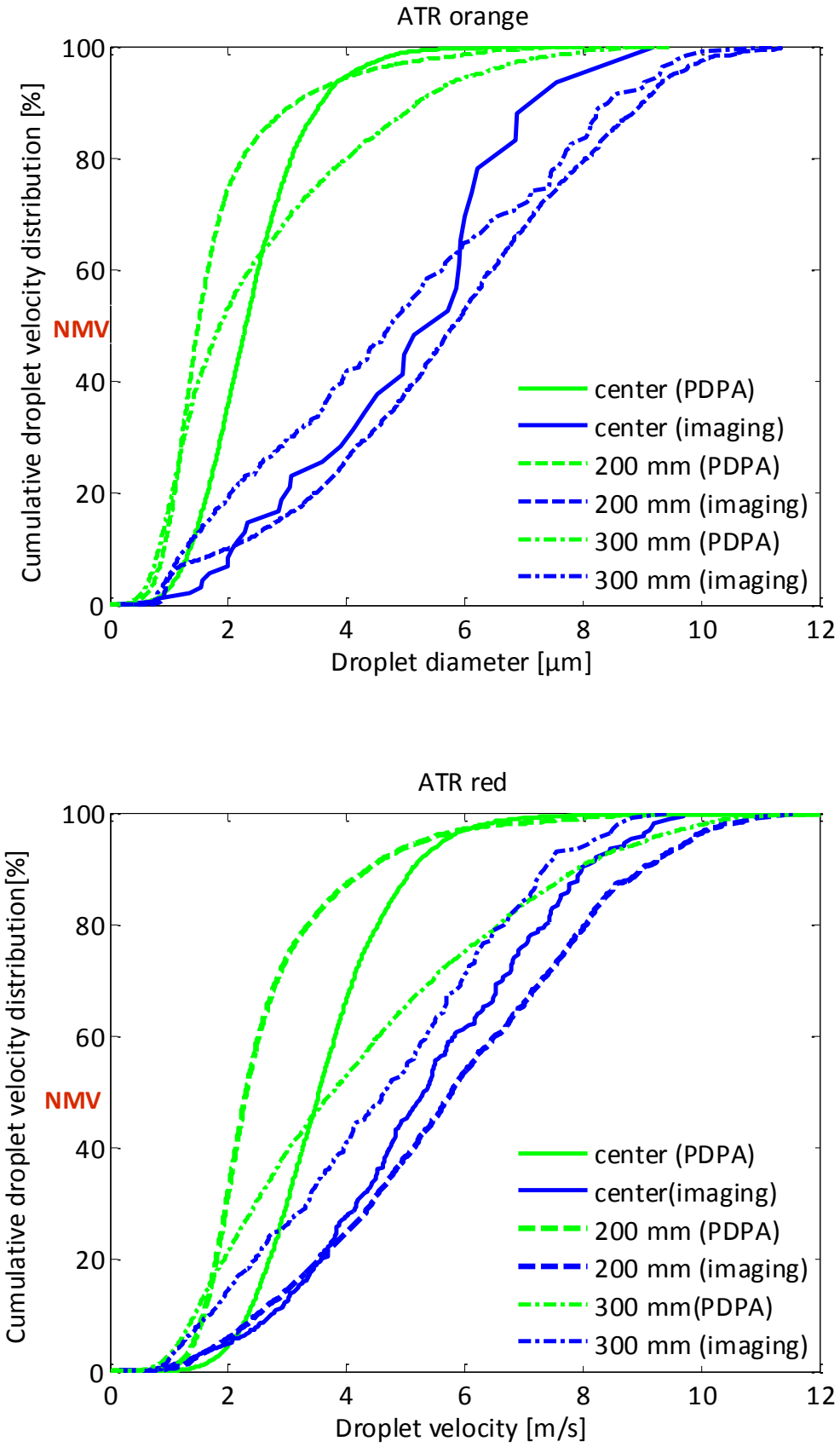

Figure 6.33. Cumulative droplet velocity distribution results using the imaging technique and PDPA laser for the five nozzle pressure combinations in three measurement point

A complete overview of the droplet velocity parameters measured with the imaging techniques and PDPA laser for the five nozzle pressure combinations can be found in Table 6.5. Average values and standard deviations with the imaging technique are based on five repetitions. Standard deviations are small, indicating a good repeatability of the measurements.

Table 6.5 Comparison between droplet velocity distribution parameters gained with the imaging techniques and PDPA laser for the five nozzle pressure combinations

		V_{vol10} (m/s)		V_{vol50} (m/s)		V_{vol90} (m/s)		VSF (-)	
		Imaging	**PDPA**	**Imaging**	**PDPA**	**Imaging**	**PDPA**	**Imaging**	**PDPA**
TeeJet XR11001	**center**	2.54 ± 0.01	1.15	6.62 ± 0.11	2.14	9.26 ± 0.02	4.47	1.01 ± 0.00	1.55
	200 mm	2.57 ± 0.00	1.37	6.05 ± 0.11	2.37	9.36 ± 0.01	5.06	1.12 ± 0.02	1.56
	400 mm	1.29 ± 0.02	0.62	24.3 ± 0.02	1.20	8.36 ± 0.01	2.53	1.65 ± 0.01	1.60
TeeJet XR11004	**center**	2.74 ± 0.02	2.34	6.32 ± 0.02	7.30	9.65 ± 0.02	14.50	1.09 ± 0.00	1.66
	200 mm	2.89 ± 0.01	2.34	6.05 ± 0.01	6.93	9.46 ± 0.02	13.28	1.09 ± 0.00	1.58
	400 mm	2.43 ± 0.01	1.13	5.98 ± 0.03	2.70	8.89 ± 0.05	7.86	1.08 ± 0.01	2.50
AI 11004	**center**	2.30 ± 0.01	2.04	5.72 ± 0.09	7.90	9.20 ± 0.03	11.04	1.21 ± 0.02	1.14
	200 mm	2.42 ± 0.02	1.72	5.59 ± 0.02	6.82	8.95 ± 0.02	9.68	1.17 ± 0.01	1.17
	400 mm	1.48 ± 0.00	1.27	3.72 ± 0.02	4.10	7.61 ± 0.02	6.79	1.65 ± 0.01	1.35
ATR orange	**center**	2.21 ± 0.06	1.04	5.82 ± 0.13	1.87	7.30 ± 0.03	3.01	0.87 ± 0.01	1.06
	200 mm	2.15 ± 0.01	0.79	6.05 ± 0.01	1.38	9.22 ± 0.03	2.76	1.17 ± 0.01	1.43
	300 mm	1.47 ± 0.03	0.67	5.93 ± 0.05	1.46	8.63 ± 0.04	4.61	1.21 ± 0.02	2.70
ATR red	**center**	2.82 ± 0.06	1.94	5.84 ± 0.03	3.01	9.31 ± 0.01	4.42	1.11 ± 0.01	0.82
	200 mm	2.71 ± 0.01	1.39	6.05 ± 0.01	2.12	9.30 ± 0.02	4.07	1.11 ± 0.01	1.27
	300 mm	1.72 ± 0.00	1.16	4.71 ± 0.04	3.26	8.35 ± 0.03	8.21	1.41 ± 0.01	2.16

6.4 CONCLUSION

This chapter presents a technique based on image processing for measuring the droplet size and velocity characteristics of agricultural hydraulic spray nozzles using the image acquisition system developed and presented in Chapter 3.

The chapter consists of two parts. In the first part, an in-focus droplet criterion based on the gray level gradient was introduced to decide whether a droplet is in focus or not. Differently sized droplets generated with a piezoelectric generator and glass nozzles in continuous mode at different distances from the focal plane and lens using a micro translation stage were measured. This enabled measurement of the gray level gradient and in-focus parameter for every droplet size. From this, a critical in-focus parameter (Infc) was established for every droplet size and an in-focus droplet criterion was deduced to decide whether a droplet is in focus or not depending on its diameter and in-focus parameter. In this study, the focused droplet zone (FDZ) was defined as the zone in which a droplet with a certain diameter is in focus and a linear relation between droplet size and FDZ was found.

In the second part, the in-focus droplet criterion was applied to spray images of different hydraulic spray nozzles and the droplet size and velocity characteristics were calculated. The effects of the nozzle type, and nozzle size and measuring position on spray droplet characteristics were studied.

The droplet size and velocity results from the imaging technique have shown that it is possible to measure the spray characteristics in a non-intrusive way using image acquisition set-up and image processing. Measured droplet sizes ranged from 24 µm up to 543 µm depending on the nozzle type and size. Droplet velocities ranged from around 0.5 m/s up to 12 m/s. Information about spray droplet size characteristics such as $D_{V0.1}$, $D_{V0.5}$, $D_{V0.9}$ and RSF as well as spray velocity characteristics such as V_{Vol10}, V_{Vol50}, V_{Vol90} and VSF, were extracted from the images. Similar effects of nozzle type and measuring position on droplet sizes as well as on droplet velocities were found with the imaging technique as with the PDPA or the droplet size and velocity, respectively.

The developed imaging technique can be seen as an alternative to the well-established PDPA laser technique. The droplet diameter and velocity characteristics showed a relatively good comparison with the results measured with the PDPA laser. When compared with the PDPA

laser, the imaging technique generally measured less small droplets and in some cases also less big droplets. Differences between both techniques can be attributed to the fact that the smallest measured droplet size with the imaging system is 24 µm while smaller droplets were measured with the PDPA. In addition, the number of smaller amount of droplets measured with the imaging technique was much smaller compared with the PDPA which increases the chance to miss one of the biggest droplets. This can be improved by taking more images. Differences in droplet velocity characteristics between both techniques can be attributed to the fact that the PDPA laser is only measuring droplet velocity in one dimension and hence underestimates the actual droplet velocity. In addition, the imaging technique applied did not allow the measurement of droplets faster than about 12 m/s based on FOV and the acquisition rate while some droplets with higher speeds were observed with the PDPA mainly for the XR 110 04. In future, the imaging system can be further improved to be able to measure at a higher frame rate with the same accuracy.

7 MACRO-SPRAY CHARACTERIZATION FROM A SINGLE NOZZLE[vi]

Agricultural pesticide sprays are applied with different types of spray nozzles each with its own spray characteristics. The objective of this chapter was to measure the macro-spray characteristics (spray angle, liquid sheet length, and spray shape) from different types of hydraulic spray nozzles using the backlight image acquisition system developed in Chapter 2 and image processing technique. Tests included five different commonly used nozzles (Albuz ATR orange and red, TeeJet XR 110 01, XR 110 04 and Al 110 04).

[vi] This chapter has been compiled from:

Vulgarakis Minov S, Cointault F, Vangeyte J, Pieters J G, Nuyttens D. 2013. Spray nozzle characterization using high speed imaging techniques. *Proceedings 9th European Conference on Precision Agriculture*. July 7 -11, Lleida, Spain. 569-576. ISBN: 978-90-8686-224-5, DOI: 10.3920/978-90-8989-778-3.

Vulgarakis Minov S, Cointault F, Vangeyte J, Pieters J G, Nuyttens D. 2014. Spray nozzle characterization using backlighted high speed imaging techniques. *Aspects of Applied Biology*. 122: 353-361.

7.1 INTRODUCTION

Agricultural nozzles produce sprays with a distribution of droplet sizes and velocities (Lefebvre, 1989) as summarized in 2.2.2.2. It is important to quantify and control these distributions because they influence the droplet trajectories and interactions with the target (Butler Ellis *et al.*, 1997).

A large range of hydraulic nozzles have been designed in which liquid under pressure is forced through an orifice so that there is sufficient velocity energy to spread out the liquid, usually in a thin sheet which becomes unstable and disintegrates into droplets of different sizes (Matthews, 2000). A minimum pressure is essential to provide sufficient velocity to overcome the contracting force of surface tension and to obtain full development of the spray pattern. An increase in pressure will increase the angle of the spray as it emerges through the orifice and also increase the flow rate in proportion to the square root of the pressure (Matthews, 2000).

The droplet spectrum depends on the nozzle output, spray angle of the nozzle and operating pressure, and this determines the spray quality (2.2.2.3). Therefore, it is important to select a nozzle that develops the desired spray pattern. The sizes of the droplets vary, in the range 10 – 1000 µm. The shape of the spray pattern of a single nozzle depends from the applied pressure at the nozzle, the height of the nozzle from the spray surface, and the angle at which the nozzle is oriented (Azimi *et al.*, 1985).

Furthermore, correct selection of spray volume is important. It will influence several spray characteristics such as drift potential, spray coverage, droplet size, hectares per tank, and pesticide effectiveness (Johnson *et al.*, 2005).

Spray droplets play an important role in the application accuracy and efficiency of plant protection products. Mechanisms of droplets leaving a nozzle and impacting the leaves are complex and difficult to quantify or model, while existing non-imaging measuring techniques are not able to fully characterize the spraying process in a non-intrusive way. Therefore accurate quantification techniques are required to evaluate the spray application process in order to maximize the economic and environmental benefits of precision farming. Moreover, spray processes occur with a relatively high speed.

The limitations of the non-imaging techniques and the improvements in digital image acquisition and processing increased the interest in using high-speed (HS) imaging techniques for spray characterization (Hijazi *et al.*, 2012) (2.4.2).

The objective of this part of the study was to measure the spray characteristics from different types of single and static hydraulic spray nozzles using the backlighted high speed imaging system developed in Chapter 3. Tests include different nozzle types (standard flat fan, air inclusion, hollow cone), nozzles sizes and spray angles. From the spray images, macro-spray characteristics (liquid sheet length, spray angle, spray shape and volume distribution pattern) were analyzed using image processing. Where possible, the results were compared with the existing non-imaging measuring techniques like a spray distribution bench (horizontal patternator).

7.2 MATERIALS AND METHODS

The macro-spray characteristics (spray angle, spray shape, and liquid sheet length) of five single hydraulic spray nozzles (7.2.1) were measured with the HS image acquisition system for spray characterization and image analysis (Chapter 3) and were compared with the results from existing non-imaging measuring techniques like the horizontal patternator (2.3.3).

7.2.1 Hydraulic spray nozzles

The spray characteristics of five different static spray nozzles were measured to evaluate the effect of nozzle type (hollow cone, standard flat fan and air inclusion flat fan nozzle), nozzle size (ISO 01 & 04) and spray angle (80° & 110°). Their properties manufacture specifications are given in Table 6.3.

Hollow cone nozzles generally provide the smallest droplet sizes. Their spray pattern consists of droplets concentrated on the outer surface of a conically shaped volume. Furthermore, this is the most popular nozzle type for orchard and vineyard spray applications. An Albuz ATR orange (600 kPa) and red (800 kPa) hollow cone nozzle with 80° spray angles were tested (Figure 7.1). Besides, Dekeyser *et al*. (2013) used the same nozzle-pressure combinations for orchard spray applications.

Figure 7.1. Albuz ATR hollow cone: orange and red nozzle

Standard flat fan nozzles are the most commonly used nozzle type for horizontal boom sprayers. They produce a flat sheet of liquid resulting in a bell shaped spray distribution, comparable to a Gaussian distribution (Huyghebaert *et al.*, 2001). A TeeJet XR 110 01 and XR 110 04, both at 400 kPa with a 110° spray angle, were tested (Figure 7.2). The ISO 04 nozzle size is commonly used in Western Europe. The small ISO 01 nozzle size was selected because of its small droplet sizes.

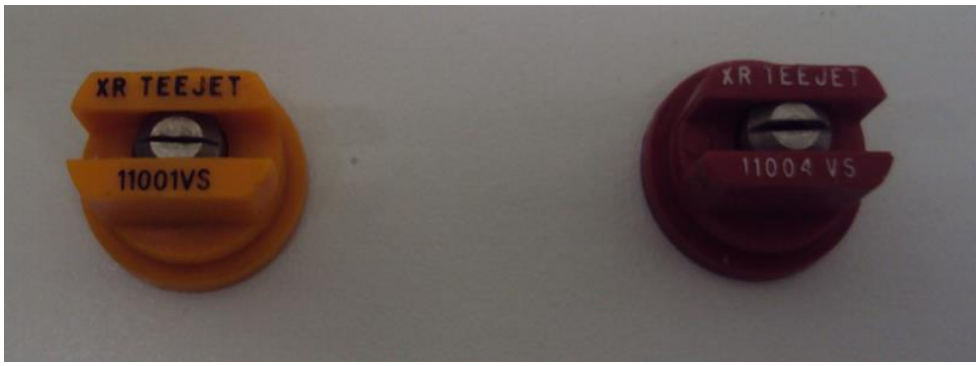

Figure 7.2. TeeJet extended range flat fan nozzles: XR 110 01 (orange) and XR 110 04 (red)

Air inclusion flat fan nozzles have two air inlets from which air is induced into the nozzle, mixing with spray liquid. As a result, the emitted spray contains large droplets, potentially with air bubbles, which reduce the risk of droplet bouncing off a leaf surface. Therefore, air inclusion nozzles are the most popular drift reducing application technique. A TeeJet AI 110 04 nozzle at 400 kPa and with a 110° spray angle was selected (Figure 7.3).

Figure 7.3. TeeJet AI 110 04 nozzle

7.2.2 Existing non-imaging techniques for spray characterization

A wide variety of non-imaging measurement techniques have been used to determine the spray nozzle characteristics. The actual flow rate of all nozzle-pressure combinations was measured in ILVO's Spray Tech Lab (2013) (Figure 7.4a).

Spray distribution measurements are mainly carried out using intrusive methods like a patternator or spray scanner. In this work, a horizontal patternator (AAMS, Maldegem, Belgium, Figure 7.4 b&c) was used to measure the cross flow distribution of the five nozzle-pressure combinations according to the International Standard ISO 5682-1(1996) in the ILVO Spray Tech Lab (2013). Water at a constant pressure (± 10 kPa) was sprayed from one static nozzle onto a 3.0 m wide channeled table and collected in a sloping section with 0.05 m wide groves which drained into calibrated collecting tubes. All nozzle-pressure combinations were tested at 3 different heights, i.e. 15, 30 and 50 cm, and in four repetitions. Nozzles were turned 180° (front/behind) between every repetition. The flat fan nozzles were installed with the longest axis of the fan perpendicular to the measuring grooves. For every nozzle setting the spray volumes in every tube, the collecting time, the relative humidity and the ambient and water temperature were registered and saved. Each measurement was stopped as soon as the amount of liquid collected in one of the tubes reached 90% of its capacity.

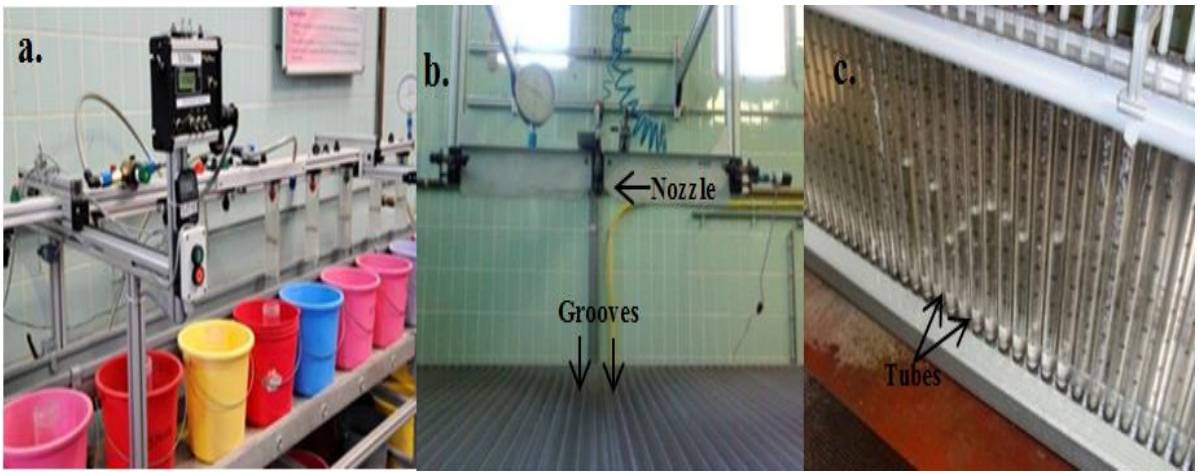

Figure 7.4. Non-imaging techniques for spray characterization at ILVO's Spray Tech Lab: (a) flow rate test bench and (b) & (c) horizontal patternator

The spray angle and spray shape of a single nozzle depend on the nozzle height, type and pressure and the angle at which the nozzle is oriented (Azimi *et al.*, 1985). The actual *spray angle* (θ) for every nozzle measurement with the horizontal patternator was trigonometrically calculated based on the nozzle height and spray pattern width defined as the distance between the centers of the last filled tubes with at least 20 mL (Figure 7.5). As it is not possible to know exactly where the spray pattern finishes (± 2.5 cm), this measuring error is brought into account while calculating the measuring accuracy on the actual spray angle (Table 7.3). The *spray shape* was estimated based on the width of the spray pattern at the three different heights and the position of the nozzle.

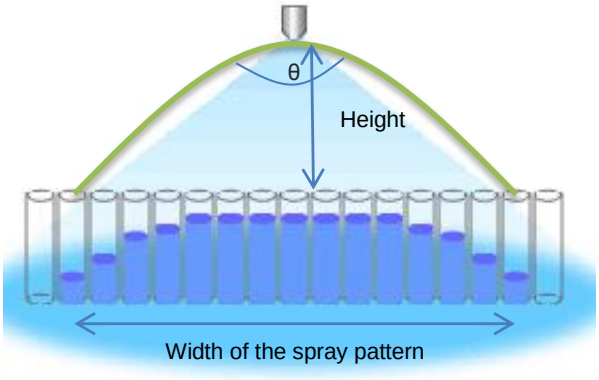

Figure 7.5. Spray angle (θ) estimation based on cross flow distribution measurement and spray height

7.2.3 Image acquisition system for spray characterization

A high-speed image acquisition system was developed for macro-spray characterization in Chapter 3 (Vulgarakis Minov *et al.*, 2015a). Figure 7.6 shows a schematic overview of the spray characterization system.

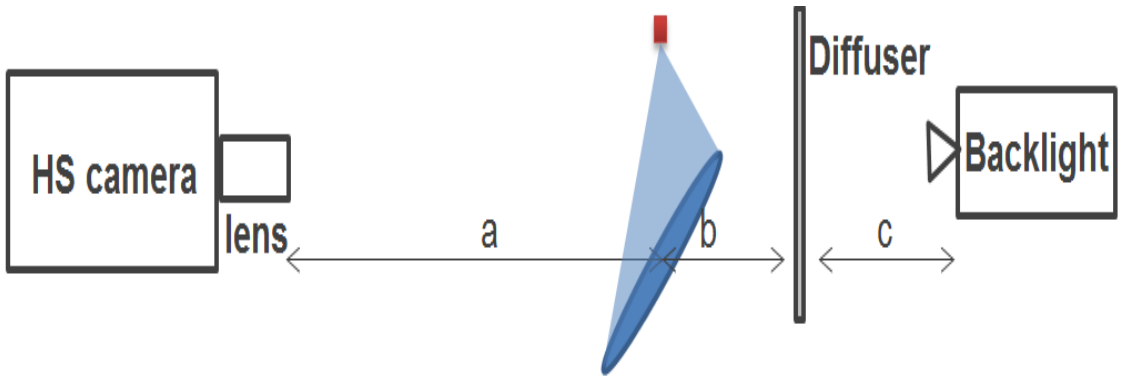

Figure 7.6. Image acquisition system for spray characterization (Vulgarakis Minov *et al.*, 2015a)

The macro spray characteristics including the spray angle, shape and liquid sheet length were investigated using an image acquisition system consisting of three main parts: a 500 W spotlight with diffuser, a HS camera IDT N3 (8-bit dynamic range, 1280 × 1024 pixels) and a macro video zoom lens (Optem, 18-108, F/2.5, 20 mm focal length). The ground glass diffuser (TECHSPEC, Edmund Optics, USA) was used to reduce the light inhomogeneity and was placed between the background light and the lens (Figure 7.6) (Lad *et al.*, 2011). The distance between the camera and nozzle was 14.3 cm resulting in a field of view (FOV) of 110 mm × 88 mm with a pixel resolution of 85.8 µm. Images were acquired at a grabbing rate of 1000 fps with an exposure time of 15 µs and + 3dB sensor gain (Massinon & Lebeau, 2012a). The captured images had 1280 × 1024 pixels with 8 bits of gray scale resolution. The Motion Studio software (IDT, Lommel, Belgium, version: 2.09, 2011) was used to view and save the images. The specifications of the system are shown in Table 7.1.

Table 7.1. Properties of the tested hydraulic spray nozzles

HS camera	IDT N3 (8-bit dynamic range, 1280 × 1024 pixels), 1000 fps
Exposure time	15 µs
Lens	Macro Video Zoom Lens (Optem, 18-108, F/2.5, 20 mm focal length)
Backlight	500 W Spotlight
Diffuser	220 ground glass diffuser
Distances a/b/c	430 mm / 80 mm / 240 mm
FOV	88.0 mm × 110 mm
Pixel resolution	85.8 µm

7.2.4 Image analysis for spray characterization

Macro-spray characteristics were determined by image analysis using dedicated algorithms developed in Matlab® (The MathWorks Co., Massachusetts). The key of automatically measuring the *spray angle* is to find the edge of the most left side and the most right side of the spray (Zhang *et al.*, 2011). The algorithm for spray angle image analysis consisted of different steps: **1**. acquiring the spray images (Figure 7.7a), **2**. noise reduction and image enhancement (Figure 7.7b), **3.** image binarization (Figure 7.7c), **4.** applying morphological operations and spray edge detection (Figure 7.7d&e) and **5**. detection of the two boundary lines of the spray angle with their orientation (Figure 7.7f). Detection of the boundary lines was the key problem for spray angle determination, so choosing the appropriate morphological operators was crucial for the detection accuracy.

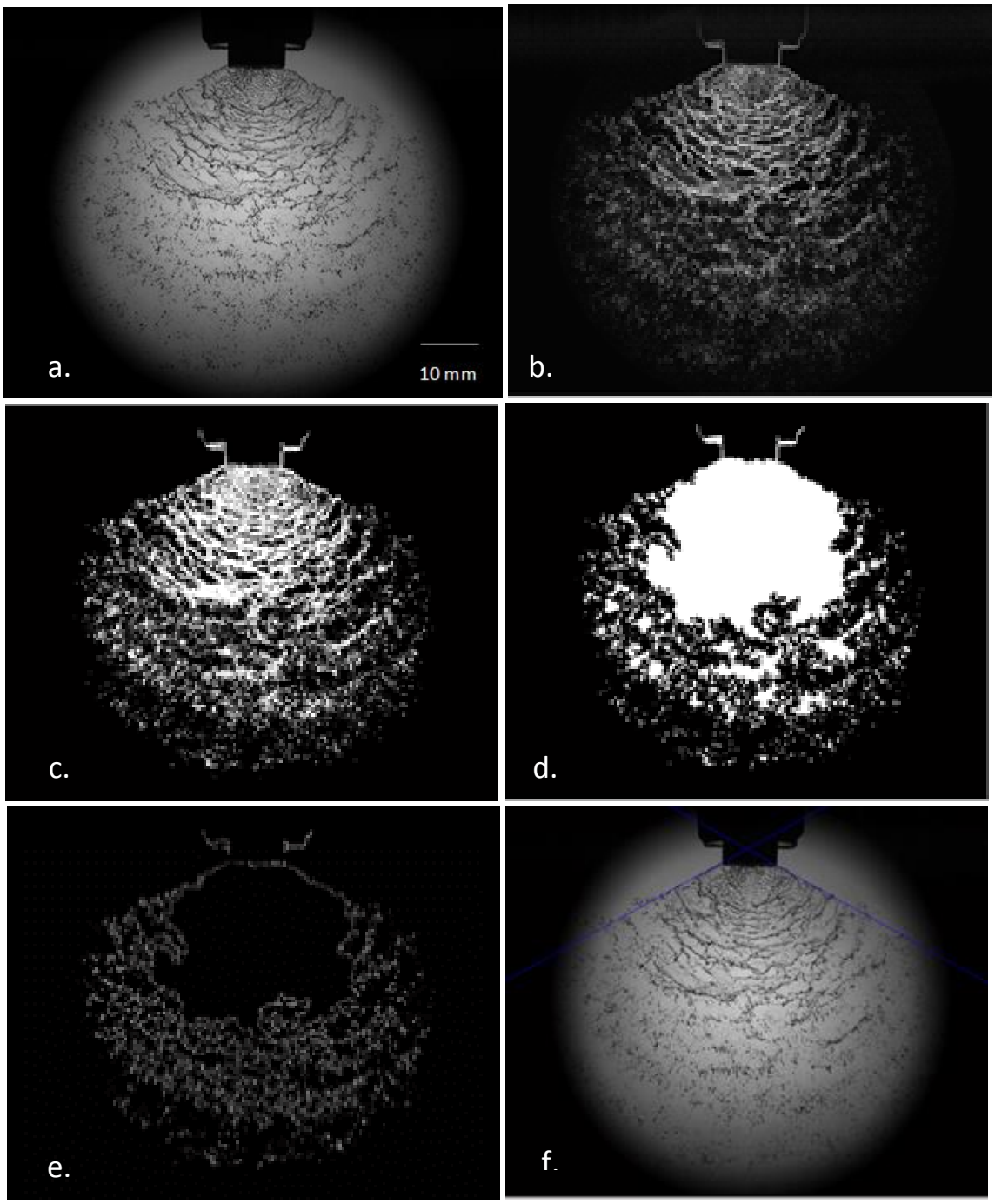

Figure 7.7. Steps in spray angle image analysis illustrated for the TeeJet XR 110 04

Determining the *spray liquid sheet length* was based on finding the biggest object and its length (starting from the nozzle exit – Figure 7.8a). For this purpose the hollow cone nozzles, with their conical spray pattern, were put at an angle of 40° towards the diffuser and a region of interest (ROI) was selected beneath the nozzle. In this way only the part of the spray which is sharp in the FOV is selected and used for the liquid sheet determination (Figure 7.8b&c).

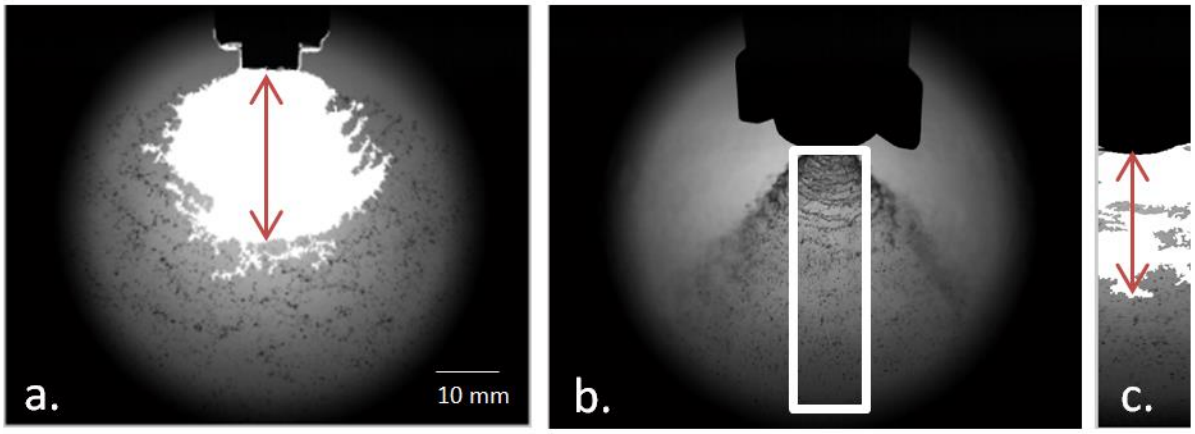

Figure 7.8. Spray liquid sheet image analysis for (a) the TeeJet XR 11004 nozzle and (b) and (c) the Albuz ATR red nozzle

Spray shape analysis was done by moving every single nozzle using a 3D positioning table (Nuyttens *et al.*, 2007a) in horizontal steps of 2.5 cm to both sides and in vertical steps of 5 cm in order to scan the spray fan. In this manner 140 images with flat fan nozzles and 68 images with hollow cone nozzles of the spray were needed to be taken and connected to view the whole spray up to 20 cm beneath the nozzle. The spray shape was achieved by edge detection (Figure 7.9). All measurements were done with tap water and repeated 5 times.

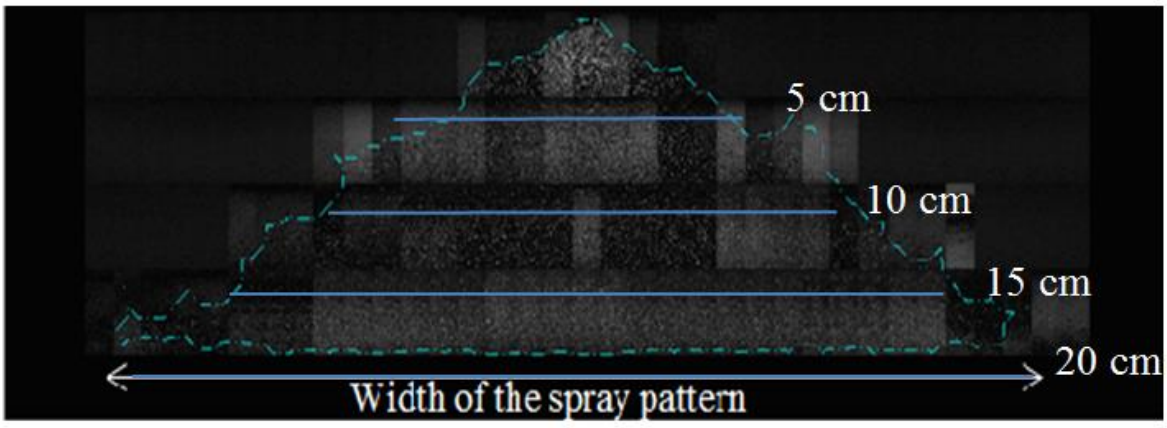

Figure 7.9. Spray shape analysis of the Tee Jet XR110 04 up to 20 cm below the nozzle

7.3 RESULTS AND DISCUSSION

7.3.1 Flow rate

The measured average flow rates (± std) of the five nozzle-pressure combinations are presented in Table 7.2 together with the nominal flow rates, the deviation from the nominal flow rate (%) and the corresponding average ambient temperature (avg ± std), the relative humidity (avg ± std) and the spray liquid temperature (avg ± std).

The flow rate of different nozzles varies according to the size of the orifice, the applied pressure and the density of the spray liquid. Flow rate increases by installing a nozzle with a larger orifice or increasing the applied pressure. As a result, in Table 7.2 it can be seen that flat fan nozzle with ISO 04 size had four times bigger flow rate than the flat fan nozzle ISO 01 at the same pressure. The maximal deviation of the nominal flow rate was 2.22 % which is clearly below the accepted value of 10% as prescribed by Vanella *et al*. (2011).

Table 7.2. Measured average flow rates of the 5 nozzle-pressure combinations and environmental conditions

Nozzle	Operating pressure (kPa)	Nominal flow rate (L min^{-1})	Actual flow rate (L min^{-1})	Deviation of the nominal flow rate (%)	Average ambient temperature (°C)	Relative humidity (%)	Spray liquid temperature (°C)
ATR orange	600	1.08	1.104 ± 0.005	2.22	17 ± 0.0	55.0 ± 0.0	22.5 ± 1.3
ATR red	800	1.73	1.740 ± 0.003	0.58	17 ± 0.0	54.7 ± 0.5	23.0 ± 1.60
XR 110 01	400	0.45	0.443 ± 0.001	-1.50	21 ± 0.0	54.7 ± 0.5	21.3 ± 0.43
XR 110 04	400	1.82	1.829 ± 0.001	0.50	16 ± 0.0	54.0 ± 0.0	15.8 ± 0.17
AI 110 04	400	1.82	1.836 ± 0.000	0.88	16 ± 0.0	56.0 ± 0.0	15.3 ± 0.18

7.3.2 Spray angle

The spray angles of the different nozzle-pressure combinations at three different heights (15, 30 and 50 cm) achieved with the horizontal patternator and with the imaging technique at the nozzle orifice (0 cm) are given in Table 7.3. In general the measured spray angles were higher than the nominal spray angles except for the Albuz red nozzle at 30 cm and the TeeJet XR 110 01 at the nozzle exit. Moreover, based on the results at 15, 30 and 50 cm, it was discovered that the actual spray angle decreased with an increase of nozzle height because of the effect of gravity. This effect was most pronounced for the finer sprays. For the hollow cone and the air inclusion nozzle, the imaging technique gave a good representation of the spray angle while the spray angle was underestimated for both standard flat fan nozzles.

7.3.3 Liquid sheet length

The smallest liquid sheet length was calculated for the TeeJet XR 110 01 nozzle (18.5 mm), followed by the two hollow cone nozzles (27.4 and 31.3 mm). The longest liquid sheets were found for the TeeJet XR 110 04 (38.9 mm) and TeeJet AI 110 04 nozzle (43.1 mm) (Table 7.3). Jasikova *et al.* (2011) measured a liquid sheet length for a full cone nozzle of 30 mm using imaging techniques.

Table 7.3. Spray angles and liquid sheet lengths of the 5 nozzles-pressure combinations

Nozzle	Pressure (kPa)	Nozzle height	Nominal spray angle	Actual spray angle (°)	Liquid sheet length (mm)
ATR orange	600	0 cm	80°	96.9 ± 6.7	27.4 ± 1.1
		15 cm		98.8 ± 7.2	
		30 cm		94.5 ± 3.6	
		50 cm		80.7 ± 2.7	
ATR red	800	0 cm	80°	86.6 ± 2.0	31.3 ± 3.1
		15 cm		98.8 ± 7.2	
		30 cm		84.9 ± 4.2	
		50 cm		80.7 ± 2.7	
XR 110 01	400	0 cm	110°	108.5 ± 1.3	18.5 ± 1.8
		15 cm		124.8 ± 2.0	
		30 cm		124.8 ± 2.0	
		50 cm		110.8 ± 1.5	
XR 110 04	400	0 cm	110°	113.8 ± 3.4	38.9 ± 1.8
		15 cm		130.3 ± 2.8	
		30 cm		128.9 ± 1.5	
		50 cm		119.0 ± 1.2	
XR 110 04	400	0 cm	110°	120.1 ± 8.7	43.1 ± 2.0
		15cm		124.8 ± 2.0	
		30 cm		124.8 ± 2.0	
		50 cm		117.5 ± 1.3	

7.3.4 Spray distribution

Figure 7.10 presents the results of the cross flow distribution measurements of the five nozzle-pressure combinations at three different heights with the results expressed in relative values (% of the total volume ± std).

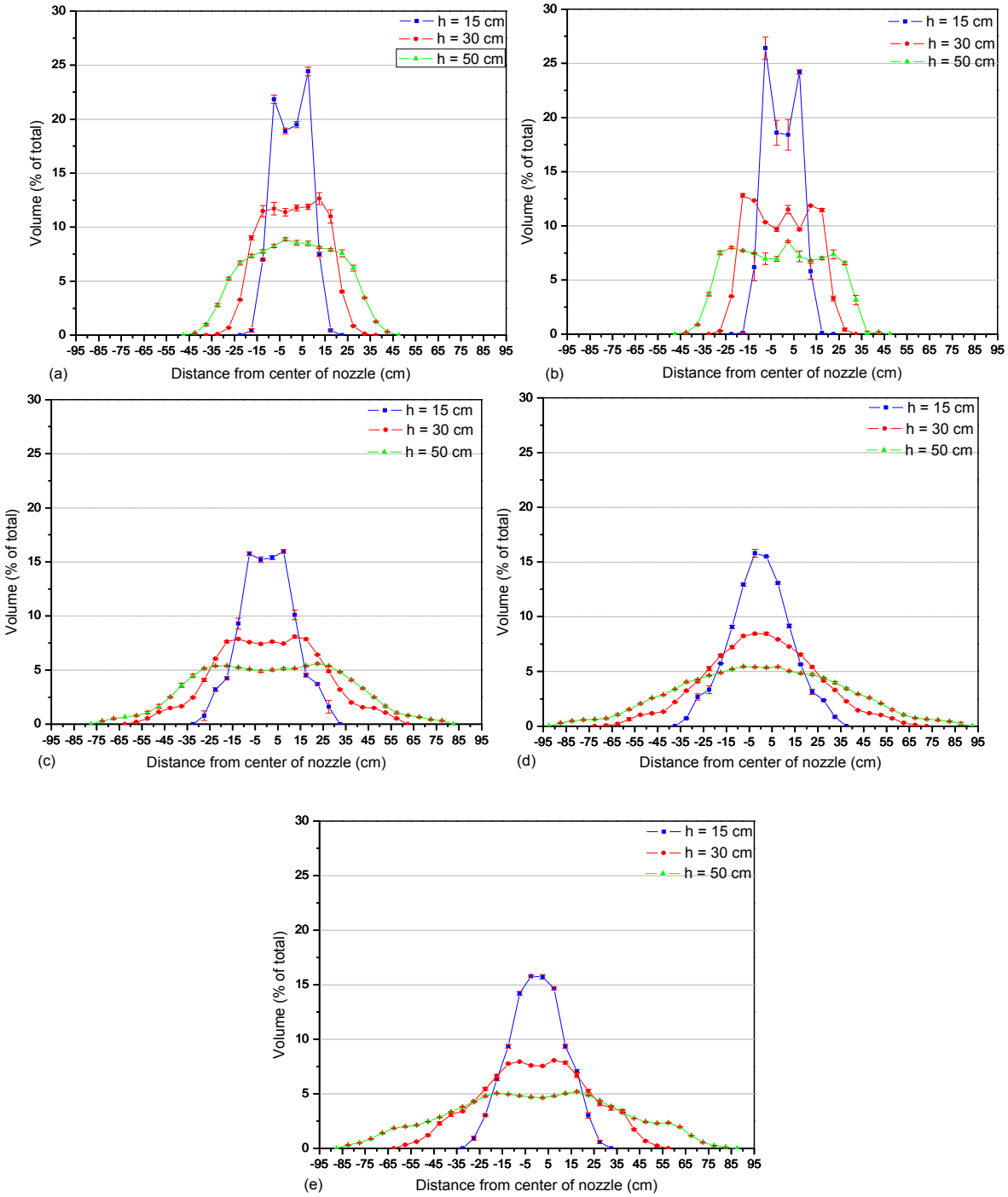

Figure 7.10. Spray distribution measurements (% and sd) at 3 different heights of the (a) Albuz ATR orange nozzle at 600 kPa, (b) Albuz ATR red nozzle at 800 kPa, (c) TeeJet XR 110 01 at400 kPa, (d) TeeJet XR 110 04 at 400 kPa and (e) TeeJet AI 110 04 at 400 kPa

These graphs give the measured spray distribution pattern with the standard deviations. Nozzle positioning is quite important due to the fact that sprayed water distribution is not even. Likewise, it is obvious from these graphs that, in general, spray nozzles have parabolic distributions and that greater nozzle-to target- distance allows the spray droplets to spread more and to create a wider individual spray pattern. At the nozzle height of 15 cm, for the flat fan nozzles, the highest percentage of the total spray volume was found directly under the nozzle and gradually decreased to both sides of the nozzle. On the other hand, at 15 cm, hollow cone type nozzles produce larger amounts of spray near the outer edges of the spray pattern and less in the center. At 30 and 50 cm heights, the spray liquid stretched over more collecting grooves and thus the discharge out of the nozzles was distributed on a larger area than compared with the 15 cm height. Moreover, the spray distributions at higher heights had smoother peaks compared to those produced at 15 cm nozzle height. So, the spray liquid distribution uniformity was dependent on the nozzle height.

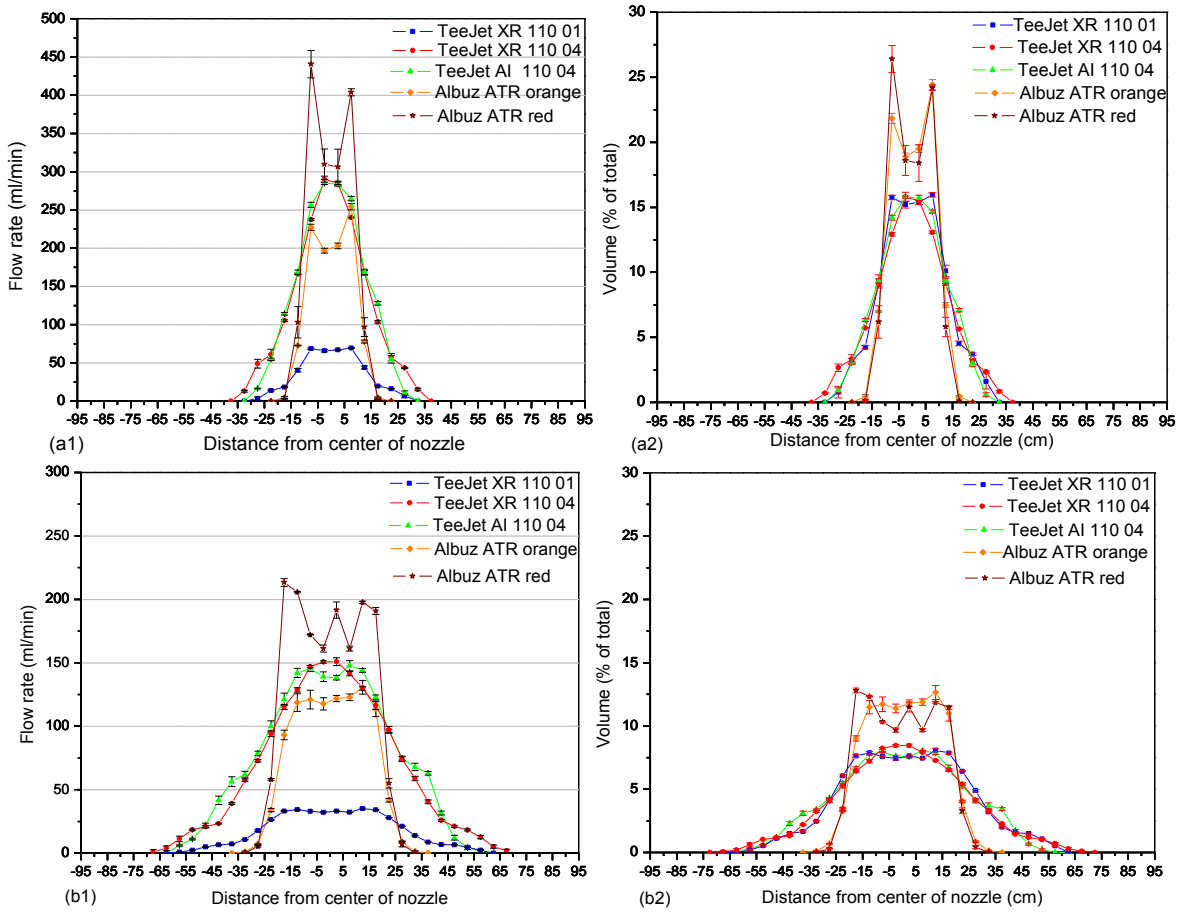

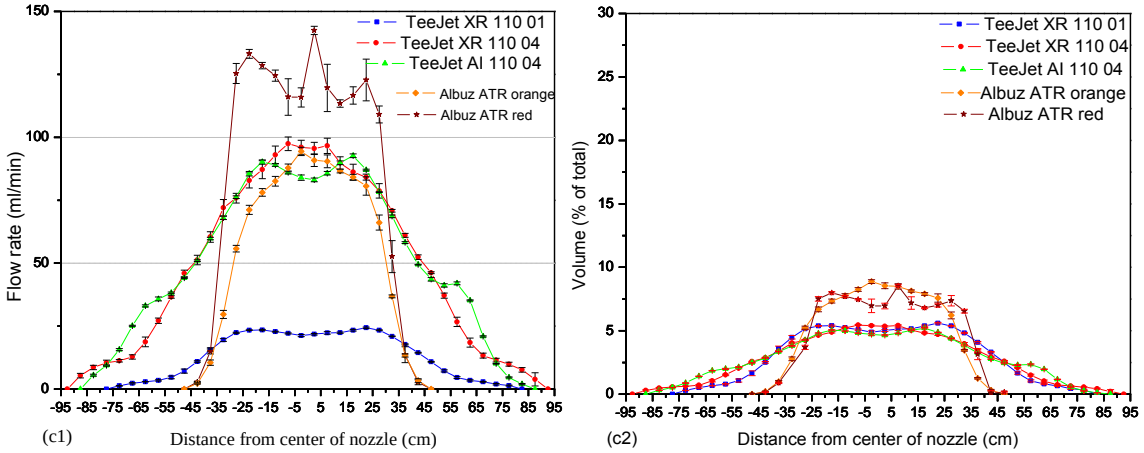

Figure 7.11. Spray distribution measurements expressed in 1. absolute (ml/min and sd) and 2. relative flow values (% and stdev.) of the five nozzle pressure combinations at heights of (a) 15 cm, (b) 30 cm and (c) 50 cm

Comparing the spray distributions between the different nozzles (Figure 7.11), it is obvious that the 110° flat fan nozzles produced a wider spray compared with the 80° hollow cone nozzles. The spray distributions generated by the TeeJet XR 110 04 and TeeJet AI 110 04 at 400 kPa were similar because of the same flow rate and spray angle. Tests with the hollow cone nozzles at 600 kPa and 800 kPa gave results with bigger standard deviations probably because of the swirling effect of this nozzle in combination with the patternator interrupting the nozzle spray.

7.3.5 Spray shape

From the spray pattern widths at 15, 30 and 50 cm (resulting from the spray distribution measurements), the spray shapes of the 5 nozzle-pressure combinations were estimated as presented in Figure 7.12. Spray shape results based on the intrusive patternator measurements of the different nozzle-pressure combinations are summarized in Figure 7.13.

Figure 7.14 presents the average spray shape of the TeeJet XR 110 04 determined using the imaging system based on 5 replicates. From this spray shape, we calculated the spray pattern width at 4 different heights (5, 10, 15 and 20 cm) and the corresponding spray angles and compared them with the patternator results at 15 cm height (Table 7.4). From the spray distribution measurements, it is clear that nozzle height had an important effect on the spray distribution. Greater nozzle to target distance allows the spray droplets to spread more and to create a wider individual spray pattern. In general, the highest spray volume was found directly under the nozzle and decreased onto both sides of the nozzle.

The higher the nozzle, the smoother the spray distribution peaks were, when compared to those produced at 15 cm nozzle height. Because of the effect of gravity, the spray shape was parabolic and the spray angle generally decreased with increased nozzle height.

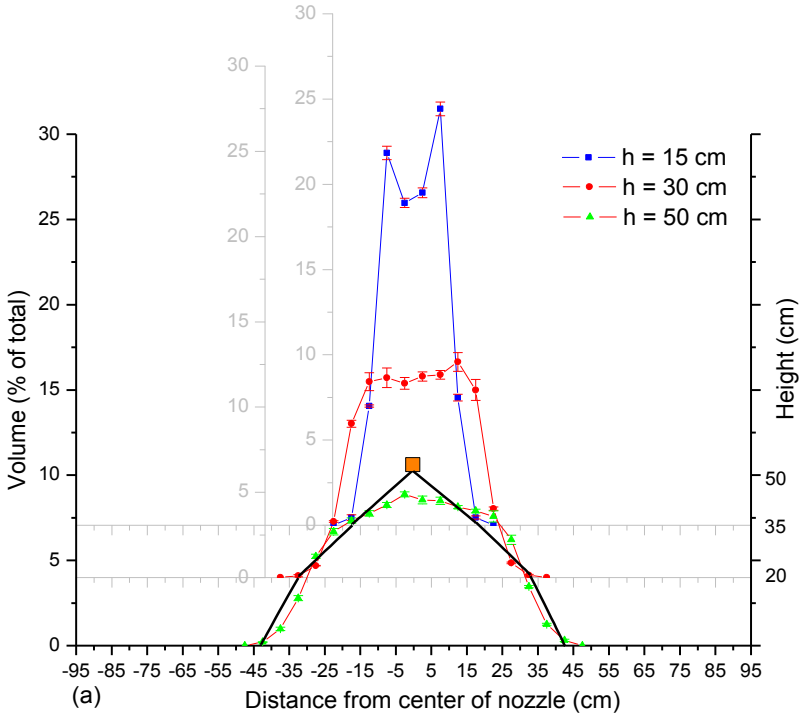

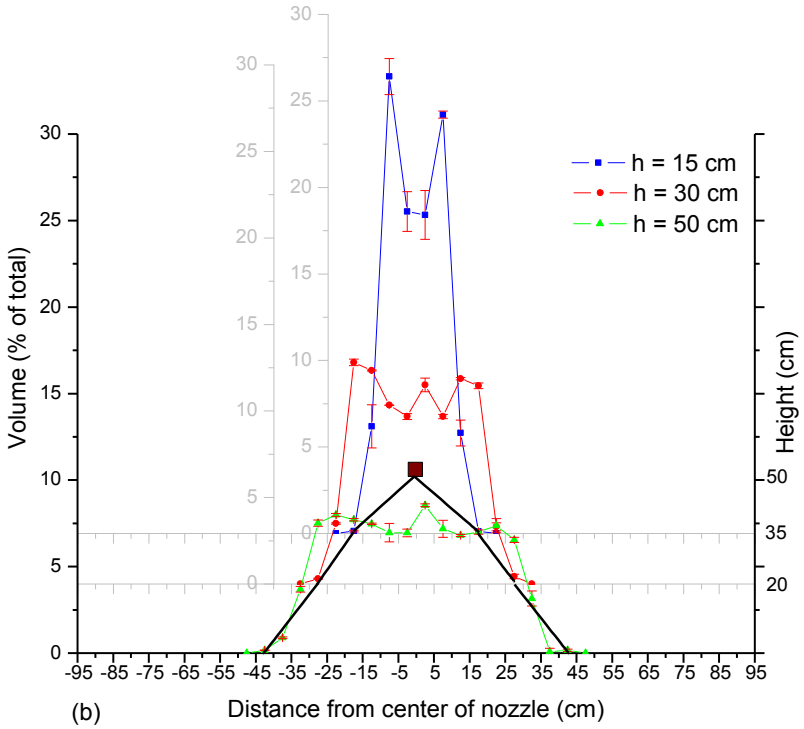

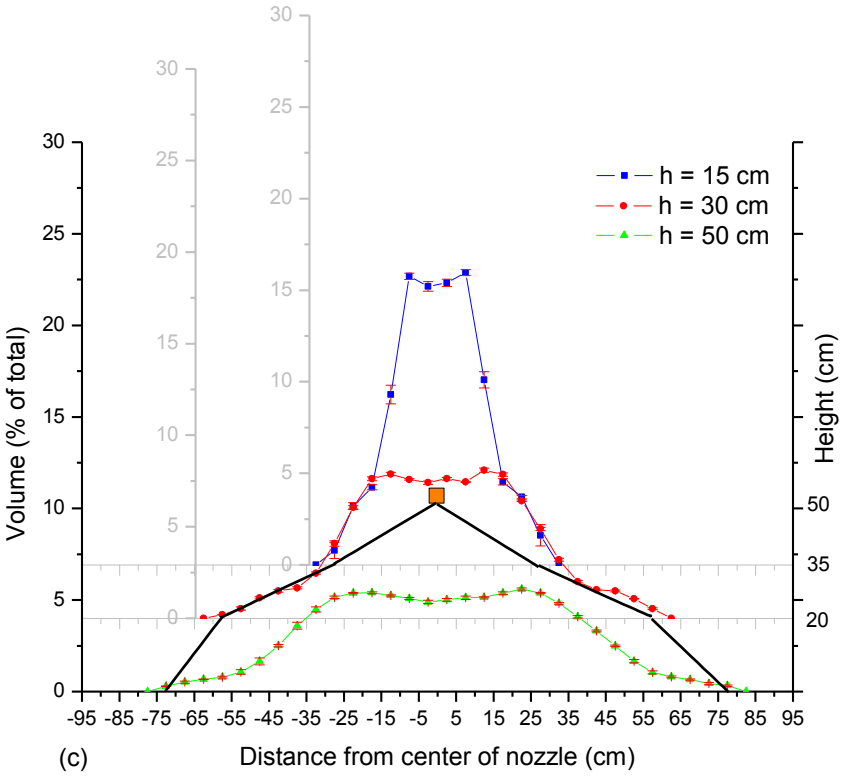
h = 15 cm
h = 30 cm
h = 50 cm
Volume (% of total)
Height (cm)
Distance from center of nozzle (cm)

(c)

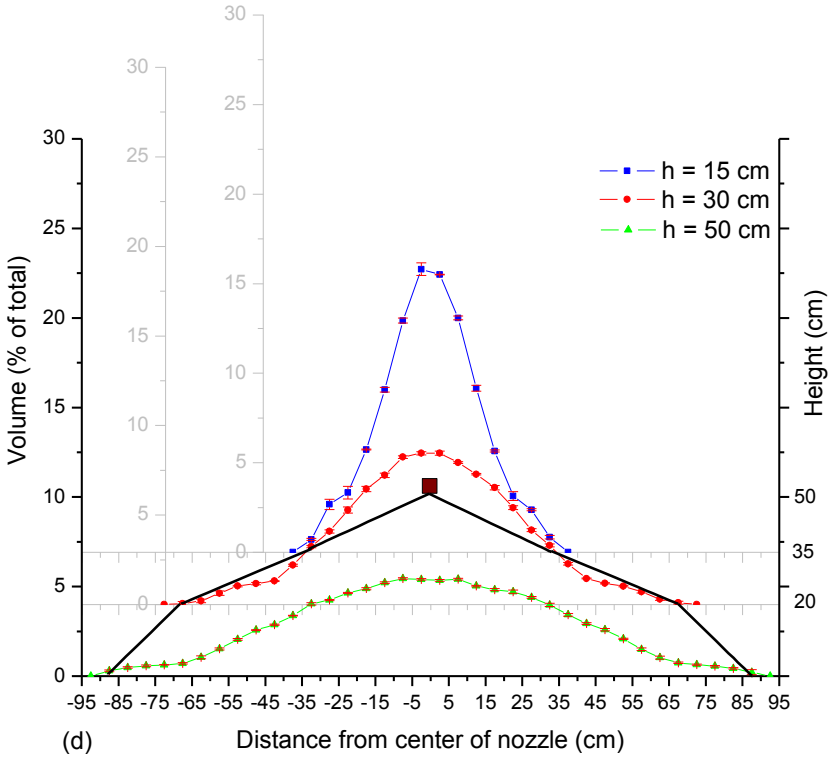
h = 15 cm
h = 30 cm
h = 50 cm
Volume (% of total)
Height (cm)
Distance from center of nozzle (cm)

(d)

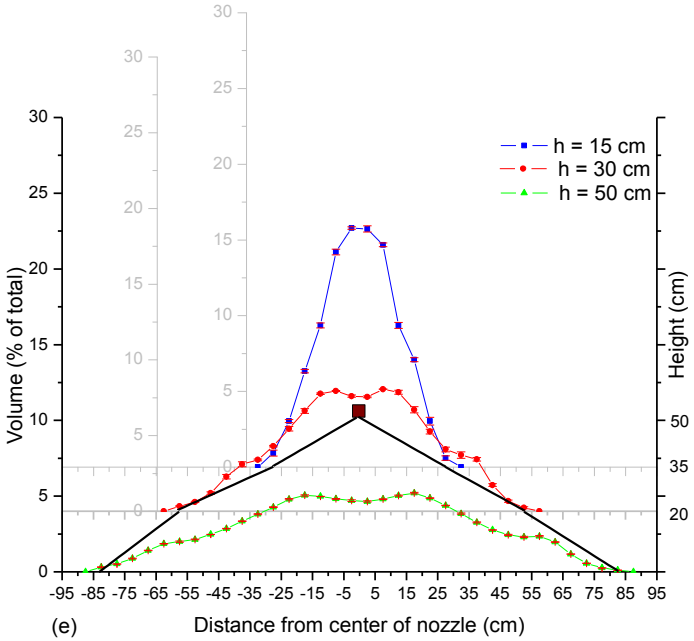

Figure 7.12. Spray angle and spray shape estimation based on spray distribution measurements at 3 different heights of the (a) Albuz ATR orange nozzle at 600 kPa, (b) Albuz ATR red at 800 kPa, (c) TeeJet XR 110 01 at 400 kPa, (d) TeeJet XR 110 04 at 400 kPa and (e) TeeJet AI 110 04 at 400 kPa

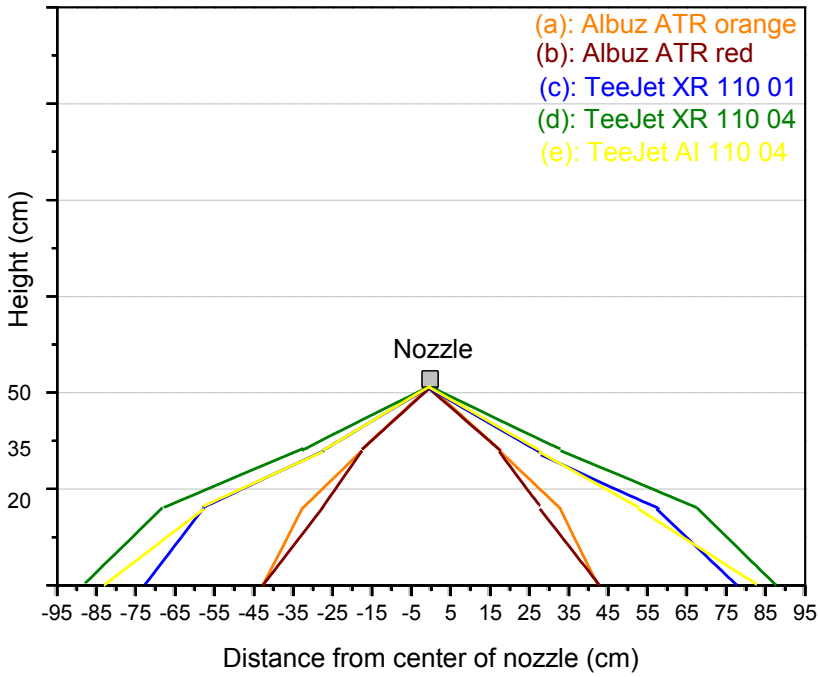

Figure 7.13. Spray angle as well as spray shape of the (a) Albuz ATR orange nozzle at 600 kPa; (b) Albuz ATR red at 800 kPa; (c) TeeJet XR 110 01 at 400 kPa; (d) TeeJet XR 110 04 at 400 kPa at 400 kPa and (e) TeeJet AI 110 04 at 400 kPa

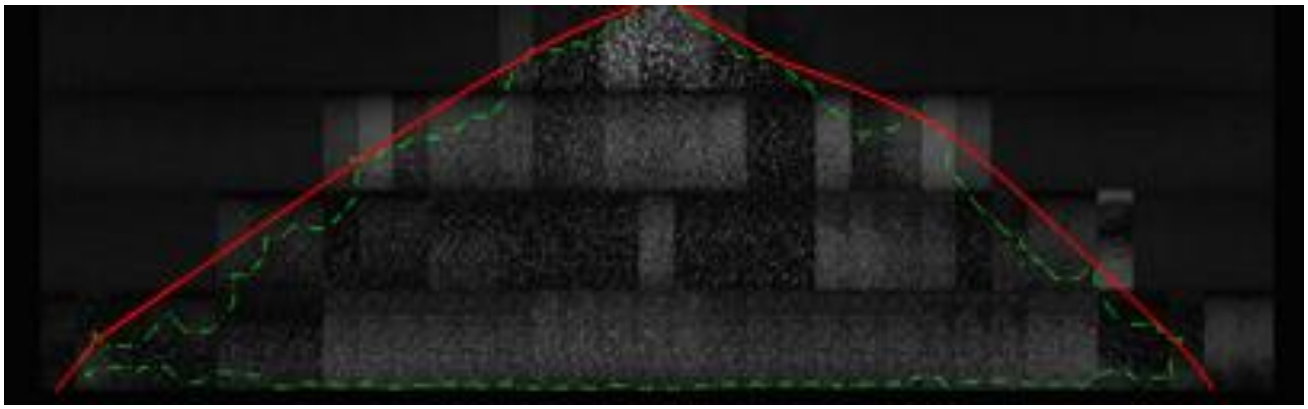

Figure 7.14. . Spray shape estimation for TeeJet XR 110 04 nozzle at 400 kPa up to 20 cm below the nozzle

Table 7.4 shows the comparison of image analysis results and horizontal patternator results. From this table, the spray angle relative error for TeeJet XR 110 04 at 15 cm height was 0.5% while for TeeJet XR 110 01 and AI 110 04, 0.6%. The spray angle relative error was bigger for the hollow cone Albuz ATR orange and red nozzles: 2.8% and 5.4%, respectively.

Accordingly, the low spray angle relative error meets well the demands for using this technique. In closing, similar results for the spray shape, pattern width and spray angle were found using the horizontal patternator and the imaging technique.

Table 7.4. Spray pattern width at 4 heights (image analysis) and at 15 cm (patternator) for the nozzle-pressure combinations

Nozzle	Nozzle height (cm)	Imaging system		Horizontal patternator		Relative error (%)
		Spray pattern width (cm)	Actual spray angle (°)	Spray pattern width (cm)	Actual spray angle (°)	Actual spray angle
ATR orange	5	12.3	101.6	-	-	-
	10	27.0	103.9	-	-	-
	15	36.8	101.6	35	98.8 ± 7.2	2.8
	20	41.7	92.4	-	-	-
ATR red	5	12.3	101.6	-	-	-
	10	22.1	95.7	-	-	-
	15	31.9	93.5	35	98.8 ± 7.2	5.4
	20	41.7	92.4	-	-	-
XR 110 01	5	22.1	131.3	-	-	-
	10	41.7	128.8	-	-	-
	15	56.4	124.0	55	124.8 ± 2.0	0.6
	20	76.1	124.5	-	-	-
XR 110 04	5	22.1	131.3	-	-	-
	10	46.6	133.6	-	-	-
	15	63.8	129.6	65	130.3 ± 2.8	0.5
	20	85.9	130.0	-	-	-
AI 110 04	5	22.1	131.3	-	-	-
	10	41.7	128.8	-	-	-
	15	56.4	124.0	55	124.8 ± 2.0	0.6
	20	76.1	124.5	-	-	-

7.4 CONCLUSION

A HS image acquisition set-up and image processing algorithms were developed to evaluate the macro-spray characteristics, i.e. spray angle, spray shape and liquid sheet length, of five different spray nozzles using image acquisition and processing. The imaging system consisted of a HS camera, a macro video zoom lens, a diffuser and a backlight spotlight. Results were compared with those obtained from traditional non-imaging techniques. The results from the imaging technique have shown that it is possible to measure the spray characteristics in a nonintrusive and correct way using a correct image acquisition set-up and dedicated image processing algorithm.

8 GENERAL CONCLUSIONS AND SUGGESTIONS FOR FUTURE WORK

8.1 GENERAL CONCLUSIONS

In the last fifty years, advances in plant protection contributed to increasing the yields and ensuring large production. Easy to apply and rather inexpensive, pesticides have proven to be very efficient. However, when pesticides are applied to crops some of the spray may not reach the target, but move outside the intended spray area. Therefore, efforts are being undertaken to their safe and efficient use which is more and more regulated by international environmental laws.

Agricultural sprays applied with different nozzle size-pressure combinations consists of range of droplet sizes and velocities (Chapter 2). Simultaneous measurement of these droplet sizes and velocities is of great significance in the spray application process. There are numerous methods for measuring droplet characteristics which can be divided into three categories: *mechanical, electrical and optical methods*. Application of these techniques may affect the spray flow behavior. A comprehensive review of these methods together with their limitations has been made in Chapter 2. Therefore, the availability of non-intrusive systems for spray characterization is of great importance.

Recent improvements in digital image processing, the high sensitivity of imaging systems and cost reductions have increased the interest in high-speed imaging techniques for agricultural applications in general and pesticide applications in specific. The prize of high speed cameras (HS) is still high and they have not yet been applied as standard measuring equipment on agricultural machines. However, for research and development activities, a high speed camera is a versatile tool which can be used in different applications where fast particles or processes must be captured and analyzed. In addition, high speed cameras allow the viewer to see and better understand the fast spray atomization process which is not the case the commonly used non-imaging droplet characterization techniques based on light scattering principles.

This thesis focused on the development and application of high speed imaging techniques for spray characterization. The general aim was to show that spray characteristics can be correctly measured with the developed imaging techniques in a non-intrusive way.

The main conclusions and achievements are summarized per chapter.

8.1.1 Development of high speed image acquisition systems based on single droplet experiments

The development of high speed image acquisition systems based on single droplet experiments was presented in Chapter 3, using a HS camera and a piezoelectric droplet generator able to to generate small droplets on demand or in continuous mode. This droplet generator can be used for studying single droplet charactristics and for the comparison with the spray droplet characteristics in a real spray application. It is also useful in many other applications where generation of wide range of uniform-sized droplets is needed e.g. calibration of droplet size measuring equipment or droplet impact studies.

Different lenses, light sources, diffusers, and exposure times were tested. The different imaging systems were evaluated based on image quality parameters (SNR, entropy ratio and contrast ratio), light stability and overexposure ratio, and the accuracy of the droplet size measurement.

The experiments resulted in dedicated image acquisition systems for measuring:

- Micro spray characteristics (droplet size and velocity). The system consisted of a HS camera with a 6 µs exposure time, a long distance microscope lens at a working distance of 430 mm resulting in a FOV of 10.5 mm x 8.4 mm, and a xenon light source used as a backlight without a diffuser. The long-distance microscope lens could deliver microscopical magnification and resolution equivalent to a standard microscope with a pixel size of 8.2 µm. Also, they give the best performance when the objective is as evenly and as brilliantly illuminated as possible. Therefore, a xenon light source was selected without diffuser.

- Macro spray characteristics (spray angle, spray shape, liquid sheet length, etc.). The system consisted of a HS camera with a 15 µs exposure time, a macro video zoom

lens at a working distance of 143 mm with a larger FOV of 88 mm x 110 mm in combination with a halogen spotlight and a diffuser resulting in a pixel size of 85.8 µm. The prize of the macro video zoom lens and spotlight on the market is affordable. With this system, attention should be paid to the light stability.

8.1.2 Droplet generation and characterization using a piezoelectric droplet generator and imaging techniques

Measurements using a single droplet generator in droplet on demand (DOD) and continuous mode were performed. The effects of operating parameters, including voltage pulse width and pulse amplitude with 4 nozzle orifice sizes (261 µm, 123 µm, 87 µm and 67 µm) on droplet diameter and droplet velocity have been characterized. Droplet sizes and velocities of the generated droplets were successfully measured with the image acquisition and image processing system developed in Chapter 3 and 4. Several conclusions were obtained:

- The experiments in DOD mode have shown that the initial droplet characteristics from the droplet generator are a function of the double pulse width and the orifice size. The pulse width values are critical parameters for droplet ejection. By changing pulse width, it was possible to control droplet velocity and droplet size diameter. In general, a decrease of t_a and an increase of t_p increased the droplet diameter. Similarly, increasing the nozzle orifice size increased the droplet diameter.
- In DOD mode, droplet sizes ranged between 134.1 µm and 461.5 µm. Foremost, the smallest and the fastest droplets were measured with the smallest nozzle orifice. The measured droplet velocities ranged between 0.08 m/s and 1.78 m/s. Besides, we noticed an effect of the pulse amplitude on the droplet diameter and velocity.
- The ratio of the droplet diameter and nozzle orifice in DOD mode ranged from 1.3 to 3.5.
- The continuous mode for every nozzle was established for a frequency resulting in a continuous droplet generation. This frequency together with different pulse amplitudes were used to test the effect on the droplet diameter, inter-droplet spacing and velocity.
- The droplet diameter was mainly controlled by the nozzle orifice. The droplet size here was between 167.2 µm and 455.8 µm.

- The nozzle orifice also influenced the droplet velocity i.e., the bigger the nozzle orifice was, the higher the droplet velocity. Obviously, there was a linear trend between the droplet diameter and velocity in continuous mode.
- The effect of the pulse amplitude on the inter-droplet spacing was statistically significant.
- The ratios between the droplet diameter and the nozzle orifice ranged from 1.3 to 3.9.
- In continuous mode, the lowest droplet velocity of 1.84 m/s was measured with the smallest nozzle orifice size while the highest droplet velocity of 4.66 m/s was measured with the biggest nozzle orifice size.
- Based on the results in both modes, similar droplet diameter sizes were produced. However, in continuous mode it was possible to achieve faster droplets which correspond better with real spray application.

8.1.3 Micro-spray characterization from a single nozzle

- An in-focus droplet criterion based on the gray level gradient was introduced to decide whether a droplet is in focus or not. From the different edge dectors, the Canny edge detector gave the best results regarding the quality of the segmentation results and in detecting droplet edges absed on gray level gradients. Differently sized droplets generated with a piezoelectric generator and glass nozzles in continuous mode at different distances from the focal plane and lens using a micro translation stage were measured. This enabled measurement of the gray level gradient and in-focus parameter for every droplet size. From here, a critical in-focus parameter (Inf_c) was established for every droplet size and an in-focus droplet criterion was deduced to decide whether a droplet is in focus or not depending on its diameter and in-focus parameter. The focused droplet zone (FDZ) is in this study defined as the zone in which a droplet with a certain diameter is in focus and a linear relation between droplet size and FDZ was found.
- The in-focus droplet criterion was applied to spray images of different hydraulic spray nozzles and the droplet size and velocity characteristics were calculated. The effects of nozzle type, nozzle size and measuring position on spray droplet characteristics were studied.

- The droplet size and velocity results from the imaging technique have shown that it is possible to measure the spray characteristics in a nonintrusive way using image acquisition set-up and image processing. Measured droplet sizes ranged from 24 µm up to 543 µm depending on the nozzle type and size. Droplet velocities ranged from around 0.5 m/s up to 12 m/s. Spray droplet size characteristics such as $D_{V0.1}$, $D_{V0.5}$, $D_{v0.9}$ and RSF as well as spray velocity characteristics such as V_{Vol10}, V_{Vol50}, V_{Vol90} and VSF, were extracted from the images. Similar effects of nozzle type and measuring position on droplet sizes as well as on droplet velocities were found with the imaging technique as with the Phase Doppler particle analyzer (PDPA) for the droplet size and velocity, respectively.
- The droplet diameter and velocity characteristics showed a relatively good correlation with the results measured with the PDPA laser. When compared with the PDPA laser, the imaging technique generally measured less small droplets and in some cases also less big droplets. Differences between both techniques can be attributed to the fact that the smallest measured droplet size with the imaging system is 24 µm while smaller droplets are measured with the PDPA. In addition, the number of smaller amount of droplets measured with the imaging technique was much smaller compared with the PDPA which increases the chance to miss one of the biggest droplets. This can be improved by taking more images. Differences in droplet velocity characteristics between both techniques can be attributed to the fact that the PDPA laser is only measuring droplet velocity in one dimension and hence underestimates the actual droplet velocity. In addition, the imaging technique applied did not allow the measurement of droplets faster than about 12 m/s based on FOV and the acquisition rate while some droplets with higher speeds were observed with the PDPA mainly for the XR 110 04. In future, the imaging system can be further improved to be able to measure at a higher frame rate with the same accuracy.
- Up to now, measurements of droplet size and velocity remain difficult in dense sprays such as those encountered in agricultural spray applications. Commonly used techniques (discussed in Chapter 2) are often limited due to multi-scattering effects, concentration and also non-spherical shapes. The advantage of this technique on the others was its ability to measure and visualize different droplet sizes and velocities by

using the developed in-focus criterion in a dense spray using a standard high speed camera and dedicated image analysis algorithms.

8.1.4 Macro-spray characterization from a single nozzle

- The spray angles of the selected nozzle-pressure combinations at the nozzle orifice (0 cm) were measured with the imaging technique. The measured spray angles were higher than the nominal spray angle except for the XR 110 01 nozzle. For the hollow cone and air inclusion nozzle, the imaging technique gave a good representation of the spray angle while the spray angle was underestimated for both standard flat fan nozzles.
- Based on the measurements with the horizontal patternator at three heights (15 cm, 30 cm and 50 cm) actual spray angle decreased with an increase of nozzle height because of the effect of gravity. This effect was the most pronounced for the finer sprays.
- The smallest liquid sheet wasfound for XR 110 01 nozzle (18.5 mm), followed by the two hollow cone nozzles (27.4 and 31.3 mm). The longest liquid sheets were found for the XR 110 04 (38.9 mm) and AI 110 04 (43.1 mm).
- From the spray shape, the spray pattern width at four heights (5, 10, 15, 20 cm) of all selected nozzles and the corresponding spray angles were calculated and compared with the results from the horizontal patternator. In general, the highest spray volume was found directly under the nozzle while the spray volume decreased on both sides of the nozzle. In addition, the higher the nozzle, the smoother were the spray distribution peaks compared with those at 15 cm nozzle height. Because of the effect of gravity, the spray shape was parabolic and the spray angle generally decreases with the increased of the nozzle height.
- A comparison of the image analysis results and horizontal patternator results at 15 cm was performed. From here, the spray angle relative error for XR 110 01 at 15 cm height was 0.5 % while for XR 110 01 and AI 110 04 was 0.6 %. The spray angle error was bigger for the hollow cone nozzle, ATR orange and ATR red: 2.8 % and 5.4 %, respectively.
- The developed image acqusition set-up for measuring the macro-spray characteristics succesfully measured the liquid sheet length from the selected nozzle-

pressure combinations. No other research has been documented measuring the size of the liquid sheet of agricultural spray applications.

- The developed algorithm measured the spray angle by defining two straight lines from the nozzle exit. This approach gave satisfactory results on the spray angle values at the nozzle exit.

8.2 SUGGESTIONS FOR FUTURE WORK

The piezoelectric droplet generator can be used in other scientific studies on droplet behavior on plant surfaces under laboratory conditions and for calibrating droplet size measuring equipment.

A number of suggestions have been identified as ways in which the implanted imaging technique may be improved for measuring the macro and micro spray characteristics.

Within the macro spray characteristics, further image processing improvements can be performed such as to calculate the spray angle at different heights (15, 30 and 50 cm) below the nozzle based on the width at each distance from the nozzle orifice.

The frame rate of the current set-up restricted the measurement of the droplet velocity. It will make a significant contribution if the HS camera could be used at bigger frame rate than 1000 fps in full resolution. In addition, the resolution could be further improved in order to be able to measure droplets below 24 µm.

Another interesting challenge is to use a real-time image processing. Moreover, instead of first saving, the images on a computer and afterwards analyzing them, the camera can transfer only the results to a computer using a network card. This will speed up the spray characterization analysis.

The developed set-up is only able to measure droplet velocities in two dimensions. Using two high speed cameras and stereovision, it would be possible to extract three dimensional information from the images.

This imaging technique has not yet been applied on a moving spray nozzle or on a real sprayer in outdoor environments. For this purpose, a new set-up should be built to solve the

problems regarding the varying lighting conditions, shocks and dirt and an algorithm to control the camera's gain and shutter parameters.

Finally, the obtained results are very useful to compare with existing spray models (e.g. CFD models).

Appendix A TABLES

Table A1. Image quality parameters (entropy ratio, contrast ratio and SNR) from the selected image parameters for the Macro Video Zoom lens/light/diffuser/exposure time combinations: entropy ratio, contrast ratio and SNR (average ± std). Mean values followed by the same letter in a column do not differ statistically ($p<0.05$; Sheffe test).

Lens	Light	Diffuser	Entropy Ratio (-)			Contrast Ratio (-)			SNR[a] (-)		
			5 µs exp. time	10 µs exp. time	15 µs exp. time	5 µs exp. time	10 µs exp. time	15 µs exp. time	5 µs exp. time	10 µs exp. time	15 µs exp. time
Macro video zoom lens	xenon	none	1.002 ± 0.013 **b**	1.006 ± 0.004 **b**	1.002 ± 0.003 **b**	1.000 ± 0.001 **b**	1.004 ± 0.002 **b**	1.003 ± 0.003 **b**	0.427 ± 0.005 **b**	0.612 ± 0.006 **b**	0.784 ± 0.006 **b**
		120[c]	1.000 ± 0.003 **b**	1.001 ± 0.002 **b**	1.005 ± 0.011 **b**	1.002 ± 0.012 **b**	1.007 ± 0.011 **b**	0.998 ± 0.004 **b**	2.075 ± 0.022 **b**	2.140 ± 0.026 **b**	2.226 ± 0.017 **b**
		220[d]	1.001 ± 0.003 **b**	1.003 ± 0.003 **b**	1.005 ± 0.011 **b**	1.006 ± 0.014 **b**	1.017 ± 0.013 **b**	1.001 ± 0.004 **b**	2.084 ± 0.036 **b**	2.095 ± 0.028 **b**	2.209 ± 0.017 **b**
	Spot-light	none	1.001 ± 0.022 **b**	0.999 ± 0.016 **b**	1.002 ± 0.015 **b**	0.988 ± 0.007 **b**	0.999 ± 0.012 **b**	1.002 ± 0.016 **b**	2.464 ± 0.013 **b**	3.122 ± 0.028 **b**	3.795 ± 0.045 **b**
		120	1.000 ± 0.008 **b**	0.995 ± 0.127 **b**	1.020 ± 0.836 **a**	1.001 ± 0.040 **b**	0.997 ± 0.124 **b**	2.350 ± 1.198 **a**	3.890 ± 0.160 **b**	11.463 ± 0.961 **b**	123.983 ± 10.553 **a**
		220	1.001 ± 0.007 **b**	1.001 ± 0.130 **b**	1.000 ± 0.974 **a**	1.002 ± 0.040 **b**	1.005 ± 0.134 **b**	2.296 ± 1.419 **a**	4.093 ± 0.161 **b**	11.523 ± 1.110 **b**	162.070 ± 22.049 **a**
	Seven-Star LED	none	1.017 ± 0.029 **b**	1.002 ± 0.008 **b**	0.996 ± 0.006 **b**	1.000 ± 0.001 **b**	1.000 ± 0.001 **b**	1.001 ± 0.002 **b**	0.574 ± 0.002 **b**	0.652 ± 0.002 **b**	0.728 ± 0.003 **b**
		120	1.000 ± 0.001 **b**	1.000 ± 0.002 **b**	0.996 ± 0.013 **b**	1.001 ± 0.002 **b**	1.000 ± 0.002 **b**	0.999 ± 0.003 **b**	1.997 ± 0.009 **b**	2.373 ± 0.004 **b**	3.279 ± 0.010 **b**
		220	1.000 ± 0.001 **b**	1.001 ± 0.002 **b**	1.000 ± 0.003 **b**	1.000 ± 0.003 **b**	1.000 ± 0.001 **b**	0.999 ± 0.003 **b**	2.115 ± 0.006 **b**	2.316 ± 0.003 **b**	3.342 ± 0.009 **b**
		220	1.007 ± 0.047 **b**	1.027 ± 0.054 **b**	1.018 ± 0.112 **b**	1.015 ± 0.065 **b**	1.015 ± 0.053 **b**	1.000 ± 0.049 **b**	0.323 ± 0.024 **b**	0.344 ± 0.024 **b**	0.402 ± 0.025 **b**

[a] SNR based on pictures with a droplet
[b] no visible droplet, image oversaturated
[c] 120 grit diffusing glass
[d] 220 grit diffusing glass

Table A2. **Image quality parameters (entropy ratio, contrast ratio and SNR) from the selected image parameters for the K2/SC Long-Distance Microscope lens/light/diffuser/exposure time combinations: Entropy ratio, Contrast ratio and SNR (average ± std). Mean values followed by the same letter in a column do not differ statistically (p<0.05; Sheffe test).**

Lens	Light	Diffuser	Entropy Ratio (-)			Contrast Ratio (-)			SNR[a] (-)		
			5 µs exp. time	10 µs exp. time	15 µs exp. time	5 µs exp. time	10 µs exp. Time	15 µs exp. time	5 µs exp. time	10 µs exp. time	15 µs exp. time
K2/SC Long -Distance Microscope lens	xenon	none	1.006 ± 0.003 **b**	1.297 ± 0.138 **b**	28.000 ± 1.000 **a**	1.036 ± 0.016 **b**	3.344 ± 0.244 **b**	92.49 ± 9.877 **a**	6.626 ± 0.103 **b**	30.895 ± 1.346 **b**	28.680 ± 0.675 **a**
		120	1.014 ± 0.078 **b**	0.995 ± 0.141 **b**	0.984 ± 0.047 **b**	1.023 ± 0.078 **b**	0.999 ± 0.062 **b**	0.988 ± 0.033 **b**	0.339 ± 0.027 **b**	0.404 ± 0.047 **b**	0.616 ± 0.045 **b**
		220	0.988 ± 0.045 **b**	1.002 ± 0.103 **b**	0.996 ± 0.092 **b**	0.991 ± 0.041 **b**	1.002 ± 0.070 **b**	1.018 ± 0.026 **b**	0.347 ± 0.018 **b**	0.414 ± 0.041 **b**	0.634 ± 0.033 **b**
	Spot-light	/	0.997 ± 0.020 **b**	1.014 ± 0.033 **b**	1.016 ± 0.014 **b**	0.996 ± 0.024 **b**	1.008 ± 0.027 **b**	1.054 ± 0.028 **b**	1.009 ± 0.071 **b**	2.650 ± 0.165 **b**	3.634 ± 0.147 **b**
		120	1.035 ± 0.106 **b**	0.993 ± 0.039 **b**	1.009 ± 0.017 **b**	0.999 ± 0.043 **b**	0.999 ± 0.035 **b**	1.002 ± 0.026 **b**	0.423 ± 0.036 **b**	0.750 ± 0.051 **b**	1.397 ± 0.075 **b**
		220	1.007 ± 0.047 **b**	1.027 ± 0.054 **b**	1.018 ± 0.112 **b**	1.015 ± 0.065 **b**	1.015 ± 0.053 **b**	1.000 ± 0.049 **b**	0.323 ± 0.024 **b**	0.344 ± 0.024 **b**	0.402 ± 0.025 **b**
	Seven-Star LED	/	1.018 ± 0.007 **b**	1.009 ± 0.004 **b**	1.009 ± 0.005 **b**	1.165 ± 0.031 **b**	1.111 ± 0.019 **b**	1.104 ± 0.017 **b**	4.581 ± 0.123 **b**	4.315 ± 0.071 **b**	4.153 ± 0.065 **b**
		120	1.014 ± 0.049 **b**	1.012 ± 0.052 **b**	1.077 ± 0.083 **b**	1.029 ± 0.060 **b**	1.003 ± 0.034 **b**	1.022 ± 0.037	0.331 ± 0.025	0.345 ± 0.017 **b**	0.410 ± 0.017 **b**
		220	1.007 ± 0.047 **b**	1.027 ± 0.054 **b**	1.018 ± 0.112 **b**	1.015 ± 0.065 **b**	1.015 ± 0.053 **b**	1.000 ± 0.049 **b**	0.323 ± 0.024 **b**	0.344 ± 0.024 **b**	0.402 ± 0.025 **b**

[a] SNR based on pictures with a droplet
[b] no visible droplet, image oversaturated
[c] 120 grit diffusing glass
[d] 220 grit diffusing glass

Appendix B LIST OF PUBLICATIONS

- **Book chapter:**

Hijazi, B., Decourselle, T., **Vulgarakis Minov, S**., Nuyttens, D., Cointault, F., Pieters, J. G. et al. (2012). The Use of High-Speed Imaging System for Applications in Precision Agriculture. In Prof.Constantin Volosencu. (Ed.), New Technologies – Trends, Innovations and Research (INTECH).

- **A1 publications:**

Vulgarakis Minov, S., Cointault, F., Vangeyte, J., Pieters, J.G., and Nuyttens, D., 2015. Development of high speed image acquisition systems for spray characterization based on single droplet experiments. Transactions of ASABE 58 (1), 27-37.

Vulgarakis Minov, S., Cointault, F., Vangeyte, J., Pieters, J.G., and Nuyttens, D., 2015. Droplet generation and characterization using piezoelectric droplet generator and high speed imaging techniques. Crop Protection 69, 18-27.

- **Conference papers:**

Vulgarakis Minov S, Cointault F, Vangeyte J, Pieters J G, Hijazi B, Nuyttens D. 2012. Development of an imaging system for single droplet characterization using a droplet generator. *Communications in Agricultural and Applied Biological Sciences*, Ghent University. 64 th International Symposium on Crop Protection, Ghent, Belgium, 22 May 2012. 77(4): 469-481;

Vulgarakis Minov S, Cointault F, Vangeyte J, Pieters J G, Nuyttens D. 2013. Measurement of single droplet characteristics using high speed imaging techniques. Proceedings of the IASTED International Conference on Signal Processing, Pattern recognition and Applications (SPPRA). February 12-14, Innsbruck, Austria. 321-326. DOI: 10.2316/P.2013.798-058; Awarded as a Best Student Paper

Vulgarakis Minov S, Cointault F, Vangeyte J, Pieters J G, Nuyttens D. 2013. Spray nozzle characterization using high speed imaging techniques. *Proceedings 9th European Conference on Precision Agriculture*. July 7 -11, Lleida, Spain. 569-576. ISBN: 978-90-8686-224-5, DOI: 10.3920/978-90-8989-778-3

Vulgarakis Minov S, Cointault F, Vangeyte J, Pieters J G, Nuyttens D. 2014. Spray nozzle characterization using backlighted high speed imaging techniques. Aspects of Applied Biology January 8 -10, Oxford, UK. 122: 353-361.

- **<u>Conference poster</u>:**

"Evaluation of the spray characteristics of a single droplet with imaging techniques", Poster, Forum for young researchers, Besancon, France, September 2012.

REFERENCES

Acharya, T. & Ray, A. K. (2005). *Image Processing: Principles and Applications*. John Wiley & Sons. 451 p.

Azimi, A. H., Carpenter, T. G. & Reichard, D. L. (1985). Nozzle spray distribution for pesticide application. *Transactions of the ASAE, **28**(5)*, 1410-1414.

Bache, D. H. & Johnstone, D. R. (1993). *Microclimate and Spray Dispersion*. Ellis Horwood Ltd. 220 p.

Baek, S. J. & Lee, S. J. (1996). A new two-frame particle tracking algorithm using match probability. *Experiments in Fluids, **22**(1)*, 23-32.

Balsari, P. & Marucco, P. (2011). The New EU Directives Requirements and the Innovation in Pesticide Application Techniques. *Journal of ASTM International, **8**(2)*, 1-21.

Barnich, O. & Droogenbroeck, M. (2011). ViBe: A universal Background subtraction algorithm for video sequences. *IEEE Transactions on Image Processing, **20**(6)*, 1709-1724.

Basi, S., Hunsche, M., Damerow, L., Lammers, P. S. & Noga, G. (2012). Evaluation of a pneumatic drop-on-demand generator for application of agrochemical solutions. *Crop Protection, **40***, 121-125.

Bayvel, L. & Orzechowski, Z. (1993). *Liquid Atomization*. Taylor & Francis Group. 475 p.

Butler Ellis, M. C., Tuck, C. R. & Miller, P. C. H. (1997). The effect of some adjuvants on sprays produced by agricultural flat fan nozzles. *Crop Protection, **16**(1)*, 41-50.

Canny, J. (1983). A computational approach to edge detection. *IEEE transactions on Pattern Analysis and Machine Intelligence, **8**(6)*, 679-698.

Castanet, G., Dunand, P., Caballina, O. & Lemoine, F. (2013). High-speed shadow imagery to characterize the size and velocity of the secondary droplets produced by drop impacts onto a heated surface. *Experiments in Fluids, **54**(3)*, 1489-1506.

Castrejon-Pita, J., Martin, G., Hoath, S. & Hutchings, I. (2008). A simple large-scale droplet generator for studies of inkjet printing. *Review of Scientific Instruments, **79**(7)*, 075108.

Cawood, P. N., Robinson, T. H. & Whittaker, S. (1995). An investigation of Alternative Application Techniques for the Control of Black-grass. In Proceedings Brighton Crop Protection Conference - Weeds. pp. 521-527.

Chigier, N. (1991). Optical imaging of spray. *Progress in Energy and Combustion Science, **17***, 211-262.

Cloeter, M. D., Qin, K., Patil, P. & Smith, B. (2010). Planar laser induced fluorescence flow visualisation applied to agricultural spray nozzles with sheet disintegration; Influence of Oil-in-Water Emulsion. In pp. 1-9.

Cointault, F., Sarrazin, P. & Paindavoine, M. (2002). High resolution low cost imaging system for particle projection analysis: application to fertilizer centrifugal spreading. *Measurement Science and Technology, **13***, 1087-1093.

Cool, S., Pieters, J. G., Mertens, K., Hijazi, B. & Vangeyte, J. (2014). A simulation of the influence of spinning on the ballistic flight of fertiliser grains. *Computers and Electronics in Agriculture, **105***, 121-131.

De Schampheleire, M., Nuyttens, D., Baetens, K., Cornelis, W., Gabriels, D. & Spanoghe, P. (2009). Effects on pesticide spray drift of the physicochemical properties of the spray liquid. *Precision Agriculture, **10**(5)*, 409-420.

Dekeyser, D., Duga, A. T., Verboven, P., Hendrickx, N. & Nuyttens, D. (2013). Assessment of orchard sprayers using laboratory experiments and CFD modelling. *Biosystems Engineering, **114**(2)*, 157-169.

Dong, X., Zhu, H. & Yang, X. (2013). Three-Dimensional Imaging system for Analyses of Dynamic Droplet Impaction and Deposit Formation on Leaves. *Transactions of ASABE, **56**(5)*, 1641-1651.

Dorr, G., Hanan, J., Hewitt, A. J., Adkins, S. & Noller, B. (2007). Modeling the Interaction of Plant Architecture and Spray Techniques. In 2007 ASABE Annual International Meeting, Technical Papers. pp. 1-10.

Dorr, G., Adkins, J., Hewitt, A., O'Donnell, C. & Noller, B. (2008). Spray deposition on plant surfaces: A modelling approach. *Functional Plant Biology, **35***, 988-996.

Dorr, J. G., Hewitt, A., Adkins, J., Hanan, J., Zhang, H. & Noller, B. (2013). A comparison of initial spray characteristics produced by agricultural nozzles. *Crop Protection, **53***, 109-117.

Etheridge, R. E., Womac, A. R. & Mueller, T. C. (1999). Characterization of the spray droplet spectra and patterns of four venture-type drift reduction nozzles. *Weed Tech., **13**(4)*, 765-770.

European Commission (2006). A thematic strategy on the sustainable use of pesticides.

European Commission (2009). Directive 2009/128/EC of the European Parliament and of the Council of 21 October 2009 establishing a framework for Community action to achieve the sustainable use of pesticides.

Evangelio, R. H. (2014). Background Subtraction for the Detection of Moving and static Objects in Video Surveillance.

FAO (2014). *Bulding a common vision for sustainable food and agriculture (Principles and Approaches)*. 56 p.

Faqiri, N. L. & Krishnan, P. (2005). Effect of nozzle pressure and wind condition on spray pattern displacement of RF5 and 110-5R nozzles. *Applied Engineering in Agriculture, **21**(5)*, 747-750.

Farooq, M., Balachandar, R. & Wolf, T. (2001). Assessment of an agricultural spray in anon-uniform cross-flow. *Transactions of the ASAE, **44**(6)*, 1455-1460.

Foqué, D. (2012). *Optimization of spray application technology in ornamental crops*. (vols. 239) Ghent University, Department of Biosystems Engineering, Faculty of Bioscience Engineering.

Foqué, D., Pieters, J. G. & Nuyttens, D. (2012). Comparing Spray Gun and Spray Boom Applications in Two Ivy Crops with Different Crop Densities. *Hortscience, **47**(1)*, 51-57.

Galeev, R. S. & Zaripov, S. K. (2003). Deposition of aerosol particles on a sphere: The role of gravity. *Aerosol Science and Technology, **37**(4)*, 325-329.

Gardiner, J. A. (1964). Measurement of the drop size distribution in water sprays by an electrical method. *Instrum.Pract., **18***, 353-356.

Gonzalez, R. C., Woods R.E. & Eddins S.L. (2004). *Digital Image Processing Using Matlab*. (vols. 609 p) Pearson Prentice Hall.

Grant, I. (1997). Particle image velocimetry: a review. In Proceedings of the Institution of Mechanical Engineers, Part C: Journal of Mechanical Engineering Science. pp. 55-76.

Haralick, R. M., Shanmugam, K. & Dieinstein, I. (1973). Textural Features for Image Classification. *IEEE Transactions ON SYSTEMS, MAN AND CYBERNETICS, **SMC-3**(6)*, 610-621.

Hatem, A. B. (1997). *Software development for particle tracking velocimetry*. University of Nottingham, United Kingdom.

Hijazi, B., Cointault, F., Dubois, J., Coudert, S., Vangeyte, J., Pieters, J. G. & Paindavoine, M. (2010). Multi phase cross-correlation method for motion estimation of fertiliser granules during centrifugal spreading. *Precision Agriculture, **11***, 684-702.

Hijazi, B., Decourselle, T., Vulgarakis Minov, S., Nuyttens, D., Cointault, F., Pieters, J. G. et al. (2012). The Use of High-Speed Imaging System for Applications in Precision Agriculture. In C. Volosencu (ed.), *New Technologies – Trends, Innovations and Research* (INTECH).

Hill, B. D. & Inaba, D. J. (1989). Use of Water-Sensitive Paper to Monitor the Deposition of Aerially Applied Insecticides. *Journal of Economic Entomology, **82**(3)*, 974-980.

Hislop, E. C. (1987). Can we achieve optimum pesticide deposits? *Aspects of Applied Biology, **14***, 153-172.

Hsuan-Chung, W. & Huey-Jiuan, L. (2010). Effects of actuating pressure waveforms on the droplet behavior in a piezoelectric inkjet. *Materials Transactions, **51**(12)*, 2269-2276.

Huyghebaert, B., Debouche, C. & Mostade, O. (2001). Flow rate quality of new flat fan nozzles. *Transactions of the ASAE, **44**(4)*, 769-773.

ILVO Spray Tech Lab (2013). ILVO BELAC accredited Spray Tech Lab.

Infinity Photo-Optical Company. (2009). Model K2/SC Long-Distance Microscope System.

International Standard ISO 5682-1. (1996). Equipment for crop protection –Spraying equipment-Part 1: Test methods of sprayer nozzles.

ISO 106225. (2005). Equipment for crop protection -- Sprayer nozzles -- Colour coding for identification.

Jain, R. & Nagel, H. (1979). On the analysis of accumulative difference pictures from image sequences of real world scenes. *IEEE Transactions on Pattern Analysis and Machine Intelligence, **PAMI-1**(2)*, 206-214.

Jasikova, D., Kotek, M., Lenc, T. & Kopecky, V. (2011). Experimental study of full cone spray nozzle by Interferometry particle sizing technique. *Recent Researches in Mechanics, **90**(3),* 1-4.

Johnson, P. D., Rimmer, D. A., Garrod, A. N. I., Helps, J. E. & Mawdsley, C. (2005). Operator exposure when applying amenity herbicides by all-terrain vehicles and controlled droplet applicators. *Annals of Occupational Hygiene, **49***, 25-32.

Ju, D., Shrimpton, J. S. & Hearn, A. (2012). A Multi-Thresholding Algorithm for sizing out of Focus Particles. *Particle & Particle Systems Characterization, **29***, 78-92.

Kashdan, J. T., Shrimpton, J. S. & Whybrew, A. (2004a). Two-phase flow characterization by automated digital image analysis. Part 1: Fundamental principles and calibration of the technique. *Particle & Particle Systems Characterization, **20**(6)*, 387-397.

Kashdan, J. T., Shrimpton, J. S. & Whybrew, A. (2004b). Two-phase flow characterization by automated digital image analysis. Part 2: Application of PDIA for sizing sprays. *Particle & Particle Systems Characterization, **21**(1)*, 15-23.

Kashdan, J. T., Shrimpton, J. S. & Whybrew, A. (2007). A digital image analysis technique for quantitative characterisation of high-speed sprays. *Optics and Lasers in Engineering, **45**(1)*, 106-115.

Khot, L. R., Salyani, M. & Sweeb, R. D. (2011). Solar and Storage Degradations of Oil- and Water-Soluble Fluorescent Dyes. *Applied Engineering in Agriculture, **27**(2)*, 211-216.

Kim, H. & Lee, S. (2002). Performance improvement of two-frame particle tracking velocimetry using a hybrid adaptive scheme. *Measurement Science & Technology, **13***, 573-582.

Kim, H. H., Kim, J. H. & Ogata, A. (2011). Time-resolved high-speed camera observation of electrospray. *Journal of Aerosol Science, **42**(4)*, 249-263.

Kim, K. S. & Kim, S. S. (1994). Drop sizing and depth-of-field correction in TV imaging. *Atomization and Sprays, **4***, 65-78.

Kirk, I. W. (2001). Droplet Spectra Classification for Fixed-Wing Aircraft Spray Nozzles. In ASAE Annual Meeting. ASAE.

Knowles, A. (2001). Adjuvants for agrochemicals. *Pesticide Outlook, **12***, 183-184.

Kowalczyk, M. (1996). Laser speckle velocimetry. In Proc.SPIE.

Kreizer, M., Ratner, D. & Liberzon, A. (2010). Real-time image processing for particle tracking velocimetry. *Experiments in Fluids, **48**(1)*, 105-110.

Kuang-Chao, F., Jhing-Yuan, C., Ching-Hua, W. & Wen-Chueh, P. (2008). Development of a drop-on-demand droplet generator for one-drop-fill technology. *Sensors and Actuators A: Physical, **147**(2)*, 649-655.

Kung, C. Y., Barnes, M. D., Lermer, N., Whitten, W. B. & Ramsey, J. M. (1999). Single-molecule analysis of ultradilute solutions with guided streams of 1lm water droplets. *Appl.Opt., **38**(9)*, 1481-1487.

Lad, N., Aroussi, A. & Muhamad Said, M. F. (2011). Droplet size Measurement for Liquid Spray using Digital Image Analysis Technique. *Journal of Applied Sciences, **11***, 1966-1972.

Lam, K. H., Sun, C. L., Kwok, K. W. & Chan, H. L. W. (2009). Piezoelectric dispenser based on a piezoelectric-metal-cavity actuator. *Review of Scientific Instruments, **80**(7)*, 075110.

Lecuona, A., Sosa, P. A., Rodriguez, P. A. & Zequeira, R. I. (2000). Volumetric characterization of dispersed two-phase flows by digital image analysis. *Measurement Science & Technology, **11**(8)*, 1152-1161.

Lee, C., Wu, C. H. & Hoopes, J. A. (2009). Simultaneous particle size and concentration measurements using a back-lighted particle imaging system. *Flow Measurement and Instrumentation, **20***, 189-199.

Lee, E. R. (2003). *Microdrop Generation*. CRC PRESS. 249 p.

Lee, S. & Kim, Y. (2004). Sizing of spray particles using image processing technique
1981. *KSME International Journal, **18**(6)*, 879-894.

Lefebvre, A. H. (1989). *Atomization and Sprays*. Hemisphere Publishing Corporation USA. 434 p.

Li, E. Q., Xu Q., Sun, J., Fuh, J. Y. H., Wong, Y. S. & Thoroddsen, S. T. (2010). Design and fabrication of a PET / PTFE-based piezoelectric squeeze mode drop-on-demand inkjet printhead with interchangeable nozzle. *Sensors and Actuators A: Physical, **163***, 315-322.

Lindemann, T. (2006). *Droplet Generation From the Nanoliter to Femtoliter Range*. (**200 ed.**) Albert-Ludwigs-Universität Freiburg.

Lipp, C. W. (2012). *Practical Spray Technology: Fundamentals and Practice*. (**1ST ed.**) Lake Innovation LLC.

Luo, J., Qi, L. H., Zhou, J. M., Xiao, Y. & Yang, F. (2011). Study on stable delivery of charged uniform droplets for freeform fabrication of metal parts. *Science China-Technological Sciences, **54**(7)*, 1833-1840.

Maggio, E. & Cavallaro, A. (2011). *Video Tracking: Theory and Practice*. (vols. 292p) Wiley.

Malot, H. & Blaisot, J. B. (2000). Droplet size distribution and sphericity measurements of low-density sprays through image analysis. *Particle & Particle Systems Characterization, **17**(4)*, 146-158.

Massinon, M. & Lebeau, F. (2012a). Experimental method for the assessment of agricultural spray retention based on high-speed imaging of drop impact on a synthetic superhydrophobic surface. *Biosystems Engineering, **112**(1)*, 56-64.

Massinon, M. & Lebeau, F. (2012b). Comparison of spray retention on synthetic superhydrophobic surface with retention on outdoor grown wheat leaves. In Aspects of Applied Biology. pp. 261-268. Association of Applied Biologists.

Materka, A. & Strzelecki, M. (1998). Texture analysis methods- A review (pp. 1-33) Technical University of Lodz.

Matthews, G. A. (2000). *Pesticide application methods*. (**Third ed.**) (vols. 432) Blackwell Science Ltd, Oxford.

Mavros, P. (2001). Flow visualization in stirred vessels - A review of experimental techniques. *Chemical Engineering Research & Design, **79**(A2)*, 113-127.

Miller, P. C. H. & Butler Ellis, M. C. (1997). Spray generation, delivery to the target and how adjuvants influence the process. *Plant Protection Quarterly, **12**(1)*, 33-38.

Miller, P. C. H. & Ellis, M. C. B. (2000). Effects of formulation on spray nozzle performance for applications from ground-based boom sprayers. *Crop Protection, **19**(8-10)*, 609-615.

Nilars, M. S. (2003). Nozzle technology and atomizer design. *Hardi International application technology course,* 5-13.

Nuyttens, D. (2007a). Drift from field crop sprayers: The influence of spray application technology determined using indirect and direct drift assessment means. PhD thesis nr. 772, KU Leuven. 293 p. ISBN 978-908826-039-1.

Nuyttens, D., Baetens, K., De Schampheleire, M. & Sonck, B. (2007b). Effect of nozzle type, size and pressure on spray droplet characteristics. *Biosystems Engineering, **97**(3)*, 333-345.

Nuyttens, D., De Schampheleire, M., Verboven, P., Brusselman, E. & Dekeyser, D. (2009). Droplet Size and Velocity Characteristics of Agricultural Sprays. *Transactions of the ASABE, **52**(5)*, 1471-1480.

Nuyttens, D., De Schampheleire, M., Verboven, P. & Sonck, B. (2010). Comparison between indirect and direct spray drift assessment methods. *Biosystems Engineering, **105**(1)*, 2-12.

Nuyttens, D., De Schampheleire, M., Baetens, K., Brusselman, E., Dekeyser, D. & Verboven, P. (2011). Drift from field crop sprayers using an integrated approach: Results from a five-year study. *Transactions of the ASABE, **54**(2)*, 403-408.

Paul, E. L., Atiemo-Obeng, V. A. & Kresta, S. M. (2004). *Handbook of Industrial Mixing Science and Practice*. (vols. 1448) JohnWiley & Sons, INC..

Permin, O., Jørgensen, L. N. & Persson, K. (1992). Deposition characteristics and biological effectiveness of fungicides applied to winter wheat and the hazards of drift when using different types of hydraulic nozzles. *Crop Protection, **11**(6)*, 541-546.

Pimentel, D. (1995). Amounts of pesticides reaching the target pests: environmental impacts and ethics. *J.Agric.Environ.Ethics, **8***, 17-29.

Pimentel, D. & Burgess, M. (2012). Small amounts of pesticides reaching target insects. *Enviro.Dev.Sustain., **14***, 1-2.

Reichard, D. L. (1990). A system for Producing Various Sizes, Numbers, and Frequencies of Uniform-Size Drops. *Transactions of the ASAE, **33**(6)*, 1767-1770.

Reichard, D. L., Cooper, J. A., Bukovac, M. J. & Fox, R. D. (1998). Using a videographic system to assess spray droplet impaction and reflection from leaf and artificial surfaces. *Pesticide Science, **53**(4)*, 291-299.

Rhodes, M. J. (2008). *Introduction to Particle Technology, 2nd Edition*. (vols. 474) John Wilery and Sons Inc. New Jersey, USA.

Rice, P. J., Rice, P. J., Arthur, E. L. & Barefoot, A. C. (2007). Advances in pesticide environmental fate and exposure assessments. *J.Agric.Food Chem., **55**(14)*, 5367-5376.

Riefler, N. & Wriedt, T. (2008). Generation of monodisperse micron-sized droplets using free adjustable signals. *Particle & Particle Systems Characterization, **25**(2)*, 176-182.

Sadeghian, H., Hojjat, Y. & Ghodsi, M. (2014). An approach to design and fabrication of a piezo-actuated microdroplet generator. *International Journal of Advanced Manufacturing Technology, **70***, 1091-1099.

Sanchez-Hermosilla, J., Rincon, V. J., Paez, F., Aguera, F. & Carvajal, F. (2011). Field evaluation of a self-propelled sprayer and effects of the application rate on spray deposition and losses to the ground in greenhouse tomato crops. *Pest Management Science, **67**(8)*, 942-947.

Saunders, R. E., Gough, J. E. & Derby, B. (2008). Delivery of human fibroblast cells by piezoelectric drop-on-demand inkjet printing. *Biomaterials, **29***, 193-203.

Schick, J. R. (1997). An Engineer's Practical Guide to Drop Size (pp. 1-15) Spraying Systems Co.

Shirolkar, J. S., Coimbra, C. F. M. & Mcquay, M. Q. (1996). Fundamental aspects of modeling turbulent particle dispersion in dilute flows. *Progress in Energy and Combustion Science, **22**(4)*, 363-399.

Sidahmed, M. M. (1996). A theory for predicting the size and velocity of droplets from pressure nozzles. *Transactions of the ASAE, **39**(2)*, 385-391.

Šikalo, S., Tropea, C. & Ganic, E. N. (2005). Impact of droplets onto inclined surfaces. *Journal of Colloid and Interface Science, **286**(2)*, 661-669.

Southcombe, E. S. E., Miller, P. C. H., Ganzelmeier, H., Van de Zande, J. C., Miralles, A. & Hewitt, A. J. (1997). The international (BCPC) spray classification system including a drift potential factor. In pp. 371-380. FARNHAM: BRITISH CROP PROTECTION COUNCIL.

Spillman, J. J. (1984). Spray Impaction, Retention and Adhesion - An Introduction to Basic Characteristics. *Pesticide Science, **15**(2)*, 97-106.

Stafford, J. V. (2000). Implementing precision agriculture in the 21st century. *Journal of Agricultural Engineering Research, **76**(3)*, 267-275.

Stainier, C., Destain, M. F., Schiffers, B. & Lebeau, F. (2006). Droplet size spectra and drift effect of two phenmedipham formulations and four adjuvants mixtures. *Crop Protection, **25**(12)*, 1238-1243.

Sumner, P. E. (2009). Soybean Sprayer Application and Calibration (pp. 8p) The University of Gerogia.

Switzer, G. L. (1991). A Versatile System for Stable Generation of Uniform Droplets. *Review of Scientific Instruments, **62**(11)*, 2765-2771.

Teske, M. E., Thistle, H. W., Hewitt, A. J. & Kirk, I. W. (2002). Conversion of droplet size distributions from PMS Optical Array Probe to Malvern Laser Diffraction. *Atomization and Sprays, **12**(1-3)*, 267-281.

Teske, M. E., Thistle, H. W., Hewitt, A. J., Kirk, I. W., Dexter, R. W. & Ghent, J. H. (2005). Rotary atomizer drop size distribution database. *Transactions of the ASAE, **48**(3)*, 917-921.

Tuceryan, M. & Jain, A. K. (1998). Texture Analysis. In Chen C.H & Pau L.F (eds.), *The Handbook of Pattern Recognition and Computer Vision* (**2nd ed.**, pp. 207-248). World Scientific Publishing Co..

Ulmke, H., Wriedt, T., Lohner, H. & Bauckhage, K. (1999). The Piezoelectric Droplet Generator - A Versatile Tool for Dispensing Applications and Calibration of Particle Sizing Instruments. In Precision Engineering - Nanotechnology (Ed.), Proceedings 1st International euspen Conference. pp. 290-293.

Ulmke, H., Wriedt, T. & Bauckhage, K. (2001). Piezoelectric droplet generator for the calibration of particle-sizing instruments. *Chemical Engineering & Technology, **24**(3)*, 265-268.

Umbaugh, S. E. (2010). *Digital image processing and analysis : human and computer vision applications with CVIP tools*. (vols. 977) CRC Press, Boca Raton, FL.

US Environmental Protection Agency (2013). Integrated Pest Management (IPM) principles.

Vanella, G., Salyani, M. & Balsari, P. (2011). Effect of the nozzle adaptor of sprayer calibrator on flow rate measurements. *Crop Protection, **30**(8)*, 1043-1047.

Vangeyte, J. & Sonck, B. (2005). Image analysis of particle trajectories. In B. Tijskens & H. Ramon (Eds.), Proceedings 1st International symposium on centrifugal fertiliser spreading. KU Leuven.

Vangeyte, J. (2013). Development and validation of a low cost technique to predict spread patterns of centrifugal fertiliser spreaders. PhD thesis nr. 1099, KU Leuven, Faculty of Bioscience Engineering. 168 p. ISBN 978-90-8826-304-0

Vulgarakis Minov, S., Cointault, F., Vangeyte, J., Pieters, J. G. & Nuyttens, D. (2013). Measurement of single droplet characteristics using high speed imaging techniques. In Proceedings of the IASTED International Conference on Signal Processing, Pattern recognition and Applications (SPPRA). pp. 321-326. ACTA Press.

Vulgarakis Minov, S., Cointault, F., Vangeyte, J., Pieters, J. G. & Nuyttens, D. (2015a). Development of High-Speed Image Acquisition Systems for Spray Characterization Based on Single-Droplet Experiments. *Transactions of ASABE, **58**(1)*, 27-37.

Vulgarakis Minov, S., Cointault, F., Vangeyte, J., Pieters, J. G. & Nuyttens, D. (2015b). Droplet generation and characterization using piezoelectric droplet generator and high speed imaging techniques. *Crop Protection, **69***, 18-27.

Wang, L., Zhang, N., Slocombe, J. W., Thierstein, G. E. & Kuhlman, D. K. (1995). Experimental Analysis of Spray Distribution Pattern Uniformity for Agricultural Nozzles. *Applied Engineering in Agriculture, **11**(1)*, 51-55.

Whisenant, S. G., Bouse, L. F., Crane, R. A. & Bovey, R. W. (1993). Droplet size and spray volume effect on honey mesquite mortality with clopyralid. *J.Range Mgmt, **46**(3)*, 257-261.

Whitney, R. W. & Roth, L. O. (1985). String Collectors for Spray Pattern-Analysis. *Transactions of the ASAE, **28**(6)*, 1749-1753.

Wright, J. F., Lidsay, A. D. & Sawyer, E. (1982). *Pesticide Tank Mix Applications, First Conference: A Symposium*. (vols. 98) ASTM International.

Yan, S., Sayad, S. & Balke, S. T. (2009). Image quality in image classification: adaptive image quality modification with adaptive classification. *Computers & Chemical Engineering, **33***, 429-435.

Yang, J. C., Chien, W., King, M. & Grosshandler, W. L. (1997). A simple piezoelectric droplet generator. *Experiments in Fluids, **23**(5)*, 445-447.

Yule, A. J. (1978). Large-Scale Structure in the mixing layer of a round jet. *Journal of Fluid Mechanics, **89**(3)*, 413-432.

Zabkiewicz, J. A. (2007). Spray formulation efficacy - holistic and futuristic perspectives. *Crop Protection, **26**(3)*, 312-319.

Zhang, N., Wang, L. & Thierstein, G. E. (2011). Measuring Nozzle Spray Uniformity Using Image-Analysis. *Transactions of the ASABE, **37***, 381-387.

Zhu, H., Reichard, D. L., Fox, R. D., Brazee, R. D. & Ozkan, H. E. (1996). Collection efficiency of spray droplets on vertical targets. *Transactions of the ASAE, **39**(2)*, 415-422.

Ziou, D. & Tabbone, S. (1998). Edge detection techniques: An overview. *International Journal of Pattern Recognition and Image Analysis, **8**(4)*, 537-559.

Zwertvaegher, I., Verhaeghe, M., Brusselman, E., Lebeau, F., Massinon, M., Nicolai, B. M. & Nuyttens, D. (2014). The impact and retention of spray droplets on a horizontal hydrophobic surface. *Biosystems Engineering, **26***, 82-91.